

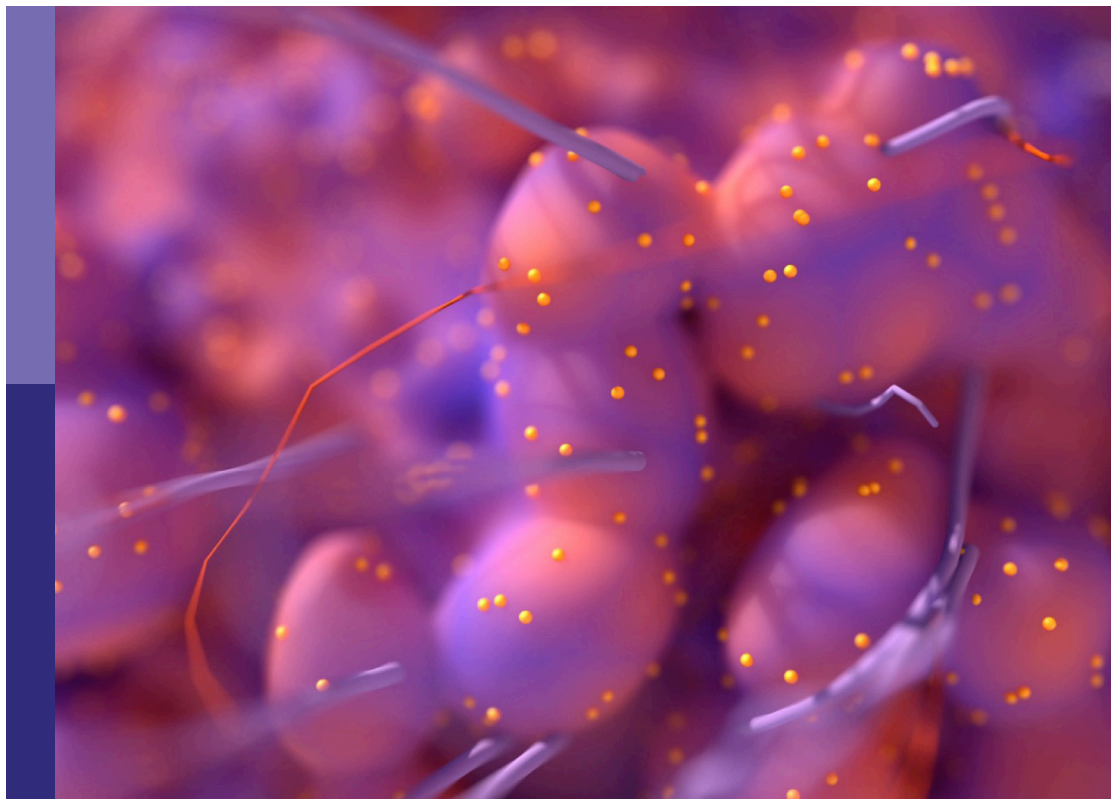
Methods in thoracic oncology

Edited by

Grigoris Stratakos, Jane Houldsworth, Jelena Stojic,
Alberto Sandri and Xiaomin Niu

Published in

Frontiers in Oncology



FRONTIERS EBOOK COPYRIGHT STATEMENT

The copyright in the text of individual articles in this ebook is the property of their respective authors or their respective institutions or funders. The copyright in graphics and images within each article may be subject to copyright of other parties. In both cases this is subject to a license granted to Frontiers.

The compilation of articles constituting this ebook is the property of Frontiers.

Each article within this ebook, and the ebook itself, are published under the most recent version of the Creative Commons CC-BY licence. The version current at the date of publication of this ebook is CC-BY 4.0. If the CC-BY licence is updated, the licence granted by Frontiers is automatically updated to the new version.

When exercising any right under the CC-BY licence, Frontiers must be attributed as the original publisher of the article or ebook, as applicable.

Authors have the responsibility of ensuring that any graphics or other materials which are the property of others may be included in the CC-BY licence, but this should be checked before relying on the CC-BY licence to reproduce those materials. Any copyright notices relating to those materials must be complied with.

Copyright and source acknowledgement notices may not be removed and must be displayed in any copy, derivative work or partial copy which includes the elements in question.

All copyright, and all rights therein, are protected by national and international copyright laws. The above represents a summary only. For further information please read Frontiers' Conditions for Website Use and Copyright Statement, and the applicable CC-BY licence.

ISSN 1664-8714
ISBN 978-2-8325-2536-4
DOI 10.3389/978-2-8325-2536-4

About Frontiers

Frontiers is more than just an open access publisher of scholarly articles: it is a pioneering approach to the world of academia, radically improving the way scholarly research is managed. The grand vision of Frontiers is a world where all people have an equal opportunity to seek, share and generate knowledge. Frontiers provides immediate and permanent online open access to all its publications, but this alone is not enough to realize our grand goals.

Frontiers journal series

The Frontiers journal series is a multi-tier and interdisciplinary set of open-access, online journals, promising a paradigm shift from the current review, selection and dissemination processes in academic publishing. All Frontiers journals are driven by researchers for researchers; therefore, they constitute a service to the scholarly community. At the same time, the *Frontiers journal series* operates on a revolutionary invention, the tiered publishing system, initially addressing specific communities of scholars, and gradually climbing up to broader public understanding, thus serving the interests of the lay society, too.

Dedication to quality

Each Frontiers article is a landmark of the highest quality, thanks to genuinely collaborative interactions between authors and review editors, who include some of the world's best academicians. Research must be certified by peers before entering a stream of knowledge that may eventually reach the public - and shape society; therefore, Frontiers only applies the most rigorous and unbiased reviews. Frontiers revolutionizes research publishing by freely delivering the most outstanding research, evaluated with no bias from both the academic and social point of view. By applying the most advanced information technologies, Frontiers is catapulting scholarly publishing into a new generation.

What are Frontiers Research Topics?

Frontiers Research Topics are very popular trademarks of the *Frontiers journals series*: they are collections of at least ten articles, all centered on a particular subject. With their unique mix of varied contributions from Original Research to Review Articles, Frontiers Research Topics unify the most influential researchers, the latest key findings and historical advances in a hot research area.

Find out more on how to host your own Frontiers Research Topic or contribute to one as an author by contacting the Frontiers editorial office: frontiersin.org/about/contact

Methods in thoracic oncology

Topic editors

Grigoris Stratakos — National and Kapodistrian University of Athens, Greece

Jane Houldsworth — Icahn School of Medicine at Mount Sinai, United States

Jelena Stojic — University of Belgrade, Serbia

Alberto Sandri — Unit of Thoracic Surgery, San Luigi Gonzaga Hospital, Italy

Xiaomin Niu — Shanghai Jiao Tong University, China

Citation

Stratakos, G., Houldsworth, J., Stojic, J., Sandri, A., Niu, X., eds. (2023). *Methods in thoracic oncology*. Lausanne: Frontiers Media SA. doi: 10.3389/978-2-8325-2536-4

Table of contents

05	Editorial: Methods in thoracic oncology Jelena Stojić and Tatjana Adžić-Vukičević
08	Study Protocol for a Randomised Controlled Trial on Pulmonary Metastasectomy vs. Standard of Care in Colorectal Cancer Patients With ≥ 3 Lung Metastases (PUCC-Trial) Severin Schmid, Heiko Becker, Ralph Fritsch, Johannes Bausch, Natalie Hunter, Carolin Jenkner, Mohamed Hassan and Bernward Passlick
16	Case Report: Clinicopathological Analysis of Minute Pulmonary Meningothelial-Like Nodules: Report of 7 Cases Ying-xia Wang, Zi Lei, Man Yang, Zhi-yuan Wang, Xuan Zhang and Guo-qing Pan
24	The prognostic influence of histological subtypes of micropapillary tumors on patients with lung adenocarcinoma ≤ 2 cm Liangdong Xu, Hangcheng Zhou, Gaoxiang Wang, Zhining Huang, Ran Xiong, Xiaohui Sun, Mingsheng Wu, Tian Li and Mingran Xie
34	Establishing a novel model of malignant airway stenosis in rabbit Xiaoxiao Lin, Liqin Zhou, Wanting Zhou, Yuping Li, Xuru Jin, Min Ye and Chengshui Chen
44	The combined role of PET/CT metabolic parameters and inflammatory markers in detecting extensive disease in small cell lung cancer Yao Hu, Jin Sun, Danming Li, Yangyang Li, Tiannv Li and Yuxiao Hu
54	Deep learning-based growth prediction for sub-solid pulmonary nodules on CT images Ri-qiang Liao, An-wei Li, Hong-hong Yan, Jun-tao Lin, Si-yang Liu, Jing-wen Wang, Jian-sheng Fang, Hong-bo Liu, Yong-he Hou, Chao Song, Hui-fang Yang, Bin Li, Ben-yuan Jiang, Song Dong, Qiang Nie, Wen-zhao Zhong, Yi-long Wu and Xue-ning Yang
65	3D deep learning versus the current methods for predicting tumor invasiveness of lung adenocarcinoma based on high-resolution computed tomography images Yilv Lv, Ying Wei, Kuan Xu, Xiaobin Zhang, Rong Hua, Jia Huang, Min Li, Cui Tang, Long Yang, Bingchun Liu, Yonggang Yuan, Siwen Li, Yaozong Gao, Xianjie Zhang, Yifan Wu, Yuchen Han, Zhanxian Shang, Hong Yu, Yiqiang Zhan, Feng Shi and Bo Ye
76	Immune cell-lipoprotein imbalance as a marker for early diagnosis of non-small cell lung cancer metastasis Wei Zhang, Weiwei Wang, Junlu Wu, Jiale Tian, Wenhui Yan, Yi Yuan, Yiwen Yao, Anquan Shang and Wenqiang Quan

- 90 **Development and validation of nomogram prognostic model for early-stage T1-2N0M0 small cell lung cancer: A population-based analysis**
Tao Ge, Shuncang Zhu, Liangdong Sun, Laibo Yin, Jie Dai, Jiayi Qian, Xiangru Chen, Peng Zhang, Jialong Zhu and Gening Jiang
- 105 **Development and validation a simple scoring system to identify malignant pericardial effusion**
Xiaxia Jin, Lingling Hu, Meidan Fang, Qiaofei Zheng, Yuan Yuan, Guoguang Lu and Tao Li
- 113 **Safety and efficacy of stereotactic ablative brachytherapy as a salvage therapy for recurrent chest wall cancer: A retrospective, multicenter study**
Bin Huo, Zhe Ji, Chuang He, Wanying Yang, Yanli Ma, Xiaodong Huo, Zhe Wang, Xinxin Zhao, Jinchao Dai, Haitao Wang, Guanglie Chen, Ruoyu Wang, Yuqing Song, Kaixian Zhang, Xuequan Huang, Shude Chai and Junjie Wang



OPEN ACCESS

EDITED AND REVIEWED BY
Lizza E.L. Hendriks,
Maastricht University Medical Centre,
Netherlands

*CORRESPONDENCE
Jelena Stojić
✉ dr.jelenastoj@gmail.com

RECEIVED 02 March 2023
ACCEPTED 20 April 2023
PUBLISHED 10 May 2023

CITATION
Stojić J and Adžić-Vukičević T (2023)
Editorial: Methods in thoracic oncology.
Front. Oncol. 13:1178236.
doi: 10.3389/fonc.2023.1178236

COPYRIGHT
© 2023 Stojić and Adžić-Vukičević. This is
an open-access article distributed under the
terms of the [Creative Commons Attribution
License \(CC BY\)](#). The use, distribution or
reproduction in other forums is permitted,
provided the original author(s) and the
copyright owner(s) are credited and that
the original publication in this journal is
cited, in accordance with accepted
academic practice. No use, distribution or
reproduction is permitted which does not
comply with these terms.

Editorial: Methods in thoracic oncology

Jelena Stojić^{1*} and Tatjana Adžić-Vukičević^{1,2}

¹Service of Pathology, University Clinical Centre, Belgrade, Serbia, ²School of Medicine, University of Belgrade, Belgrade, Serbia

KEYWORDS

methodology, oncology, thorax, small cell lung cancer, non-small lung cancer

Editorial on the Research Topic Methods in thoracic oncology

Lung carcinoma is the most common tumor of the thoracic region and therefore requires a serious multidisciplinary approach in diagnostics, treatment, and in determining the prognosis and outcomes of each specific case, using biochemical, radiologic, and pathohistological methods and parameters. A contemporary multidisciplinary approach is also adopted for other tumors of the thoracic region. In the last two decades, for thoracic tumors, and especially lung carcinoma, various predictive markers that influence treatment options and thus also the outcome of diseases and the quality of life of patients have been developed.

All accepted and published papers have very studiously examined possibilities for establishing new methods, i.e. new prognostic parameters in thoracic oncology. Since the studies included large numbers of patients, we may consider their results relevant. Topics covered by these studies ranged from biochemical and metabolic properties to the microenvironment of malignant cells of both types of primary lung carcinoma, as well as secondary, metastatic lung carcinoma. Some studies also presented rare thoracic and lung tumors and the ways they were diagnosed, underlining the importance of pathologic examinations in their diagnostics. The contribution of imaging tools to the prognostics of malignant diseases in thoracic oncology was also emphasized, particularly in correlation with the metabolic changes observed. One of the ways of studying the introduction of new methods was by using experimental animal models.

The studies covered all common histological types of lung carcinoma, as well as the most common secondary or metastatic intestinal or colorectal carcinoma and chest wall tumors. A rare variant of the most aggressive papillary subtype of lung adenocarcinoma of size $\leq 20\text{mm}$ (pTNM: T1-2N0M0) was also presented in this Research Topic. The rare minute pulmonary meningotheial-like nodules were described, and one of the articles considered their specific clinical, radiological, morphological, and immunohistological features. The article also described a cytological investigation for the purpose of differentiating malignant from benign cells in pericardial effusion. This cytological study gained validation of the scoring system for their differentiation, which is a challenge in daily practice. An original experimental investigation of malignant airway stenosis in rabbits was for the first time published in the global literature. Two studies investigated biochemical and metabolic mechanisms of remodeling the microenvironment in NSCLC and SCLC progression and metastasis.

The details of each of these articles are the following:

The new predicting method in the evaluation of staging of SCLC combines the role of PET/CT metabolic parameters, systemic immune-inflammation marker (SII), maximum standardized uptake value (SUVmax), metabolic tumor volume (MTV), total lesion glycolysis (TLG), systemic immune-inflammation marker (SII), maximum standardized uptake value (SUVmax), metabolic tumor volume (MTV), and total lesion glycolysis (TLG) with inflammatory markers, namely, neutrophil/lymphocyte ratio (NLR), platelet/lymphocyte (PLR), and monocyte/lymphocyte ratio (MLR). The binary stage system, extensive-stage disease (ED) and limited-stage disease, was included in 119 patients with previous pathological diagnoses of SCLC who had performed PET/CT scans. The authors detected that baseline markers and tumor metabolic parameters were associated with a binary stage in SCLC patients. ED-SCLC could be predicted on PET/CT scans in patients with associated high levels of MTV/MLR based on metabolic tumor volume and systemic inflammatory response (Hu et al.).

In another multidisciplinary and multicentric study researchers tried to find a correlation between immune cells and high-density lipoprotein as the markers for early detection of metastatic NSCLC. The authors investigated the value of blood-related indicators: neutrophil/leukocyte (NLR), lymphocyte/monocyte (LMR), high-density lipoprotein (HNR), high-density lipoprotein/monocyte (HMR), and combined assays in metastatic NSCLC. The researchers concluded that NLR, LMR, HNR, and HMR levels had diagnostic values for metastatic NSCLC. This investigation provides a mechanism for remodeling the microenvironment prior to NSCLC metastasis. The idea is to continue the research in the future, including more patients with metastatic NSCLC for better evaluation of investigated markers and adopt it as a new method (Zhang et al.).

Two studies investigated the performance of the imaging method of 3D deep learning that automatically predicts tumor invasiveness in intraoperative frozen tissue sections, comparing it with the results of an interobserver study between radiologists on high-resolution CT scan (HRCT) and surgeons in conditions where pathologists established diagnosis of low-risk adenocarcinoma (pre-IAC), adenocarcinoma *in situ* (AIS), or minimally invasive adenocarcinoma (MIA). The deep learning approach will be a valuable guiding strategy during surgery (Lv et al.). In the second study, the deep learning method was established as a recommended prediction model for the detection of sub-solid tumor nodule growth pattern, mass, and measures, intended to successfully manage them during follow-up periods, based on approximately 2,500 investigated lung tumors (Liao et al.).

The group of authors tried to provide the development and validation of a nomogram for predicting individual survival (OS) and lung cancer-specific survival (LCSS) prognostic model for the early-stage T1-2N0M0 subset of SCLC. A retrospective population-based study included approximately 1,600 patients with SCLC from the SEER database, divided into two cohorts depending on the year of diagnosis. This investigation provided a new nomogram showing certain reliability that could aid clinicians in improving the prognosis, treatment strategy, and new design of future clinical trials suitable for web servers as well. (Ge et al.).

Chest wall tumors, including metastatic lung, breast and thymic carcinoma, mesothelioma, and sarcoma used to be surgically treated. The authors of a retrospective, multicentric study strongly suggested salvage brachytherapy (SABT) as a safe and efficient method. This type of therapy shows promising efficient follow-up in patients with Karnofsky scores higher than 80 (ECOG 0 and 1), who received a dose greater than 130Gy and had tumors larger than 40mm (Huo et al.).

Pulmonary adenocarcinoma rarely has a micropapillary (MP) pattern. Authors investigated preoperatively diagnosed MPs $\leq 20\text{mm}$ (pTNM: T1-2N0M0) in 390 patients in different proportions. The prognosis depends on the type of resection and lymph node dissection. Lobectomy and systemic lymph node dissection are recommended for patients with a micropapillary histological component of $>5\%$ and sublobular resection and limited lymph node dissection are recommended for patients with a micropapillary histological component of $\leq 5\%$. The authors will evaluate the feasibility of this method in the future (Xu et al.).

Metastatic intestinal adenocarcinoma or colorectal carcinoma (CRC) in lung parenchyma was investigated in patients meeting established criteria. The leading criterion was three or more metastatic nodules in the lung parenchyma in this trial. The conclusion could be that new biomarkers are needed for better risk stratification and identification of patients with a high risk for CRC recurrence after metastasectomy without conventional markers. Circulating DNA (ctDNA) will be analyzed at various pre-and post-surgical time points as well as in surgically untreated patients to characterize its role as a clinically useful biomarker in patients with CRC undergoing pulmonary mastectomy. This trial will provide stronger evidence for the performance of pulmonary metastasectomy and potentially better patient selection (Schmid et al.).

The etiology of pericardial effusion was emphasized as very significant in patients with diagnosed tumors in the surrounding tissues. The authors suggested a scoring system for differentiating malignant from benign cells in pericardial effusion. Included parameters are loss of weight (3 points), no fever (4 points), and mediastinal lymph node enlargement (6 points). In pericardial effusion, the parameters are the presence of adenosine deaminase (5 points), effusion lactate dehydrogenase (7 points), and carcinoembryonic antigen (10 points). The cut point is 16 for differentiating malignant from benign cells. The reviewers remark that pericardial effusion pathology can resolve the dilemma with cell morphology and immunohistochemistry as an updated model (Jin et al.).

The rabbit model is available for stent implantation in case of tumors growing in the bronchial tree, particularly in the trachea. This method is safe and effective for stent implantation due to it facilitating the treatment approach. The author recommends this model for preclinical animal studies on bronchoscopic interventional treatments (Wang et al.).

In a multidisciplinary approach, combining clinical, radiological, morphological pattern, and immunohistochemical findings, seven cases of minute pulmonary meningotheelial-like nodules (MPMN) were diagnosed and described, incidentally detected with lung carcinoma and pneumonia, and in three cases occurred alone, with the appearance of multiple, medium hardness,

and greyish-white solid tumors. A typical growing pattern through widened alveolar septa, morphology, and immunoprofile confirmed MPMNs (Wang et al.).

All published articles could be summarized as novelties in multidisciplinary methods in thoracic oncology. All of them are interesting and attractive for readers, from pulmonologists and thoracic surgeons to thoracic pathologists and oncologists. We expect these studies to inspire researchers to recommend and adopt new methods that might contribute to diagnostics and help determine prognostic and predictive methods in thoracic oncology.

Author contributions

This is the editorial of accepted papers that will be published in the journal with specific topic “Editorial: Methods in Thoracic Oncology”. This paper is the summary of all accepted papers where the new methodology in thoracic oncology is suggested or old methods that are improved. As editor, I analyzed all accepted papers and presented a new methodology and contributions, i.e. obtained results introducing a new methodology. The co-author

helped with clinical experiences interpreting obtained result in eleven accepted papers. All authors contributed to the article and approved the submitted version.

Conflict of interest

The authors declare that the research was conducted in the absence of any commercial or financial relationships that could be construed as a potential conflict of interest.

Publisher's note

All claims expressed in this article are solely those of the authors and do not necessarily represent those of their affiliated organizations, or those of the publisher, the editors and the reviewers. Any product that may be evaluated in this article, or claim that may be made by its manufacturer, is not guaranteed or endorsed by the publisher.



Study Protocol for a Randomised Controlled Trial on Pulmonary Metastasectomy vs. Standard of Care in Colorectal Cancer Patients With ≥ 3 Lung Metastases (PUCC-Trial)

Severin Schmid^{1*}, Heiko Becker², Ralph Fritsch³, Johannes Bausch⁴, Natalie Hunter⁴, Carolin Jenkner⁴, Mohamed Hassan¹ and Bernward Passlick¹

¹ Department of Thoracic Surgery, Medical Center – University of Freiburg, Faculty of Medicine, University of Freiburg, Freiburg, Germany, ² Department of Medicine I, Medical Center – University of Freiburg, Faculty of Medicine, University of Freiburg, Freiburg, Germany, ³ Department of Medical Oncology and Hematology – University Hospital of Zurich, Zurich, Switzerland, ⁴ Clinical Trials Unit, Medical Center, Faculty of Medicine, University of Freiburg, Freiburg, Germany

OPEN ACCESS

Edited by:

Marcello Migliore,
University of Catania, Italy

Reviewed by:

Norman Williams,
University College London,
United Kingdom
Dai-Yuan Ma,
Affiliated Hospital of North Sichuan
Medical College, China

*Correspondence:

Severin Schmid
SeverinSchmid@gmx.net

Specialty section:

This article was submitted to
Thoracic Oncology,
a section of the journal
Frontiers in Oncology

Received: 06 April 2022

Accepted: 19 May 2022

Published: 11 July 2022

Citation:

Schmid S, Becker H, Fritsch R, Bausch J, Hunter N, Jenkner C, Hassan M and Passlick B (2022) Study Protocol for a Randomised Controlled Trial on Pulmonary Metastasectomy vs. Standard of Care in Colorectal Cancer Patients With ≥ 3 Lung Metastases (PUCC-Trial). *Front. Oncol.* 12:913896. doi: 10.3389/fonc.2022.913896

This is a multicentre prospective randomised controlled trial for patients with 3 or more resectable pulmonary metastases from colorectal carcinoma. The study investigates the effects of pulmonary metastasectomy in addition to standard medical treatment in comparison to standard medical treatment plus possible local ablative measures such as SBRT. This trial is intended to demonstrate an overall survival difference in the group undergoing pulmonary metastasectomy. Further secondary and exploratory endpoints include quality of life (EORTC QLQ-C30, QLQ-CR29 and QLQ-LC29 questionnaires), progression-free survival and impact of mutational status. Due to the heterogeneity and complexity of the disease and treatment trajectories in metastasised colorectal cancer, well powered trials have been very challenging to design and execute. The goal of this study is to create a setting which allows treatment as close to the real life conditions as possible but under well standardised conditions. Based on previous trials, in which patient recruitment in the given setting hindered successful study completion, we decided to (1) restrict inclusion to patients with 3 or more metastases (since in case of lesser, surgery will probably be the preferred option) and (2) allow for real world standard of care (SOC) treatment options before and after randomisation including watchful waiting (as opposed to a predefined treatment protocol) and (3) possibility that patient can receive SOC externally (to reduce patient burden). Moreover, we chose to stipulate 12 weeks of systemic treatment prior to possible resection to further standardize treatment response and disease course over a certain period of time. Hence, included patients will be in the disease state of oligopersistence rather than primary oligometastatic. The trial was registered in the German Clinical Trials Register (DRKS-No.: DRKS00024727).

Keywords: colorectal (colon) cancer, pulmonary metastasectomy, overall survival (OS), quality of life, metastasis

INTRODUCTION

Pulmonary metastasectomy (PM) is a widely applied treatment for metastasised colorectal cancer (mCRC) based on findings from a vast abundance of retrospective trials (1–5). The only prospective trial on pulmonary mCRC has not shown any survival benefit for patients undergoing PM compared to systemic therapy only (6). Although the trial failed to reach its recruitment target and was thus underpowered the observed survival of 47% after 4 years in the control group is far better than expected and crucial when assuming a potential benefit from PM (7). Other prospective randomised trials have demonstrated a benefit for progression-free as well as overall survival by radical local ablative treatments in metastasised solid cancers including lung, breast, colorectal cancer (CRC) and others (8–11). Local ablative measures in these trials were either exclusively or mostly non-surgical consisting of stereotactic body radiation therapy (SBRT) and radiofrequency ablation. Moreover, the only trial exclusively including patients with hepatic metastases from CRC suffered, although randomised, from serious imbalances regarding number of metastases in the investigated groups (8).

Generally, the application of local ablative measures in metastasised cancers remains controversial. Some argue that systemic diseases should be treated as such and hence therapy should be confined to systemic treatment alone (12). Others believe that radical local measures result in survival advantages due to cytoreduction and removal of sites which are insufficiently treated by the medical treatment. Also, these sites could be capable of seeding new metastases. The significance of tumour cell release by secondary tumours for further metastatisation remains unclear, however, there is clinical and experimental evidence showing a beneficial effect of aggressive local ablative treatment in oligometastasis on further metastatisation (13–19).

Current guidelines of the European Society of Medical Oncology (ESMO) recommend resection of pulmonary metastases in cases in which R0-resection is feasible, however under consideration of relative contraindications based on the tumour biology as well as patient-related factors such as comorbidities and personal expectations (20).

The factors currently defining tumor biology include presence of a higher number of metastases, meta- vs. synchronicity of metastatisation and a short interval from diagnosis of the primary to first manifestation of metastasis [disease-free-interval (DFI)]. Due to the lack of strong evidence the interpretation of these relative contraindications is highly variable and the chosen treatment modalities depend largely on the treating institution and discipline. A benefit from surgical resection has never been proven in prospective trials even in patients with small numbers of metastases (1–3). Nevertheless, surgery in these patients is generally applied and considered treatment of choice in many countries. This is based primarily on retrospective data which shows a favourable prognosis in patients with completely resectable metastases, even if there are more than 3 lesions (2, 5). If surgical resection in comparison to the current standard of care proves superior in the study

presented here, PM could be implicated as standard of care option also in patients with multiple metastases and thus help to improve long-term survival of these patients; on the other hand, a negative finding could result in abandoning the practice of PM at least in a selected cohort.

To our knowledge there is currently only one ongoing other multi-centric prospective randomised controlled trial on PM conducted by the MD Anderson Cancer Center in Texas, USA which started recruitment in July 2018 (NCT03599752). Patients are categorised into low and high risk before being randomised. Low risk patients are randomised to either PM + systemic treatment or PM alone. High-risk patients are randomised to either PM + systemic treatment or systemic treatment alone. Primary outcome measures are progression-free survival (PFS) in the low-risk group and overall survival (OS) in the high-risk group.

Although past prospective randomised trials either failed to reach the targeted recruitment numbers and/or suffered from patient heterogeneity we hope that further, carefully designed prospective trials, as the one we present here, can provide additional insight into the potential benefits of surgical removal of pulmonary metastases in patients with CRC.

METHODS AND ANALYSIS

Design

This is a multicentre prospective randomised controlled trial for patients with 3 or more resectable pulmonary metastases from CRC. PUCC investigates the effects of pulmonary metastasectomy in addition to standard medical treatment in comparison to standard of care, i.e. medical treatment and/or alternative local ablative measures such as stereotactic body radiation therapy (SBRT).

This trial is intended to demonstrate an overall survival benefit in the group undergoing pulmonary metastasectomy. For the trial start a total of about 15 sites have agreed to participate in this multicentre trial. Then, if necessary more sites will be included and in case of recruitment failure, the respective sites will be replaced. The planned recruiting period is 2 years.

Endpoints

The primary endpoint is overall survival (OS). OS is defined as the time from randomisation until death from any cause with censoring at the last date alive. The primary objective is to assess the effect of pulmonary metastasectomy compared to standard of care consisting of systemic therapy and possible SBRT where indicated on OS.

Secondary endpoints are

- Progression-free survival (PFS), defined as the time from randomisation until disease progression or death from any cause.
 - PFS assessment will be performed locally, usually in a multidisciplinary setting (e.g. tumour board) but at least by a radiologist and oncologist/thoracic surgeon.

- Definitions of progressive disease (PD) can consist of but are not limited to: unequivocal tumour growth of known metastatic lesions, new metastatic lesions, local recurrence.
- PFS will be determined from serial CT scans, PET-CT or MRT with censoring at the last date alive and progression-free.
- Complete remission, defined as no radiologic sign of residual disease and pathologically complete (R0) resection if applicable.
- Quality of life (QoL) using the EORTC QLQ-C30, QLQ-CR29 and QLQ-LC29 questionnaires at 3, 6, 12, 24 and 36 months after randomisation.

Participants

Patients with at least 3 technically resectable (R0) pulmonary metastases from colorectal cancer will be enrolled into this trial. A total of 152 patients are planned to be randomised at a 1:1 ratio (about half of the patients to each treatment arm).

Main Inclusion Criteria

1. Histologically confirmed colorectal adenocarcinoma
2. ≥ 3 technically resectable (R0) pulmonary metastases
3. Male or female patients aged ≥ 18 years without upper age limit
4. Resected primary tumour with intent to cure (sole prior (chemo) radiation of a rectal cancer with documented complete remission is permitted)
5. In case of previous treatment of hepatic metastases: no radiologic sign of active hepatic disease at the time of trial randomisation
6. A minimum of 12 weeks of systemic therapy with the last treatment applied within 6 months prior to randomisation
7. Good performance status (ECOG 0-1)
8. Sufficient pulmonary reserve (FEV1 $>60\%$, DLCO $>60\%$)

Main Exclusion Criteria

1. Active extra-thoracic tumour disease (including primary tumour *in situ*)
2. Prior resection of lung metastases (diagnostic resection is allowed)
3. Requirement of a pneumonectomy to achieve complete resection
4. Other malignancy in the past 5 years (except non-melanoma skin cancer or *in situ* cancer)
5. Histologically proven intrathoracic lymph node metastasis (except resectable single level mediastinal, hilar and pulmonary) as defined at <https://radiopaedia.org/articles/thoracic-lymph-node-stations>
6. Known or uncontrolled brain metastases
7. Known BRAF V600E mutation (unknown BRAF mutation status does not constitute an exclusion criterion)
8. Prior $>2^{\text{nd}}$ line therapy, i.e. TAS-102 (Lonsurf[®]) or regorafenib
9. Medical condition which poses a high risk to undergo systemic treatment and/or surgery as defined by the investigator

Treatment

All trial participants must have received at least 12 weeks of standard systemic treatment, with the last treatment applied within 6 months prior to randomisation. Chemotherapy can have been carried out at the discretion of the treating oncologist and according to local standards/guideline recommendations and must have consisted of a cytotoxic therapy (monotherapy, doublet or triplet) with or without a VEGF- or EGFR-directed therapy.

If the patients are randomised to Arm A, the pulmonary metastasectomy surgery should be performed as soon as possible after completion of systemic therapy (as defined in inclusion criterion 6) but no sooner than 4 weeks after last application of systemic therapy.

Before trial enrolment, all patients will require restaging *via* PET-CT or CT-thorax and -abdomen or CT-thorax plus MRI abdomen within 6 weeks before randomisation. If a patient has 3 or more isolated lung metastases, the patient will be assessed for trial inclusion by an experienced thoracic surgeon, preferably in the setting of a multidisciplinary tumour board. If the metastases are amenable to surgical resection and the inclusion criteria are met, then the patient will be randomised (**Figure 1**).

Experimental Treatment (Arm A)

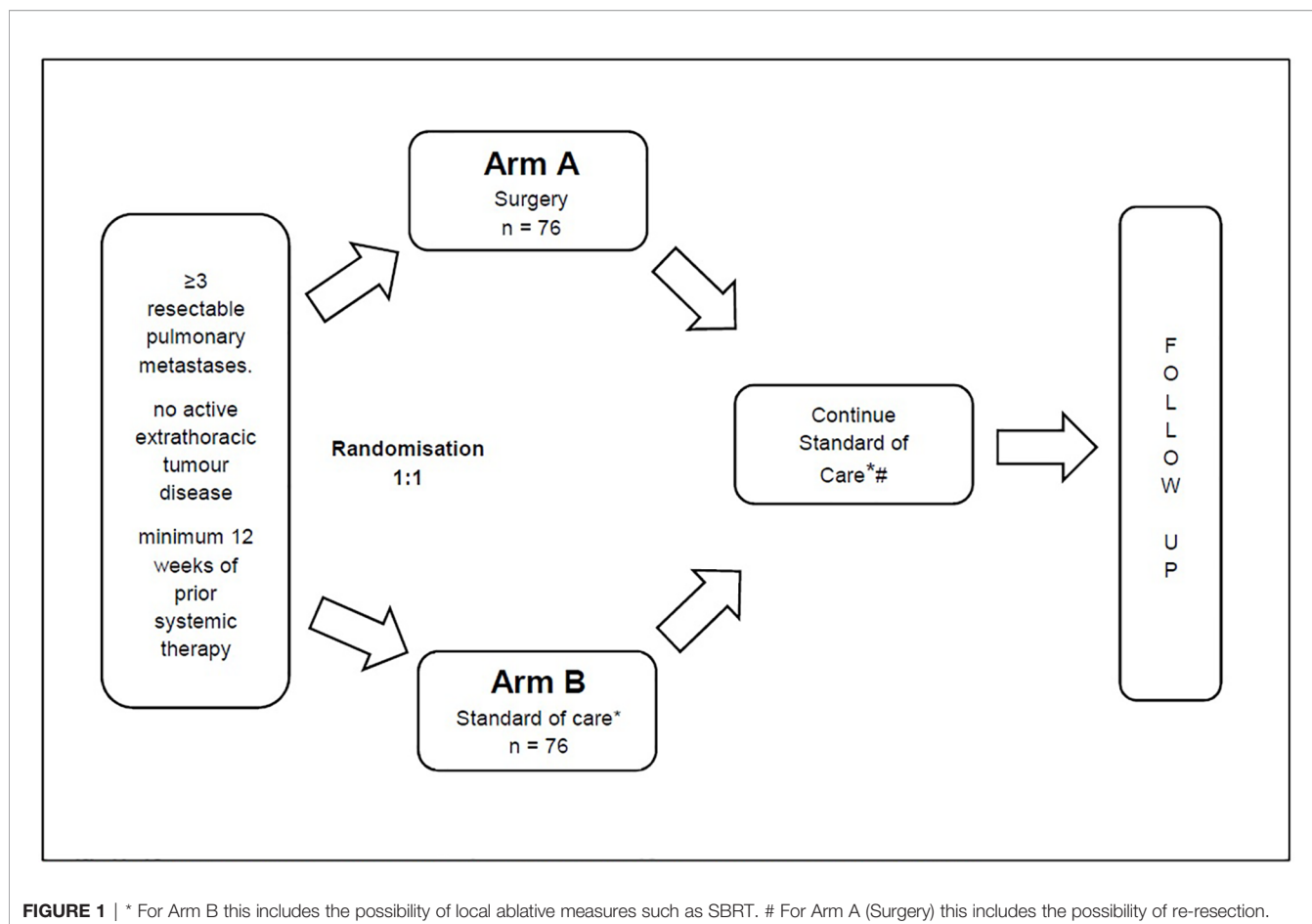
After randomisation into the experimental treatment arm patients will undergo uni- or bilateral surgical resection of the pulmonary metastases.

In case of bilateral disease patients will undergo one side first and after 3-5 weeks the other side. A CT scan of the thorax should be performed after the first surgery and before the second. Remaining metastases after resection on the ipsilateral side do not result in trial exclusion or pose a contraindication to resection of the remaining side. If the lesions are amenable to safe and complete resection, lesions can be removed by the means of minimally invasive surgery. Also, according to surgeon's preference single-stage bilateral resection *via* sternotomy can be carried out. Single stage bilateral thoracotomy is not recommended. Anatomical resection (segmentectomy, lobectomy) can be applied if it is required to provide safe R0-resection.

Any currently available standard-device can be used for resection according to local standards. If cautery or laser-devices are used the resulting defects should be sutured with a monofilament absorbable suture (e.g. PDSTM).

In case of diffuse metastasisation and/or pleural carcinosis the surgery must be aborted. Systematic lymphadenectomy or sampling is recommended in patients in Arm A. If mediastinal lymph node metastases are ruled out by PET-CT and/or endobronchial ultrasound guided biopsy (EBUS), lymphadenectomy can be omitted.

After completion of surgical treatment in Arm A the patients will continue with systemic treatment according to the standard of care. Postoperative continuation of systemic therapy will be decided upon investigator's discretion. If adjuvant treatment is chosen, then this should preferably consist of fluorouracil (alternatively capecitabine) and oxaliplatin. Given the lack of benefit of regimens containing irinotecan, EGFR-targeted agents



and VEGF-targeted agents in the adjuvant treatment of stage II or III colon cancer, these should only be used on an individual basis in the postoperative setting.

In the experimental arm, it is encouraged that patients undergo re-resection in case of disease progression/recurrence if the respective oncologic principles apply.

Control Treatment (Arm B)

After randomisation into the control arm patients will continue standard of care consisting of systemic therapy. Standard of care should follow common oncologic recommendations. SBRT can be applied upon investigator's discretion.

Data on the standard anti-tumour care (chemotherapy and SBRT) will be collected and analysed **Figure 2**.

Informed Consent Procedure

Before enrolment in the clinical trial, the patient will be informed that participation in the clinical trial is voluntary and that he/she may withdraw from the clinical trial at any time without having to give reasons and without penalty or loss of benefits to which the patient is otherwise entitled. The treating physician will provide the patient with information about the treatment methods to be compared and the possible risks involved. At the same time, the nature, significance, implications, expected

benefits and potential risks of the clinical trial and alternative treatment will be explained to the patient. The patient's written consent must be obtained before any trial-specific tests/treatments. For this purpose, the written consent form will be personally dated and signed by the trial patient and the investigator conducting the informed consent discussion.

Randomisation Methodology

Randomisation will be performed, stratified by site, in blocks of variable length aiming for large block lengths in a ratio of 1:1 to ensure a balanced distribution of the treatments and reduce selection bias. The block lengths will be documented separately and will not be disclosed to the sites. Central randomisation will be performed web based using the RedCapTM tool to conceal treatment allocation.

Data Management and Monitoring

The data management will be performed with REDCapTM, a fully web based remote data entry (RDE) system (also called eCRF). The system is based on web forms and is developed and maintained by the REDCap Consortium (redcap@vanderbilt.edu). The technical specifications of the database will be described in the codebook delivered automatically by the REDCapTM system.

Visit schedule and assessments	Screening/ Randomisation	pulmonary metasta- sectomy ⁽¹⁾	3 Mo ± 2 W	6 Mo ± 2 W	9 Mo ± 2 W	12 Mo ± 2 W	15 Mo ± 2 W	18 Mo ± 2 W	21 Mo ± 2 W	24 Mo ± 4 W	30 Mo ± 4 W	36 Mo ± 4 W	≥ 42 – 60 Mo Phone FU Visits every 3 Mo until EOS (defined as 36 Mo after Rando of the last pt) ± 4 W
Visit Number	1	1a (only in Arm A)	2	3	4	5	6	7	8	9	10	11	
Time frame	4 weeks		36 months										up to 2 years (24 Mo)
Informed consent, Registration, Demographic data	X												Overall survival and anti-tumour therapy
MH incl. prior treatment, height, weight	X												
Physical examination	X												
Inclusion/exclusion criteria	X												
Data on disease/ mutation status	X												
Randomisation (Rando)	Rando ⁽²⁾												
Treatment Arm A (surgery)		X	surgery plus systemic treatment according to standard of care										
Treatment Arm B (control)			systemic treatment incl. SBRT as applicable according to standard of care										
ECOG Performance Status	X												
QoL questionnaires ⁽³⁾	X		X	X		X				X		X	
Laboratory (Hematology & Clinical Chemistry) ⁽⁴⁾	X	(X)	X	X ⁽⁷⁾	X ⁽⁷⁾	X ⁽⁷⁾	X ⁽⁷⁾	X ⁽⁷⁾	X ⁽⁷⁾	X ⁽⁷⁾	X ⁽⁷⁾	X ⁽⁷⁾	
CT chest/abdomen or PET-CT or CT-chest/ MRI abdomen (must not exceed assessments as defined by local clinical routine) ⁽⁵⁾	X ⁽⁵⁾	(X) ⁽⁵⁾	X	X ⁽⁷⁾	X ⁽⁷⁾	X ⁽⁷⁾		X ⁽⁷⁾		X ⁽⁷⁾	X ⁽⁷⁾	X ⁽⁷⁾	
Lung function testing including DLCO	X			X ⁽⁷⁾		X ⁽⁷⁾				X ⁽⁷⁾			
Adverse events (CTCAE)		X	X										
Documentation of nights in hospital ⁽⁶⁾	X	X	X	X	X	X							

FIGURE 2 | EOS, End of Study; FU, Follow-Up; MH, Medical history; Mo, month(s); pt(s), patient(s); Rando, randomisation; SBRT, Stereotactic Radiation Therapy; W, week(s). (1) Investigations during the treatment period are performed at the discretion of the treating physician and according to the respective treatment arm. (2) Randomisation has to be performed as close as possible to potential start of surgery. (3) Quality of life (QoL) will be assessed using the EORTC QLQ-C30, QLQ-CR29 and QLQ-LC29 questionnaires. (4) Laboratory includes LDH, CEA, CA19-9, CRP (see section 7.8.8 Blood tests). (5) Not older than 6 weeks at the time of randomisation. (6) Number of nights in hospital will be documented starting from the randomisation date and until the end of the month 12. (7) Might be assessed externally, if not possible at trial site due to Covid19.

Details on data management (software, procedures, responsibilities, etc.) will be described in a data management plan prior to the trial. During the trial, the performance of data management and any deviations from the data management plan will be documented in a data management plan. Technical specifications of the trial data base and all data checks will be documented in a data validation plan.

The trial data base has been fully validated before any data entry will be performed. Data entry personnel will not be given access to the trial data base until they have been trained. The investigator or a designated person will record the participation in the trial, the frequency of the trial visits, the relevant medical data, the concomitant treatment and the occurrence of adverse events in the medical record of each trial patient, as timely as possible. An audit trail provide a data history which data were entered, changed or deleted, by whom and when.

Data will be checked during data entry by so-called built-in edit checks. The data will be further reviewed for completeness, consistency, plausibility, and regarding protocol violations and other distinctive problems (e.g. cumulative missings) using SAS software. The resulting queries will be sent to the investigator for correction or verification of the documented data. All programs which can be used to influence the data or data quality will be validated (e.g. edit check and data validation programs for import of external data, etc.).

Concomitant treatments or procedures entered into the eCRF will be coded using the WHO Drug Reference List. Adverse

Events will be coded using the Medical dictionary for regulatory activities (MedDRA) terminology.

Information about trial patients will be kept confidential and managed under the applicable laws and regulations. Those regulations require a signed patient authorisation informing the patient of the following:

- what protected health information (PHI) will be collected from patients in this trial;
- who will have access to that information and why;
- who will use or disclose that information;
- the rights of a research patient to revoke their authorisation for use of their PHI.

In the event that a patient revokes authorisation to collect or use PHI, the investigator, by regulation, retains the ability to use all information collected prior to the revocation of patient authorisation. For patients that have revoked authorisation to collect or use PHI, attempts should be made to obtain permission to collect at least vital status (i.e. that the patient is alive) at the end of their scheduled trial phase. The data collection system for this trial uses built-in security features to prevent unauthorised access to confidential participant information, including an encrypted transport protocol for data transmission from the participating sites to the trial database. The trial database is located on a server of the IT facility of Medical Center - University of Freiburg. Employees of the Clinical Trials Unit charged with hosting the eCRF and the trial database are obliged

to maintain data confidentiality and to comply with data protection regulation.

Biostatistical Planning and Analysis

The sample size calculation is based on the primary endpoint overall survival. A median OS time of approximately 27 months under standard of care is assumed, while the median OS time is expected to increase to about 55 months under standard of care (without SBRT) and pulmonary metastasectomy (2, 21). This corresponds to a hazard ratio of 2.04 between the treatment arms (medical treatment vs. medical treatment and pulmonary metastasectomy). The effect of medical treatment and pulmonary metastasectomy will be assessed by a log-rank test at two-sided significance level of 5% and by estimation of the hazard ratio with corresponding asymptotic two-sided 95% confidence interval. The null hypothesis is rejected, if the confidence interval does not contain one. Under the above assumptions, the trial is planned to detect a difference between medical treatment and pulmonary metastasectomy over medical treatment alone with a power of 90%, which requires a total number of 83 events to be observed. To account for the possibility that the observed hazard ratio may be diminished by non-compliance and/or drop-out of patients, the sample size is calculated to achieve a power of 90%. The required number of patients to be randomised to observe this amount of events depends on the length of follow-up. With a recruitment period of 2 years, an additional follow-up period after the end of recruitment of 3 years (maximum length of follow up 5 years) it can safely be assumed that a sufficient number of events will have been observed by the end of the trial if a total of 152 patients (76 per group) are available for analysis (software used, e.g. nQuery Advisor 8.3).

Definition of Populations Included in the Analyses

Efficacy analyses will be performed primarily in the full analysis set (FAS) according to the intention-to-treat (ITT) principle. This means that the patients will be analysed in the treatment arms to which they were randomised, irrespective of whether they refused or discontinued the treatment or whether other protocol violations occurred.

The per-protocol (PP) population is a subset of the FAS and is defined as the group of patients who had no major protocol violations, received a predefined minimum dose of the treatment and underwent the examinations required for the assessment of the endpoints at relevant, predefined times. The analysis of the PP population will be performed for the purpose of a sensitivity analysis. Safety analyses will be performed in the safety population. Patients in the safety population are analysed as belonging to the treatment arm defined by treatment received. Patients are included in the respective treatment arm, if treatment was started/if they received at least one dose of trial treatment.

Primary Endpoint

The effects of standard of care with and without metastasectomy with respect to the primary endpoint overall survival will be estimated and tested by Cox regression. The regression model will include treatment and trial site as independent variables, as

well as, metachronicity vs. synchronicity and, previous treatment of hepatic metastasis and colon- or rectal cancer. As estimate of the effect size, the hazard ratio between the two treatment arms will be given with the corresponding asymptotic two-sided 95% confidence interval. The two-sided test on difference between standard of care with metastasectomy and standard of care at significance level 5% will be based on the corresponding asymptotic two-sided 95% confidence interval from the Cox regression model. Overall survival will be analysed irrespective of the occurrence of intercurrent events. This is consistent with the treatment policy strategy of the estimands framework.

Secondary Endpoints for Efficacy

Descriptive analyses of the secondary endpoints will be performed in similar regression models as for the primary endpoint, as appropriate for the respective type of data. Differences between treatment groups will be calculated with 95% CIs. Progression free survival and complete remission will be measured from randomisation and be analysed using Cox regression as described for the primary endpoint. Endpoints with competing events will be estimated using the Aalen Johanson estimator. Endpoints without competing events will be estimated using the Kaplan Meier estimator. Quality of life measures (EORTC QLQ-C30, QLQ-CR29 and QLQ-LC29) will be analysed descriptively by treatment arm and time point using linear regression. Changes from baseline will be described. Differences in the number of courses of systemic therapy and in the time on systemic therapy will be summarised descriptively by treatment arm using the FAS. The impact of the mutational status on treatment response and survival (on PFS and OS) performed in similar regression models as for primary endpoint adjusted for the mutational status.

DISCUSSION

Despite its wide application pulmonary metastasectomy in mCRC remains controversial. Past trials have shown ambiguous results which might be at least partially due to difficulties recruiting and/or imbalances in the investigated groups (6, 8, 11). PM are very well tolerated procedures with close to zero mortality and very little morbidity in this often relatively fit patient collective (5, 22). If the situation allows, the treating physician tends to recommend PM to the patient as the common assumption is a prolonged survival when metastases are completely removed. However, as outlined above, this assumption is primarily based on retrospective data, as it has never been formally demonstrated in a prospective trial. Interestingly, one would assume that patients also tend to want to undergo complete removal of metastases, however data from the PulMiCC-trial has shown that patients often seem to prefer non-surgical treatment in case of a well-informed decision (6, 23).

Nevertheless, multiple prospective randomised trials suggest a survival benefit from radical local treatments in oligometastatic cancers (9–11). Hence there is an urgent need for more homogeneous and adequately powered trials in CRC. Considering the discussed issues regarding the heterogeneity in the patient collective, complexity of treatment trajectories,

regional differences in treatment choices as well as the aforementioned various biases, well-powered clinical trials have been challenging to design and execute. The goal of this study is to create a setting which allows treatment as close to the real-life conditions as possible but under well standardised conditions. Based on previous trials, in which patient recruitment in the given setting hindered successful study completion, we decided to (1) restrict inclusion to patients with 3 or more metastases (since in case of lesser, surgery will probably be the preferred option) and (2) allow for real world standard of care treatment options before and after randomization including watchful waiting (as opposed to a predefined treatment protocol) and (3) possibility that patient can receive SOC externally (to reduce patient burden). Moreover, we chose to stipulate 12 weeks of systemic treatment prior to possible resection to further standardize treatment response and disease course over a certain period of time. Hence, included patients will be in the disease state of oligopersistence. To increase the feasibility of the trial we took several measures to minimize documentation burden: e.g. certain events are only documented in the experimental arm and radiology data on disease progression is limited to no evidence of disease and evidence of disease, which is then further differentiated into progressive and non-progressive disease. Furthermore, to adequately assess the treatment burden, we included quality of life questionnaires, evaluations regarding the application of chemotherapy, as well as nights spend in hospital. This should reflect the possible negative impact of surgery but also chemotherapy on quality of life during the course of the disease. Finally, novel biomarkers are needed for better risk stratification and identification of patients with high risk for CRC recurrence after surgical metastasectomy, outperforming conventional parameters such as CEA, number of metastases, or the disease-free interval. Therefore, in selected centres circulating DNA (ctDNA) will be analysed at various pre- and post-surgical time points as well as in patients not undergoing surgery to characterize its role as a clinically useful biomarker in patients with mCRC undergoing curative-intent pulmonary metastasectomy within the prospective Pucc trial. With further, well-standardised prospective data we hope to

provide stronger evidence for performance of PM and potentially better patient selection.

DATA AVAILABILITY STATEMENT

The original contributions presented in the study are included in the article/supplementary material. Further inquiries can be directed to the corresponding author.

ETHICS STATEMENT

The studies involving human participants were reviewed and approved by Medical Ethical Committee of Freiburg University Medical Center, No. 21-1612. The patients/participants provided their written informed consent to participate in this study.

AUTHOR CONTRIBUTIONS

Conceptualisation: SS, HB, RF, CJ and BP. Project planning: SS, HB, RF, JB, NH, CJ and BP. Writing: SS, HB, CJ. Statistical counseling: CJ. Funding acquisition: SS and RF. Editing: SS, HB, RF, JB, NH, CJ and BP. All authors provided review of the manuscript. All authors read and approved the final manuscript. All authors contributed to the article and approved the submitted version.

FUNDING

The Pucc trial is funded by the Deutsche Forschungsgemeinschaft (DFG, German Research Foundation) – project number 418151269. The trial design has been peer-reviewed and approved by the funding body.

REFERENCES

- Pfannschmidt J, Dienemann H, Hoffmann H. Surgical Resection of Pulmonary Metastases From Colorectal Cancer: A Systematic Review of Published Series. *Ann Thorac Surg* (2007) 84(1):324–38. doi: 10.1016/j.athoracsur.2007.02.093
- Okumura T, Boku N, Hishida T, Ohde Y, Sakao Y, Yoshiya K, et al. Surgical Outcome and Prognostic Stratification for Pulmonary Metastasis from Colorectal Cancer. *Ann Thorac Surg* (2017) 104(3):979–87. doi: 10.1016/j.athoracsur.2017.03.021
- Nanji S, Karim S, Tang E, Brennan K, McGuire A, Pramesh CS, et al. Pulmonary Metastasectomy for Colorectal Cancer: Predictors of Survival in Routine Surgical Practice. *Ann Thorac Surg* (2018) 105(6):1605–12. doi: 10.1016/j.athoracsur.2018.02.007
- Renaud S, Seiflinger J, Lawati Y, Guerrero F, Falcoz PE, Massard G, et al. Anatomical Resections Improve Survival Following Lung Metastasectomy of Colorectal Cancer Harboring KRAS Mutations. *Ann Surg* (2018) 270:1170–77. doi: 10.1097/SLA.0000000000002829
- Moneke I, Funcke F, Schmid S, Osei-Agyemang T, Passlick B. Pulmonary Laser-Assisted Metastasectomy is Associated With Prolonged Survival in Patients With Colorectal Cancer. *J Thorac Dis* (2019) 11(8):3241–49. doi: 10.21037/jtd.2019.08.73
- Milosevic M, Edwards J, Tsang D, Dunning J, Shackcloth M, Batchelor T, et al. Pulmonary Metastasectomy in Colorectal Cancer: Updated Analysis of 93 Randomized Patients – Control Survival is Much Better Than Previously Assumed. *Colorectal Dis* (2020) 22(10):1314–24. doi: 10.1111/codi.15113
- Franko J, Shi Q, Meyers JP, Maughan TS, Adams RA, Seymour MT, et al. Prognosis of Patients With Peritoneal Metastatic Colorectal Cancer Given Systemic Therapy: An Analysis of Individual Patient Data From Prospective Randomised Trials From the Analysis and Research in Cancers of the Digestive System (ARCAD) Database. *Lancet Oncol* (2016) 17(12):1709–19. doi: 10.1016/S1470-2045(16)30500-9
- Ruers T, Van Coevorden F, Punt CJA, Pierie JE, Borel-Rinkes I, Ledermann JA, et al. Local Treatment of Unresectable Colorectal Liver Metastases: Results of a Randomized Phase II Trial. *J Natl Cancer Inst* (2017) 109(9):1–10. doi: 10.1093/jnci/djx015

9. Gomez DR, Blumenschein GR, Lee JJ, Hernandez M, Ye R, Camidge DR, et al. Local Consolidative Therapy Versus Maintenance Therapy or Observation for Patients With Oligometastatic Non-Small-Cell Lung Cancer Without Progression After First-Line Systemic Therapy: A Multicentre, Randomised, Controlled, Phase 2 Study. *Lancet Oncol* (2016) 17(12):1672–82. doi: 10.1016/S1470-2045(16)30532-0
10. Iyengar P, Wardak Z, Gerber DE, Tumati V, Ahn C, Hughes RS, et al. Consolidative Radiotherapy for Limited Metastatic Non-Small-Cell Lung Cancer. *JAMA Oncol* (2018) 4(1):e173501. doi: 10.1001/jamaoncol.2017.3501
11. Palma DA, Olson R, Harrow S, Gaede S, Louie AV, Haasbeek C, et al. Stereotactic Ablative Radiotherapy Versus Standard of Care Palliative Treatment in Patients With Oligometastatic Cancers (SABR-COMET): A Randomised, Phase 2, Open-Label Trial. *Lancet* (2019) 393(10185):2051–8. doi: 10.1016/S0140-6736(18)32487-5
12. Åberg T, Treasure T. Analysis of Pulmonary Metastasis as an Indication for Operation: An Evidence-Based Approach. *Eur J Cardiothorac Surg* (2016) 50(5):792–8. doi: 10.1093/ejcts/ezw140
13. Kovaleva V, Geissler A-L, Lutz L, Fritsch R, Makowicz F, Wiesemann S, et al. Spatio-Temporal Mutation Profiles of Case-Matched Colorectal Carcinomas and Their Metastases Reveal Unique *De Novo* Mutations in Metachronous Lung Metastases by Targeted Next Generation Sequencing. *Mol Cancer* (2016) 15(1):63. doi: 10.1186/s12943-016-0549-8
14. Kaifi JT, Kunkel M, Das A, Harouaka RA, Dicker DT, Li G, et al. Circulating Tumor Cell Isolation During Resection of Colorectal Cancer Lung and Liver Metastases: A Prospective Trial With Different Detection Techniques. *Cancer Biol Ther* (2015) 16:699–708. doi: 10.1080/15384047.2015.1030556
15. Le U-T, Bronsert P, Picardo F, Riethdorf S, Haager B, Rylski B, et al. Intraoperative Detection of Circulating Tumor Cells in Pulmonary Venous Blood During Metastasectomy for Colorectal Lung Metastases. *Sci Rep* (2018) 8(1):8751. doi: 10.1038/s41598-018-26410-8
16. Jamal-Hanjani M, Wilson GA, McGranahan N, Birkbak NJ, Watkins TBK, Veeriah S, et al. Tracking the Evolution of Non-Small-Cell Lung Cancer. *N Engl J Med* (2017) 376(22):2109–21. doi: 10.1056/NEJMoa1616288
17. Abbosh C, Birkbak NJ, Wilson GA, Jamal-Hanjani M, Constantin T, Salari R, et al. Phylogenetic ctDNA Analysis Depicts Early-Stage Lung Cancer Evolution. *Nature* (2017) 545(7655):446–51. doi: 10.1038/nature22364
18. Steinert G, Schölch S, Niemiets T, Iwata N, García SA, Behrens B, et al. Immune Escape and Survival Mechanisms in Circulating Tumor Cells of Colorectal Cancer. *Cancer Res* (2014) 74(6):1694–704. doi: 10.1158/0008-5472.CAN-13-1885
19. Rahbari NN, Bork U, Kircher A, Nimitz T, Schölch S, Kahlert C, et al. Compartmental Differences of Circulating Tumor Cells in Colorectal Cancer. *Ann Surg Oncol* (2012) 19(7):2195–202. doi: 10.1245/s10434-011-2178-1
20. Van Cutsem E, Cervantes A, Nordlinger B, Arnold D. The ESMO Guidelines Working Group. Metastatic Colorectal Cancer: ESMO Clinical Practice Guidelines for Diagnosis, Treatment and Follow-Up. *Ann Oncol* (2014) 25(April 2002):iii1–9. doi: 10.1093/annonc/mdl260
21. Heinemann V, von Weikersthal LF, Decker T, Kiani A, Vehling-Kaiser U, Al-Batran SE, et al. FOLFIRI Plus Cetuximab Versus FOLFIRI Plus Bevacizumab as First-Line Treatment for Patients With Metastatic Colorectal Cancer (FIRE-3): A Randomised, Open-Label, Phase 3 Trial. *Lancet Oncol* (2014) 15(10):1065–75. doi: 10.1016/S1470-2045(14)70330-4
22. Hassan M, Graeter T, Dietrich I, Kemna LJ, Passlick B, Schmid S. Surgical Morbidity and Lung Function Changes After Laser-Assisted Pulmonary Metastasectomy: A Prospective Bicentric Study. *Front Surg* (2021) 8:646269. doi: 10.3389/fsurg.2021.646269
23. Treasure T, Farewell V, Macbeth F, Batchelor T, Milosevic M, King J, et al. The Pulmonary Metastasectomy in Colorectal Cancer Cohort Study: Analysis of Case Selection, Risk Factors and Survival in a Prospective Observational Study of 512 Patients. *Colorectal Dis* (2021) 23:1793–803. doi: 10.1111/codi.15651

Author Disclaimer: The funder was not involved in the development of the protocol. The funder did not influence the trial design and will not take part in data collection, analysis and interpretation or in writing the manuscript.

Conflict of Interest: The authors declare that the research was conducted in the absence of any commercial or financial relationships that could be construed as a potential conflict of interest.

Publisher's Note: All claims expressed in this article are solely those of the authors and do not necessarily represent those of their affiliated organizations, or those of the publisher, the editors and the reviewers. Any product that may be evaluated in this article, or claim that may be made by its manufacturer, is not guaranteed or endorsed by the publisher.

Copyright © 2022 Schmid, Becker, Fritsch, Bausch, Hunter, Jenkner, Hassan and Passlick. This is an open-access article distributed under the terms of the Creative Commons Attribution License (CC BY). The use, distribution or reproduction in other forums is permitted, provided the original author(s) and the copyright owner(s) are credited and that the original publication in this journal is cited, in accordance with accepted academic practice. No use, distribution or reproduction is permitted which does not comply with these terms.



Case Report: Clinicopathological Analysis of Minute Pulmonary Meningothelial-Like Nodules: Report of 7 Cases

OPEN ACCESS

Edited by:

Xiaomin Niu,
Shanghai Jiao Tong University, China

Reviewed by:

Fiori Alite,
Geisinger Commonwealth School of
Medicine, United States
Muhammad Usman Tariq,
Armed Forces Hospital Al Hada,
Saudi Arabia

*Correspondence:

Xuan Zhang
snoopykm@126.com
Guo-qing Pan
guoqing_pan@163.com

[†]These authors have contributed
equally to this work

Specialty section:

This article was submitted to
Thoracic Oncology,
a section of the journal
Frontiers in Oncology

Received: 12 May 2022

Accepted: 23 June 2022

Published: 19 July 2022

Citation:

Wang Y-x, Lei Z, Yang M,
Wang Z-y, Zhang X and
Pan G-q (2022) Case Report:
Clinicopathological Analysis of
Minute Pulmonary Meningothelial-Like
Nodules: Report of 7 Cases.
Front. Oncol. 12:942517.
doi: 10.3389/fonc.2022.942517

Ying-xia Wang^{1†}, Zi Lei^{1†}, Man Yang^{2†}, Zhi-yuan Wang¹, Xuan Zhang^{3*}
and Guo-qing Pan^{1*}

¹ Department of Pathology, The First Affiliated Hospital of Kunming Medical University, Kunming, China, ² Department of Pathology, Fuyuan County People's Hospital of Qujing City, Fuyuan, China, ³ School of Pharmaceutical Sciences and Yunnan Key Laboratory of Pharmacology for Natural Products, Kunming Medical University, Kunming, China

Objective: To investigate the clinical manifestations, radiologic features, pathological features, and immunophenotype of minute pulmonary meningothelial-like nodules (MPMNs).

Method: This is a retrospective observational study. We collected the clinical data of 7 cases of MPMNs, and performed comprehensive characterization using a combination of clinical, morphological, radiologic and immunohistochemical assessments.

Results: Of the 7 cases of MPMNs, 6 were female and 1 was male. The median age was 55 years. All MPMNs were multiple in lung with the size from 0.01 to 0.5cm. Chest CT examination showed ground-glass attenuation or solid nodules. Four cases were concomitant with carcinoma and/or pneumonia, and 3 cases occurred alone. Four of the 7 patients had no obvious symptoms; 3 patients had chest pain or cough or shortness of breath or hemoptysis. Multiple white nodules were found macroscopically, and the diseased cells grew along the alveolar septum, with relatively normal morphology, rich cytoplasm, unclear cell boundary, and uniform nucleus with delicate chromatin and without atypia; and the diseased cells showed nest or whorls distribution. EMA, PR, CD56 and vimentin were positive in all cases by immunohistochemistry.

Conclusions: MPMNs are rare benign lesions in the lung, often multiple, usually less than 0.5cm in diameter, most of which have no obvious clinical symptoms. MPMNs are often found by chest CT, and occur independently or concomitant with other lesions. The positive immunohistochemical staining of EMA, PR, CD56, vimentin supports the diagnosis.

Keywords: minute pulmonary meningothelial-like nodules, benign lesions, pathological features, immunophenotype, radiographic manifestations

HIGHLIGHTS

- Minute pulmonary meningothelial-like nodules (MPMNs) are rare benign lesions in the lung that most often occur in middle-aged and elderly women.
- Chest CT examination shows ground-glass attenuation or solid nodules.
- The morphology of diseased cells shows characteristics of meningothelial cells.
- Positive immunohistochemistry for EMA, PR, CD56, and vimentin supports the diagnosis of MPMNs.

INTRODUCTION

Minute pulmonary meningothelial-like nodules (MPMNs) are rare, small benign lesions in the lungs that are usually found incidentally in surgical specimens and in routine pathology examinations of autopsy specimens (1, 2). Korn et al. first reported this disease in 1960 (3). The occurrence of MPMNs is associated with many diseases, such as pulmonary thromboembolism, interstitial lung disease, and lung adenocarcinoma; they are sometimes found as concomitant diseases of the main disease of the lung (prevalent in lung cancer cases) or can occur alone (4–6).

MPMNs are usually asymptomatic and are not easily detected clinically. The early diagnosis rate of MPMNs has improved with the popularization of chest thin-section computed tomography (CT) in lung cancer screening (7). The CT presentation of MPMNs is multiple micronodules, usually less than 0.5 cm in diameter, with ground glass-like changes (8). It is difficult to distinguish MPMNs from lung carcinoma *in situ* or microinvasive adenocarcinoma on imaging; thus, intraoperative or postoperative pathological examination and immunophenotypic identification are required to confirm the diagnosis. MPMNs are reactive proliferative lesions of pulmonary meningeal epithelial cells, and their morphologic structure and immunohistochemical examination show that they are similar to meningiomas, with the morphologic features and immunotype of meningeal epithelial cells (9).

As a rare disease, MPMNs have been reported in relatively few studies, with a few reports in out of China and rare reports in China. Therefore, MPMNs are poorly understood by clinicians, radiologists, and pathologists. In this paper, we report 7 cases of MPMNs and review the relevant literature to discuss the clinical manifestations, imaging features, pathological characteristics, and immunophenotypes of MPMNs and summarize their diagnostic points in order to improve physicians' understanding of this disease.

MATERIALS AND METHODS

General Information

The clinical data of 7 patients with MPMNs confirmed by the pathology department of our hospital from December 2020 to

April 2021 were collected, among which 3 cases occurred in the lower lobe of the left lung, 3 cases occurred in the lower lobe of the right lung, and 1 case occurred in the upper lobe of the left lung. Multiple nodules with ground glass density were found by CT through Artificial Intelligence(AI) scanning and confirmation of experienced radiologists, and couldn't be differentiated with carcinoma. The nodules were removed by thoracoscopic surgery for frozen section diagnosis to determine the scope of surgery, and postoperative paraffin sections and immunohistochemical staining were performed for further typing.

Intraoperative Frozen Pathological Examination

The tissues collected by thoracoscopy were immediately cut to look for the nodules. The lesioned nodules were cut into 1.5x1.5x0.2-cm tissue blocks, treated with a frozen embedding agent, placed in a -20°C frozen sectioning machine. After embedding, the tissues were cut into 5-μm slices, fixed in alcoholic ether for 1 min, and then subjected to hematoxylin and eosin (HE) staining.

Paraffin Pathological Section Examination

After the frozen sections were cut, the remaining tissue blocks were first fixed in neutral formaldehyde for 6-8 h, put into a dehydrator for overnight dehydration, taken out and embedded into wax blocks using an embedding machine, then cut into 4-μm thin slices. The slices were baked for 30 min, then dewaxed, de-benzene, washed, stained with hematoxylin, restained with blue, stained with eosin, washed, dehydrated, made transparent, and sealed, and their morphological characteristics were observed under optical microscopy.

Immunohistochemical Staining

The En-Vision 2-step method was used: they were repaired under high pressure, primary and secondary antibodies were added, submitted to color development with diaminobenzidine (DAB), and submitted to hematoxylin staining of cell nuclei, and then underwent dehydration, transparency, and sealing.

RESULTS

Clinical and Imaging Features

The clinical and imaging data of the 7 cases of MPMNs in this study are shown in **Table 1**. Age-sex distribution: 6 patients were female (31-56 years old, mean 49.5 years old) and 1 case was an elderly male. Number, diameter and location of nodules: all had multiple microscopic nodules <0.5 mm in diameter; 6 patients had nodules in the lower lobe of the lung, and 1 had nodules in the upper lobe. Concomitant lesions: 3 patients had no concomitant lesions, 2 patients had invasive adenocarcinoma of the lung (one of them also had a bronchial adenoma), 1 had nonkeratinizing squamous cell carcinoma and organizing pneumonia, and 1 had organizing pneumonia and atypical adenomatous nodules. Clinical symptoms: 4 patients had no clinical symptoms, and the pulmonary nodules were found

during physical examination; 1 patient had chest pain with radiating pain in the right shoulder; 1 patient had cough with a small amount of yellow sputum; and 1 patient had recurrent cough and shortness of breath with hemoptysis. Imaging manifestations: multiple micronodules, mostly ground glass density nodules, were seen on chest CT (**Figure 1**).

Pathomorphological Features

Macroscopic Features

Multiple grayish-white solid nodules with medium hardness, irregular morphology and well demarcated borders, 0.1-0.5 cm in diameter, were seen in the specimens of all 7 cases.

Intraoperative Frozen Section

Microscopic Features

Widened alveolar septum, visible hyperplastic epithelioid cells growing along the alveolar septum with round or ovoid cells that were uniform in size, arranged in a complex layer, and without heterogeneity. It was difficult to distinguish from atypical adenomatous hyperplasia in frozen sections. Only 1 case was diagnosed as a benign lesion, and the typing was pending postoperative paraffin section results, while the other 6 cases were all diagnosed as atypical alveolar epithelial hyperplasia pending postoperative paraffin section results (**Figure 2**).

Postoperative Paraffin Section Microscopic Features

Microscopically, the lesion was still clearly demarcated from the surrounding lung tissue, without a capsule; the alveolar septa were widened, the lesion cells grew along the alveolar septum, the air cavity was open, and some of the lesion cells grew around blood vessels. The lesion cells were round or ovoid and uniform in size. The cell morphology was relatively normal, without

atypia. The cytoplasm was abundant, and the cell boundary was unclear. The nucleus was light stained, and delicate chromatin was evenly distributed (**Figure 3**).

Immunophenotypic Characteristics

Of the 7 MPMNs, 7 were positive for PR, EMA, CD56 and vimentin, with 100% positivity; and 7 were negative for Syn, Chromogranin-A, TTF-1, NapsinA, Pan-CK, and CD68, with 100% negativity; the Ki-67 index was < 3% in all cases, with the range from less than 1% to less than 3%, as shown in **Figure 4**.

DISCUSSION

MPMNs are benign meningeal epithelial-like proliferative lesions occurring in the interstitial lung stroma and are most common in women over 60 years of age; they are often accompanied by other diseases, including lung cancer, chronic lung disease, congestive heart failure, and thromboembolic disease (1, 2, 10–12). Among the 7 patients with MPMNs in this study, there were 6 female patients with an average age of 49.5 and 1 elderly male patient, indicating that MPMNs tend to occur in women and the age of onset tends to be younger, which may be due to the increasing use of chest CT lung cancer screening in routine physical examinations, which has increased the early diagnosis rate of MPMNs. Among the 7 MPMN patients, 3 had no concomitant lesions, 2 had concomitant invasive lung adenocarcinoma (one with accompanying bronchial adenoma), 1 also had nonkeratinizing squamous cell carcinoma and organizing pneumonia, and 1 also had organizing pneumonia and atypical adenomatous nodules. These results suggested that MPMNs can occur either alone or

TABLE 1 | Clinical and Imaging data of 7 MPMN Cases.

Case number	Age (years)	Sex	Location	Number and diameter of nodules	Associated lesions	Symptoms	Radiographic manifestations
1	30-35	Female	Lower lobe of the left lung	Multiple, 0.1 cm	Microinvasive adenocarcinoma of the lung, bronchial adenoma	Asymptomatic; pulmonary nodules found on physical examination	Multiple ground glass nodules with slightly blurred borders
2	40-45	Female	Upper lobe of the left lung	Multiple, 0.1 cm	Multiple invasive lung adenocarcinoma	Asymptomatic; pulmonary nodules found on physical examination	Multiple masses in the left lung and multiple microscopic nodules in both lungs
3	50-55	Female	Lower lobe of the right lung	Multiple, 0.3-0.5 cm in diameter	None	Asymptomatic; pulmonary nodules found on physical examination	Multiple ground glass density micro-nodules in both lungs
4	50-55	Female	Lower lobe of the left lung	Multiple, 0.01-0.05 cm in diameter	None	Asymptomatic; pulmonary nodules found on physical examination	Multiple microscopic nodules in both lungs, some of which were ground glass nodules
5	50-55	Female	Lower lobe of the right lung	Multiple, 0.4-0.5 cm in diameter	None	Chest pain radiating to the right shoulder	Multiple microscopic nodules in both lungs
6	56-60	Female	Lower lobe of the right lung	Multiple, 0.1-0.4 cm in diameter	Organizing pneumonia, atypical adenomatous nodules	Cough with a small amount of yellow sputum	Nodular foci in the dorsal segment of the right lower lobe with multiple micronodules in both lungs
7	66-70	Male	Lower lobe of the left lung	Multiple, 0.1 cm in diameter	Nonkeratinizing squamous cell carcinoma, organizing pneumonia	Recurrent cough, shortness of breath, hemoptysis	Mass in the hilar region of the lower lobe of the left lung with multiple small nodules in both lungs

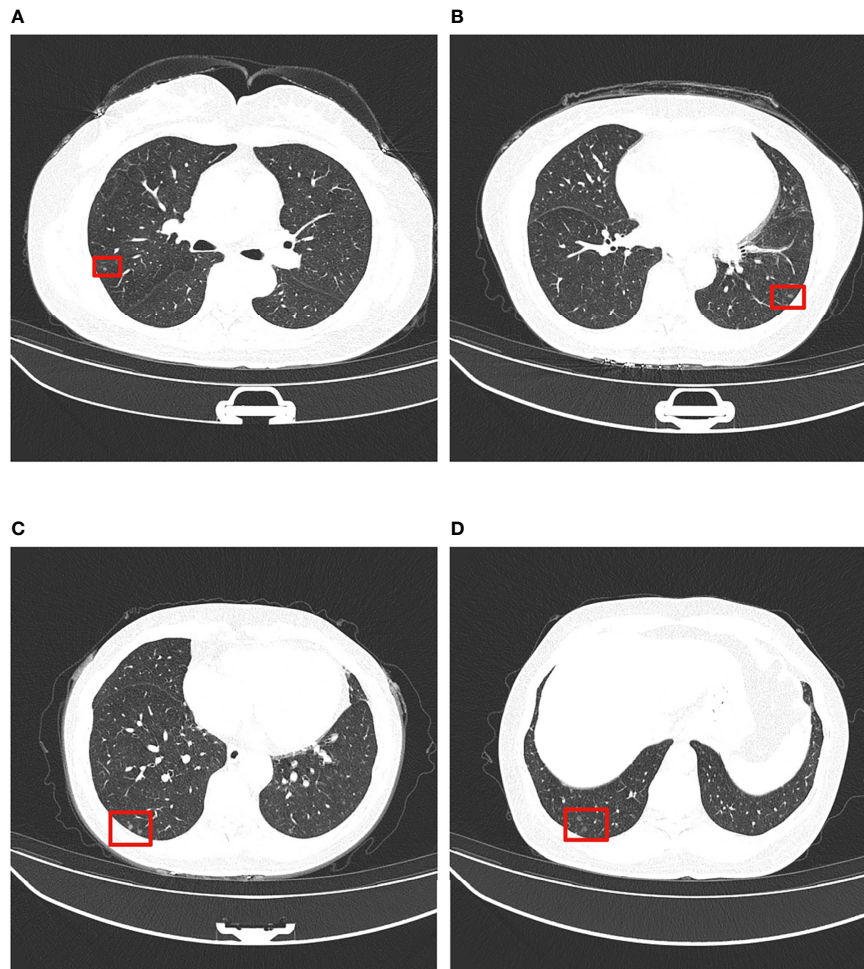


FIGURE 1 | Typical thin-section CT presentation of MPMNs. Multiple ground glass density shadows in the middle and lower lobes of the left and right lungs (shown in red boxes), 0.2-0.4 cm in diameter, with irregular shadows and slightly blurred boundary. (A-D) show ground glass density nodules in left and right lungs at different CT sections.

concomitant with other lesions, including malignant or benign tumors and inflammatory lesions.

Patients with MPMNs usually have no obvious clinical symptoms, and the nodules are only detected on chest CT examination or accidentally at visits for symptoms associated with other lung diseases. In the present study, multiple pulmonary nodules were found in specimens of all 7 patients on chest CT examination through Artificial Intelligence(AI) scanning and confirmation of experienced radiologists. Of the 7 patients with MPMNs, 4 had no obvious clinical symptoms, 1 had chest pain radiating to the right shoulder; 1 had cough with a small amount of yellow sputum; and 1 case had recurrent cough with shortness of breath and hemoptysis. The true incidence of MPMNs may be underestimated due to the insidious nature of their clinical symptoms. Clinicians, radiologists, and pathologists should increase their awareness of and concern about MPMNs.

The typical CT presentation of MPMNs is multiple microscopic nodules ranging from 0.2-0.5 cm in diameter with

ground glass-like changes (8, 13); a small number of MPMNs also present with diffuse thin-walled cystic cavities on CT (14, 15). All 7 patients with MPMNs in this study presented with multiple microscopic nodules visible on chest CT with diameters in the range from 0.01-0.5 cm; most of the nodules were ground glass density nodules, and no diffuse thin-walled cystic cavities were found, consistent with the typical CT presentation of MPMNs. However, the CT presentation of MPMNs is similar to that of malignant pulmonary nodules, and it is difficult to distinguish MPMNs from malignant pulmonary nodules based only on the imaging presentation, making it prone to misdiagnosis (16). Therefore, the diagnosis of MPMNs needs to be confirmed by pathomorphological examination of surgical biopsy tissue.

MPMNs need to be differentiated from meningiomas, bronchial adenomas and adenocarcinomas *in situ* in terms of pathomorphology. MPMNs are typically characterized by proliferative lung mesenchymal cells with clear borders, usually

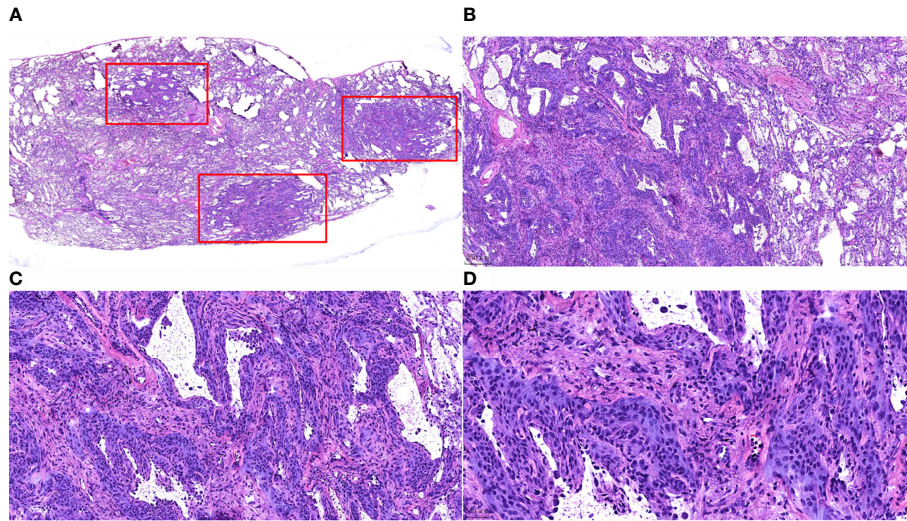


FIGURE 2 | Morphological characteristics of intraoperative frozen sections of MPMNs. **(A)** Frozen section HE staining x7.2. Three nodules (shown in the red box) with irregular morphology and clear borders are visible in the lung tissue. **(B)** x40 shows 1 of the nodules growing around the blood vessels. **(C)** Frozen section, HE staining, x100. The lesion cells are growing along the alveolar septum, with an open air cavity and the proliferation of interstitial fibrous tissue. **(D)** Frozen section, HE staining, x200. Well-differentiated cells were observed without atypia, with a smooth nuclear membrane, a low nucleo-cytoplasmic ratio and no pathological nuclear division.

without an envelope, and homogeneous round or ovoid swirling arrangements of cells that can grow along the alveolar septa or around blood vessels; these cells are without obvious atypia and resemble meningeal epithelial cells, with fine chromatin, inconspicuous nucleoli, and rare mitotic figures (1, 13, 14, 16–18). Meningiomas usually form encapsulated masses with solid,

nested clusters of tumor cells, usually without alveolar lumen and residual alveolar epithelial cells. Bronchial adenomas are bilayered structures formed by epithelial cells and continuously arranged basal cells: the epithelial layer is structurally diverse and can be papillary or glandular luminal cells; the cell morphology may be consistent with mucous cells, alveolar epithelial cells, or

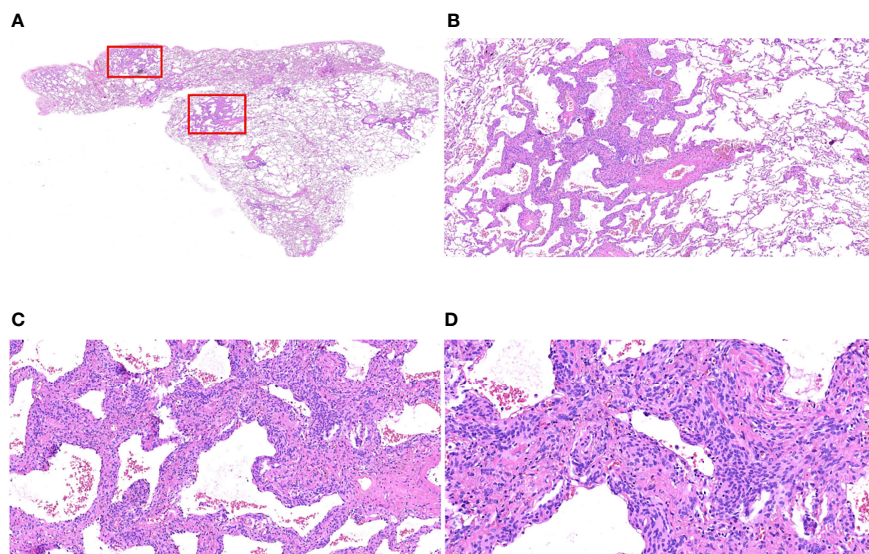


FIGURE 3 | Morphological characteristics of postoperative paraffin sections of MPMNs. **(A)** Paraffin section HE x7.2 with an open alveolar cavity, uniform distribution of fine bronchi, several areas of widened alveolar septa and dense cells (shown in the red box) still clearly demarcated from the surrounding lung tissue, without an envelope. **(B)** x40 HE shows widened alveolar septa, lesion cells growing along the alveolar septa and an open air cavity. **(C)** HE x100 lesion cells partially growing around the blood vessels. **(D)** HE x200 shows that the lesion cells are round or ovoid, with relatively normal morphology, abundant cytoplasm, unclear cell demarcation, light stained nuclei with delicate chromatin and without atypia.

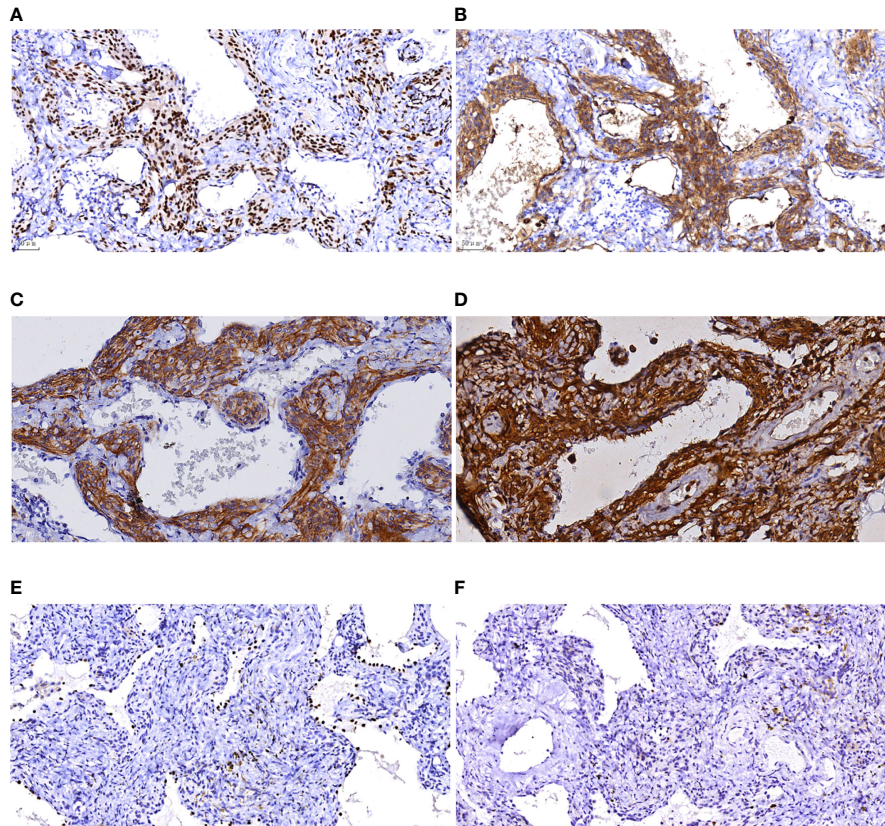


FIGURE 4 | Immunohistochemical results of MPMNs. **(A)** x200 The cells were nuclear positive for PR; **(B)** x200 The cells were cytoplasmic positive for EMA; **(C)** x200 The cells were cytoplasmic positive for CD56; **(D)** x200 The cells were both nuclear and cytoplasmic positive for vimentin; **(E)** x200 Normal type II alveolar epithelial cells were positive and meningeal epithelial-like cells were negative for TTF-1; **(F)** x200 The number of Ki-67 positive cells was <1%.

ciliated columnar epithelial cells without atypia, and exfoliated tumor cells may float in the mucus in the alveolar lumen. Adenocarcinoma *in situ* is usually a monolayer arrangement with no basal cells, atypia of the cells, variable sizes of nuclei, and visible mitotic figures.

In the present study, multiple grayish-white solid nodules with medium hardness, irregular morphology and well demarcated borders, 0.1-0.5 cm in diameter, were found macroscopically in the specimens of all 7 cases. Microscopically, the lesion was still clearly demarcated from the surrounding lung tissue, without an capsule; the alveolar septa were widened, the lesion cells grew along the alveolar septum, the air cavity was open, and some of the lesion cells grew around blood vessels. The lesion cells were round or ovoid and uniform in size. The cell morphology was relatively normal, without atypia. The cytoplasm was abundant, and the cell boundary was unclear. The nucleus was light stained, and delicate chromatin was evenly distributed. All pathological findings mentioned above were consistent with the typical pathological morphological features of MPMNs.

Immunohistochemical detection of specific cellular markers can clarify the cellular immunophenotypic characteristics and determine the cellular origin. In this study, the immunohistochemical results revealed that PR, EMA, CD56, and vimentin were all positively

expressed and Chromogranin-A, TTF-1, Napsin A, and CD68 were negative in 7 cases of MPMNs; additionally, the Ki-67 index was <3%, suggesting that the proliferating cells were consistent with the phenotypic characteristics of meningeal epithelial cells, which is consistent with literature reports (7, 16, 19). As a result of the combination of microscopic pathomorphological features and immunophenotypic characteristics, the diagnosis of MPMNs was confirmed in all 7 cases.

All 7 patients of this study were followed up for 13 to 17 months. All patients received chest CT examination once every six months during follow-up period and no nodules were found. Six patients recovered well without symptoms or adverse events after removal of nodules by thoracoscopic surgery, suggesting that the prognosis of MPMNs is good. Pleural effusion and abdominal pain occurred in only 1 patient combined with multiple invasive lung adenocarcinoma, however, both chest CT and abdominal ultrasonography showed no nodules or mass.

CONCLUSION

In summary, minute pulmonary meningothelial-like nodules (MPMNs) are rare benign lesions in the lung that most often

occur in middle-aged and elderly women. They are often multiple, usually less than 0.5 cm in diameter, most often do not have obvious clinical symptoms, are often detected by chest CT, and can occur alone or concomitant with other lung lesions. Positive immunohistochemistry for EMA, PR, CD56, and vimentin supports the diagnosis. Clinicians, radiologists, and pathologists should increase their attention to and awareness of this disease. Our report will provide references for diagnosis of MPMNs.

STRENGTHS AND LIMITATIONS OF THIS STUDY

This is a rare case series, MPMNs have been reported in relatively few studies, with a few reports out of China and rare reports in China.

This study performed comprehensive characterization of MPMNs using a combination of clinical, morphological, radiologic and immunohistochemical assessments.

There were only 7 cases in this study and the results were not checked using statistical tools.

DATA AVAILABILITY STATEMENT

The original contributions presented in the study are included in the article. Further inquiries can be directed to the corresponding authors.

REFERENCES

- Mizutani E, Tsuta K, Maeshima AM, Asamura H, Matsuno Y. Minute Pulmonary Meningothelial-Like Nodules: Clinicopathologic Analysis of 121 Patients. *Hum Pathol* (2009) 40(5):678–82. doi: 10.1016/j.humpath.2008.08.018
- Asakawa A, Horio H, Hishima T, Yamamichi T, Okui M, Harada M. Clinicopathologic Features of Minute Pulmonary Meningothelial-Like Nodules. *Asian Cardiovasc Thorac Ann* (2017) 25(7-8):509–12. doi: 10.1177/0218492317731390
- Korn D, Bensch K, Liebow AA, Castleman B. Multiple Minute Pulmonary Tumors Resembling Chemodectomas. *Am J Pathol* (1960) 37(6):641–72.
- Churg AM, Warnock ML. So-Called "Minute Pulmonary Chemodectoma": A Tumor Not Related to Paragangliomas. *Cancer* (1976) 37:1759–69. doi: 10.1002/1097-0142(197604)37:4<1759::aid-cnrcr2820370422>3.0.co;2-3
- Gaffey MJ, Mills SE, Askin FB. Minute Pulmonary Meningothelial-Like Nodules: A Clinicopathologic Study of So-Called Minute Pulmonary Chemodectoma. *Am J Surg Pathol* (1988) 12:167–75. doi: 10.1097/0000478-198803000-00001
- Spain DM. Intrapulmonary Chemodectomas in Subjects With Organizing Pulmonary Thromboemboli. *Am Rev Respir Dis* (1967) 96:1158–64. doi: 10.1164/arrd.1967.96.6.1158
- Lin D, Yu Y, Wang H, Fang Y, Yin J, Shen Y, et al. Radiological Manifestations, Histological Features and Surgical Outcomes of Pulmonary Meningothelial Proliferation: A Case Series and Rethinking. *Transl Lung Cancer Res* (2020) 9(4):1159–68. doi: 10.21037/tlcr-19-699
- Sellami D, Gotway MB, Hanks DK, Webb WR. Minute Pulmonary Meningothelial-Like Nodules: Thin-Section CT Appearance. *J Comput Assist Tomogr* (2001) 25(2):311–3. doi: 10.1097/00004728-200103000-00028
- Ionescu DN, Sasatomi E, Aldeeb D, Omalu BI, Finkelstein SD, Swalsky PA, et al. Pulmonary Meningothelial-Like Nodules: A Genotypic Comparison With Meningiomas. *Am J Surg Pathol* (2004) 28(2):207–14. doi: 10.1097/0000478-200402000-00008
- Mukhopadhyay S, El-Zammar OA, Katzenstein AL. Pulmonary Meningothelial-Like Nodules: New Insights Into a Common But Poorly Understood Entity. *Am J Surg Pathol* (2009) 33:487–95. doi: 10.1097/PAS.0b013e31818b1de7
- Suster S, Moran CA. Diffuse Pulmonary Meningotheliomatosis. *Am J Surg Pathol* (2007) 31(4):624–31. doi: 10.1097/01.pas.0000213385.25042.cf
- Gleason JB, Valentin R, Almedia P, Martinez N, Bejarano PA. Diffuse Pulmonary Meningotheliomatosis: A Literature Review of a Rare Diffuse Parenchymal Lung Disease With Unclear Clinical Significance. *J Assoc Chest Physicians* (2017) 5:18–25. doi: 10.4103/2320-8775.196647
- Lee SK, Kim GJ, Kim YJ, Leem AY, Hwang ED, Kim SK, et al. Minute Pulmonary Meningothelial-Like Nodules Simulating Hematogenous Lung Metastasis: A Case Report. *Tuberc Respir Dis (Seoul)* (2013) 75(2):67–70. doi: 10.4046/trd.2013.75.2.67
- Harada M, Aono Y, Yasui H, Uto T, Sato J, Imokawa S, et al. Minute Pulmonary Meningothelial-Like Nodules Showing Multiple Ring-Shaped Opacities. *Intern Med* (2019) 58(21):3149–52. doi: 10.2169/internalmedicine.2108-18
- Kraushaar G, Ajlan AM, English JC, Müller NL. Minute Pulmonary Meningothelial-Like Nodules: A Case of Incidentally Detected Diffuse Cystic Micronodules on Thin-Section Computed Tomography. *J Comput Assist Tomogr* (2010) 34(5):780–2. doi: 10.1097/RCT.0b013e3181e47c28
- Peng XX, Yan LX, Liu C, Wang SY, Li WF, Gao X, et al. Benign Disease Prone to be Misdiagnosed as Malignant Pulmonary Nodules: Minute Meningothelioid Nodules. *Thorac Cancer* (2019) 10(5):1182–7. doi: 10.1111/1759-7714.13061
- Kamiya K, Yoshizu A, Kashizaki F, Hida N, Hayashi H. Minute Pulmonary Meningothelial-Like Nodules Coexisting With Pulmonary Cryptococcosis Mimicking Lung Cancer. *Gen Thorac Cardiovasc Surg* (2013) 61(11):659–62. doi: 10.1007/s11748-012-0169-1

ETHICS STATEMENT

The studies involving human participants were reviewed and approved by Ethical Review Board of the First Affiliated Hospital of Kunming Medical University. The patients/participants provided their written informed consent to participate in this study. Written informed consent was obtained from the participant for the publication of this case report.

AUTHOR CONTRIBUTIONS

Y-xW, ZL and MY have contributed equally to this work and share first authorship. Y-xW collected data, wrote the manuscript. ZL designed the project, analyzed the data and revised the paper. MY Collected and analyzed the data. XZ and G-qP designed the project and revised the paper. Z-yW assisted in case collection and analyzed the data. All authors contributed to the article and approved the submitted version.

FUNDING

This study was supported by grants from the National Natural Science Foundation of China (No. 81660431), the Joint Projects of Applied Basic Research of Kunming Medical University and Yunnan Provincial Department of science and Technology(No. 2019FE001-220), the Science Project of Yunnan Provincial Department of Education (No. 2018JS202).

18. Kuroki M, Nakata H, Masuda T, Hashiguchi N, Tamura S, Nabeshima K, et al. Minute Pulmonary Meningothelial-Like Nodules: High-Resolution Computed Tomography and Pathologic Correlations. *J Thorac Imaging* (2002) 17(3):227–9. doi: 10.1097/00005382-200207000-00008
19. Niho S, Yokose T, Nishiwaki Y, Mukai K. Immunohistochemical and Clonal Analysis of Minute Pulmonary Meningothelial-Like Nodules. *Hum Pathol* (1999) 30(4):425–9. doi: 10.1016/s0046-8177(99)90118-1

Conflict of Interest: The authors declare that the research was conducted in the absence of any commercial or financial relationships that could be construed as a potential conflict of interest.

Publisher's Note: All claims expressed in this article are solely those of the authors and do not necessarily represent those of their affiliated organizations, or those of the publisher, the editors and the reviewers. Any product that may be evaluated in this article, or claim that may be made by its manufacturer, is not guaranteed or endorsed by the publisher.

Copyright © 2022 Wang, Lei, Yang, Wang, Zhang and Pan. This is an open-access article distributed under the terms of the Creative Commons Attribution License (CC BY). The use, distribution or reproduction in other forums is permitted, provided the original author(s) and the copyright owner(s) are credited and that the original publication in this journal is cited, in accordance with accepted academic practice. No use, distribution or reproduction is permitted which does not comply with these terms.



OPEN ACCESS

EDITED BY

Alberto Sandri,
San Luigi Gonzaga Hospital, Italy

REVIEWED BY

Hang Su,
Tongji University, China
Qingyuan Huang,
Fudan University, China

*CORRESPONDENCE

Mingran Xie
xmr1981@ustc.edu.cn
Tian Li
ahslyxwkl@163.com

[†]These authors have contributed
equally to this work and share
first authorship

SPECIALTY SECTION

This article was submitted to
Thoracic Oncology,
a section of the journal
Frontiers in Oncology

RECEIVED 27 May 2022

ACCEPTED 18 July 2022

PUBLISHED 10 August 2022

CITATION

Xu L, Zhou H, Wang G, Huang Z,
Xiong R, Sun X, Wu M, Li T and Xie M
(2022) The prognostic influence of
histological subtypes of micropapillary
tumors on patients with lung
adenocarcinoma ≤ 2 cm.
Front. Oncol. 12:954317.
doi: 10.3389/fonc.2022.954317

COPYRIGHT

© 2022 Xu, Zhou, Wang, Huang, Xiong,
Sun, Wu, Li and Xie. This is an open-
access article distributed under the
terms of the [Creative Commons
Attribution License \(CC BY\)](#). The use,
distribution or reproduction in other
forums is permitted, provided the
original author(s) and the copyright
owner(s) are credited and that the
original publication in this journal is
cited, in accordance with accepted
academic practice. No use,
distribution or reproduction is
permitted which does not comply with
these terms.

The prognostic influence of histological subtypes of micropapillary tumors on patients with lung adenocarcinoma ≤ 2 cm

Liangdong Xu^{1,2†}, Hangcheng Zhou^{3†}, Gaoxiang Wang^{1,2},
Zhining Huang^{1,2}, Ran Xiong², Xiaohui Sun², Mingsheng Wu²,
Tian Li^{2*} and Mingran Xie^{1,2*}

¹Department of Thoracic Surgery, Affiliated Provincial Hospital of Anhui Medical University, Hefei, China, ²Department of Thoracic Surgery, The First Affiliated Hospital of University of Science and Technology of China (USTC), Division of Life Sciences and Medicine, University of Science and Technology of China, Hefei, China, ³Department of Pathology, The First Affiliated Hospital of University of Science and Technology of China (USTC), Division of Life Sciences and Medicine, University of Science and Technology of China, Hefei, China

Objective: This study aimed to explore the value of micropapillary histological subtypes in predicting the specific surgical specificity and lymph node metastasis prognosis of early lung adenocarcinoma.

Methods: A total of 390 patients with lung adenocarcinoma were included who underwent surgery in the Department of Thoracic Surgery of the Affiliated Provincial Hospital of Anhui Medical University from January 2016 to December 2017. The data were analysed with SPSS 26.0 statistical software, and the clinicopathological data of the two groups were compared with the chi-square test. The survival rate was calculated by the Kaplan-Meier method, and the difference in survival rate between groups was analysed by the log-rank test. Multivariate survival analysis was performed using the Cox model.

Results: Univariate analysis of the clinicopathological data of the patients showed that the micropapillary histological subtype was significantly associated with the survival rate of patients ($p=0.007$). The clinicopathological data of the patients were substituted into the Cox model for multivariate analysis, and the results showed that the micropapillary histological subtype was an independent prognostic factor affecting the survival rate of the patients ($p=0.009$). The average survival time of Group A (micronipple composition $> 5\%$) was 66.7 months; the 1-year, 3-year, and 5-year survival rates were 98.8%, 93.0%, and 80.9%, respectively. The survival of the lobectomy group was better than that of the sublobectomy group and the survival of patients with systematic dissection was better than that of patients with limited lymph node dissection. The average survival time of Group B (micronipple composition $\leq 5\%$) was 70.5 months; the 1-year, 3-year, and 5-year survival rates were 99.3%, 95.4%, and 90.6%, respectively. There was no

difference in the survival rate between the lobectomy group and sublobectomy group, and there was also no difference in survival between systematic lymph node dissection and limited lymph node dissection, The survival rate of Group B was significantly better than that of Group A.

Conclusion: The micropapillary histological component is an independent risk factor after surgery in patients with ≤ 2 cm lung adenocarcinoma. When the proportion of micropapillary components is different, the prognosis of patients is different when different surgical methods and lymph node dissections are performed. Lobectomy and systematic lymph node dissection are recommended for patients with a micropapillary histological composition $>5\%$; sublobar resection and limited lymph node dissection are recommended for patients with a micropapillary histological composition $\leq 5\%$.

KEYWORDS

non-small cell lung cancer, micropapillary component, sublobar resection, prognosis, survival

Introduction

At present, lung cancer is the malignant tumor with the highest mortality rate in the world, of which non-small-cell lung cancer (NSCLC) accounts for 80%-85%, with the most common histological type being adenocarcinoma (1, 2). With the development of imaging technology and the widespread use of low-dose spiral CT, an increasing number of small pulmonary nodules (≤ 2 cm) are found and confirmed as early lung adenocarcinoma by postoperative pathology (3, 4). For resectable non-small-cell lung cancer, lobectomy and mediastinal lymph node dissection are still the main comprehensive treatments (5, 6). According to the new classification proposed by the International Association for Lung Cancer Research (IASLC), the American Thoracic Society (ATS) and the European Respiratory Society (ERS), lung adenocarcinoma can be divided into five histological subtypes. Studies have shown that lung adenocarcinoma dominated by acinar type shows a good prognosis, while micropapillary-based lung adenocarcinoma is associated with poor prognosis (7–9). Whether patients with micropapillary histological subtypes of lung adenocarcinoma can benefit from sublobectomy has not been studied, and the relationship between micropapillary components and lymph node metastasis is unclear. In this study, we aimed to explore the value of micropapillary histological subtypes in predicting the specific surgical specificity and lymph node metastasis prognosis of early lung adenocarcinoma and to select the best surgical scheme for optimal individualized treatment and prognosis stratification.

Methods

Patient selection

This study retrospectively analysed 1403 patients with NSCLC who underwent surgery in the Department of Thoracic Surgery of the Affiliated Provincial Hospital of Anhui Medical University from January 2016 to December 2017. Inclusion criteria were: 1) patients with primary lung adenocarcinoma confirmed by postoperative pathology; 2) tumor size ≤ 2 cm; 3) postoperative pathological stage was pT1-2N0M0; and 4) R0 resection. Exclusion criteria were: 1) received neoadjuvant therapy; 2) patients with multiple nodules; 3) incomplete medical records. Based on the above criteria, a total of 390 patients with lung adenocarcinoma were included in this study.

This study was approved by the Ethics Committee of the Provincial Hospital affiliated with Anhui Medical University.

Research content

The study involves a comparative analysis of general clinicopathological data of patients and the relationship between micropapillary histological subtype components and survival rate.

We compared the effects of different surgical and lymph node dissection methods on the survival rate of patients with different micropapillary histological subtypes.

Surgery and lymph node dissection

The surgical methods include lobectomy and sublobectomy, and sublobectomy also includes wedge resection and segmentectomy.

The indications of sublobectomy are determined by the general physical state of the patient and CT findings. Sublobectomy was performed for peripheral lesions located outside the parenchyma of the lung or for CT shadows dominated by ground glass nodules. Sublobectomy was performed in patients with poor cardiopulmonary function, combined with basic cardiopulmonary diseases, or who were too old to tolerate lobectomy, regardless of tumor size or presence of solid components on CT. Wedge resection or segmentectomy depends on the tumor location and surgical skill of the surgeon.

According to the recommendation from the National Comprehensive Cancer Network, systematic lymph node dissection included 6 groups of lymph nodes, of which 3 groups were intrapulmonary and hilar, and 3 groups included mediastinal lymph nodes (10). Systemic hilar and mediastinal lymph node dissection routinely explores and dissects the 2R, 3A, 3P, 4R, 7-10 groups of lymph nodes and intrapulmonary lymph nodes on the right side and routinely explores and dissects the 4L, 5-10 group lymph nodes and intrapulmonary lymph nodes on the left side. Limited lymph node dissection includes regional lymph node dissection, lymph node sampling dissection or no lymph node dissection. Limited lymph node dissection will be performed according to the tumor size, intraoperative pathology and overall physical status of the patient.

Histological evaluation

The pathological staging was based on the IASLC TNM staging system (8th edition) (11). The pathological sections of all patients were blind reviewed and reclassified by two senior clinical pathologists in our hospital. When there were differences in the diagnosis between the two physicians, they were re-examined and classified by another clinical pathologist.

According to the IASLC/ATS/ERS classification system of lung adenocarcinoma, lung adenocarcinoma can be divided into five subtypes: lepidic, acinar, papillary, micropapillary and solid. The percentage of each tissue subtype was recorded in increments of 5%. If micropapillary components accounted for 5% of the tumor, one subtype was considered to exist. The pattern with the largest proportion was defined as the histologically dominant pattern. In this study, micropapillary composition > 5% was defined as Group A, and micropapillary composition ≤ 5% was defined as Group B.

Postoperative follow-up

Follow-up was carried out in two ways: outpatient regular follow-up and telephone follow-up. The patients were followed

up with every 4 months for years 1-2, every half-year for years 3-5, and once a year from the 6th year. The relevant clinical information (including chest and brain CT, bone scan, abdominal and adrenal ultrasound, etc.) and the survival of the patients were obtained.

Overall survival was defined as the time from surgery to death from any cause. The end point of follow-up was March 2022.

Statistical analysis

The data were analysed with SPSS 26.0 statistical software, and the clinicopathological data of the two groups were compared with the chi-square test. The survival rate was calculated by the Kaplan–Meier method, and the difference in survival rate between groups was analysed by the log-rank test. Multivariate survival analysis was performed using the Cox model. $P < 0.05$ indicates that the difference is statistically significant.

Results

Patient characteristics

The clinicopathological data of 390 patients with ≤ 2 cm lung adenocarcinoma who underwent lung surgery were included in this study, including 86 patients in Group A and 304 patients in Group B. There were 14 patients with the predominant subtype of micropapillary in Group A, while those in Group B were not predominantly micropapillary. The proportion of the micropapillary dominant subtype in Group A was higher than that in Group B, and there was statistical significance in the main pathological subtypes ($p < 0.001$). There was no statistical significance in sex, age, smoking history, preoperative comorbidities, tumor location, maximum tumor diameter, visceral pleural invasion, surgical method, or lymph node dissection method ($p > 0.05$). (Table 1).

Univariate and multivariate analysis of patient prognosis

Univariate analysis of the clinicopathological data of the patients showed that the micropapillary histological subtype was significantly associated with the survival rate of patients ($p = 0.007$) (Table 2). The clinicopathological data of the patients were substituted into the Cox model for multivariate analysis, and the results showed that the micropapillary histological subtype was an independent prognostic factor affecting the survival rate of the patients ($p = 0.009$) (Table 2).

TABLE 1 Baseline characteristics of the study population.

	Group A (n = 86)	Group B (n = 304)	χ^2	P Value
Sex			0.068	0.794
Male	37	126		
Female	49	178		
Age, year			0.189	0.664
≤60	45	151		
>60	41	153		
Smoking history			2.094	0.148
Yes	16	38		
No	70	266		
Preoperative comorbidities			0.350	0.554
Yes	41	134		
No	45	170		
Tumor location			2.114	0.715
RUL	26	109		
RML	9	27		
RLL	10	45		
LUL	29	86		
LLL	12	37		
Tumor diameter, cm			3.333	0.068
≤1	21	106		
>1, ≤2	65	198		
VPI			2.867	0.090
Present	21	60		
Absent	65	244		
Operation type			2.546	0.111
Lobectomy	58	176		
Sublobectomy	28	128		
Lymph node dissection type			2.167	0.141
SLND	59	182		
LLND	27	122		
Histologically dominant pattern			87.833	<0.001
Lepidic	15	162		
Acinar	39	124		
Papillary	13	9		
Micropapillary	14	0		
Solid	5	9		

RUL, right upper lung; RML, right middle lung; RLL, right lower lung; LUL, left upper lung; LLL, left lower lung; VPI, visceral pleural invasion; SLND, systematic lymph node dissection; LLND, limited lymph node dissection; Preoperative complication includes high blood pressure, diabetes, arrhythmia, asthma, and so forth.

Survival of patients in each group

A total of 390 patients were followed from January 2016 to March 2022, with a total follow-up period of 75.0 months and a median follow-up period of 57.0 months. Thirty-five patients were lost to follow-up. The average survival time of the whole group of patients was 69.8 months; the 1-year, 3-year, and 5-year survival rates were 99.2%, 94.8%, and 88.5%, respectively. The average survival time of Group A was 66.7 months; the 1-year, 3-year, and 5-year survival rates were 98.8%, 93.0%, and 80.9%, respectively, and the average survival time of Group B was 70.5 months; the 1-year, 3-year, and 5-year survival rates were 99.3%, 95.4%, and 90.6%, respectively. The survival rate of Group B was significantly better than that of Group A, and the result was statistically significant ($p=0.007$) (Figure 1).

The prognostic effect of micropapillary histological components in patients with different surgical methods and different lymph node dissections

The patients in Group A were divided into the lobectomy group and sublobectomy group, and a survival curve analysis was performed. It was found that the survival of the lobectomy group was better than that of the sublobectomy group, and the result was statistically significant ($p=0.008$). (Figure 2) Systematic lymph node dissection and limited lymph node dissection were used for survival analysis. The survival of patients with systematic dissection was better than that of patients with limited lymph node dissection, and the result was statistically significant ($p=0.028$). (Figure 3).

TABLE 2 The prognostic factors associated with overall survival of patients in groups A, B by univariate analysis and multivariate Cox regression.

Variables	Case	Univariate		Multivariate	
		Mean survival time (month) (95% CI)	P Value	OR (95%CI)	P Value
Sex			0.946	–	0.949
Male	163	69.8			
Female	227	69.8			
Age, year			0.433	–	0.356
≤60	196	70.7			
>60	194	69			
Smoking history			0.361	–	0.461
Yes	54	69.2			
No	336	70			
Preoperative comorbidities			0.183	–	0.187
Yes	175	68.7			
No	215	70.7			
Tumor location			0.384	–	0.074
RUL	135	70.7			
RML	36	66.4			
RLL	55	65			
LUL	115	71.1			
LLL	49	70			
Tumor diameter, cm			0.273	–	0.182
≤1	127	68.8			
>1	263	70.3			
VPI			0.09	–	0.129
Present	81	68.4			
Absent	309	70.2			
Operation type			0.139	–	0.088
Lobectomy	234	70.5			
Sublobectomy	156	68.8			
Lymph node dissection type			0.94	–	0.875
SLND	241	70			
LLND	149	70.2			
Micropapillary component			0.007	0.436 (0.234–0.813)	0.009
>5%	86	66.7			
≤5%	304	70.5			

RUL, right upper lung; RML, right middle lung; RLL, right lower lung; LUL, left upper lung; LLL, left lower lung; VPI, visceral pleural invasion; SLND, systematic lymph node dissection; LLND, limited lymph node dissection; Preoperative complication includes high blood pressure, diabetes, arrhythmia, asthma, and so forth.

The patients in Group B were divided into the lobectomy group and sublobectomy group, and a survival curve analysis was carried out. There was no difference in the survival rate between the two groups, and the result was not statistically significant ($p=0.844$). (Figure 4) There was no difference in survival between systematic lymph node dissection and limited lymph node dissection, and the results were not statistically significant ($p=0.159$) (Figure 5).

Discussion

The survival and prognosis of patients with lung cancer are related to many clinical and pathological factors. Many studies have

reported that the micropapillary components of lung adenocarcinoma are closely related to lymph node metastasis, vascular tumor thrombus, visceral pleural invasion and airway diffusion (12, 13). This may be an independent risk factor for postoperative local metastasis and recurrence of early-stage NSCLC, and this is of high value for predicting the biological behaviour of tumours. This study also found that the micropapillary histological subtype component was an independent risk factor in patients with lung adenocarcinoma ≤ 2 cm after surgery, and when the proportion of micropapillary components was different, the prognoses of patients who underwent different surgical methods and lymph node dissection were different. Lobectomy and systematic lymph node dissection in patients with micropapillary histology $>5\%$ have better long-term survival. The surgical method

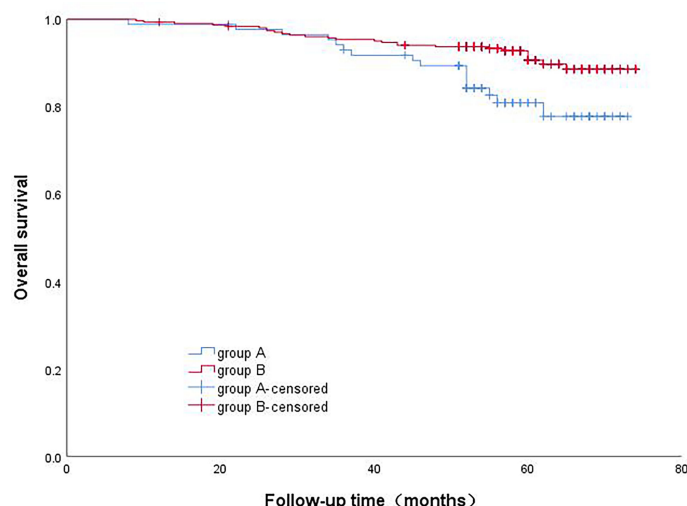


FIGURE 1
Comparison of patients survival rate with different micropapillary proportions.

and lymph node dissection have no significant effect on the survival of patients in whom the histological composition of the micropapillary is $\leq 5\%$. This indicates that the micropapillary component has a certain value for the specific surgical approach of early-stage lung adenocarcinoma and prognosis in lymph node metastasis.

In this study, 390 patients with non-small cell lung adenocarcinoma who underwent pulmonary nodule surgery were grouped according to the proportion of micropapillary histological components. Through multivariate and survival

analyses, we found that the long-term survival of patients with $> 5\%$ micropapillary components was significantly lower than that of patients with $\leq 5\%$ micropapillary components, and the histological component of the micropapillary was an independent risk factor. Tamás Zombori et al. (14) found that the prognosis of patients with acinar lung adenocarcinoma is fairly good, while those patients with solid and micropapillary histological components are more prone to recurrence, metastasis, and an overall worse prognosis. In the study of Jun-ichi Nitadori et al. (15), IASLC/ATS/ERS classification was used

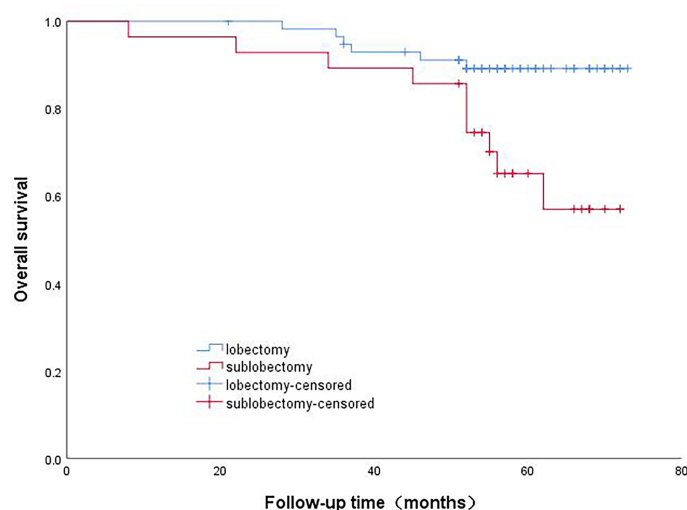


FIGURE 2
Survival curve of patients with micropapillary composition $> 5\%$ with different surgical methods.

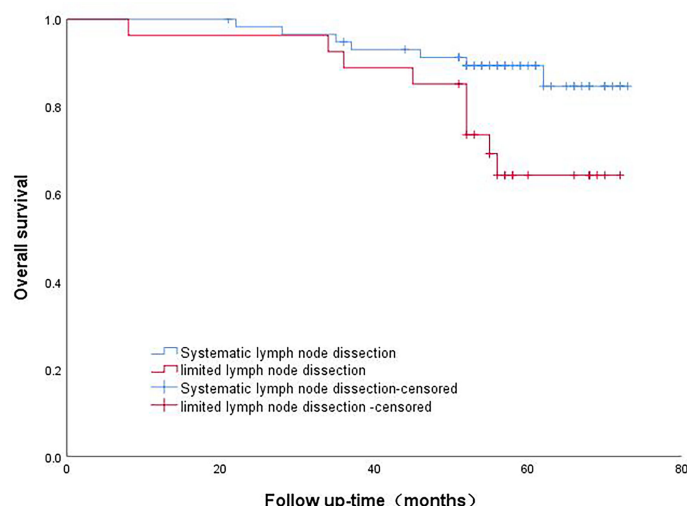


FIGURE 3

Survival curve analysis of patients with micropapillary component >5% with different lymph node dissection methods.

to determine that the presence of 5% or more micropapillary components was independently associated with the risk of recurrence in patients treated by lung wedge resection. Katsuya Watanabe et al. (16) studied 1289 patients with lung adenocarcinoma who underwent pneumonectomy from 2008 to 2015. It was found that the risk curve of patients with micropapillary components showed a broad peak within one year after operation, while those without micropapillary histological components showed some gentle peaks approximately two years after operation. In stage I patients, the

presence of micropapillary components was associated with a poor recurrence-free survival rate and early recurrence but not in advanced patients. This indicates that patients with micropapillary components have a high risk of early postoperative recurrence, and the risk of recurrence exists for a long time. Even after complete resection of stage I lung adenocarcinoma, micropapillary components are still associated with poor prognosis. The results of this study are similar, and the prognosis of patients without micropapillary components is better than that of patients with micropapillary components.

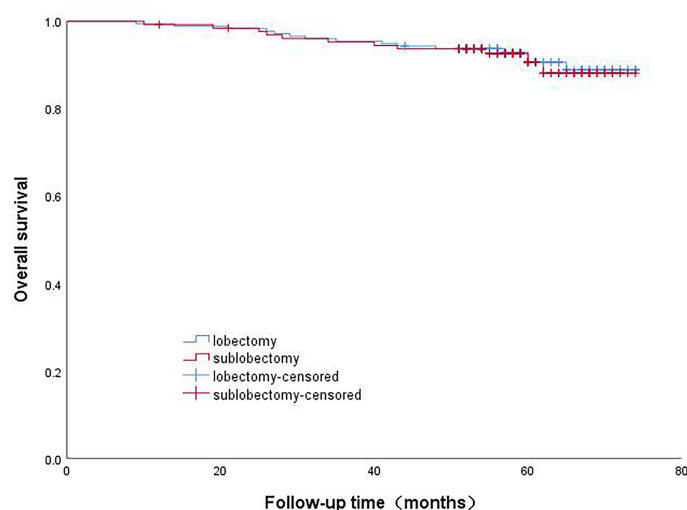


FIGURE 4

Survival curve of patients with micropapillary composition $\leq 5\%$ with different surgical methods.

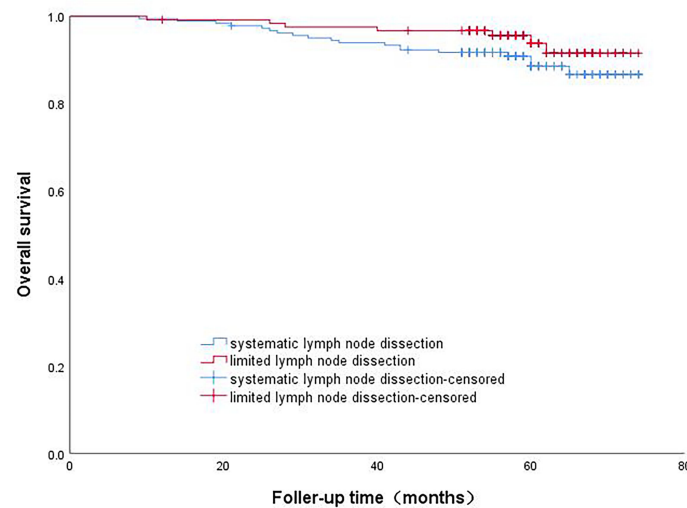


FIGURE 5

Survival curve analysis of patients with micropapillary component $\leq 5\%$ with different lymph node dissection methods.

Because of these studies, the micropapillary histological components are of great significance in precisely selecting suitable patients for sublobar resection.

For resectable NSCLC, comprehensive treatment is still based on lobectomy and mediastinal lymph node dissection (5, 6). In the Japanese JCOG0802 study, the overall survival of sublobectomy was significantly better than that of lobectomy in these early patients (more people died of other diseases in the lobectomy group). Although the local recurrence rate is increased, greater preservation of lung parenchyma increases the room for subsequent treatment, such as in cases of disease progression and secondary primary cancer (17, 18). In this study, it was found that when the proportion of histological components of micropapillae was different, the survival of patients after different operations was different. When the micropapillary histological components were more than 5%, the survival rate of lobectomy was higher, while in the patients with micropapillary histological components lower than 5%, there was no significant difference in survival rate after different surgical methods. Yao et al. (19) found that patients with subcentimetre lung adenocarcinoma with micropapillary components had a poor prognosis, and wedge resection was associated with a higher risk of recurrence than anatomic lung resection (segmentectomy and lobectomy), which was similar to our results.

Lymph node metastasis is the most reliable indicator of staging and prognosis of patients with lung cancer, but excessive lymph node dissection may increase the time of operation and drainage and may damage the nerve, blood vessel and lymphoid structure in the mediastinum, resulting in increased postoperative complications. In our study, when the

micropapillary components were more than 5%, the survival rate after systemic lymph node dissection was higher, while in patients with micropapillary components $\leq 5\%$, the survival rate showed no significant change after undergoing different lymph node dissections. Sun et al. (20) analysed the clinicopathological data of 1160 patients with ≤ 2 cm invasive lung adenocarcinoma who underwent surgery from seven medical institutions from January 2012 to December 2015. It was found that limited mediastinal lymph node dissection was an independent prognostic factor for N2 lymph node metastasis in patients with micropapillary and solid components $>5\%$. The recurrence-free survival and overall survival time of patients who underwent systemic lymph node dissection were better than those who underwent limited lymph node dissection. In patients whose sum of micropapillary and solid components $\leq 5\%$, the prognosis of localized lymph node dissection was similar to that of systemic lymph node dissection. This is also similar to our research results.

The results of this study may be based on the following reasons. First, micropapillary lung adenocarcinoma has special structural characteristics. Its tumor cells are small and cuboid, grow in papillary clusters without fibrous vascular axes, and can be attached to the alveolar wall or fall off into the alveolar cavity. Because of its unique “inside-out” growth mode, the tumor cell cluster has a strong invasive behaviour, which spreads easily, is more prone to vascular and interstitial invasion, and is prone to early recurrence and metastasis (21, 22). Second, when the patient has micropapillary histological subtype components, the tumor resection margin is insufficient after sublobectomy, and the tumor is more likely to metastasize and recur. Third, when the patient has micropapillary histological subtype

components, the number of lymph node dissection stations and the number of lymph nodes were significantly reduced when the patient underwent limited lymph node dissection, and the lymph node postoperative pathology showed false negatives. No accurate lymph node staging was provided for patients with lung cancer, and postoperative adjuvant treatment was not available in time, which shortened the survival time of patients.

Our research also has some limitations. First, this is a retrospective study, which may lead to limited data and some selection bias. To verify our findings, it is necessary to conduct randomized trials in the future. Second, the sample size of patients is limited. Third, the heterogeneity of the tumours will inevitably have some potential impact on the diagnosis of pathological sections. At present, due to the limitation of intraoperative frozen pathological conditions, many medical centres cannot fully judge the micropapillary histological subtype components according to intraoperative pathology. Although preoperative biopsy can well predict histological composition, the availability of samples is limited, and this invasive procedure may lead to many complications. The relationship between imaging data and micropapillary components needs further confirmation to guide clinical decision-making.

Conclusions

The micropapillary histological component is an independent risk factor after surgery in patients with ≤ 2 cm lung adenocarcinoma. When the proportion of micropapillary components is different, the prognosis of patients is different when different surgical methods and lymph node dissections are performed. Lobectomy and systematic lymph node dissection are recommended for patients with a micropapillary histological composition $>5\%$; sublobar resection and limited lymph node dissection are recommended for patients with a micropapillary histological composition $\leq 5\%$. The feasibility of this strategy needs to be prospectively validated in future work. It is believed that more data are needed to better clarify this issue.

Data availability statement

The original contributions presented in the study are included in the article/supplementary material. Further inquiries can be directed to the corresponding authors.

Ethics statement

The studies involving human participants were reviewed and approved by the Affiliated Provincial Hospital of Anhui Medical

University. Written informed consent for participation was not required for this study in accordance with the national legislation and the institutional requirements.

Author contributions

LX: Conceptualization, methodology, software, investigation, writing - original draft, writing - review, and editing. HZ: Conceptualization, methodology, investigation, histological evaluation. GW: Methodology, software, investigation. ZH: Methodology, software, investigation. RX: Visualization, investigation. XS: Visualization, investigation. MW: Visualization, investigation. TL: Writing - original draft, writing - review, and editing. MX: Funding acquisition, writing - review, and editing. All authors contributed to the article and approved the submitted version.

Funding

This work was supported by the grants from the National Natural Science Foundation of China and Key research and development projects in Anhui Province (NO.81973643 and 202004j07020017).

Acknowledgments

The authors thank Yuehong-Shen for their help with data collection and preparation of figures.

Conflict of interest

The authors declare that the research was conducted in the absence of any commercial or financial relationships that could be construed as a potential conflict of interest.

Publisher's note

All claims expressed in this article are solely those of the authors and do not necessarily represent those of their affiliated organizations, or those of the publisher, the editors and the reviewers. Any product that may be evaluated in this article, or claim that may be made by its manufacturer, is not guaranteed or endorsed by the publisher.

References

- Kim C, Xi L, Cultraro C, Wei F, Jones G, Cheng J, et al. Longitudinal circulating tumor DNA analysis in blood and saliva for prediction of response to osimertinib and disease progression in EGFR-mutant lung adenocarcinoma. *Cancers* (2021) 13(13):3342. doi: 10.3390/cancers13133342
- Siegel R, Miller K, Fuchs H, Jemal A. Cancer statistics, 2022. *CA: Cancer J Clin* (2022) 72(1):7–33. doi: 10.3322/caac.21708
- Yi J, Choi P, Bang J, Jeong S, Cho J. Systemic air embolism after computed tomography-guided hook wire localization: two case reports and literature review. *J Thorac Dis* (2018) 10(1):E59–64. doi: 10.21037/jtd.2017.12.04
- Park S, Yoon J, Park K, Lee S. Prediction of occult lymph node metastasis using volume-based PET parameters in small-sized peripheral non-small cell lung cancer. *Cancer imaging: Off Publ Int Cancer Imaging Soc* (2015) 15:21. doi: 10.1186/s40644-015-0058-9
- Berman A, Jabbour S, Vachani A, Robinson C, Choi J, Mohindra P, et al. Empiric radiotherapy for lung cancer collaborative group multi-institutional evidence-based guidelines for the use of empiric stereotactic body radiation therapy for non-small cell lung cancer without pathologic confirmation. *Trans Lung Cancer Res* (2019) 8(1):5–14. doi: 10.21037/tlcr.2018.12.12
- Zhang Z, Miao J, Chen Q, Fu Y, Li H, Hu B. Assessment of non-lobe-specific lymph node metastasis in clinical stage IA non-small cell lung cancer. *Thorac Cancer* (2019) 10(7):1597–604. doi: 10.1111/1759-7714.13121
- Choi S, Jeong J, Lee S, Shin K, Jeong S, Park T, et al. Clinical implication of minimal presence of solid or micropapillary subtype in early-stage lung adenocarcinoma. *Thorac Cancer* (2021) 12(2):235–44. doi: 10.1111/1759-7714.13754
- Lee G, Lee H, Jeong J, Han J, Cha M, Lee K, et al. Clinical impact of minimal micropapillary pattern in invasive lung adenocarcinoma: Prognostic significance and survival outcomes. *Am J Surg Pathol* (2015) 39(5):660–6. doi: 10.1097/pas.0000000000000399
- Yanagawa N, Shiono S, Abiko M, Ogata S, Sato T, Tamura G. New IASLC/ATS/ERS classification and invasive tumor size are predictive of disease recurrence in stage I lung adenocarcinoma. *Journal of thoracic oncology: Official publication of the international association for the study of lung cancer. J Thorac Oncol.* (2013) 8(5):612–8. doi: 10.1097/JTO.0b013e318287c3eb
- Sun W, Su H, Liu J, Zhang L, Chen C. Impact of histological components on selecting limited lymphadenectomy for lung adenocarcinoma ≤ 2 cm. *Lung Cancer* (2020), 150:36–43. doi: 10.1016/j.lungcan.2020.1009.1016
- Hung J, Yeh Y, Jeng W, Wu K, Huang B, Wu Y, et al. Predictive value of the international association for the study of lung cancer/American thoracic Society/European respiratory society classification of lung adenocarcinoma in tumor recurrence and patient survival. *J Clin Oncol: Off J Am Soc Clin Oncol* (2014) 32(22):2357–64. doi: 10.1200/jco.2013.50.1049
- Yoshimoto T, Matsubara D, Soda M, Ueno T, Amano Y, Kihara A, et al. Mucin 21 is a key molecule involved in the incohesive growth pattern in lung adenocarcinoma. *Cancer Sci* (2019) 110(9):3006–11. doi: 10.1111/cas.14129
- Morimoto J, Nakajima T, Suzuki H, Nagato K, Iwata T, Yoshida S, et al. Impact of free tumor clusters on prognosis after resection of pulmonary adenocarcinoma. *J Thorac Cardiovasc Surg* (2016) 152(1):64–72.e61. doi: 10.1016/j.jtcvs.2016.03.088
- Zombori T, Nyári T, Tiszlavicz L, Pálfoldi R, Csada E, Géczi T, et al. The more the micropapillary pattern in stage I lung adenocarcinoma, the worse the prognosis—a retrospective study on digitalized slides. *Virchows Archiv: an Int J Pathol* (2018) 472(6):949–58. doi: 10.1007/s00428-018-2337-x
- Nitadori J, Bograd A, Kadota K, Sima C, Rizk N, Morales E, et al. Impact of micropapillary histologic subtype in selecting limited resection vs lobectomy for lung adenocarcinoma of 2 cm or smaller. *J Natl Cancer Inst* (2013) 105(16):1212–20. doi: 10.1093/jnci/djt166
- Watanabe K, Sakamaki K, Ito H, Yokose T, Yamada K, Nakayama H, et al. Impact of the micropapillary component on the timing of recurrence in patients with resected lung adenocarcinoma. *Eur J Cardio-Thoracic Surg: Off J Eur Assoc Cardio-thoracic Surg* (2020) 58(5):1010–8. doi: 10.1093/ejcts/ezaa138
- Nakamura K, Saji H, Nakajima R, Okada M, Asamura H, Shibata T, et al. A phase III randomized trial of lobectomy versus limited resection for small-sized peripheral non-small cell lung cancer (JCOG0802/WJOG4607L). *Japanese J Clin Oncol* (2010) 40(3):271–4. doi: 10.1093/jjco/hyp156
- Saji H, Okada M, Tsuboi M, Nakajima R, Suzuki K, Aokage K, et al. Segmentectomy versus lobectomy in small-sized peripheral non-small-cell lung cancer (JCOG0802/WJOG4607L): A multicentre, open-label, phase 3, randomised, controlled, non-inferiority trial. *Lancet (London England)* (2022) 399(10335):1607–17. doi: 10.1016/s0140-6736(21)02333-3
- Yao J, Zhu E, Li M, Liu J, Zhang L, Ke H, et al. Prognostic impact of micropapillary component in patients with node-negative subcentimeter lung adenocarcinoma: A Chinese cohort study. *Thorac Cancer* (2020) 11(12):3566–75. doi: 10.1111/1759-7714.13702
- Sun W, Su H, Liu J, Zhang L, Li M, Xie H, et al. Impact of histological components on selecting limited lymphadenectomy for lung adenocarcinoma ≤ 2 cm. *Lung Cancer (Amsterdam Netherlands)* (2020) 150:36–43. doi: 10.1016/j.lungcan.2020.09.016
- Xu Z, Wang J, Zhang Y, Wu S, Ma L, Qin Y, et al. Xp11.2 translocation/TFE3 gene fusion renal cell carcinoma with a micropapillary pattern: Cases report and literature review. *Am J Trans Res* (2019) 11(1):327–39.
- Zhang H, Huang W, Liu C, Giaccone G, Zhao X, Sun X, et al. The prognostic value of non-predominant micropapillary pattern in a large cohort of resected invasive lung adenocarcinoma measuring ≤ 3 cm. *Front Oncol.* (2021) 11:657506. doi: 10.3389/fonc.2021.657506



OPEN ACCESS

EDITED BY

Xiaomin Niu,
Shanghai Jiao Tong University, China

REVIEWED BY

Alessandro Gonfiotti,
University of Florence, Italy
Gang Hou,
China-Japan Friendship Hospital,
China

*CORRESPONDENCE

Chengshui Chen
chenchengshui@wmu.edu.cn

SPECIALTY SECTION

This article was submitted to
Thoracic Oncology,
a section of the journal
Frontiers in Oncology

RECEIVED 01 June 2022

ACCEPTED 25 July 2022

PUBLISHED 18 August 2022

CITATION

Lin X, Zhou L, Zhou W, Li Y, Jin X,
Ye M and Chen C (2022) Establishing a
novel model of malignant airway
stenosis in rabbit.
Front. Oncol. 12:959309.
doi: 10.3389/fonc.2022.959309

COPYRIGHT

© 2022 Lin, Zhou, Zhou, Li, Jin, Ye and
Chen. This is an open-access article
distributed under the terms of the
[Creative Commons Attribution License](#)
(CC BY). The use, distribution or
reproduction in other forums is
permitted, provided the original
author(s) and the copyright owner(s)
are credited and that the original
publication in this journal is cited, in
accordance with accepted academic
practice. No use, distribution or
reproduction is permitted which
does not comply with these terms.

Establishing a novel model of malignant airway stenosis in rabbit

Xiaoxiao Lin¹, Liqin Zhou¹, Wanting Zhou¹, Yuping Li¹,
Xuru Jin¹, Min Ye¹ and Chengshui Chen^{2,3*}

¹Department of Pulmonary and Critical Care Medicine, First Affiliated Hospital of Wenzhou Medical University, Wenzhou, China, ²The Quzhou Affiliated Hospital of Wenzhou Medical University, Quzhou People's Hospital, Quzhou, China, ³Key Laboratory of Interventional Pulmonology of Zhejiang Province, First Affiliated Hospital of Wenzhou Medical University, Wenzhou, China

Background: Malignant central airway stenosis is a life-threatening condition. However, treatment of malignant airway stenosis remains challenging. There is currently a severe lack of an excellent animal model of malignant airway stenosis to facilitate treatment approaches. This is the first study to establish a rabbit model of malignant airway stenosis for bronchoscopic interventional studies.

Materials and methods: New Zealand White rabbits were used in this study, randomly divided into group A (18 rabbits) and group B (6 rabbits). A VX2 fragment suspension was injected into the submucosal layer of rabbits' airway by bronchoscopy. Bronchoscopic examinations were performed once a week after VX2 tumor implantation to observe tumor growth and the degree of airway stenosis. Randomly, three rabbits were generally dissected after a weekly bronchoscopic examination in group A. The rabbits that reached grade III airway stenosis underwent stent implantation in group B.

Results: A total of 24 rabbits were successfully implanted with the VX2 fragment suspension in the airway without significant adverse events, and the success rate of the tumor growth was 100%. The degree of airway stenosis reaching grade III took 2 to 3 weeks after implantation of the VX2 tumor. The median survival time of rabbit models without stent implantation and rabbits with stent implantation was 32.5 and 32.0 days, respectively.

Conclusions: The implanting method is safe and effective for the establishment of a rabbit model of malignant airway stenosis. When the tumor grows to 2 to 3 weeks, the rabbit model is available for stent implantation. We recommend the models for more preclinical animal studies on bronchoscopic interventional treatments.

KEYWORDS

malignant airway stenosis, animal model, rabbit, bronchoscopy, VX2

Introduction

Malignant central airway stenosis is a life-threatening condition caused by malignant tumors, most commonly occurring in locally advanced lung cancer (1, 2). For patients ineligible for surgery due to poor general condition or an advanced tumor stage, bronchoscopic intervention is a useful treatment option, including photodynamic therapy, tumor ablation, cryotherapy, and airway stenting (3). However, treatment of malignant airway stenosis remains challenging and is variable among clinicians and institutions (4, 5). Besides other techniques, stent-related technologies continue to overcome the current complications of stents, such as migration, infection, and granulation tissue formation (6). Recently, novel stents, new laser, and spray cryotherapy with a novel multimodal approach have been gradually designed to solve malignant airway stenosis (7–11). However, the ideal bronchoscopic technique does not currently exist, and studies on new techniques are necessary and significant.

Although many of these technical changes can be evaluated directly in the patient, clinical investigation often needs preliminary support from animal studies. However, there is currently a severe lack of an excellent animal model of malignant airway stenosis to facilitate treatment-related studies.

The VX2 tumor, a squamous cell cancer model, which was firstly proposed by Shope and Hurst (12) in 1933, has been implanted in many sites of rabbits, including the liver, kidney, lung, esophagus, and muscle (13–15). Although the rabbits belong to moderate-to-large-sized models and have been used to study benign airway stenosis in stent-related research (16, 17), there have been no reports on establishing a rabbit model with malignant airway stenosis.

This is the first study that aims to develop a rabbit model of malignant airway stenosis in which we describe the use of submucosal VX2 fragments in the tracheal wall and to investigate the safety and efficiency of the method, as well as the characteristics of the airway stenosis model. Furthermore, we observed the feasibility of stent implantation in the novel model.

Materials and methods

Animal and tumor

Male or female New Zealand White rabbits (Kelian Rabbit Professional Cooperative, Hangzhou, China) weighing between 2.5 and 3.5 kg were used in this study. The VX2 tumor previously stored at -80°C was obtained from the Surgery Laboratory in the First Affiliated Hospital of Wenzhou Medical University. All experimental procedures were approved by the Laboratory Animal Center of Wenzhou Medical University (ID: wyd2021-0289) and were performed

in accordance with the National Institute of Health's Guide for the Care and Use of Laboratory Animals.

Tumor propagation and implantation preparation

Four rabbits with hind-limb tumors were used to propagate and maintain VX2 tumors. Approximately 0.2 ml of saline with VX2 tumor tissue fragments, which could pass through a 1-ml syringe connecting with an 18-gauge needle, was injected deeply into the hind limb of gluteal muscles of rabbits. After 2–3 weeks, the animals were executed and the hind-limb tumors were processed. All VX2 tumors were cleaned from the surrounding normal tissue, and necrotic portions of the tumors were removed.

The collected tumors were cut into small pieces approximately 0.5 mm in diameter, which could pass through the 20-gauge needle, and preserved in saline for fragment implantation. Approximately 0.6 ml tumor fragment suspension was placed in a 1-ml syringe connecting with a 20-gauge transfusion needle (Figure 1A).

Endoscopic implantation of VX2 fragment suspension

A total of 24 rabbits were included in the process and randomly divided into group A and group B. Group A (18 rabbits) was used to observe the characteristics of the airway stenosis model, and group B (6 rabbits) was implanted with a metal stent when malignant stenosis occurred in the rabbit airway.

Each rabbit was firstly anesthetized by injection with 3% pentobarbital sodium (1 ml/kg) *via* the ear vein and then secured in supine position. Its anterior neck was exposed, and then preoperative hair removal was prepared. A medical tooth pad was fixed in the oral cavity of the rabbit. An ordinary bronchoscope with an outer diameter of 4.9 mm (UE Medical Corporation, Zhejiang, China) was inserted into the airway from the tooth pad, and 1 ml of lidocaine (2%) was injected into the vocal area to reduce the intense cough reaction of the rabbit.

Then the anterior neck between two tracheal cartilages was punctured with the 20-gauge transfusion needle in the guidance of a light source of the bronchoscope (Figure 1B). The puncture site was approximately located 1 cm away from the upper part of the manubrium sternum. After inserting through the skin, subcutaneous tissue, and anterior tracheal wall to the airway, a puncture was made using the needle across the mucosa into the submucosal layer in the tracheal membrane. When the whole inclined surface of the needle enters into the submucosal layer, which could be clearly seen by a bronchoscope, approximately 0.15 ml of VX2 fragment suspension was then injected into the

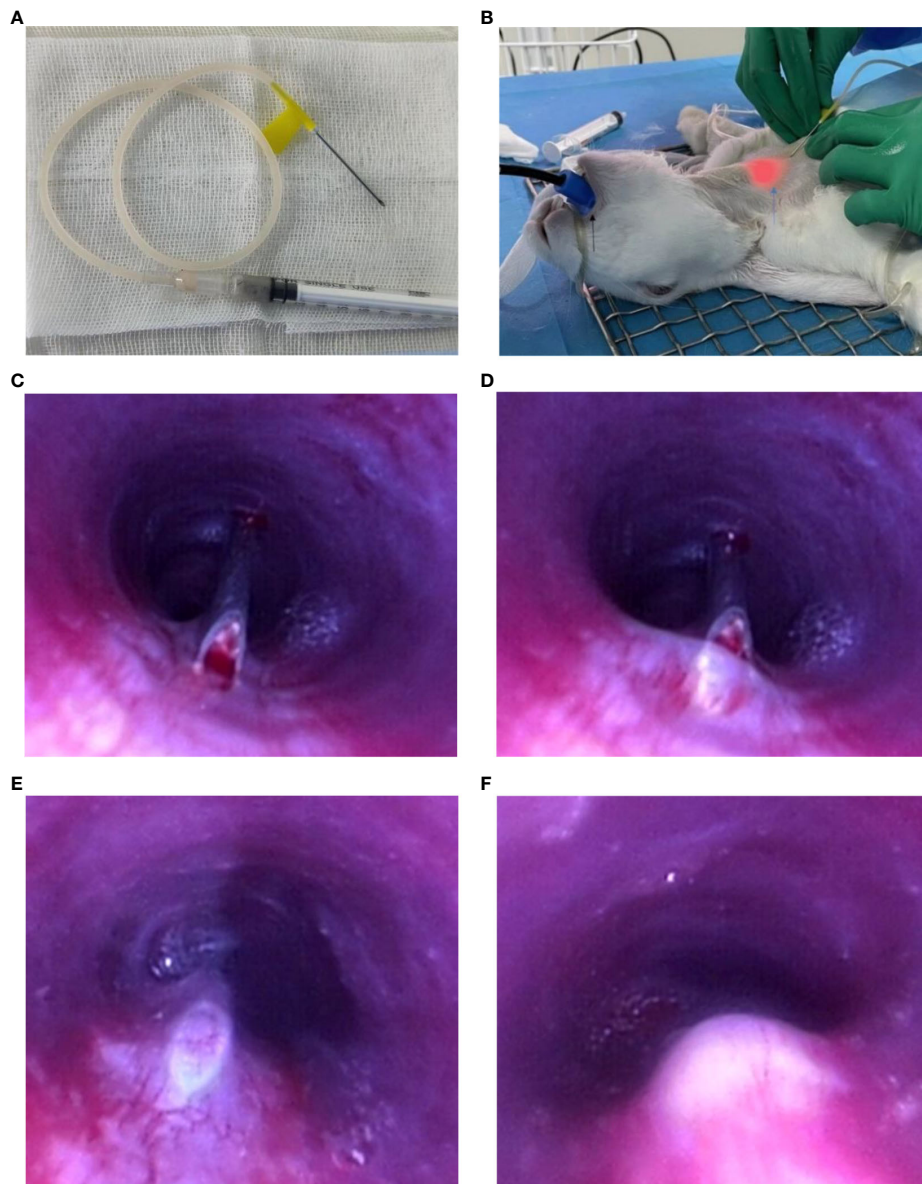


FIGURE 1

Endoscopic implantation of VX2 fragment suspension. Preparation before implantation: **(A)** VX2 fragment suspension in a 1-ml syringe connecting with a 20-gauge transfusion needle. **(B)** The black arrow points to the medical tooth pad; blue arrow points to the light source of the bronchoscope; Procedure of endoscopic implantation: **(C–E)** The 20-gauge needle entering into the submucosal layer. **(F)** Injection of VX2 fragment suspension.

submucosal layer of the rabbit's airway. Finally, the needle was rapidly evacuated from the airway. The operational process is vividly shown in [Figures 1C–F](#) and [Video 1](#). The implantation site was approximately 5 cm away from the tracheal carina, which was the equivalent of 3 cm away from the glottis of the rabbit. During the procedure, a 50-ml syringe was put into the working channel of the bronchoscope to artificially provide oxygen to the rabbit. The complications of the procedure, such as apnea, death, and massive hemorrhage, were assessed and

accessed immediately after the procedure. After implantation, the rabbits were intramuscularly injected with 200,000 U penicillin at once.

Endoscopic follow-up

Bronchoscopic examinations were performed once a week after VX2 tumor implantation to observe tumor growth and the

degree of airway stenosis. The anesthesia procedure was the same as that described before. Referring to the published classification system of airway stenosis (18), four grades were used to evaluate the airway stenosis under endoscopy: grade I stenosis less than or equal to a 25% decrease in the lumen cross-sectional area; grade II stenosis more than 25% but less than or equal to 50%; grade III stenosis more than 50% but less than or equal to 75%; and grade IV stenosis more than 75%.

Survival time and necropsy

In group A, randomly three rabbits were generally dissected after a weekly bronchoscopic examination. In other words, every three rabbits were executed in the first, second, third, and fourth weeks after tumor implantation. The remaining six rabbits, without stent implantation, were observed until they had inability to survive. A humane endpoint was used in this study, at which the animal models would be humanely sacrificed when they had significant symptoms of dyspnea and wheeze and then their health was so weak that they could not stand and eat food.

The rabbits were injected with 3% pentobarbital sodium (1 ml/kg) *via* the ear vein and then injected with 20 ml of air. General necropsy examinations involved the organs of the tracheal wall, esophagus, lung, liver, and kidney, to clarify tumor invasion and metastasis. The length and width and height of the VX2 tumor in the trachea were measured by a vernier caliper. All the tumors were evaluated histologically. Hematoxylin–eosin (HE)-stained histopathology is the gold standard for the diagnosis of carcinoma.

Stent implantation

In group B, a self-expandable metal stent (8 mm in diameter and 30 mm in length) was implanted when the degree of airway stenosis in the rabbit reached grade III. Firstly, the distance from the distal end of the airway tumor to medical teeth was measured by bronchoscopy and a guidewire was inserted across the stenosis into the main bronchus. Then the delivery device was gently passed over the guidewire and the stent was released according to the measured distance before. After withdrawing the delivery device, ideal positioning of the stent was assessed and adjusted endoscopically. Finally, bronchoscopic examinations were performed every week to observe the stent-related complications and airway restenosis.

Results

Safety of experimental procedure

All 24 rabbits tolerated the bronchoscopy procedure without clinically significant adverse events. When implanting VX2

fragment suspension, no apnea or massive hemorrhage, or even death, occurred (Table 1). It would only take 60 s from bronchoscope inserting into the airway to bronchoscope withdraw.

Success rate of tumor growth

In the first week after tumor implantation, small nodules attached to the outer wall of the trachea in all living rabbits. All rabbits were confirmed to have tumor growth in their airway by dissection and then histopathology. The success rate of tumor growth in the rabbit airway was 100% (Table 1).

Tracheal tumor feature

In group A, the macroscopic external and internal views of the tracheal tumor are as shown in Figures 2A, B. The mean length of the airway tumor is 9.7 mm in the first week; 20.7 mm in the second week; 25.0 mm in the third week; 31.6 mm in the fourth week; and 42 mm in the last rabbits. Furthermore, the mean width (height) is respectively 5.5 (4.5) mm, 12.7 (10.3) mm, 15.2 (13.1) mm, 19.9 (15.3) mm, and 32.3 (20.5) mm in different periods of rabbits (Figure 2C).

In histopathological examination, the tumor cells grew vigorously in the first 3 weeks. Moreover, some tumors (22.2%, 2/9) showed slightly necrotic portions in the second and third weeks. However, the tumors showed obviously necrotic portions in the fourth week (Figures 2D–F).

TABLE 1 The observational data in the study.

Observation	Number	Percent
Implanting VX2 fragment suspension		
Success	24/24	100%
Hemorrhage	0/24	0%
Apnea	0/24	0%
Death	0/24	0%
Success rate of tumor growth	24/24	100%
Success rate of stenosis model in group A		
First week	8/18	44.4%
Second week	13/15	86.7%
Third week	12/12	100%
Implanting stent in group B		
Success rate	6/6	100%
Complication		
Airway restenosis	4/6	66.7%
Airway cancerous fistula	1/6	16.7%
Granulation tissue formation	1/6	16.7%

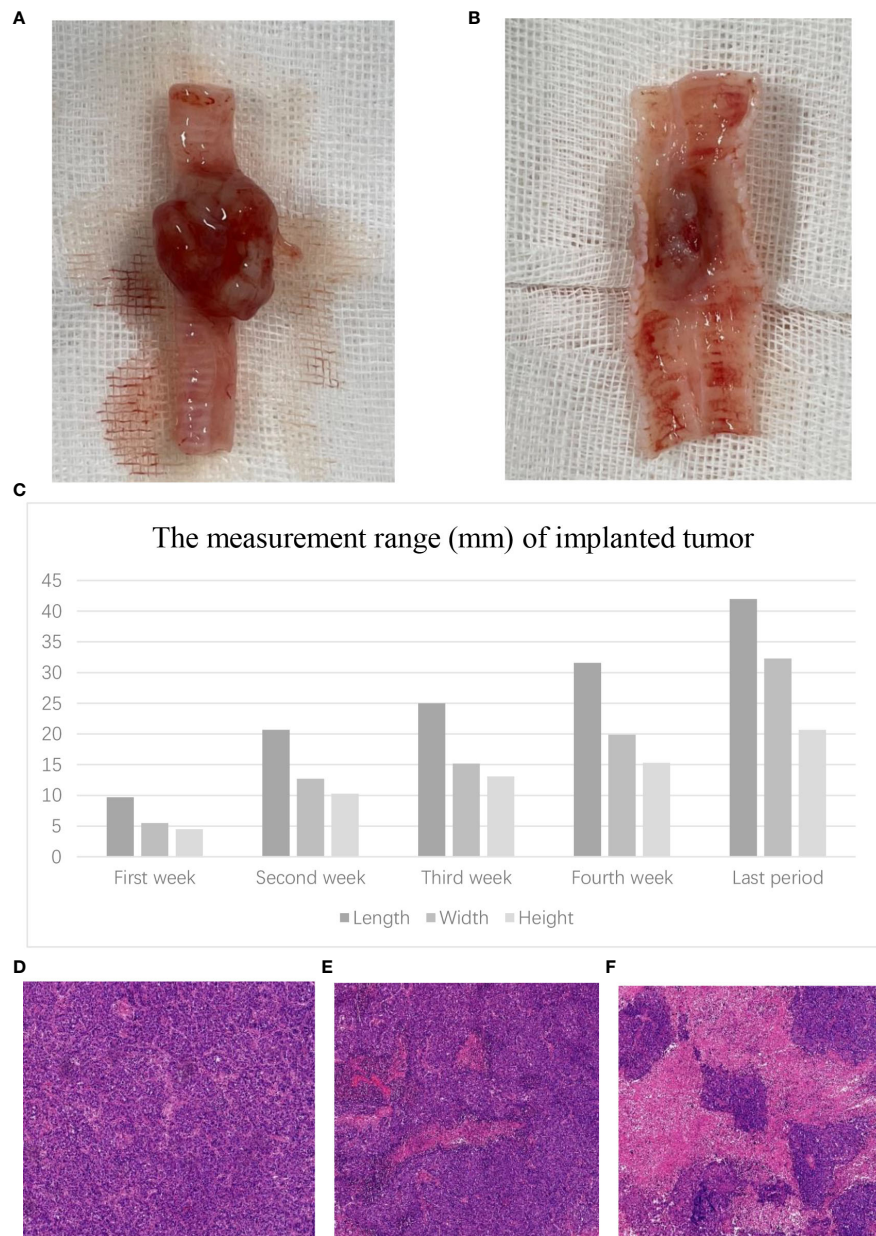


FIGURE 2

Tumor growth in the airway. (A) Macroscopic external view of the tracheal tumor. (B) Macroscopic internal view of the tracheal tumor. (C) The measurement range of the VX2 tumor in different periods. Microscopic view of the tracheal tumor. (D) Tumor cells grew vigorously. (E) Tumor showed slightly necrotic portions. (F) Tumor showed obviously necrotic portions.

Success rate of establishing malignant airway stenosis

In group A, during the bronchoscopic follow-up after tumor implantation, non-appreciable airway stenosis, I grade stenosis,

and grade II stenosis were observed in 56% (10/18), 39% (7/18), and 5% (1/18) rabbits in the first week, respectively.

In the second week, the percentages of non-appreciable stenosis, grade I stenosis, grade II stenosis, and grade III stenosis were 13% (2/15), 34% (5/15), 40% (6/15), and 13%

(2/15), respectively. Moreover, in the third week, the percentages of grade II stenosis, grade III stenosis, and grade IV stenosis were 42% (5/12), 42% (5/12), and 16% (2/12), respectively. In the fourth weekly bronchoscopic examination, three rabbits (33%) showed grade III airway stenosis and six rabbits (67%) showed grade IV stenosis. The data are summarized in Table 2. Moreover, rabbits with grade IV airway stenosis had symptoms of breathing difficulties and weakness and suffered from massive mucilage secretion plugging in the distal airway.

TABLE 2 Degree of airway stenosis in different weeks after tumor implantation.

Rabbit, no. (%)	Non-appreciate	I grade	II grade	III grade	IV grade
First week, 18	10 (56%)	7 (39%)	1 (5%)		
Second week, 15	2 (13%)	5 (34%)	6 (40%)	2 (13%)	
Third week, 12			5 (42%)	5 (42%)	2 (16%)
Fourth week, 9				3 (33%)	6 (67%)

Airway stenosis types

The gross classical appearance of the tumors varied from small submucosal microbulge to larger mass in bronchoscopy. In rabbits with malignant airway stenosis in the study, different structural stenosis types including extrinsic compression of the airway, tumor invasion of the airway wall or intraluminal tumor, and a combination growth are shown in Figure 3.

Tumor distant metastasis

The airway tumor did not metastasize to other organs of rabbits in the first and second weekly necropsy examinations. In the third week, one rabbit was observed to have diffuse pulmonary metastases. In the fourth week, three rabbits were verified with diffuse pulmonary metastases while one of them was attacked by metastatic esophageal carcinoma. The remaining rabbits with their survival time of more than 28 days all showed pulmonary metastases; one of them also had

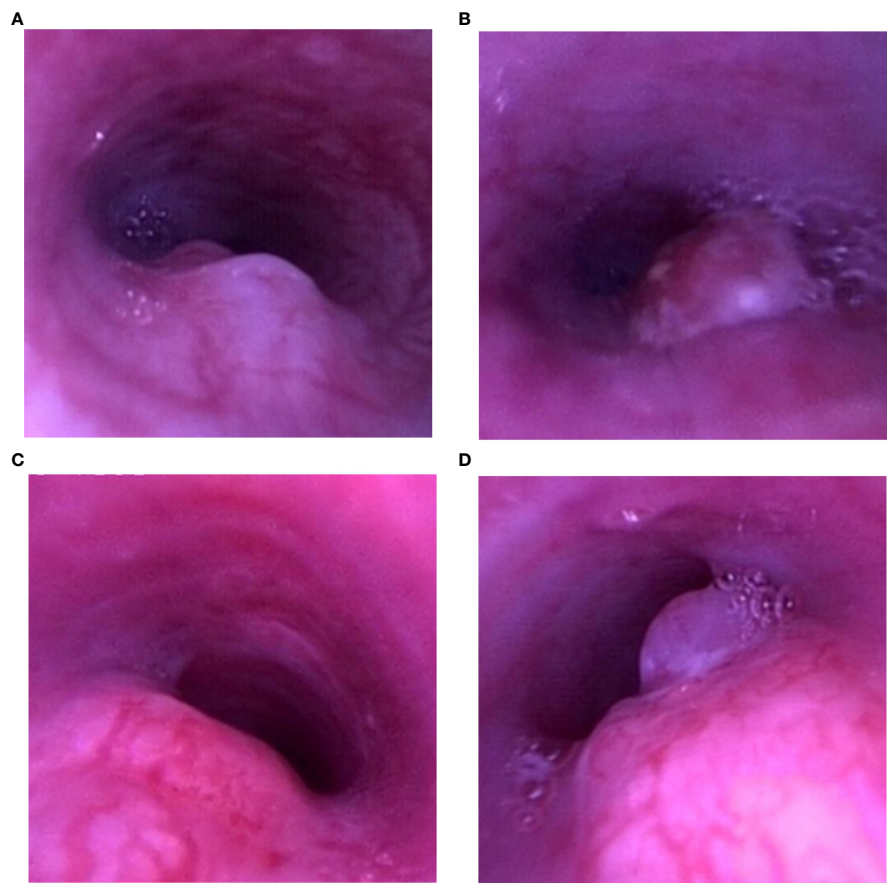


FIGURE 3 Airway stenosis types. (A) Tumor invasion of the airway wall. (B) Intraluminal tumor. (C) Extrinsic compression of the airway. (D) Combination growth.

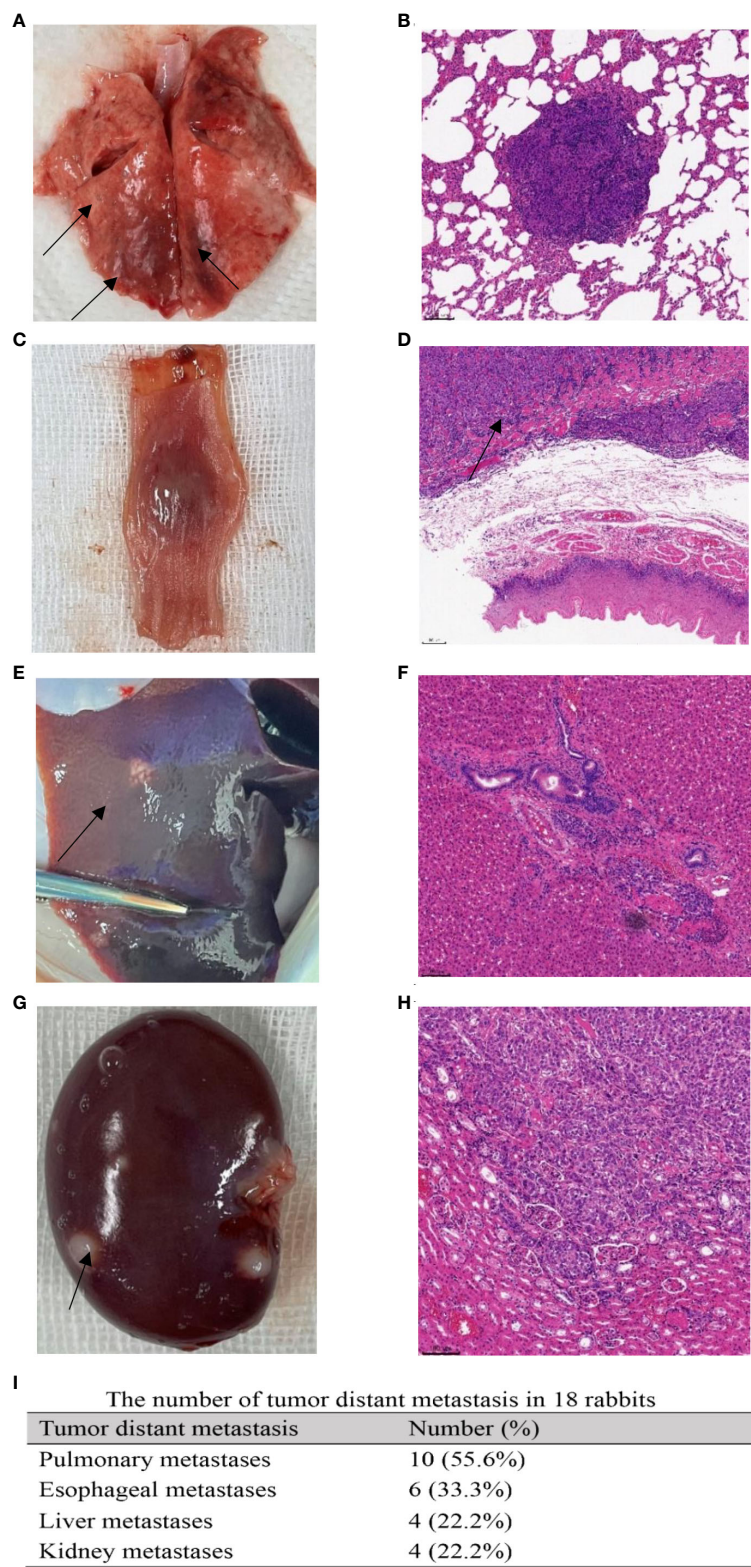


FIGURE 4
Tumor distant metastases. Macroscopic view of tumor metastases: (A) pulmonary metastasis (black arrow); (C) esophageal metastasis; (E) hepatic metastasis (black arrow); (G) renal metastasis (black arrow). Microscopic observation of tumor metastases: (B) pulmonary metastasis; (D) esophageal metastasis. The black arrow points to cancer cells infiltrating the esophageal muscular layer. (F) Hepatic metastasis. (H) Renal metastasis. (I) The number of tumor distant metastases in 18 rabbits.

esophageal metastasis, and four of them presented with multiple metastatic organs including lung, esophagus, liver, and kidney. The manifestations of metastatic lesions and corresponding histopathology are demonstrated in Figure 4.

Survival time of the rabbit models

The remaining six rabbits in group A suffered from respiratory failure. Before they received humane sacrifice, the bronchoscopic examination presented grade IV stenosis on the airway. The survival time of rabbits varied from 31 to 34 days, and the median survival time was 32.5 days after VX2 tumor implantation.

Stent-related complications

In group B, the time of airway showing grade III stenosis was 3 weeks in four rabbits and 2 weeks in other rabbits. The metal stents were successfully implanted into the narrow airway of six rabbits. Moreover, the airway of all six rabbits recovered patency at once after stent implantation (Figure 5). The median survival time of relevant rabbits was 32.0 days after VX2 tumor implantation. Four rabbits died of severe airway restenosis and one died of airway cancerous fistula, and the remaining one rabbit suffered granulation tissue formation and mucus plugging. The observational data in the study are shown in Table 2.

Discussion

In the current study, the bronchoscopic procedure was minimally invasive with a high success rate of implantation and establishment of a malignant airway stenosis model. The

adequate follow-up data showed a degree of airway stenosis in different periods, different airway stenosis types, survival time, tumor growth, and metastases of rabbits after VX2 implantation, which indicated that the animal models were reliable for mimicking the disease of human malignant central airway stenosis. When the tumor grows to 2 to 3 weeks, the rabbit model is available for stent implantation.

Malignant central airway stenosis is a serious condition that causes the death of patients. Patients with malignant airway stenosis always have a poor prognosis because of respiratory obstructions and reduced quality of life. Interventional bronchoscopy, especially airway stenting, is an available treatment to palliation of symptoms. However, adequate animal studies are necessary to evaluate the efficacy and safety of bronchoscopy-related treatments. In a recent study, animals were not under disease conditions and were only used to assess the safety of a stent loaded with ^{125}I seeds, due to the current lack of animal models of malignant airway stenosis (19). Therefore, a reliable animal model of malignant airway stenosis is sorely needed.

Small animal models, such as mice, are reasonable options for evaluating systemic therapy but have limitations for evaluating bronchoscopic technologies. Even though the airway structure of large animal models are more similar to humans, management of dogs or pigs is extremely difficult for researchers. However, New Zealand White rabbits are readily available and relatively inexpensive as models and are sufficiently large to allow the oral insertion of bronchoscope to their airway. Moreover, rabbits allow for research on bronchoscopic interventional treatments (20, 21). Prof. Li et al. implanted a novel stent into a rabbit airway to evaluate its function (17). Nakagishi et al. studied the application of photodynamic therapy for a benign airway stenosis rabbit model under bronchoscopy (22). All in all, the New Zealand White rabbit is a rational model to be adopted to perform the animal trial.

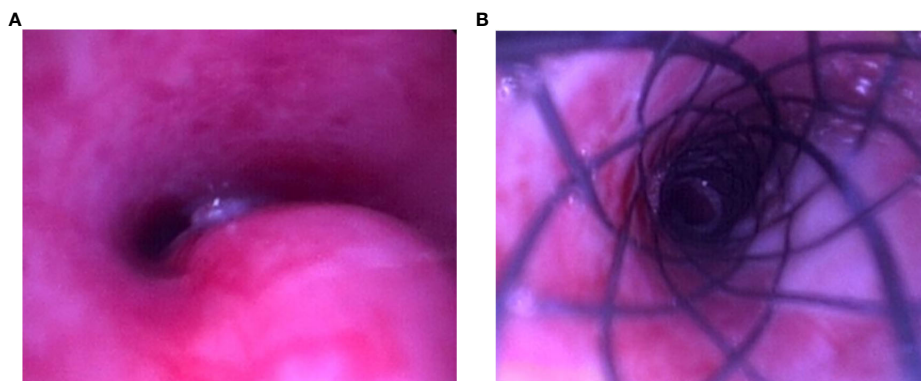


FIGURE 5
Stent implantation. (A) Malignant airway stenosis. (B) Airway opened.

According to our observations, the bronchoscope could smoothly pass through the airway of rabbits. Moreover, rabbits could tolerate the bronchoscopy procedure without severe complications. The rabbit model of malignant airway stenosis exhibits the characteristics of malignant stenosis and shows potential use for research on the efficiency of bronchoscopic treatments.

It has been reported that the success rate of tumor growth by the implantation of a VX2 fragment approximately 1 mm in diameter was higher than that by implantation of VX2 cells in the liver of rabbits (23, 24). The current data demonstrated that the method of implanting VX2 fragment suspension into the submucosal layer of the rabbit airway using a bronchoscope resulted in a 100% success in tumor growth.

It is a significant advantage on tumor implantation and then follow-up under bronchoscopic monitoring. The operational process could be clearly seen by bronchoscopy, and the condition of malignant airway stenosis was observed dynamically. Moreover, there was no apnea and death of rabbits during bronchoscopy.

Occlusion of >50% of the trachea in central malignant airway stenosis always leads to obvious clinical symptoms of patients and requires bronchoscopic interventional treatments. In the study, the degree of airway stenosis reaching grade III only took 2 to 3 weeks after implantation of a VX2 tumor. It signifies that the researchers can rapidly and conveniently establish a malignant stenosis model in rabbits, which is conducive to further studies on airway treatment. The supplementary experiment showed that a rabbit model with malignant airway stenosis could tolerate stenting implantation and then respiratory obstructions could be alleviated, although the bare metal stent did not obviously increase the survival time of rabbits because of tumor ingrowth and stent-related complications during the follow-up. These results indicate that it is safe and feasible to perform bronchoscopic intervention in our animal models. Moreover, the tumor tissue showed obviously necrotic portions after tumor growth at 4 weeks, which may be followed by an occurrence of an airway cancerous fistula. Therefore, we consider that the rabbit model is available for bronchoscopic interventional studies when the tumor grows at 2 to 3 weeks.

A limitation of the model we created, however, is that the types of malignant airway stenosis could not be controlled after VX2 implantation. In addition, we just chose one dose (0.15 ml) of VX2 tissue suspension. Future studies are needed to observe the relationship between stenosis types and the amount of VX2 suspension.

In conclusion, the implanting method described above is safe and effective for the establishment of a rabbit model of malignant airway stenosis to mimic the progression of this human disease. When the tumor grows at 2 to 3 weeks, the rabbit model is available for stent implantation. We recommend the model for more preclinical animal studies on bronchoscopic interventional treatments.

Data availability statement

The original contributions presented in the study are included in the article/[Supplementary Material](#). Further inquiries can be directed to the corresponding author.

Ethics statement

The animal study was reviewed and approved by Laboratory Animal Center of Wenzhou Medical University (ID: wydw2021-0289).

Author contributions

XL was a major contributor in writing the manuscript. CC and YL designed the study. MY and XJ analyzed the data. LZ and WZ performed the study. All authors contributed to the manuscript revision and read and approved the submitted version.

Funding

The study was supported by grants from the Key Laboratory of Interventional Pulmonology of Zhejiang Province (2019E10014) and the Zhejiang Provincial Key Research and Development Program (2020C03067).

Conflict of interest

The authors declare that the research was conducted in the absence of any commercial or financial relationships that could be construed as a potential conflict of interest.

Publisher's note

All claims expressed in this article are solely those of the authors and do not necessarily represent those of their affiliated organizations, or those of the publisher, the editors and the reviewers. Any product that may be evaluated in this article, or claim that may be made by its manufacturer, is not guaranteed or endorsed by the publisher.

Supplementary material

The Supplementary Material for this article can be found online at: <https://www.frontiersin.org/articles/10.3389/fonc.2022.959309/full#supplementary-material>

SUPPLEMENTARY VIDEO 1
Procedure of endoscopic implantation.

References

- Murgu SD, Egressy K, Laxmanan B, Doblare G, Ortiz-Comino R, Hogarth DK. Central airway obstruction: Benign strictures, tracheobronchomalacia, and malignancy-related obstruction. *Chest* (2016) 150:426–41. doi: 10.1016/j.chest.2016.02.001
- Global Burden of Disease Cancer Collaboration, Fitzmaurice C, Akinyemiju TF, Al Lami FH, Alam T, Alizadeh-Navaei R, et al. Global, regional, and national cancer incidence, mortality, years of life lost, years lived with disability, and disability-adjusted life-years for 29 cancer groups 1990 to 2016: A systematic analysis for the global burden of disease study. *JAMA Oncol* (2018) 4:1553–68. doi: 10.1200/JCO.2018.36.15_suppl.1568
- Gorden JA, Ernst A. Endoscopic management of central airway obstruction. *Semin Thorac Cardiovasc Surg* (2009) 21:263–73. doi: 10.1053/j.semtcvs.2009.08.002
- Ost David E, Ernst A, Grosu HB, Lei X, Diaz-Mendoza J, Slade M, et al. Complications following therapeutic bronchoscopy for malignant central airway obstruction: Results of the AQUIRE registry. *Chest* (2015) 148:450–71. doi: 10.1378/chest.14-1530
- Phillips MJ. Malignant airway obstruction: What to do? *Respirology* (2018) 23:803–4. doi: 10.1111/resp.13343
- Ost DE, Shah AM, Lei X, Godoy MCB, Jimenez CA, Eapen GA, et al. Respiratory infections increase the risk of granulation tissue formation following airway stenting in patients with malignant airway obstruction. *Chest* (2012) 141:1473–81. doi: 10.1378/chest.11-2005
- Shan Q, Huang W, Shang M, Wang Z, Xia N, Xue Q, et al. Customization of stent design for treating malignant airway stenosis with the aid of three-dimensional printing. *Quant Imaging Med Surg* (2021) 11:1437–46. doi: 10.21037/qims-20-727
- Hohenforst-Schmidt W, Zarogoulidis P, Pitsiou G, Linsmeier B, Tsavlis D, Kioumis I, et al. Drug eluting stents for malignant airway obstruction: A critical review of the literature. *J Cancer* (2016) 7:377–90. doi: 10.7150/jca.13611
- Wang Y, Lu J, Guo J-H, Zhu GY, Zhu HD, Chen L, et al. A novel tracheobronchial stent loaded with I seeds in patients with malignant airway obstruction compared to a conventional stent: A prospective randomized controlled study. *EBioMedicine* (2018) 33:269–75. doi: 10.1016/j.ebiom.2018.06.006
- Gesierich W, Reichenberger F, Fertl A, Haeussinger K, Sroka R. Endobronchial therapy with a thulium fiber laser, (1940 nm). *J Thorac Cardiovasc Surg* (2014) 147:1827–32. doi: 10.1016/j.jtcvs.2013.12.038
- Benn BS, Krishna G. A novel multimodal approach to treating proximal tracheal obstructions with spray cryotherapy. *J Thorac Dis* (2019) 11:613–7. doi: 10.21037/jtd.2018.11.134
- Shope RE, Hurst EW. Infectious papillomatosis of rabbits : with a note on the histopathology. *J Exp Med* (1933) 58:607–24. doi: 10.1084/jem.58.5.607
- Prins FM, Kerkmeijer LGW, Pronk AA, Vonken EPA, Meijer RP, Bex A, et al. Renal cell carcinoma: Alternative nephron-sparing treatment options for small renal masses, a systematic review. *J Endourol* (2017) 31:963–75. doi: 10.1089/end.2017.0382
- Huang J, Shuang J, Xiong G, Wang X, Zhang Y, Tang X, et al. Establishing a rabbit model of malignant esophagostenosis using the endoscopic implantation technique for studies on stent innovation. *J Transl Med* (2014) 12:40. doi: 10.1186/1479-5876-12-40
- Gregor A, Fujino K, Bernards N, Kinoshita T, Motooka Y, Inage T, et al. Rabbit VX2 lung tumor models can form early nodal metastases. *World J Surg Oncol* (2019) 17:231. doi: 10.1186/s12957-019-1774-6
- Nakagishi Y, Morimoto Y, Fujita M, Ozeki Y, Maehara T, Kikuchi M, et al. Rabbit model of airway stenosis induced by scraping of the tracheal mucosa. *Laryngoscope* (2005) 115:1087–92. doi: 10.1097/01.MLG.0000163105.86513.6D
- Li Z, Jiao D, Zhang W, Ren K, Qiu L, Tian C, et al. Antibacterial and antihyperplasia polylactic acid/silver nanoparticles nanofiber membrane-coated airway stent for tracheal stenosis. *Colloids Surf B Biointerfaces* (2021) 206:111949. doi: 10.1016/j.colsurfb.2021.111949
- Freitag L, Ernst A, Unger M, Kovitz K, Marquette CH. A proposed classification system of central airway stenosis. *Eur Respir J* (2007) 30:7–12. doi: 10.1183/09031936.00132804
- Wang Y, Guo J-H, Zhu G-Y, Zhu HD, Chen L, Lu J, et al. A novel self-expandable, radioactive airway stent loaded with I seeds: A feasibility and safety study in healthy beagle dog. *Cardiovasc Intervent Radiol* (2017) 40:1086–93. doi: 10.1007/s00270-017-1639-8
- Motooka Y, Fujino K, Gregor A, Bernards N, Chan H, Inage T, et al. Endobronchial ultrasound-guided radiofrequency ablation of lung tumors and mediastinal lymph nodes: A preclinical study in animal lung tumor and mediastinal adenopathy models. *Semin Thorac Cardiovasc Surg* (2020) 32:570–8. doi: 10.1053/j.semtcvs.2020.02.003
- Nakagishi Y, Morimoto Y, Fujita M, Morimoto N, Ozeki Y, Maehara T, et al. Photodynamic therapy for airway stenosis in rabbit models. *Chest* (2008) 133:123–30. doi: 10.1378/chest.07-1410
- Nakagishi Y, Morimoto N, Fujita M, Ozeki Y, Maehara T, Kikuchi M, et al. Amelioration of airway stenosis in rabbit models by photodynamic therapy with talaporfin sodium (NPe6). *Photochem Photobiol* (2009) 85:714–8. doi: 10.1111/j.1751-1097.2008.00472.x
- Chen JH, Lin YC, Huang YS, Chen TJ, Lin WY, Han KW, et al. Induction of VX2 carcinoma in rabbit liver: comparison of two inoculation methods. *Lab Anim* (2004) 38:79–84. doi: 10.1258/00236770460734434
- Sun J-H, Zhang Y-L, Nie C-H, Yu XB, Xie HY, Zhou L, et al. Considerations for two inoculation methods of rabbit hepatic tumors: Pathology and image features. *Exp Ther Med* (2012) 3:386–90. doi: 10.3892/etm.2011.435



OPEN ACCESS

EDITED BY

Grigoris Stratakis,
National and Kapodistrian University of
Athens, Greece

REVIEWED BY

Semra Paydaş,
Çukurova University, Turkey
Changjing Zuo,
Second Military Medical University,
China

*CORRESPONDENCE

Jin Sun
wander21@126.com

SPECIALTY SECTION

This article was submitted to
Thoracic Oncology,
a section of the journal
Frontiers in Oncology

RECEIVED 03 June 2022

ACCEPTED 11 August 2022

PUBLISHED 14 September 2022

CITATION

Hu Y, Sun J, Li D, Li Y, Li T and Hu Y
(2022) The combined role of PET/CT
metabolic parameters and
inflammatory markers in detecting
extensive disease in small cell
lung cancer.
Front. Oncol. 12:960536.
doi: 10.3389/fonc.2022.960536

COPYRIGHT

© 2022 Hu, Sun, Li, Li, Li and Hu. This is
an open-access article distributed under
the terms of the [Creative Commons
Attribution License \(CC BY\)](#). The use,
distribution or reproduction in other
forums is permitted, provided the
original author(s) and the copyright
owner(s) are credited and that the
original publication in this journal is
cited, in accordance with accepted
academic practice. No use,
distribution or reproduction is
permitted which does not comply with
these terms.

The combined role of PET/CT metabolic parameters and inflammatory markers in detecting extensive disease in small cell lung cancer

Yao Hu¹, Jin Sun^{2*}, Danming Li³, Yangyang Li²,
Tiannv Li² and Yuxiao Hu¹

¹Department of PET/CT Center, Jiangsu Cancer Hospital and Jiangsu Institute of Cancer Research and the Affiliated Cancer Hospital of Nanjing Medical University, Nanjing, China, ²Department of Nuclear Medicine, The First Affiliated Hospital of Nanjing Medical University, Nanjing, China, ³Department of Radiation Oncology, The First Affiliated Hospital of Nanjing Medical University, Nanjing, China

The combined role of inflammatory markers [including neutrophil/lymphocyte ratio (NLR), platelet/lymphocyte ratio (PLR), monocyte/lymphocyte ratio (MLR), and systemic immune-inflammation index (SII)] and PET/CT metabolic parameters [including maximum standardized uptake value (SUVmax), mean standardized uptake value (SUVmean), metabolic tumor volume (MTV), and TLG (total lesion glycolysis)] at baseline in evaluating the binary stage [extensive-stage disease (ED) and limited-stage disease (LD)] of small cell lung cancer (SCLC) is unclear. In this study, we verified that high metabolic parameters and inflammatory markers were related to the binary stage of SCLC patients, respectively ($p < 0.05$). High inflammatory markers were also associated with high MTV and TLG in patients with SCLC ($p < 0.005$). Moreover, the incidences of co-high metabolic parameters and inflammatory markers were higher in ED-SCLC ($p < 0.05$) than those in LD-SCLC. Univariate logistic regression analysis demonstrated that ^{Co-high} MTV/NLR, ^{Co-high} MTV/MLR, ^{Co-high} MTV/SII, ^{Co-high} TLG/NLR, ^{Co-high} TLG/MLR, and ^{Co-high} TLG/SII were significantly related to the binary stage of SCLC patients ($p = 0.00$). However, only ^{Co-high} MTV/MLR was identified as an independent predictor for ED-SCLC (odds ratio: 8.67, 95% confidence interval CI: 3.51–21.42, $p = 0.000$). Our results suggest that co-high metabolic parameters and inflammatory markers could be of help for predicting ED-SCLC at baseline. Together, these preliminary findings may provide new ideas for more accurate staging of SCLC.

KEYWORDS

SCLC, inflammatory markers, metabolic parameters, PET/CT, MTV/MLR

Introduction

Lung cancer is one of the main causes of cancer-related death in the world (1, 2). According to pathology, lung cancer is mainly divided into adenocarcinoma, squamous cell carcinoma, small cell lung cancer (SCLC), and so on. Among them, SCLC accounts for about 15%, with the characteristics of early metastasis, easy recurrence, and low 5-year survival rate (as low as 5%–10%) (2). According to a binary stage method in most of the articles, SCLC is classified into limited-stage disease (LD-SCLC) confined to the ipsilateral hemithorax and extensive-stage disease (ED-SCLC) spread beyond the ipsilateral hemithorax, the former including contralateral mediastinal and ipsilateral supraclavicular lymph nodal metastases and the latter including hematogenous metastases and malignant pleural or pericardial effusion (3). The management of different stages are completely different in SCLC patients (4). Chemoradiotherapy is the standard treatment of LD-SCLC patients. While a proposed treatment program for ED-SCLC is systemic chemotherapy, which could offer rapid responses and the best palliation. The median survival times of LD-SCLC and ED-SCLC are only 15–20 months and 8–13 months (4), respectively. Therefore, correct staging is pivotal regarding the selection of appropriate and effective treatment strategies for individual patients with SCLC.

^{18}F -fluorodeoxyglucose (^{18}F -FDG) positron-emission tomography (PET)/computed tomography (CT), providing both functional and morphological data, is a systemic non-invasive imaging technique and used in tumor staging, treatment responses and recurrence diagnosis (5, 6). Maximum standardized uptake value (SUVmax), mean standardized uptake value (SUVmean), metabolic tumor volume (MTV), and total lesion glycolysis (TLG) are used as semi-quantitative parameters of PET/CT, which reflect the local metabolism and the biological aggressiveness of tumors (7). However, the use of PET/CT is still controversial since some previous studies showed that false-positive results affected stage for SCLC patients by using PET/CT (5). Hence, the metabolic parameters *via* PET/CT are not sufficient to evaluate the binary stage of SCLC. The FDG uptake in lesions is affected by many different factors including infection and inflammation (8). The SCLC patients with normal blood counts are advised to conduct a bone marrow biopsy in order to exclude bone marrow involvement (4). Recent studies have confirmed that inflammation plays significant roles in tumor microenvironment, where it influences tumor development, progression, and treatment response (9). Meanwhile, a growing body of evidence indicated that increased levels of serum inflammatory markers such as neutrophil/lymphocyte ratio (NLR), platelet/lymphocyte ratio (PLR), monocyte/lymphocyte ratio (MLR), and systemic immune-inflammation index (SII) correlated with the stage of malignancies [e.g., non-small cell lung cancer (NSCLC) (10), renal cell carcinoma (11),

and colon cancer (12)]. Drawing on the above discoveries, the combined evaluation of metabolic parameters and inflammatory markers may be highly effective in detecting binary stage for SCLC at baseline.

However, to our knowledge, there are rare studies on the correlation between PET/CT semi-quantitative parameters and inflammatory markers in detecting the binary stage of SCLC. Therefore, the purpose of this study was to evaluate the relationship between inflammatory markers (NLR, PLR, MLR, and SII) in peripheral blood and semi-quantitative parameters (SUVmax, SUVmean, MTV, and TLG) *via* PET/CT and their combined role on detecting ED-SCLC.

Materials and methods

Subjects

All patients with SCLC underwent PET/CT scanning between January 2016 and June 2019 at the First Affiliated Hospital of Nanjing Medical University. Clinical data such as gender, age, smoking history, and hematological parameters [e.g., neutrophil (N), monocyte (M), lymphocyte (L), and platelet (P) counts] closest to the day of PET/CT scanning were collected. The Department of Clinical Laboratory of the First Affiliated Hospital of Nanjing Medical University performed the data analyses. Inflammatory markers based on N, M, L, and P—NLR, MLR, PLR, and SII—were calculated using the formula N/L , M/L , P/L , and $P \times N/L$, respectively. The inclusion criteria were as follows (1): diagnosed with SCLC by surgical or biopsy specimens (2); did not undergo any treatment before PET/CT scanning and inflammatory marker measurement (3); PET/CT scanning performed within 1 week after inflammatory marker measurement (4); diagnosis of pleural effusion, pericardial effusion, lymph node, and distant organ metastasis by pathological examination and imaging examination such as contrast enhanced CT (CECT), PET/CT, and magnetic resonance imaging (MRI); and (5) without other tumors and without other diseases that alter hematological parameters. The study was approved by the Ethics Committee of the First Affiliated Hospital of Nanjing Medical University.

^{18}F -FDG PET/CT scanning

^{18}F -FDG PET/CT (Biograph 16HR; Siemens, Germany) examinations were acquired after fasting for 6 h and 60–75 min after intravenous injection of ^{18}F -FDG (3.70–5.55 MBq/kg weight). The blood glucose level was below 120 mg/dl in all included patients before tracer injection. All patients had normal tidal breathing during PET and CT scans. Patients underwent low-dose CT scans (120–140 kV, 65 mA and 5.0 mm slice), followed by PET scans with six to eight bed positions (2 min per

bed positions) per patient based on the height. The PET images were reconstructed with attenuation corrected CT using the ordered subset expectation maximization (OSEM) algorithm. Then, all data were transferred in DICOM format to the Beth Israel PET/CT viewer plugin for FIJI and displayed as axial, coronal, and sagittal images. The SUVmax, SUVmean, MTV, and TLG of all lesions were delineated semiautomatically by the Beth Israel PET/CT viewer plugin for FIJI (<http://sourceforge.net/projects/bifijiplugins/>) (ImageJ distribution) (13).

Statistical analysis

Data were analyzed using SPSS 25.0 software (SPSS, IL, USA). Data in accordance with normal distribution were expressed as the mean \pm standard deviation (SD) values, while non-normal distribution data were expressed as median (interquartile interval). Statistical differences between groups were assessed by *t*-test or Mann–Whitney *U* test. *t*-test was performed for data in accordance with normal distribution, while non-normal distribution data were analyzed by Mann–Whitney *U* test. A Chi-square test was performed for rate comparisons. Receiver operating characteristic (ROC) curve analysis was performed to find optimal cutoff values of NLR, MLR, SII, MTV, and TLG to predict ED-SCLC. The area under curve (AUC) was calculated as a measure of the accuracy of the test. Logistic regression analysis was used to assay the association of patients' clinical features, inflammatory markers, and metabolic parameters in detecting ED-SCLC. *p*-value < 0.05 was considered to be statistically significant.

Results

Patients' characteristics

A total of 119 patients met the inclusion criteria and were enrolled in our study. Of these 119 patients, the median age was 64 (range: 25–91) years; 105 (64.6%) were male; 14 were female; 92 had a history of smoking; 47 SCLC patients were diagnosed with ED-SCLC, which spread beyond the ipsilateral hemithorax (Table 1). Median SUVmax, SUVmean, MTV, and TLG values for all lesions and median NLR, PLR, MLR, and SII values of the patients are shown in Table 1.

Correlation of inflammatory markers with clinical features and binary stage of SCLC

In patients with SCLC, NLR, PLR, MLR, and SII were significantly higher in ED-SCLC than LD-SCLC ($p > 0.05$, Table 2). Furthermore, we found that MLR is higher in patients older than 64 years. NLR, MLR, and SII are higher in male patients than female patients. NLR and SII are higher in patients with smoking than those without smoking (Table 2). With a cutoff value of 2.64, 170.67, 0.31, and 583.1, high NLR, PLR, MLR, and SII could respectively predict ED-SCLC ($p < 0.05$, Figure 1).

Correlation of metabolic parameters of SCLC with clinical features and binary stage of SCLC

In patients with SCLC, SUVmean, MTV, and TLG were higher in ED-SCLC compared to those in LD-SCLC, respectively ($p > 0.05$), whereas SUVmax in patients with ED and those with LD were not significantly different (Table 3). With a cutoff value of 7.69, 61.36, and 405.85, high MTV and TLG could separately predict ED-SCLC ($p < 0.05$, Figure 2), while ROC analysis revealed that SUVmax could not predict ED-SCLC ($p = 0.123$ and 0.087). There were no significant differences in SUVmax, SUVmean, MTV, and TLG observed in SCLC patients with different age and smoking (Table 3).

Correlation of high metabolic parameters of SCLC with increased inflammatory markers

All SCLC patients were divided into low-MTV (or low-TLG) and high-MTV (or high-TLG) groups by cutoff values of 61.36 (or 405.85) (the cutoff value predicting ED-SCLC). The results showed that the NLR, PLR, MLR, and SII were higher in the high-MTV or high-TLG patients than in the low-MTV or low-TLG patients, respectively ($p < 0.05$, Table 4).

Correlation of co-high metabolic parameters/inflammatory markers with binary stage of SCLC

Patients with SCLC were grouped into ^{co-low} MTV/NLR or ^{co-low} MTV/MLR or ^{co-low} MTV/SII, ^{low} MTV/^{high} NLR or ^{low} MTV/^{high} MLR or ^{low} MTV/^{high} SII, ^{high} MTV/^{low} NLR or ^{high} MTV/^{low} MLR, and ^{co-high} MTV/NLR or ^{co-high} MTV/MLR groups, respectively, based on the corresponding cutoff values (the cutoff value predicting ED-SCLC). TLG was the same as above. The results showed that the incidences of ^{Co-high} MTV/NLR, ^{Co-high} MTV/PLR, ^{Co-high} MTV/MLR, ^{Co-high} MTV/SII, ^{Co-high} TLG/NLR, ^{Co-high} TLG/PLR, ^{Co-high} TLG/MLR, and ^{Co-high} TLG/SII were higher in ED-SCLC patients than those in LD-SCLC, respectively ($p = 0.000$, Table 5). The incidences of ^{Co-high} MTV/NLR, ^{Co-high} MTV/MLR, ^{Co-high} MTV/SII, ^{Co-high} TLG/NLR, ^{Co-high} TLG/MLR, and ^{Co-high} TLG/SII were higher in male patients than those in female patients, respectively (Table 5). The incidences of ^{Co-high} MTV/MLR and ^{Co-high} TLG/MLR were higher in patients older than 64 years. However, the MTV and TLG of all lesions and NLR, PLR, MLR, or SII status did not exhibit a significant relationship with smoking.

Univariate analysis revealed that ^{Co-high} MTV/NLR ($p = 0.000$), ^{Co-high} MTV/PLR ($p = 0.001$), ^{Co-high} MTV/MLR ($p = 0.000$), ^{Co-high} MTV/SII ($p = 0.000$), ^{Co-high} TLG/NLR ($p = 0.000$), ^{Co-high} TLG/PLR ($p = 0.005$), ^{Co-high} TLG/MLR ($p = 0.000$), ^{Co-high} TLG/SII ($p = 0.001$), and smoking were related to the binary stage of SCLC (Table 6). Multivariate analysis further revealed that only ^{Co-high} MTV/MLR [odds ratio (OR): 8.67, 95% CI: 3.51–21.42, $p = 0.000$] was an independent predictor for ED-SCLC (Table 6). However, the gender and age did not exhibit a significant relationship with the binary stage of SCLC (Table 6).

TABLE 1 Patient characteristics.

	Number (<i>n</i> = 119)	Value
Gender		
Male	105 (88.2%)	
Female	14 (11.8%)	
Age		
≤64	59 (49.6%)	
>64	60 (50.4%)	
Smoking		
Yes	92 (77.3%)	
No	27 (22.7%)	
Tumor Stage		
LD-SCLC	72 (60.5%)	
ED-SCLC	47 (39.5%)	
Inflammatory markers		
NLR		2.63 (0.30, 17.86)
PLR		132.49 (48.70, 561.19)
MLR		0.28 (0.04, 2.49)
SII		541.01 (47.88, 2,410.20)
Metabolic parameters		
SUVmax		12.78 (5.39, 47.34)
SUVmean		6.87 (3.17, 21.49)
MTV		65.58 (2.95, 1,208.91)
TLG		468.25 (19.77, 6,965.86)

Discussion

In this study, our results revealed that the baseline inflammatory markers (NLR, MLR, PLR, and SII) and metabolic parameters (MTV and TLG) were significantly correlated with the binary stage of SCLC. In addition, hematological parameters (NLR, MLR, PLR, and SII) were significantly associated with MTV and TLG in SCLC patients. More importantly, co-high semi-quantitative parameters (MTV

and TLG) and hematological parameters (NLR, MLR, PLR, and SII) were significantly related to ED-SCLC, but only ^{Co-high} MTV/MLR was identified as an independent predictor for ED-SCLC.

Growing evidence has demonstrated that inflammatory markers (NLR, PLR, MLR, and SII) in peripheral blood have been suggested to be correlated with the stage of different tumors, such as NSCLC (10), renal cell carcinoma (11), and colon cancer (12). Oner et al. (11) demonstrated that NLR and

TABLE 2 Analysis of inflammatory markers in patients with SCLC (*n* = 119).

	NLR	<i>p</i>	PLR	<i>p</i>	MLR	<i>p</i>	SII	<i>p</i>
Age								
≤64	2.48 (1.00, 8.69)	0.992	143.59 (54.40, 390.00)	0.103	0.26 (0.04, 2.06)	0.019	580.32 (136.54, 2410.20)	0.116
>64	2.87 (0.30, 17.86)		117.91 (48.70, 561.19)		0.35 (0.08, 2.49)		496.51 (47.88, 2201.47)	
Gender								
Male	2.86 (2.01, 3.61)	0.005	132.71 (105.73, 168.22)	0.062	0.28 (0.22, 0.42)	0.007	565.83 (403.96, 802.21)	0.007
Female	1.72 (0.66, 14.68)		99.35 (48.70, 441.18)		0.21 (0.04, 0.47)		316.10 (123.22, 2201.47)	
Smoking								
Yes	2.78 (0.30, 16.40)	0.036	138.88 (54.40, 561.19)	0.125	0.29 (0.08, 2.49)	0.079	595.21 (47.88, 2410.20)	0.025
No	1.96 (0.66, 17.86)		113.66 (48.70, 366.97)		0.25 (0.04, 1.86)		425.75 (123.22, 1988.99)	
Tumor Stage								
LD-SCLC	2.23 (0.30, 6.87)	0.001	123.11 (48.70, 390.00)	0.019	0.26 (0.04, 2.06)	0.002	460.84 (47.88, 2410.20)	0.007
ED-SCLC	3.17 (1.00, 17.86)		149.33 (54.40, 561.19)		0.37 (0.08, 2.49)		737.47 (136.54, 2201.47)	

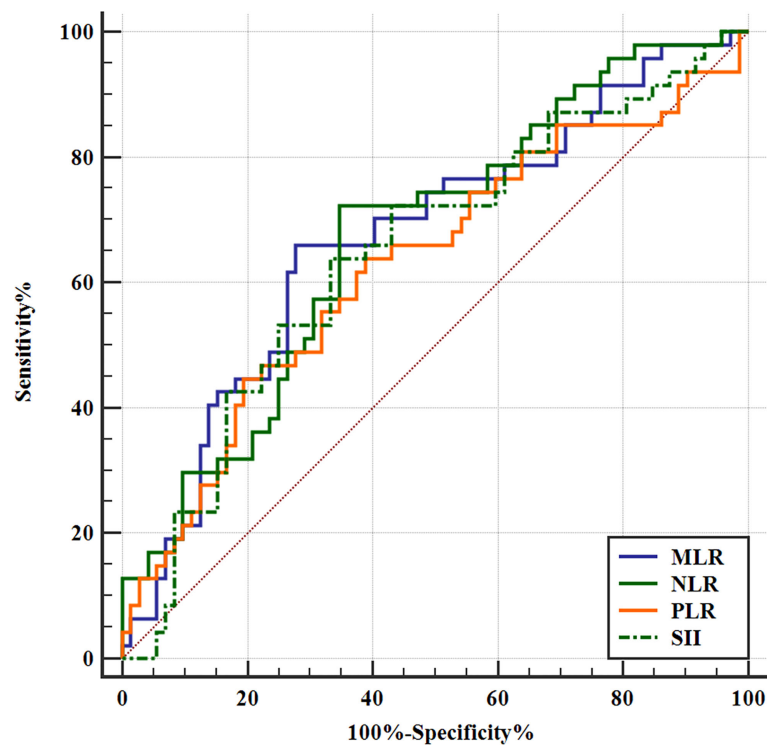


FIGURE 1

Receiver operating characteristic (ROC) curves of inflammatory markers for predicting binary stage of SCLC. NLR, PLR, MLR, and SII could predict the binary stage of SCLC. The ROC curve analysis of the NLR to predict ED-SCLC. With an NLR of 2.64 as the threshold, the sensitivity and specificity in the prediction of ED-SCLC were 72.34% and 65.28%, respectively. The AUC was 0.672 (95% confidence interval [CI]: 0.580–0.756; $p = 0.0006$). The ROC curve analysis of the PLR to predict ED-SCLC. With an PLR of 170.67 as the threshold, the sensitivity and specificity for the prediction of ED-SCLC were 44.68% and 80.56%, respectively. The AUC was 0.628 (95% CI: 0.535–0.715; $p = 0.0178$). The ROC curve analysis of the MLR to predict ED-SCLC. With an MLR of 0.31 as the threshold, the sensitivity and specificity for the prediction of ED-SCLC were 65.96% and 70.83%, respectively. The AUC was 0.669 (95% CI: 0.577–0.753; $p = 0.0010$). The ROC curve analysis of the SII to predict ED-SCLC. With an SII of 583.1 as the threshold, the sensitivity and specificity for the prediction of ED-SCLC were 63.83% and 66.67%, respectively. The AUC was 0.646 (95% CI: 0.553–0.731; $p = 0.0055$).

TABLE 3 Analysis of metabolic parameters of SCLC on PET/CT scanning ($n = 119$).

	SUVmax	<i>p</i>	SUVmean	<i>p</i>	MTV (cm^3)	<i>p</i>	TLG (g)	<i>p</i>
Age		0.987		0.782		0.564		0.644
≤64	12.83 (5.39, 47.34)		6.84 (3.33, 21.49)		71.28 (4.29, 1,208.91)		476.35 (28.85, 5,530.39)	
>64	12.78 (5.85, 25.53)		7.02 (3.17, 20.88)		64.34 (2.95, 1,091.43)		461.58 (19.77, 6,965.86)	
Gender		0.817		0.332		0.040		0.096
Male	12.78 (5.39, 47.34)		6.86 (3.17, 21.49)		71.28 (2.95, 1,208.91)		482.41 (19.77, 6,965.86)	
Female	12.88 (7.06, 21.20)		7.42 (3.90, 13.28)		31.92 (7.24, 120.97)		237.66 (34.54, 1,606.65)	
Smoking		0.172		0.133		0.211		0.198
Yes	13.02 (5.39, 47.34)		7.07 (3.17, 21.49)		72.13 (2.95, 1,208.91)		487.74 (19.77, 6,965.86)	
No	11.91 (6.12, 25.53)		6.24 (3.49, 11.94)		41.58 (7.24, 1,091.43)		317.70 (34.54, 5,556.47)	
Tumor Stage		0.788		0.018		0.000		0.000
LD-SCLC	12.78 (5.85, 26.12)		7.42 (3.32, 14.88)		38.93 (2.95, 299.21)		290.37 (19.77, 4,267.74)	
ED-SCLC	12.83 (5.39, 47.34)		6.43 (3.17, 36.25)		161.81 (7.58, 1,208.91)		1126.64 (43.66, 6,965.86)	

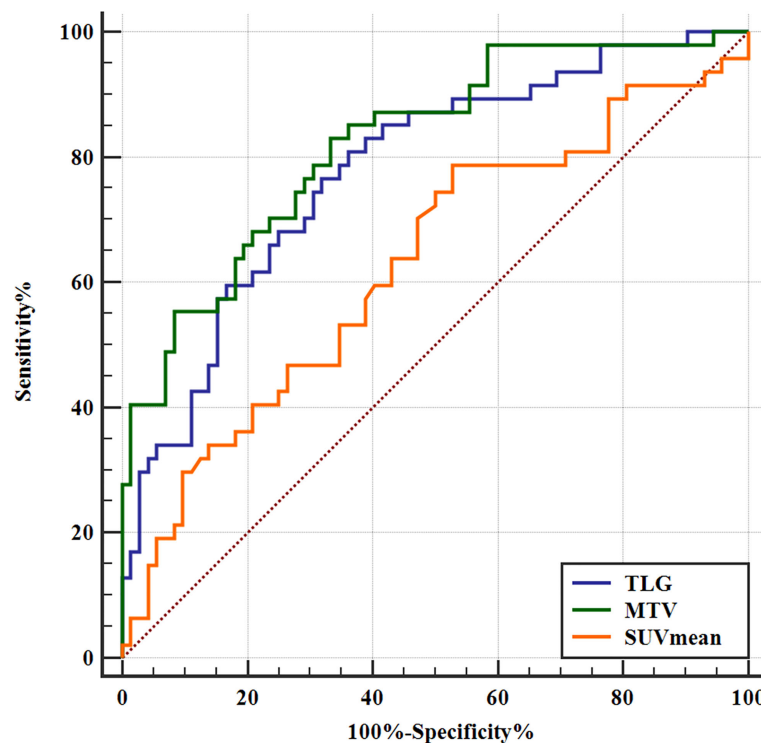


FIGURE 2

Receiver operating characteristic (ROC) curves of SUVmean, MTV, and TLG for predicting binary stage of SCLC. The SUVmean, MTV, and TLG could predict tumor stage. The ROC curve analysis of the SUVmean to predict ED-SCLC. With an SUVmean of 7.69 as the threshold, the sensitivity and specificity in the prediction of ED-SCLC were 78.72% and 47.22%, respectively. The AUC was 0.628 (95% CI: 0.535–0.715; $p = 0.0166$). The ROC curve analysis of the MTV to predict ED-SCLC. With an MTV of 61.36 as the threshold, the sensitivity and specificity in the prediction of ED-SCLC were 82.98% and 66.67%, respectively. The AUC was 0.823 (95% CI: 0.742–0.887; $p < 0.0001$). The ROC curve analysis of the TLG to predict ED-SCLC. With a TLG of 405.85 as the threshold, the sensitivity and specificity for the prediction of ED-SCLC were 80.85% and 63.89%, respectively. The AUC was 0.779 (95% CI: 0.694–0.850; $p < 0.0001$).

LMR predicted the late stage in renal cell carcinoma. In a study of colon cancer and NSCLC, Uludag et al. (12) and Goksel et al. (10) showed that NLR and PLR were significantly higher in late stage than those in early stage. In accordance with the previous studies, our study suggested that hematological parameters (NLR, PLR, MLR, and SII) were correlated with the binary stage in patients with SCLC. High NLR, MLR, and SII can be caused by increased neutrophils and monocytes or/and decreased lymphocytes in peripheral blood. Inflammation cells are known to be considered as part of the tumor microenvironment and promote development (14). Monocytes

or neutrophils could directly form complexes with tumor cells and mediate migration in blood vessel (15). The complexes help metastatic seeds escape immune surveillance, while lymphocytes prevent the development of cancer by secreting protective inflammatory factors (16). Platelets also secrete inflammatory factors (e.g., vascular endothelial growth factor, VEGF) to facilitate tumor angiogenesis and metastasis (17). All the above theories suggested that baseline NLR, MLR, PLR, and SII might predict ED SCLC.

SUVmax reflects the maximum value of tumor metabolism. However, MTV and TLG are calculated based on the volume of

TABLE 4 Correlation of inflammatory markers with different MTV or TLG levels of SCLC.

	MTV (cm ³)		<i>p</i>	TLG (g)		<i>p</i>
	≤61.36 (56)	>61.36 (63)		≤405.85 (55)	>405.85 (64)	
NLR	2.13 (0.30, 6.31)	3.13 (1.00, 17.86)	0.000	2.14 (0.30, 8.69)	3.12 (1.00, 17.86)	0.001
PLR	118.22 (48.70, 384.62)	164.71 (154.40, 561.19)	0.001	120.30 (48.70, 384.62)	164.30 (54.40, 561.19)	0.001
MLR	0.25 (0.08, 0.81)	0.34 (0.04, 2.49)	0.008	0.26 (0.08, 0.81)	0.34 (0.04, 2.49)	0.019
SII	438.80 (47.88, 2233.15)	750.17 (136.54, 2410.20)	0.000	443.40 (47.88, 2233.15)	743.82 (136.54, 2410.20)	0.000

TABLE 5 Relationship of metabolic parameters and inflammatory markers with binary stage of SCLC.

	Tumor Stage		<i>p</i>	Gender		<i>p</i>
	LD-SCLC	ED-SCLC		Female	Male	
Co-low MTV/NLR	37	2	0.000	9	30	0.013
Low MTV/ ^{High} NLR	11	6		0	17	
High MTV/ ^{Low} NLR	10	11		3	18	
Co-high MTV/NLR	14	28		2	40	
Co-low MTV/PLR	44	6	0.000	9	41	0.207
Low MTV/ ^{High} PLR	4	2		0	6	
High MTV/ ^{Low} PLR	14	20		2	32	
Co-high MTV/PLR	10	19		3	26	
Co-low MTV/MLR	36	3	0.000	9	30	0.007
Low MTV/ ^{High} MLR	12	5		0	17	
High MTV/ ^{Low} MLR	15	13		4	24	
Co-high MTV/MLR	9	26		1	34	
Co-low MTV/SII	39	4	0.000	9	34	0.035
Low MTV/ ^{High} SII	9	4		0	13	
High MTV/ ^{Low} SII	9	13		3	19	
Co-high MTV/SII	15	26		2	39	
Co-low TLG/NLR	36	2	0.000	9	29	0.012
Low TLG/ ^{High} NLR	10	7		0	17	
High TLG/ ^{Low} NLR	11	11		3	19	
Co-high TLG/NLR	15	27		2	40	
Co-low TLG/PLR	43	6	0.000	9	40	0.183
Low TLG/ ^{High} PLR	3	3		0	6	
High TLG/ ^{Low} PLR	15	20		2	33	
Co-high TLG/PLR	11	18		3	26	
Co-low TLG/MLR	35	3	0.000	9	29	0.007
Low TLG/ ^{High} MLR	11	6		0	17	
High TLG/ ^{Low} MLR	16	13		4	25	
Co-high TLG/MLR	10	25		1	34	
Co-low TLG/SII	38	4	0.000	9	33	0.033
Low TLG/ ^{High} SII	8	5		0	13	
High TLG/ ^{Low} SII	10	13		3	20	
Co-high TLG/SII	16	25		2	39	

interest (VOI); thus, they may be better to reflect tumor metabolism and burden. In the previous study, ¹⁸F-FDG PET/CT is used as a reliable molecular imaging method for staging patients with SCLC (5). In the present study, we also explored the application of semi-quantitative parameters *via* ¹⁸F-FDG PET/CT to assess the binary stage in patients with SCLC. Our study demonstrated that SUVmean, MTV, and TLG were related to the binary stage of SCLC patients, but SUVmax was not. Apostolova et al. (18) reported that MTV and SUVmax were associated with stage in patients with NSCLC. In another study, Dolan et al. (19) demonstrated that an elevated TLG was correlated with TNM stage of NSCLC. In addition, Hu et al. (20) found that MTV and TLG were related to the stage in patients with adenocarcinoma, and only MTV was associated with stage in patients with squamous cell carcinoma. Based on

the above findings, the relationships between different metabolic parameters and the stage of lung cancer were not identical, but they could be used to evaluate the tumor stage for lung cancer. Although the pathological type and tumor stage in the present study are different from the previous studies, our results also supported this.

In addition, with the increase of MTV and TLG of SCLC patients, hematological parameters of NLR, PLR, MLR, and SII were elevated. A previous study reported that there were positive correlations between NLR and metabolic parameters (SUVmax, SUVmean, MTV, TLG, whole-body MTV, and TLG) *via* PET/CT in patients with SCLC (21). However, the PLR, MLR, and SII were respectively associated with MTV and TLG of SCLC in our study, which have not been reported before. To our knowledge, the underlying mechanism of relationship between

TABLE 6 Univariate and multivariate logistic regression analysis of potential relationships between patients' characteristics and binary stage of SCLC.

	Univariate <i>p</i> -value	Multivariate <i>p</i> -value	OR	95% CI for OR	
				Lower	Upper
Gender	0.057	0.184	4.50	0.96	21.12
Age	0.910	0.314	1.04	0.50	2.12
Smoking	0.042	0.163	2.81	1.04	7.62
Co-high MTV/NLR	0.000	0.241	6.11	2.68	13.93
Co-high MTV/PLR	0.001	0.416	4.21	1.73	10.21
Co-high MTV/MLR	0.000	0.000	8.67	3.51	21.42
Co-high MTV/SII	0.000	0.270	4.71	2.10	10.56
Co-high TLG/NLR	0.000	0.437	5.13	2.28	11.54
Co-high TLG/PLR	0.005	0.615	3.44	1.44	8.22
Co-high TLG/MLR	0.000	0.405	7.05	2.92	16.99
Co-high TLG/SII	0.001	0.432	3.98	1.79	8.84

inflammatory markers and metabolic parameters is undergoing investigation. A similar relationship between metabolic parameters and inflammatory markers was demonstrated in other cancers including colorectal cancer (22) and NSCLC (10). Xu et al. (22) suggested that SUVmax, MTV, and TLG were significantly associated with LMR and NLR. In a study of NSCLC, Goksel et al. (10) reported that MTV and TLG were positively related to NLR and PLR. These relationships between semi-parameters and hematological parameters in patients with different malignancies may be explained by certain opinions. On the one hand, inflammatory cells infiltrate primary tumors, resulting in the increase of ^{18}F -FDG uptake (23). On the other hand, the hypoxia promotes the secretion of VEGF by inflammatory cells, resulting in tumor angiogenesis and increase of ^{18}F -FDG uptake within tumor (24). The local tumor metabolism may have resulted from tumor metabolic itself and inflammatory cells (25). Interestingly, in the present study, we observed that the co-high MTV (or TLG) and inflammatory markers (NLR, PLR, MLR, and SII) were associated with ED-SCLC, but only $^{\text{co-high}}$ MTV/MLR was considered as an independent predictor for ED-SCLC. MTV represents the metabolic tumor volume of all lesions, and MLR reflects the host's systemic inflammatory response. These findings mean that $^{\text{co-high}}$ MTV/MLR might be not only more accurate, but also effective for detecting ED-SCLC in the present study. Therefore, the correlation between metabolic parameters *via* ^{18}F -FDG PET/CT and inflammatory markers needs further research. In a word, our results preliminarily demonstrated the synergistic effect of tumor metabolic activity with inflammatory markers in assessing the binary stage of SCLC.

SCLC has a close association with smoking, which is considered a factor in the development of SCLC (26, 27). Smoking has been proven to associate with inflammatory markers such as NLR, eosinophil-to-lymphocyte ratio (ELR),

and lymphocyte-to-monocyte ratio (LMR) (28). In this study, although there was no significant correlation between inflammatory markers of NLR, PLR, MLR, and SII or metabolic parameters with smoking status, the incidences of $^{\text{Co-high}}$ MTV/MLR, $^{\text{Co-high}}$ MTV/SII, $^{\text{Co-high}}$ TLG/MLR, and $^{\text{Co-high}}$ TLG/SII were higher in smokers than nonsmokers. Furthermore, smoking was not an independent predictor for the binary stage of SCLC, which is due to only few patients being never-smokers in this study. However, understanding the association between smoking, inflammation markers, tumor metabolism, and binary stage in SCLC patients needs additional research in the future.

There are some limitations in this study. Firstly, as a retrospective study, there are some limitations such as a great gender ratio difference, the lack of a control matched group, and the absence of a rigorous control of the inflammation-related lung diseases (e.g., obstructive pneumonia, interstitial pneumonia, and chronic obstructive pulmonary disease). Secondly, the sample size was relatively small and all patients were only from a single center. A multi-center prospective study with a larger sample size should be carried out in the future.

Conclusion

In conclusion, our results demonstrate that the baseline inflammatory markers (NLR, MLR, and SII) and tumor metabolic parameters are associated with the binary stage in patients with SCLC. Moreover, the co-high MTV/MLR based on metabolic tumor volume and systemic inflammatory response could be of help for predicting the ED-SCLC. However, further investigation needs to evaluate the combined role of inflammatory markers and tumor metabolic parameters *via* PET/CT in detecting ED-SCLC at baseline.

Data availability statement

The original contributions presented in the study are included in the article/Supplementary Material. Further inquiries can be directed to the corresponding author.

Ethics statement

The studies involving human participants were reviewed and approved by the Ethics Committee of the First Affiliated Hospital of Nanjing Medical University. The patients/participants provided their written informed consent to participate in this study.

Author contributions

JS, YH, YL, DL, TL, and YXH directly participated in the planning, execution or analysis of the study. JS, YH, and TL designed the study and interpreted the results. DL and YL contributed to collection of clinical dates. JS and YH drafted the manuscript. All authors contributed to the article and approved the submitted version.

References

1. Siegel RL, Miller KD, Fuchs HE, Jemal A. Cancer statistics, 2021. *CA Cancer J Clin* (2021) 71(1):7–33. doi: 10.3322/caac.21654
2. Kalemkerian GP. Small cell lung cancer. *Semin Respir Crit Care Med* (2016) 37(5):783–96. doi: 10.1055/s-0036-1592116
3. Kalemkerian GP, Loo BW, Akerley W, Attia A, Bassetti M, Bumber Y, et al. NCCN guidelines insights: Small cell lung cancer, version 2. 2018. *J Natl Compr Canc Netw* (2018) 16(10):1171–82. doi: 10.6004/jncn.2018.0079
4. Dingemans AC, Fruh M, Ardizzoni A, Besse B, Faivre-Finn C, Hendriks LE, et al. Small-cell lung cancer: ESMO clinical practice guidelines for diagnosis, treatment and follow-up(). *Ann Oncol* (2021) 32(7):839–53. doi: 10.1016/j.annonc.2021.03.207
5. Martucci F, Pascale M, Valli MC, Pesce GA, Froesch P, Giovanella L, et al. Impact of (18)F-FDG PET/CT in staging patients with small cell lung cancer: A systematic review and meta-analysis. *Front Med (Lausanne)* (2019) 6:336. doi: 10.3389/fmed.2019.00336
6. Farsad M. FDG PET/CT in the staging of lung cancer. *Curr Radiopharm* (2020) 13(3):195–203. doi: 10.2174/1874471013666191223153755
7. Wang Y, Han R, Wang Q, Zheng J, Lin C, Lu C, et al. Biological significance of (18)F-FDG PET/CT maximum standard uptake value for predicting EGFR mutation status in non-small cell lung cancer patients. *Int J Gen Med* (2021) 14:347–56. doi: 10.2147/IJGM.S287506
8. Reinfeld BI, Madden MZ, Wolf MM, Chytil A, Bader JE, Patterson AR, et al. Cell-programmed nutrient partitioning in the tumour microenvironment. *Nature* (2021) 593(7858):282–8. doi: 10.1038/s41586-021-03442-1
9. Grivennikov SI, Greten FR, Karin M. Immunity, inflammation, and cancer. *Cell* (2010) 140(6):883–99. doi: 10.1016/j.cell.2010.01.025
10. Goksel S, Cengiz A, Ozturk H, Yurekli Y. Prognostic impact of the (18)F-fluorodeoxyglucose positron-emission tomography/computed tomography metabolic parameters and correlation with hematological inflammatory markers in lung cancer. *J Cancer Res Ther* (2021) 17(4):925–30. doi: 10.4103/jcrt.JCRT_1046_20

Funding

This work was supported by grants from the National Jiangsu Provincial Health and Family Planning Commission Foundation (H2018029) and Research Project of Jiangsu Cancer Hospital (No. ZJ202122). These funders did participate in design, data collection, and analysis of the present study and have no role in the decision to publish the manuscript.

Conflict of interest

The authors declare that the research was conducted in the absence of any commercial or financial relationships that could be construed as a potential conflict of interest.

Publisher's note

All claims expressed in this article are solely those of the authors and do not necessarily represent those of their affiliated organizations, or those of the publisher, the editors and the reviewers. Any product that may be evaluated in this article, or claim that may be made by its manufacturer, is not guaranteed or endorsed by the publisher.

11. Oner I, Sackan F, Ozdemir D. Evaluation of the preoperative haematological parameters predicting the high T-stage and fuhrman grade in renal cell carcinoma. *J Coll Physicians Surg Pak* (2022) 32(4):461–6. doi: 10.29271/jcpsp.2022.04.461
12. Uludag SS, Sanli AN, Zengin AK, Ozcelik MF. Systemic inflammatory biomarkers as surrogate markers for stage in colon cancer. *Am Surg* (2022) 88(6):1256–62. doi: 10.1177/0003134821995059
13. Schindelin J, Arganda-Carreras I, Frise E, Kaynig V, Longair M, Pietzsch T, et al. Fiji: an open-source platform for biological-image analysis. *Nat Methods* (2012) 9(7):676–82. doi: 10.1038/nmeth.2019
14. Greten FR, Grivennikov SI. Inflammation and cancer: Triggers, mechanisms, and consequences. *Immunity* (2019) 51(1):27–41. doi: 10.1016/j.immuni.2019.06.025
15. Kalafati L, Mitroulis I, Verginis P, Chavakis T, Kourtzelis I. Neutrophils as orchestrators in tumor development and metastasis formation. *Front Oncol* (2020) 10:581457. doi: 10.3389/fonc.2020.581457
16. Zhao W, Wang P, Jia H, Chen M, Gu X, Liu M, et al. Lymphocyte count or percentage: which can better predict the prognosis of advanced cancer patients following palliative care? *BMC Cancer* (2017) 17(1):514. doi: 10.1186/s12885-017-3498-8
17. Best MG, Wesseling P, Wurdinger T. Tumor-educated platelets as a noninvasive biomarker source for cancer detection and progression monitoring. *Cancer Res* (2018) 78(13):3407–12. doi: 10.1158/0008-5472.CAN-18-0887
18. Apostolova I, Ego K, Steffen IG, Buchert R, Wertz H, Achenbach HJ, et al. The asphericity of the metabolic tumour volume in NSCLC: correlation with histopathology and molecular markers. *Eur J Nucl Med Mol Imaging*. (2016) 43(13):2360–73. doi: 10.1007/s00259-016-3452-z
19. Dolan RD, Maclay JD, Abbass T, Colville D, Buali F, MacLeod N, et al. The relationship between (18)F-FDG-PETCT-derived tumour metabolic activity, nutritional risk, body composition, systemic inflammation and survival in patients with lung cancer. *Sci Rep* (2020) 10(1):20819. doi: 10.1038/s41598-020-77269-7

20. Hu WD, Wang HC, Wang YB, Cui LL, Chen XH. Correlation study on 18F-FDG PET/CT metabolic characteristics of primary lesion with clinical stage in lung cancer. *Q J Nucl Med Mol Imaging*. (2021) 65(2):172–7. doi: 10.23736/S1824-4785.19.03146-7
21. Mirili C, Guney IB, Paydas S, Seydaoglu G, Kapukaya TK, Ogul A, et al. Prognostic significance of neutrophil/lymphocyte ratio (NLR) and correlation with PET-CT metabolic parameters in small cell lung cancer (SCLC). *Int J Clin Oncol* (2019) 24(2):168–78. doi: 10.1007/s10147-018-1338-8
22. Xu J, Li Y, Hu S, Lu L, Gao Z, Yuan H. The significant value of predicting prognosis in patients with colorectal cancer using (18)F-FDG PET metabolic parameters of primary tumors and hematological parameters. *Ann Nucl Med* (2019) 33(1):32–8. doi: 10.1007/s12149-018-1299-z
23. Kubota R, Yamada S, Kubota K, Ishiwata K, Tamahashi N, Ido T. Intratumoral distribution of fluorine-18-fluorodeoxyglucose *in vivo*: high accumulation in macrophages and granulation tissues studied by microautoradiography. *J Nucl Med* (1992) 33(11):1972–80.
24. Kwilas AR, Donahue RN, Tsang KY, Hodge JW. Immune consequences of tyrosine kinase inhibitors that synergize with cancer immunotherapy. *Cancer Cell Microenviron* (2015) 2(1):e677. doi: 10.14800/ccm.677
25. Du S, Sun H, Gao S, Xin J, Lu Z. Metabolic parameters with different thresholds for evaluating tumor recurrence and their correlations with hematological parameters in locally advanced squamous cell carcinoma: an observational (18)F-FDG PET/CT study. *Quant Imaging Med Surg* (2019) 9(3):440–52. doi: 10.21037/qims.2019.02.09
26. Hamilton G, Rath B. Smoking, inflammation and small cell lung cancer: recent developments. *Wien Med Wochenschr* (2015) 165(19–20):379–86. doi: 10.1007/s10354-015-0381-6
27. Schuller HM. The impact of smoking and the influence of other factors on lung cancer. *Expert Rev Respir Med* (2019) 13(8):761–9. doi: 10.1080/17476348.2019.1645010
28. Cekici Y, Yilmaz M, Secen O. New inflammatory indicators: association of high eosinophil-to-lymphocyte ratio and low lymphocyte-to-monocyte ratio with smoking. *J Int Med Res* (2019) 47(9):4292–303. doi: 10.1177/0300060519862077



OPEN ACCESS

EDITED BY

Xiaomin Niu,
Shanghai Jiao Tong University, China

REVIEWED BY

Song Xu,
Tianjin Medical University General
Hospital, China
Qiang Yan,
Taiyuan University of Technology,
China

*CORRESPONDENCE

Xue-ning Yang
yangxuening@gdph.org.cn
Yi-long Wu
syylwu@live.cn

[†]These authors have contributed
equally to this work

SPECIALTY SECTION

This article was submitted to
Thoracic Oncology,
a section of the journal
Frontiers in Oncology

RECEIVED 25 July 2022

ACCEPTED 20 September 2022

PUBLISHED 12 October 2022

CITATION

Liao R-q, Li A-w, Yan H-h, Lin J-t,
Liu S-y, Wang J-w, Fang J-s, Liu H-b,
Hou Y-h, Song C, Yang H-f, Li B,
Jiang B-y, Dong S, Nie Q, Zhong W-z,
Wu Y-l and Yang X-n (2022) Deep
learning-based growth prediction
for sub-solid pulmonary nodules
on CT images.
Front. Oncol. 12:1002953.
doi: 10.3389/fonc.2022.1002953

COPYRIGHT

© 2022 Liao, Li, Yan, Lin, Liu, Wang,
Fang, Liu, Hou, Song, Yang, Li, Jiang,
Dong, Nie, Zhong, Wu and Yang. This is
an open-access article distributed under
the terms of the [Creative Commons
Attribution License \(CC BY\)](https://creativecommons.org/licenses/by/4.0/). The use,
distribution or reproduction in other
forums is permitted, provided the
original author(s) and the copyright
owner(s) are credited and that the
original publication in this journal is
cited, in accordance with accepted
academic practice. No use,
distribution or reproduction is
permitted which does not comply with
these terms.

Deep learning-based growth prediction for sub-solid pulmonary nodules on CT images

Ri-qiang Liao^{1†}, An-wei Li^{2†}, Hong-hong Yan^{1†}, Jun-tao Lin¹,
Si-yang Liu¹, Jing-wen Wang², Jian-sheng Fang²,
Hong-bo Liu², Yong-he Hou³, Chao Song³, Hui-fang Yang³,
Bin Li⁴, Ben-yuan Jiang¹, Song Dong¹, Qiang Nie¹,
Wen-zhao Zhong¹, Yi-long Wu^{1*} and Xue-ning Yang^{1*}

¹Guangdong Lung Cancer Institute, Guangdong Provincial People's Hospital, Guangdong Academy of Medical Sciences, Guangzhou, China, ²Guangzhou Shiyuan Electronics Co., Ltd, Guangzhou, China, ³Yibicom Health Management Center, CVTE, Guangzhou, China, ⁴Automation Science and Engineering, South China University of Technology, Guangzhou, China

Background: Estimating the growth of pulmonary sub-solid nodules (SSNs) is crucial to the successful management of them during follow-up periods. The purpose of this study is to (1) investigate the measurement sensitivity of diameter, volume, and mass of SSNs for identifying growth and (2) seek to establish a deep learning-based model to predict the growth of SSNs.

Methods: A total of 2,523 patients underwent at least 2-year examination records retrospectively collected with sub-solid nodules. A total of 2,358 patients with 3,120 SSNs from the NLST dataset were randomly divided into training and validation sets. Patients from the Yibicom Health Management Center and Guangdong Provincial People's Hospital were collected as an external test set (165 patients with 213 SSN). Trained models based on LUNA16 and Lndb19 datasets were employed to automatically obtain the diameter, volume, and mass of SSNs. Then, the increase rate in measurements between cancer and non-cancer groups was studied to evaluate the most appropriate way to identify growth-associated lung cancer. Further, according to the selected measurement, all SSNs were classified into two groups: growth and non-growth. Based on the data, the deep learning-based model (SiamModel) and radiomics model were developed and verified.

Results: The double time of diameter, volume, and mass were 711 vs. 963 days ($P = 0.20$), 552 vs. 621 days ($P = 0.04$) and 488 vs. 623 days ($P < 0.001$) in the cancer and non-cancer groups, respectively. Our proposed SiamModel performed better than the radiomics model in both the NLST validation set and external test set, with an AUC of 0.858 (95% CI 0.786–0.921) and 0.760

(95% CI 0.646–0.857) in the validation set and 0.862 (95% CI 0.789–0.927) and 0.681 (95% CI 0.506–0.841) in the external test set, respectively. Furthermore, our SiamModel could use the data from first-time CT to predict the growth of SSNs, with an AUC of 0.855 (95% CI 0.793–0.908) in the NLST validation set and 0.821 (95% CI 0.725–0.904) in the external test set.

Conclusion: Mass increase rate can reflect more sensitively the growth of SSNs associated with lung cancer than diameter and volume increase rates. A deep learning-based model has a great potential to predict the growth of SSNs.

KEYWORDS

sub solid pulmonary nodules, growth, mass, deep learning, radiomics

Introduction

Lung cancer is the leading cause of cancer death, with an estimated 1.8 million deaths (18.0%) worldwide in 2020 (1). However, low-dose computed tomography (LDCT) is an effective screening tool for reducing lung cancer mortality in high-risk individuals (2). With the popularization of the LDCT for lung cancer screening, the detection rate for pulmonary nodules, particularly sub-solid nodules (SSNs), has been significantly improved (3).

SSNs, which include both ground-glass (GGNs) and part-solid (PSNs) nodules, have a higher likelihood of malignancy than solid nodules regardless of size (4). Although SSNs have a good prognosis when treated early, they are at serious risk of overdiagnosis and overtreatment (5). Further, predicting the growth of SSNs is crucial to the successful management of SSNs during follow-up periods. Compared with diameter and volume, an increase in mass is an early indicator of growth. However, manual measurement of tumor quality requires many human resources and is difficult to carry out in routine clinical practice (6). Artificial intelligence (AI) has provided great improvements in cancer imaging (7). For example, many studies have used radiomics and deep learning to progress their fields (8–12). However, in the field of SSNs, little progress has been made with the use of AI or other automatic methods.

Therefore, the aim of this study is to investigate the most sensitive measurement of diameter, volume, and mass, using automatic methods, for identifying the growth of SSNs, and further, to establish a deep learning-based model to predict the growth of SSNs based on consecutive computed tomography (CT) scans to provide evidence for follow-up and treatment plans.

Materials and methods

Study protocol

We retrospectively analyzed sub-solid nodule cases from the National Lung Screening Trial (NLST) (2) from August 2002 to December 2009, Yibicom Health Management Center from August 2017 to January 2022, and Guangdong Provincial People's Hospital from July 2011 to September 2021. The inclusion criteria for Yibicom Health Management Center and Guangdong Provincial People's Hospital were as follows: (a) $30 \leq \text{aged} \leq 80$ years old; (b) underwent at least 2-year examination records with thin-section (2.5 mm) CT images; (c) at least one sub-solid nodule; and (d) the diameter 5 and 30 mm of the sub-solid nodule on initial CT images. The exclusion criteria were as follows: (a) only received one CT examination; (b) follow-up time was less than 2 years from the first CT examination; and (c) combined with other malignant tumors with history of less than 5 years, except for lung cancer. If the patient had multiple sub-solid nodules, the largest of the two nodules meeting the above conditions was selected for the study.

In total, 2,358 patients with 3,120 SSNs from the NLST dataset were enrolled and were randomly divided into the training set (1,894 patients with 2,493 SSNs) and validation set (464 patients with 627 SSNs), according to the ratio of 8:2 (Figure 1). In addition, 165 patients with 213 SSNs from Yibicom Health Management Center and Guangdong Provincial People's Hospital were collected as an external test set (Figure 2).

CT examinations

Axial images from 7,177 LDCT/CT examinations (6,812 CT examinations of 2,358 patients from NLST, 365 CT examinations of 165 patients from our two hospitals) were included in this study and were reconstructed by standard or lung kernel. If there were more than three available CT examinations, the latest three exams were enrolled. In total, 9,411 sub-solid nodule volumes from the axial images were extracted to assess the growth (Figures 1, 2).

Image analysis

In order to analyze the changes in diameter, volume, and mass of SSNs over consecutive years, we followed the method in Fang et al., to pair the same nodules between different CT scans (13). Our data organization approach aimed to ascertain the diameter, volume, and mass change of SSNs in consecutive CT scans (Figure 3). A semiautomatic pipeline was developed to process the consecutive CT scans. First, we detected and identified the SSNs on original CT scans. We then performed 3D image registration for the second (T_i) and third (T_{i+1}) CT scans in terms of the first scan (T_{i-1}) and paired 3D volumes of interest (VOIs) containing SSNs to match the same sub-solid nodule at different time points. Next, we employed a segmenter to automatically crop out the lesion of nodules in VOIs to calculate their diameter, volume, and mass.

After automatically annotating, we performed a manual review to acquire reliable labels.

Specifically, two popular CT datasets, Lung Nodule Analysis (LUNA)16 (14) and Lung Nodule Database (LNDb) (15), were used to train our models (detector and segmenter), in which the detector for VOI identification was a 3D variant of CenterNet (16) and the segmenter for lesion segmentation was a multi-scale 3D UNet (17). The results of the detector on LUNA16 were FROC = 0.966, recall = 0.978, and precision = 0.654. The segmenter has a dice of 0.838 on LUNA16.

Growth measurement

There were three measurements for evaluating the growth of nodule, after semiautomatic acquisition of the nodule mask (1): the diameter, which was the longest side of the smallest circumscribed rectangle on the maximal surface of the nodule mask; (2) the volume (V in mm^3), which was computed by multiplying the voxel number and the volume of a single voxel; and (3) the mass, which was computed as follows: $M = V \times (A + 1,000)/1,000$ (18), where A is the average CT attenuation value (HU) and V is the volume of the nodule.

The SSNs from NLST were divided into cancer group and non-cancer group according to follow-up confirmation results. For each SSN, we calculated the increase rates of the diameter, volume, and mass during follow-up, respectively,

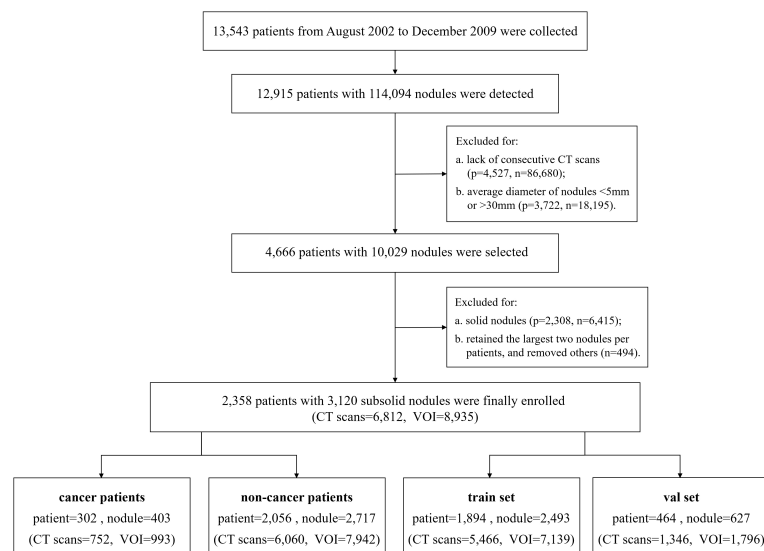


FIGURE 1
Flowchart of case selection on the NLST data set.

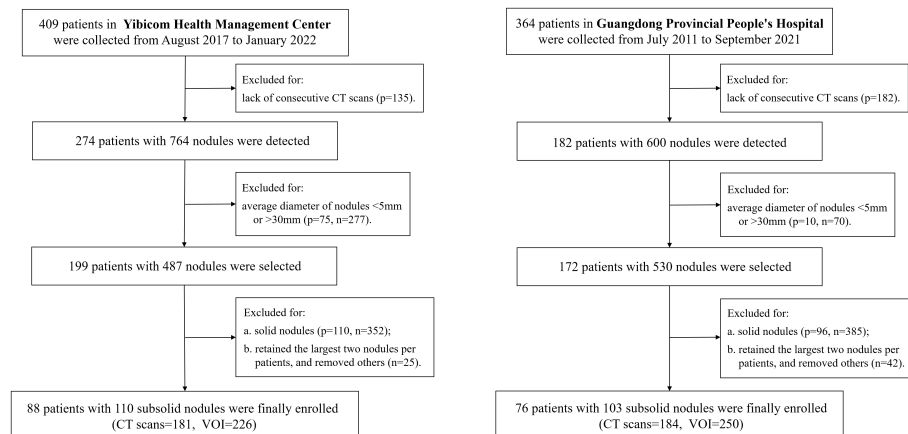


FIGURE 2
Flowchart of case selection on the external data set.

then compared the three relative rates between the cancer group and non-cancer group to evaluate the most appropriate way for identifying the growth.

Growth prediction model

According to the selected measurement, all SSNs were classified into two groups: growth group and non-growth group. The deep learning-based model and radiomics model were developed using the training set and were verified in the validation and test sets, respectively.

The radiomics model was the logistic regression model based on radiomics features, which was extracted from the shape and appearance of SSN in 3D VOIs and selected by the Least Absolute Shrinkage and Selection Operator (LASSO) (19). In total, 1,218 features were extracted and 60 features were selected for modeling the logistic regression model.

Following selection (13), the deep learning-based model was identified (called SiamModel, Figure 4), where FG_t , FL_t , and FL_{t-1} represent global feature embedding of T_t VOI, local feature embedding of T_t VOI, and local feature embedding of T_{t-1} VOI, respectively. A learnable embedding FL_{t-1} was provided if T_{t-1} VOI was unavailable, which occurred when there were only two CT scans. For a given subject, the 3D VOI pairs (T_{t-1} and T_t) taken from CT scans at sequential time points were fed into the Siamese encoder for extracting feature embedding. After fusing the features using the spatial-temporal mixer (STM) module (13), the fully connected layer was used to predict the growth probability. It was worth mentioning that the global information of VOIs was changeless on T_{t-1} and T_t . Hence, we only learned global feature embedding from T_t without T_{t-1} . However, the local information of the same nodule in T_{t-1} and T_t was different and highly discriminative for growth prediction. Therefore, we learned local feature embeddings from both T_{t-1} and T_t to capture the evolving local information.

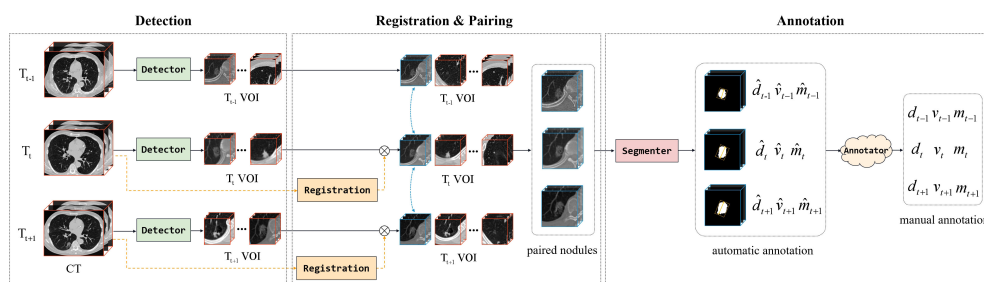


FIGURE 3
The pipeline of organizing the dataset, including CT scan registration, ROI pairing, and class annotation. The letters d, v, and m denote the diameter, volume, and mass of lung nodules, respectively.

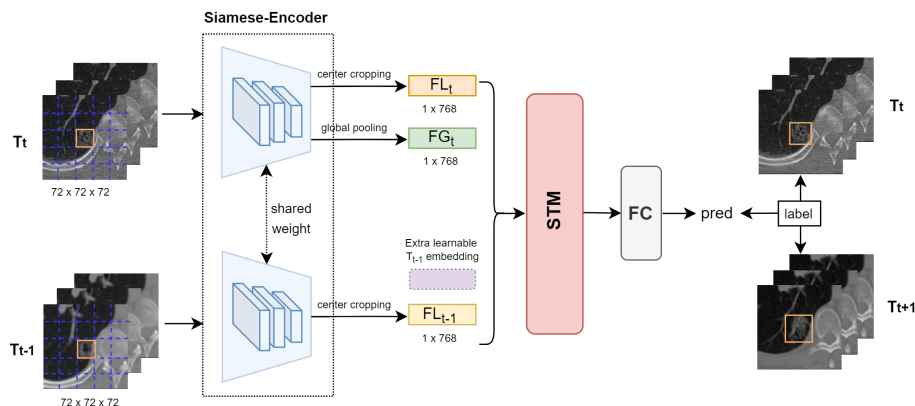


FIGURE 4

Overview of our proposed deep learning-based growth prediction model (called SiamModel), where FG_t , FL_t , and FL_{t-1} represent global feature embedding of T_t VOI, local feature embedding of T_t VOI, and local feature embedding of T_{t-1} VOI, respectively. The two encoders, whose backbone was ViT-B, in the Siamese-encoder shared weights.

To efficiently leverage changing information of SSNs in both non-growth and growth groups, we took the weighted smooth-L1 loss instead of cross-entropy loss to train our model, as follows:

$$L = \alpha \times \text{SmoothL}_1(p, y) \times I_{\geq} + \text{SmoothL}_1(p, -y) \times (1 - I_{\geq}) \quad (1)$$

In this model, p and y are the model output and ground truth of the relative growth rate, respectively. The indicator function $I_{y \geq r} = 1$ if $y \geq r$, and 0 otherwise, and r was set to 0.1. α is the imbalance coefficient and was set to 1.0, 2.0, 3.0, 4.0, and 5.0 for our experiments, where we found that 3.0 was the best value.

The model was trained from scratch for 100 epochs with the AdamW optimizer (20), with a weight decay of 0.05 and a momentum of 0.9. The batch size was set as 16, and learning rate from $10e-6$ to $lr \times \text{Batchsize}/64$ in the first five epochs, where $lr = 5e-4$, and then scheduled by the cosine annealing strategy (20).

Statistical analysis

Python 3.6.8 software with `scipy.stats` (1.8) and `sklearn.metrics` (1.0) packages was employed for data processing and statistical analysis. The reported statistical significance levels were all two-sided, and $P < 0.05$ was considered statistically significant.

Continuous variables were expressed as means \pm standard deviations and compared with t-tests. Categorical variables were expressed by frequency and compared using the χ^2 test. The discriminatory ability of these growth prediction models was

evaluated with receiver operating characteristic (ROC) curves. Then, the non-parametric bootstrap was used to estimate the variability around each of the performance measures.

Results

Growth-to-variability ratio

In total, 3,120 SSNs from 2,358 patients in the NLST dataset, including 2,983 (96%) GGNs and 137 (4%) part-solid nodules (PSNs), were selected for the study. Most patients with a total of 2,695 SSNs received at least three CT scans. To evaluate the best way for identifying the sub-solid nodule growth, we divided those SSNs from NLST into the cancer group (403 SSNs) and non-cancer group (2,717 SSNs) according to follow-up confirmation results. The increase rate and doubling time (21) of diameter, volume, and mass were calculated respectively (Table 1). The P-values of the measurements (without diameter double time) compared between cancer and non-cancer groups were less than 0.05. In addition, mass had the smallest P-value, indicating that the difference in mass was more pronounced for cancer and non-cancer groups. In addition, mass had the shortest double time in the cancer group, which means mass has a better sensitivity for growth.

The mean time between the first and last CT examinations of the selected SSNs was 739 days (range, 521–1,274 days). During this period, the diameter, volume, and mass of the SSNs in the cancer group increased with a mean of 14%, 90%, and 121%, respectively, while in the non-cancer group the mean increased at 4%, 26%, and 19%, respectively. For distinguishing growth in the cancer and non-cancer groups, the increase rate in mass was

TABLE 1 Different rates of change (between the latest two consecutive examine) in the NLST dataset.

Type		Cancer	Non-cancer	P-value
Number**		187	2508	–
Diameter	Rate	0.07 ± 0.23	0.01 ± 0.16	0.002
	Double time*	711 (638, 894)	793 (716, 899)	0.2
Volume	Rate	0.49 ± 2.05	0.06 ± 0.66	0.005
	Double time*	552 (344, 725)	621 (458, 801)	0.04
Mass	Rate	0.74 ± 3.39	0.08 ± 0.83	0.009
	Double time*	488 (321, 630)	623 (463, 799)	<0.001

Double time* (Q1, Q3): selected within [1, 1,000] for statistics. Number**: SSNs with consecutive Tt–1, Tt, and Tt+1.

more significant than those in volume and diameter (Figure 5). When the mass increased at greater than 25%, the SSNs showed a significant growth trend and were more likely to deteriorate into lung cancer.

($P = 0.04$) was significantly different between the growth and non-growth groups.

Growth and non-growth subsolid nodule characteristics

According to the above analysis, the growth of SSNs was defined as an increase in mass at 25% within 1 year. There were 2,493 SSNs (174 growth, 2,319 non-growth), 627 SSNs (38 growth, 589 non-growth), and 213 SSNs (9 growth, 204 non-growth) in the training, validation, and external test sets, respectively (Table 2). In the training and validation sets from NLST, there were significant differences in average CT value ($P < 0.01$) and diameter ($P < 0.001$) between the growth and non-growth groups. However, in the external test set, only diameter

Model performance comparison

The deep learning-based and radiomics models were developed using the training set and were verified in the validation and test sets. The AUC of SiamModel was 0.858 (95% CI 0.786–0.921) in the validation set and 0.862 (95% CI 0.789–0.927) in the external test set (Table 3). The comparable results between the validation and external test sets showed that SiamModel had good generalization ability.

Compared with STM (13), our SiamModel obtained better performance with the AUC of 0.858 (95% CI 0.786–0.921) vs. 0.823 (95% CI 0.731–0.898) in the validation set and 0.862 (95% CI 0.789–0.927) vs. 0.806 (95% CI 0.693–0.902) in the external test set, which indicated the superiority of our proposed weighted smooth-l1 loss for SSN growth prediction.

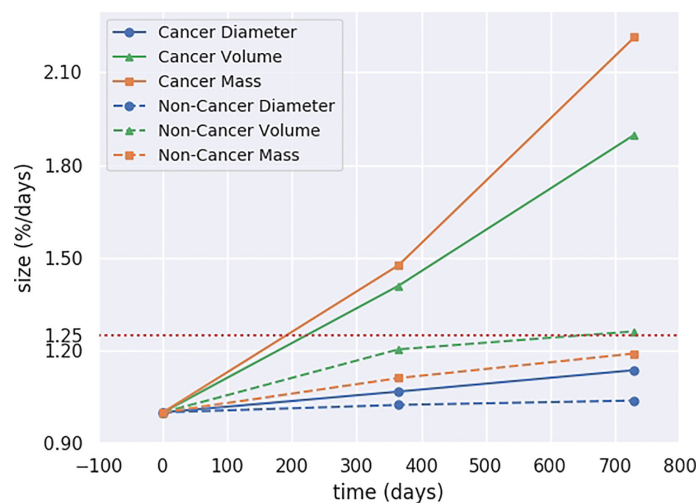


FIGURE 5
Progression in mass, volume, and diameter of SSNs.

TABLE 2 The characteristics of patients and sub-solid nodules and the results of univariate analysis on training, validation, and external test sets.

Dataset	Characteristics	Growth (Q ₁ , Q ₃)	Non-growth (Q ₁ , Q ₃)	T/χ^2 value	P value
NLST train set	Number	174	2319	–	–
	Age (years)	63 (59, 67)	62 (58, 66)	1.48	0.14
	Gender (male/female)	102/72	1312/1007	0.2	0.66
	Average CT value (HU)	-598.4 (-692.1, 538.7)	-640.6 (-703.3, -589.7)	4.1	<0.001
	Diameter (mm)	9.6 (5, 12.2)	5.6 (4, 6)	8.1	<0.001
	Texture (GGNs/PSNs)	142/32	2247/72	90.82	0
	Number	38	589	–	–
NLST Val Set	Age (years)	65 (61, 69)	62 (58, 66)	3.6	<0.001
	Gender (male/female)	19/19	363/226	1.57	0.21
	Average CT value (HU)	-564.2 (-679.8, -454.1)	-630.1 (-684.3, -581.1)	2.72	<0.01
	Diameter (mm)	12.9 (5.8, 20.5)	5.6 (4.0, 6.4)	6.03	<0.001
	Texture (GGNs/PSNs)	19/19	363/226	31.6	0
	Number	9	204	–	–
	Age (years)	58 (47, 67)	53 (46, 61)	0.83	0.43
External test set	Gender (male/female)	4/5	84/120	0.02	0.88
	Average CT value (HU)	-553.2 (-700.1, -460.9)	-657.5 (-723.2, 600.9)	1.51	0.17
	Diameter(mm)	9.6 (7.1, 12)	6.2 (4, 7.1)	2.47	0.04
	Texture (GGNs/PSNs)	8/1	202/2	1.16	0.28

Assuming all T_{t-1} scans were unavailable in datasets (using only T_t VOI as input), the performance of SiamModel and radiomics model was compared as shown in Table 3 and Figure 6. In the NLST validation set, the AUC values of SiamModel and radiomics model were 0.855 (95% CI 0.793–0.908) and 0.760 (95% CI 0.646–0.857), respectively, and 0.821 (95% CI 0.725–0.904) and 0.681 (95% CI 0.506–0.841) in the external test set. Therefore, our SiamModel performed better than the radiomics model in both the NLST validation set and external test set (Figure 6).

Comparing one using only T_t VOI as input, we saw that our SiamModel with two VOIs (T_{t-1} and T_t) as input could perform slightly better, with an AUC of 0.858 vs. 0.855 in the NLST validation set and 0.862 vs. 0.821 in the external test set.

Examples of model prediction

Figure 7 provides examples predicted by our SiamModel in the external test set.

The probability of growth was calculated as shown in Eq. 2, where p and th are the model output and threshold selected for sensitivity and specificity as shown in Table 3, respectively, and τ is the sharpening coefficient, set as 0.1 to map p to 0–1:

$$prob = \frac{e(p - th)/\tau}{1 + e(p - th)/\tau} \quad (2)$$

The predicted result with $prob \geq 0.5$ indicated the growth, which required more attention from doctors and relatively intensive follow-up.

TABLE 3 Performance of different models using only one CT scan in the validation and external test sets.

Data set	Method	AUC (95% CI)	Sensitivity (95% CI)	Specificity (95% CI)	PPV (95% CI)	NPV (95% CI)
NLST val	SiamModel (our)	0.858 (0.786-0.921)	0.632 (0.485-0.786)	0.921 (0.898-0.942)	0.341 (0.239-0.456)	0.975 (0.961-0.987)
	SiamModel (once, our)	0.855 (0.793-0.908)	0.843 (0.724-0.952)	0.651 (0.613-0.692)	0.136 (0.094-0.184)	0.985 (0.973-0.995)
	STM[13]	0.823 (0.731-0.898)	0.764 (0.622-0.897)	0.738 (0.702-0.774)	0.157 (0.109-0.217)	0.98 (0.965-0.991)
	Radiomics (once)	0.76 (0.646-0.857)	0.763 (0.615-0.889)	0.465 (0.424-0.506)	0.085 (0.059-0.114)	0.968 (0.947-0.986)
External test	SiamModel (our)	0.862 (0.789-0.927)	0.893 (0.625-1.000)	0.749 (0.685-0.807)	0.134 (0.056-0.230)	0.994 (0.980-1.000)
	SiamModel (once, our)	0.821 (0.725-0.904)	0.889 (0.625-1.000)	0.669 (0.608-0.731)	0.106 (0.040-0.179)	0.993 (0.977-1.000)
	STM[13]	0.806 (0.693-0.902)	0.895 (0.636-1.000)	0.574 (0.507-0.664)	0.083 (0.034-0.141)	0.992 (0.972-1.000)
	Radiomics (once)	0.681 (0.506-0.841)	0.663 (0.333-1.000)	0.528 (0.461-0.599)	0.059 (0.019-0.107)	0.972 (0.939-1.000)

Discussion

Our study first compared the effectiveness of diameter, volume, and mass for assessing SSN growth based on the big data from NLST and found that mass had a better sensitivity to assess SSN growth. Then, we developed the deep learning-based model (SiamModel) to predict the mass growth of SSNs and achieved good performance in both the validation set (AUC = 0.858) and the external test set (AUC = 0.862).

For pulmonary nodules discovered in screening or incidentally, the first task was to assess risk of malignancy. There are several models (22–24) which combined clinical and radiographic factors to estimate the malignancy probability and achieve fair performance (25). For those indeterminate nodules,

follow-up would be recommended (26). The growth pattern of lung nodules (18, 27) would increase the accuracy rate to diagnose malignant nodules and reduce the false positives, although some benign nodules would grow (28).

In addition, there are several methods to measure nodule growth, such as diameter, volume, and mass. Nodule growth or the solid component in part-solid nodule growth is defined as an increase in diameter of more than 1.5 mm in Lung-Reporting and Data Systems (RADS) (27) and in the National Comprehensive Cancer Network (NCCN) algorithm (NCCN 2022 screening). While 2 mm was chosen as the threshold for defining growth in both overall nodule size and the solid component of a part-solid nodule in the Fleischner Society (24), I-ELCAP requires different sizes of growth according to

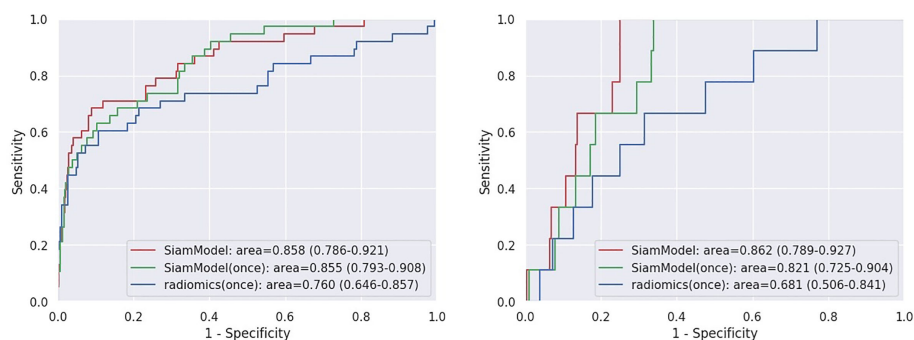


FIGURE 6

Receiver operating characteristic (ROC) curves on NLST validation set (left) and external test set (right). SiamModel (once) and radiomics (once) are only using Tt VOI as input.

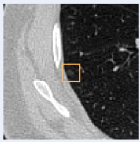
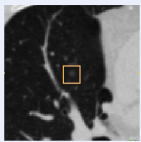
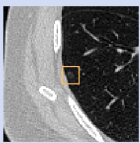
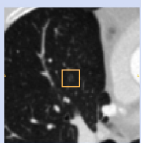
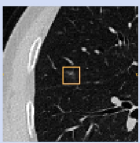
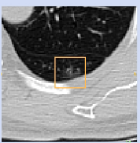
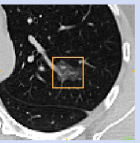
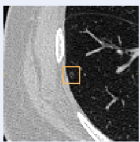
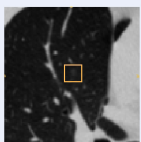
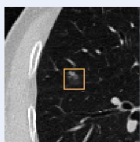
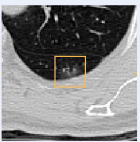
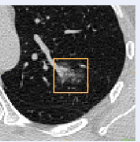
T_{t-1}			NAN	NAN	NAN
T_t					
T_{t+1}					
prob	0.182	0.192	0.627	0.686	0.999

FIGURE 7
Examples of predicting the growth probability by our method in the external test set.

initial diameter of nodules (I-ELCAP protocol. Available at <https://www.ielcap.org/protocols> Accessed June 14,2022). Because the investigator of NELSON thought volume measurements are more accurate than size by means of semiautomatic software calculation, growth was defined as a change in volume of at least 25% growth of pulmonary nodules (29, 30) and volume measurement was also recommended in the British Thoracic Society pulmonary nodule management guidelines (22). Additionally, the volume doubling time (VDT) of SSN would be longer, and VDT may not be sensitive to different indolent lung cancers from benign nodules. Our study also showed a mean of VDT cancer growth and non-cancer growth (552 vs. 621 days, $P = 0.04$) and was close to the NLST databases.

Furthermore, Hoop et al. (6) compared measurements of diameter, volume, and mass in 52 pulmonary GGNs and found that mass is the best method for identifying malignant GGNs and detection of growth of GGNs. Our study also found that mass growth was the most sensitive method to identify the growth of SSNs, since the growth of mass might reflect the volume, density, or solid component growth. Compared with Hoop et al.'s study (6), we investigated growth rate in SSNs from NLST and validated the data in a larger number of patients. Moreover, we used an automatic machine learning method to measure volume and mass, which would reduce the consumption of time and labor.

Initial size (31), CT attenuation (3), and history of lung cancer (30) were associated with GGN growth according to the first-time CT results and clinical factors. For those pulmonary nodules which require follow-up, previous studies focus on classifying and few rely on prediction factors for the GGO

growth. Radiomics and deep learning techniques have been investigated to detect, segment, and classify in the field of pulmonary nodule management (7, 32) in the past 10 years. Radiomics could extract the high quantitative image features from medical imaging (32, 33) and build high-performance models with limited datasets. Several studies (34) have demonstrated that radiomic signatures can differentiate malignant and benign nodules with a sensitivity ranging from 76.2 to 92.9% and a specificity ranging from 72.7 to 96.1%. The combined radiographic factor or supervised machine learning with the radiomics model could achieve better performance (34, 35). In the traditional radiomics methods to classify pulmonary nodules (11), large amounts of labor are required for manual tumor segmentation and feature extraction. Deep learning algorithms could detect and segment pulmonary nodules automatically and build predictive models. Ardila et al. (8) developed a predictive model of the risk of lung cancer by the 3D deep learning method and achieved algorithms that were comparable to, or could even outperform, radiologists with or without prior CT imaging. A Lung Cancer Prediction Convolutional Neural Network model (36) was also found to outperform the Brock model to predict risk of lung cancer. A deep machine learning algorithm developed by Huang et al. (21) was compared with Lung-RADS and volume doubling time to inform lung cancer incidence with 1, 2, and 3 years. As for growth of pulmonary nodules, Tao et al. (18) first manually segmented 313 lung nodules in 246 patients in their hospital then developed a convolutional neural network (CNN) to model the imagery change in the nodules from the baseline CT image to the follow-up CT image and achieved an AUC of 0.857 for solid nodules and 0.843 for GGNs in differentiating growth and non-

growth nodules. Compared with Tao et al. (18), we first trained the detection and segmentation models on LUNA16 and LNDb datasets and then used them to identify and segment SSNs automatically which was easily reproducible. As for the growth of SSNs, we developed a deep learning-based model, called SiamModel. In the independent external test set, our SiamModel could predict the growth of SSNs with good performance (AUC = 0.862) and showed a significant improvement, compared with the radiomics model.

This study has the following limitations: (a) the growth and non-growth SSNs were extremely imbalanced in our external test set, so a validation bias might exist; and (b) the training set only contained low-dose CT scans, but the external set enrolled both normal CT and low-dose CT scans, therefore, it is still necessary to expand the training and test sets with more normal CT scans in further study; and (c) we defined an increase of at least 25% in mass as the growth of SSNs without an exact derivation which should be tested in further clinical practice.

Mass increase rate can reflect the growth of SSNs associated with lung cancer more sensitively than diameter and volume increase rates. Further, we established a deep learning-based model (called SiamModel) that could better predict the growth of SSNs on the base of mass, compared with the radiomics model.

Data availability statement

The original contributions presented in the study are included in the article/supplementary material. Further inquiries can be directed to the corresponding authors.

Ethics statement

This study was reviewed and approved by Guangdong Provincial People's Hospital (KY-Z-2022-125-01). Written informed consent for participation was not required for this study in accordance with the national legislation and the institutional requirements.

References

1. Sung H, Ferlay J, Siegel RL, Laversanne M, Soerjomataram I, Jemal A, et al. Global cancer statistics 2020: Globocan estimates of incidence and mortality worldwide for 36 cancers in 185 countries. *CA Cancer J Clin* (2021) 71:209–49. doi: 10.3322/caac.21660
2. Aberle DR, Adams AM, Berg CD, Black WC, Clapp JD, Fagerstrom RM, et al. Reduced lung-cancer mortality with low-dose computed tomographic screening. *N Engl J Med* (2011) 365:395–409. doi: 10.1056/NEJMoa1102873
3. Gao C, Li J, Wu L, Kong D, Xu M, Zhou C. The natural growth of subsolid nodules predicted by quantitative initial ct features: A systematic review. *Front Oncol* (2020) 10:318. doi: 10.3389/fonc.2020.00318
4. Singh R, Kalra MK, Homayounieh F, Nitiwarangkul C, McDermott S, Little BP, et al. Artificial intelligence-based vessel suppression for detection of sub-solid nodules in lung cancer screening computed tomography. *Quant Imaging Med Surg* (2021) 11:1134–43. doi: 10.21037/qims-20-630
5. Sun Q, Huang Y, Wang J, Zhao S, Zhang L, Tang W, et al. Applying CT texture analysis to determine the prognostic value of subsolid nodules detected during low-dose CT screening. *Clin Radiol* (2019) 74:59–66. doi: 10.1016/j.crad.2018.07.103
6. de Hoop B, Gietema H, van de Vorst S, Murphy K, van Klaveren RJ, Prokop M. Pulmonary ground-glass nodules: increase in mass as an early indicator of growth. *Radiology* (2010) 255:199–206. doi: 10.1148/radiol.09090571

Author contributions

XY contributed to conception and design of the study. RL wrote the first draft of the manuscript and analyze data. AL organized the database. HHY performed the statistical analysis. JL, SL, BJ, SD, QN, WZ contributed to collect clinical data. BL, YW, JF, HL, YH, CS, HFY contributed to analyze data. YW supervised the study. All authors contributed to manuscript revision, read, and approved the submitted version.

Funding

This work was supported by the research fund from Guangzhou Municipal Science and Technology Bureau (grant no. 202201011664 to XY).

Conflict of interest

XY, YW, RL, HHY, JL, SL, BJ, SD, QN, WZ are employed by Guangdong Provincial People's Hospital. BL is employed by South China University of Technology. Authors AL, JW, JF and HL are employed by Guangzhou Shiyuan Electronics Co., Ltd.

The remaining authors declare that the research was conducted in the absence of any commercial or financial relationships that could be construed as a potential conflict of interest.

Publisher's note

All claims expressed in this article are solely those of the authors and do not necessarily represent those of their affiliated organizations, or those of the publisher, the editors and the reviewers. Any product that may be evaluated in this article, or claim that may be made by its manufacturer, is not guaranteed or endorsed by the publisher.

7. Bi WL, Hosny A, Schabath MB, Giger ML, Birkbak NJ, Mehrta A, et al. Artificial intelligence in cancer imaging: Clinical challenges and applications. *CA Cancer J Clin* (2019) 69:127–57. doi: 10.3322/caac.21552
8. Ardila D, Kiraly AP, Bharadwaj S, Choi B, Reicher JJ, Peng L, et al. End-to-end lung cancer screening with three-dimensional deep learning on low-dose chest computed tomography. *Nat Med* (2019) 25:954–61. doi: 10.1038/s41591-019-0447-x
9. Ather S, Kadir T, Gleeson F. Artificial intelligence and radiomics in pulmonary nodule management: current status and future applications. *Clin Radiol* (2020) 75:13–9. doi: 10.1016/j.crad.2019.04.017
10. Li R, Xiao C, Huang Y, Hassan H, Huang B. Deep learning applications in computed tomography images for pulmonary nodule detection and diagnosis: A review. *Diagno (Basel)* (2022) 12(2):298. doi: 10.3390/diagnostics12020298
11. Fahmy D, Kandil H, Khelifi A, Yaghi M, Ghazal M, Sharafeldeen A, et al. How ai can help in the diagnostic dilemma of pulmonary nodules. *Cancers (Basel)* (2022) 14(7):1840. doi: 10.3390/cancers14071840
12. Murchison JT, Ritchie G, Senyszak D, Nijwenning JH, van Veenendaal G, Wakkie J, et al. Validation of a deep learning computer aided system for CT based lung nodule detection, classification, and growth rate estimation in a routine clinical population. *PLoS One* (2022) 17:e0266799. doi: 10.1371/journal.pone.0266799
13. Fang J, Wang J, Li A, Yan Y, Hou Y, Song C, et al. Siamese Encoder-based spatial-temporal mixer for growth trend prediction of lung nodules on ct scans. *arXiv* (2022) 2206.03049. doi: 10.1007/978-3-031-16431-6_46
14. Setio AAA, Traverso A, de Bel T, Berens MSN, Bogaard CVD, Cerello P, et al. Validation, comparison, and combination of algorithms for automatic detection of pulmonary nodules in computed tomography images: The LUNA16 challenge. *Med Image Anal* (2017) 42:1–13. doi: 10.1016/j.media.2017.06.015
15. Pedrosa J, Aresta G, Ferreira C, Rodrigues M, Leitao P, Carvalho AS, et al. LNDb: A lung nodule database on computed tomography. *arXiv* (2019). doi: 10.48550/arXiv.1911.08434
16. Zhou X, Wang D, Kr̄ahenbūhl P. Objects as points. *arXiv* (2019) 1904.07850. doi: 10.48550/arXiv.1904.07850
17. Kushnure DT, Talbar SN. MS-UNet: A multi-scale UNet with feature recalibration approach for automatic liver and tumor segmentation in CT images. *Comput Med Imaging Graph* (2021) 89:101885. doi: 10.1016/j.compmedimag.2021.101885
18. Tao G, Zhu L, Chen Q, Yin L, Li Y, Yang J, et al. Prediction of future imagery of lung nodule as growth modeling with follow-up computed tomography scans using deep learning: a retrospective cohort study. *Transl Lung Cancer Res* (2022) 11:250–62. doi: 10.21037/tlcr-22-59
19. Tibshirani R. Regression shrinkage and selection via the lasso. *J R Stat Soc: Ser B (Methodological)* (1996) 58:267–88. doi: 10.1111/j.2517-6161.1996.tb02080.x
20. Loshchilov I, Hutter F. Stochastic gradient descent with warm restarts. *Proceedings 5th Int Conf Learn Represent* (2016). 1–16. Available at: <https://arxiv.org/abs/1608.03983v1>
21. Huang P, Lin CT, Li Y, Tammemagi MC, Brock MV, Atkar-Khattra S, et al. Prediction of lung cancer risk at follow-up screening with low-dose CT: a training and validation study of a deep learning method. *Lancet Digit Health* (2019) 1:e353–e62. doi: 10.1016/S2589-7500(19)30159-1
22. Baldwin DR, Callister ME. The British thoracic society guidelines on the investigation and management of pulmonary nodules. *Thorax* (2015) 70:794–8. doi: 10.1136/thoraxjnl-2015-207221
23. Gould MK, Ananth L, Barnett PG. A clinical model to estimate the pretest probability of lung cancer in patients with solitary pulmonary nodules. *Chest* (2007) 131:383–8. doi: 10.1378/chest.06-1261
24. Bankier AA, MacMahon H, Goo JM, Rubin GD, Schaefer-Prokop CM, Naidich DP. Recommendations for measuring pulmonary nodules at ct: A statement from the Fleischner society. *Radiology* (2017) 285:584–600. doi: 10.1148/radiol.2017162894
25. Zhang K, Wei Z, Nie Y, Shen H, Wang X, Wang J, et al. Comprehensive analysis of clinical logistic and machine learning-based models for the evaluation of pulmonary nodules. *JTO Clin Res Rep* (2022) 3:100299. doi: 10.1016/j.jtocr.2022.100299
26. Wood DE, Kazerooni EA, Aberle D, Berman A, Brown LM, Eapen GA, et al. *NCCN guidelines® insights: Lung cancer screening, version 1.2022* (2022). Available at: <https://nccn.org/view/journals/nccn/20/7/article-p754.xml>.
27. Pinsky PF, Gierada DS, Black W, Munden R, Nath H, Aberle D, et al. Performance of lung-rads in the national lung screening trial: A retrospective assessment. *Ann Intern Med* (2015) 162:485–91. doi: 10.7326/M14-2086
28. Zhang R, Tian P, Qiu Z, Liang Y, Li W. The growth feature and its diagnostic value for benign and malignant pulmonary nodules met in routine clinical practice. *J Thorac Dis* (2020) 12:2019–30. doi: 10.21037/jtd-19-3591
29. van Klaveren RJ, Oudkerk M, Prokop M, Scholten ET, Nackaerts K, Vernhout R, et al. Management of lung nodules detected by volume CT scanning. *N Engl J Med* (2009) 361:2221–9. doi: 10.1056/NEJMoa0906085
30. de Koning HJ, van der Aalst CM, de Jong PA, Scholten ET, Nackaerts K, Heuvelmans MA, et al. Reduced lung-cancer mortality with volume ct screening in a randomized trial. *N Engl J Med* (2020) 382:503–13. doi: 10.1056/NEJMoa1911793
31. Hiramatsu M, Inagaki T, Inagaki T, Matsui Y, Satoh Y, Okumura S, et al. Pulmonary ground-glass opacity (GGO) lesions-large size and a history of lung cancer are risk factors for growth. *J Thorac Oncol* (2008) 3:1245–50. doi: 10.1097/JTO.0b013e318189f526
32. Lambin P, Leijenaar RTH, Deist TM, Peerlings J, de Jong EEC, van Timmeren J, et al. Radiomics: the bridge between medical imaging and personalized medicine. *Nat Rev Clin Oncol* (2017) 14:749–62. doi: 10.1038/nrclinonc.2017.141
33. Lambin P, Rios-Velazquez E, Leijenaar R, Carvalho S, van Stiphout RG, Granton P, et al. Radiomics: extracting more information from medical images using advanced feature analysis. *Eur J Cancer* (2012) 48:441–6. doi: 10.1016/j.ejca.2011.11.036
34. Wu YJ, Wu FZ, Yang SC, Tang EK, Liang CH. Radiomics in early lung cancer diagnosis: From diagnosis to clinical decision support and education. *Diagno (Basel)* (2022) 12(5):1064. doi: 10.3390/diagnostics12051064
35. Tan M, Ma W, Sun Y, Gao P, Huang X, Lu J, et al. Prediction of the growth rate of early-stage lung adenocarcinoma by radiomics. *Front Oncol* (2021) 11:658138. doi: 10.3389/fonc.2021.658138
36. Massion PP, Antic S, Ather S, Arteta C, Brabec J, Chen H, et al. Assessing the accuracy of a deep learning method to risk stratify indeterminate pulmonary nodules. *Am J Respir Crit Care Med* (2020) 202:241–9. doi: 10.1164/rccm.201903-0505OC



OPEN ACCESS

EDITED BY

Alberto Sandri,
San Luigi Gonzaga Hospital, Italy

REVIEWED BY

Yuetao Wang,
First People's Hospital of Changzhou,
China
Fabrizio Minervini,
University of Lucerne, Switzerland

*CORRESPONDENCE

Bo Ye
yeb00430@sjtu.edu.cn
Feng Shi
feng.shi@uii-ai.com

[†]These authors have contributed
equally to this work

SPECIALTY SECTION

This article was submitted to
Thoracic Oncology,
a section of the journal
Frontiers in Oncology

RECEIVED 16 July 2022

ACCEPTED 30 September 2022

PUBLISHED 21 October 2022

CITATION

Lv Y, Wei Y, Xu K, Zhang X, Hua R,
Huang J, Li M, Tang C, Yang L, Liu B,
Yuan Y, Li S, Gao Y, Zhang X, Wu Y,
Han Y, Shang Z, Yu H, Zhan Y, Shi F
and Ye B (2022) 3D deep learning
versus the current methods for
predicting tumor invasiveness of
lung adenocarcinoma based on
high-resolution computed
tomography images.
Front. Oncol. 12:995870.
doi: 10.3389/fonc.2022.995870

COPYRIGHT

© 2022 Lv, Wei, Xu, Zhang, Hua, Huang,
Li, Tang, Yang, Liu, Yuan, Li, Gao, Zhang,
Wu, Han, Shang, Yu, Zhan, Shi and Ye.
This is an open-access article
distributed under the terms of the
Creative Commons Attribution License
(CC BY). The use, distribution or
reproduction in other forums is
permitted, provided the original
author(s) and the copyright owner(s)
are credited and that the original
publication in this journal is cited, in
accordance with accepted academic
practice. No use, distribution or
reproduction is permitted which does
not comply with these terms.

3D deep learning versus the current methods for predicting tumor invasiveness of lung adenocarcinoma based on high-resolution computed tomography images

Yilv Lv^{1†}, Ying Wei^{2†}, Kuan Xu¹, Xiaobin Zhang¹, Rong Hua¹,
Jia Huang³, Min Li⁴, Cui Tang⁵, Long Yang⁶, Bingchun Liu⁷,
Yonggang Yuan⁸, Siwen Li⁹, Yaozong Gao², Xianjie Zhang²,
Yifan Wu², Yuchen Han¹⁰, Zhanxian Shang¹⁰, Hong Yu¹¹,
Yiqiang Zhan², Feng Shi^{2*} and Bo Ye^{1*}

¹Department of Thoracic Surgery, Shanghai Chest Hospital, Shanghai Jiao Tong University, Shanghai, China, ²Department of Research and Development, Shanghai United Imaging Intelligence Co., Ltd., Shanghai, China, ³Department of Oncologic Surgery, Shanghai Chest Hospital, Shanghai Jiao Tong University, Shanghai, China, ⁴Department of Radiology, Shanghai Municipal Hospital of Traditional Chinese Medicine, Shanghai University of Traditional Chinese Medicine, Shanghai, China, ⁵Department of Radiology, Yangpu Hospital, Tongji University, Shanghai, China, ⁶Department of Thoracic Surgery, Affiliated Hospital of Gansu Medical College, Pingliang, China, ⁷Department of Thoracic Surgery, Weifang People's Hospital, Weifang, China, ⁸Department of Thoracic Surgery, Qilu Hospital of Shandong University, Qingdao, China, ⁹Department of Thoracic Surgery, Qingyuan People's Hospital, Guangzhou Medical University, Guangzhou, China, ¹⁰Department of Pathology, Shanghai Chest Hospital, Shanghai Jiao Tong University, Shanghai, China, ¹¹Department of Radiology, Shanghai Chest Hospital, Shanghai Jiao Tong University, Shanghai, China

Background: Different pathological subtypes of lung adenocarcinoma lead to different treatment decisions and prognoses, and it is clinically important to distinguish invasive lung adenocarcinoma from preinvasive adenocarcinoma (adenocarcinoma *in situ* and minimally invasive adenocarcinoma). This study aims to investigate the performance of the deep learning approach based on high-resolution computed tomography (HRCT) images in the classification of tumor invasiveness and compare it with the performances of currently available approaches.

Methods: In this study, we used a deep learning approach based on 3D conventional networks to automatically predict the invasiveness of pulmonary nodules. A total of 901 early-stage non-small cell lung cancer patients who underwent surgical treatment at Shanghai Chest Hospital between November 2015 and March 2017 were retrospectively included and randomly assigned to a training set (n=814) or testing set 1 (n=87). We subsequently included 116 patients who underwent surgical treatment and intraoperative frozen section between April 2019 and January 2020 to form testing set 2. We compared the performance of our deep learning approach in

predicting tumor invasiveness with that of intraoperative frozen section analysis and human experts (radiologists and surgeons).

Results: The deep learning approach yielded an area under the receiver operating characteristic curve (AUC) of 0.946 for distinguishing preinvasive adenocarcinoma from invasive lung adenocarcinoma in the testing set 1, which is significantly higher than the AUCs of human experts ($P < 0.05$). In testing set 2, the deep learning approach distinguished invasive adenocarcinoma from preinvasive adenocarcinoma with an AUC of 0.862, which is higher than that of frozen section analysis (0.755, $P = 0.043$), senior thoracic surgeons (0.720, $P = 0.006$), radiologists (0.766, $P > 0.05$) and junior thoracic surgeons (0.768, $P > 0.05$).

Conclusions: We developed a deep learning model that achieved comparable performance to intraoperative frozen section analysis in determining tumor invasiveness. The proposed method may contribute to clinical decisions related to the extent of surgical resection.

KEYWORDS

computer-aided diagnosis, lung adenocarcinoma, intraoperative frozen section, tumor invasiveness, artificial intelligence, non-small cell lung (NSCLC)

1 Introduction

Lung cancer ranks second in the most commonly diagnosed cancer and remains the leading cause of cancer death worldwide (1, 2). With the widespread implementation of low-dose computed tomography (CT) screening and regular physical examinations, a substantial number of early-stage lung cancers have been detected (3). Surgical resection remains the gold standard for early-stage lung cancer treatment, and the mode of surgery is lobectomy (4). However, an increasing number of studies and single-institution trials have demonstrated that sublobar resection may yield comparable outcomes in selected patients with early-stage non-small cell lung cancer (NSCLC) (5, 6). Sublobar resection can preserve the lung parenchyma, which is particularly valuable for patients with poor pulmonary reserve or those who are likely to require subsequent additional resection (5). Therefore, sublobar resection is extremely important in the treatment of patients with early-stage NSCLC.

A consistent method has not been established to identify the optimal candidates for sublobar resection of NSCLC with a low likelihood of recurrence. Patients with ground-glass opacity-dominant clinical stage IA adenocarcinomas are suitable for sublobar resection, as confirmed by the latest clinical trial (7). In the new multidisciplinary classification of pulmonary adenocarcinoma by the International Association for the Study of Lung Cancer (IASLC)/American Thoracic Society (ATS)/European Respiratory Society (ERS), the disease-specific survival for adenocarcinoma *in situ* (AIS) and minimally invasive adenocarcinoma (MIA) are 100% or nearly 100%, respectively, after complete resection. Invasive lung adenocarcinoma (IAC) is more aggressive and has a worse prognosis than AIS and MIA, suggesting that sublobar resection is only appropriate for patients with MIA or AIS (8, 9).

Currently, there are three methods to evaluate pathological aggressiveness and the suitability of sublobar resection in patients with early-stage lung adenocarcinoma: preoperative biopsy, CT imaging, and intraoperative frozen section analysis. Small lesions are difficult to locate, while biopsy samples may not be representative (10, 11). In addition, whether preoperative biopsy increases the likelihood of early-stage lung cancer recurrence remains controversial (12, 13). Intraoperative frozen section analysis has traditionally been used to assess tumor invasiveness and guide surgical management. However, the technique does have certain limitations: Several studies have shown that the accuracy and sensitivity of intraoperative frozen sections are

Abbreviations: AUC, area under the curve; NSCLC, non-small cell lung cancer; IASLC, International Association for the Study of Lung Cancer; ATS, American Thoracic Society; ERS, European Respiratory Society; AIS, adenocarcinoma *in situ*; MIA, minimally invasive adenocarcinoma; IAC, invasive lung adenocarcinoma; pre-IAC, preinvasive lung adenocarcinoma; AI, artificial intelligence; CNN, convolutional neural network; LPA, lepidic predominant adenocarcinoma.

relatively low for subcentimeter pulmonary nodules (14, 15). There has been a strong focus on identifying pathological invasiveness according to imaging findings. CT imaging can reportedly distinguish preinvasive lung adenocarcinoma (pre-IAC; AIS and MIA) from IAC, although the small sample sizes and ambiguous appearances of these findings prevent its routine adoption in clinical practice (16–20). It is therefore a great challenge for radiologists or experts to diagnose a large number of detected pulmonary nodules, as these methods are time-consuming and error-prone when interpreting nodules. Therefore, we need a more straightforward and precise method to determine the pathological aggressiveness of all types of nodules based on CT imaging, not just ground-glass nodules.

In recent years, artificial intelligence (AI) techniques coupled with radiological imaging have played an essential role in automatically predicting the tumor invasiveness of pulmonary adenocarcinomas from CT scans (21–25). Deep learning, a popular research area of AI, enables end-to-end models to obtain self-learned features and achieves promising results using input data without the need for manual feature extraction (26). Deep learning algorithms have been widely applied to many problems, such as lung nodule detection, segmentation, and classification (27, 28).

The purpose of this study was to develop a computer-aided approach to accurately and automatically discriminate the invasiveness of lung adenocarcinomas in routine chest CT images. We built a deep learning model and investigated the utility of the model in predicting pathological invasiveness among patients with early-stage lung adenocarcinoma. In addition, we compared the performance of the deep learning model with that of observers and intraoperative frozen section diagnoses to determine the best method of distinguishing pre-IAC from IAC in clinical practice.

2 Methods

2.1 Ethical considerations

This retrospective study adhered to the Declaration of Helsinki and relevant ethical policies in China. The study protocol was approved by the Institutional Review Board and Ethics Committee of Shanghai Chest Hospital (No. IS2180). The requirement for patient consent was waived because of the retrospective study design.

2.2 Data collection

This study retrospectively reviewed the medical records of 2671 consecutive patients with NSCLC who underwent surgical resection in Shanghai Chest Hospital between November 2015 and March 2017 to develop the training set and testing set 1. An

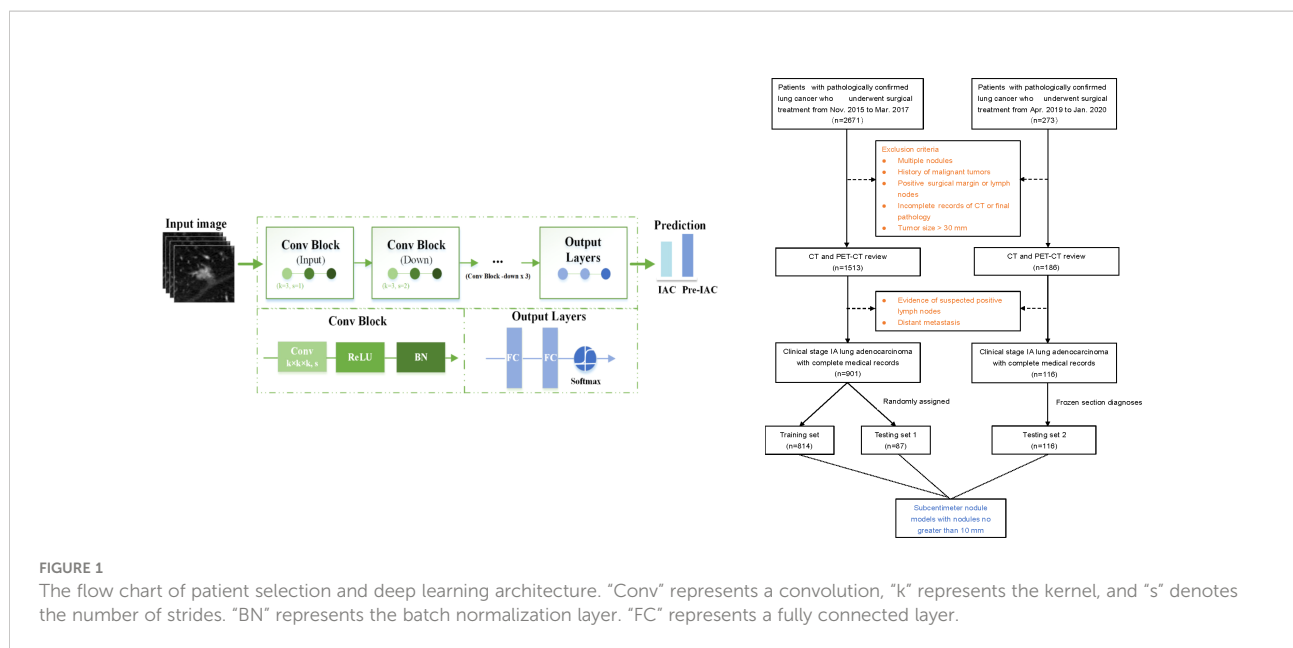
additional dataset of 273 patients who underwent surgery between April 2019 and January 2020 was separately identified and formed an additional testing set (i.e., testing set 2). The inclusion criteria were as follows: (1) stage 0 or IA lung adenocarcinoma confirmed by final pathology according to the 8th Edition of the TMN Classification (29); (2) availability of preoperative thin-section CT (0.625 mm–1.25 mm) images; and (3) resected nodules were sent for paraffin sectioning, and the final pathological results were available. The exclusion criteria were as follows: (1) multiple pulmonary nodules; (2) previous history of malignant tumor; (3) pathologically confirmed positive surgical margin or lymph nodes; (4) incomplete records of CT or pathology quality and (5) pulmonary nodule with size greater than 30mm. Finally, 901 patients with early-stage lung adenocarcinoma were enrolled and testing set 1 using a stratified random sampling method, and 116 patients were enrolled in the testing set 2. To compare the accuracy of intraoperative frozen section analysis with that of artificial intelligence-based CT image analysis, frozen section diagnoses of the independent testing set 2 were collected (Figure 1).

2.3 CT image acquisition, classification, and pathological evaluation

All preoperative CT scans were obtained at full inspiration to avoid respiratory motion artifacts. Brilliance iCT and Ingenuity (Philips Medical Systems, Netherlands) scanners were used to scan CT images at an efficient dose of 120 kV tube energy and 200 mA. All CT data were acquired in the supine position at full inspiration. High-resolution images were acquired with a reconstruction slice thickness of 1 mm and no overlap, and a lung window (window width: 1500, window level: -500) was used for film reading.

For frozen section diagnosis, resected tumor tissues were preserved in a sterile, sealed plastic bag; they were sent to the pathology department within 5 min after resection. Essential tumor information was recorded; one block of the largest tumor tissue was separated from the sample and sectioned using a CM-3050s freezing microtome (Leica, Nussloch, Germany). Before sectioning, the tissue block was frozen at -24°C for 5 min in OCT compound (SAKURA Tissue-Tek; Torrance, CA, USA). One or two slices (5 µm each) were collected and placed on glass slides. The slides were fixed in methanol/glacial acetic acid for 10–20 s and then subjected to routine hematoxylin and eosin staining (Figure 2). The predominant pattern was defined according to the histologic component with the greatest percentage.

For paraffin-embedded sections, any remaining tissues that had been collected during surgery were fixed in 10% formaldehyde, embedded in paraffin, continuously sectioned at 5 µm, and subjected to hematoxylin and eosin staining for postoperative pathological analysis. Final pathology was also established *via* elastic fiber staining and immunohistochemical assessment of cytokeratin 7, thyroid transcription factor-1, and



napsin A (all antibodies from Cell Signaling Technology; Danvers, MA, USA) in paraffin-embedded sections.

Frozen section and final pathology diagnoses came from blind assessments by two pathologists (Y.H. and Z.S., chest pathologists with more than 20 years of experience in pathological diagnosis) according to the IASLC/ATS/ERS classification (8). Two pathologists reevaluated the diagnoses to reach a consensus if a discrepancy presented. AIS and MIA were combined to form a low-risk group that was called pre-IAC.

2.4 Nodule labeling and segmentation

All lung nodules with nodule diameters greater than 3 mm on each CT scan were automatically localized with 3D bounding boxes and automatically segmented using a research tool (30) developed by Shanghai United Imaging Intelligence Co., Ltd. A total of 1017 nodules were ultimately included as regions of interest (ROIs), and each of them was reviewed and confirmed by at least two senior radiologists. [Supplementary Material Figure S1](#) illustrates the size distribution of pre-IAC and IAC nodules on diameter.

2.5 Deep learning model construction

In the data preprocessing step, we first used the lung window (window width: 1500, window level: -400) for CT images normalization by Z-score standardization method. Then we truncated the normalized intensity value into the range of [-1,1], which means the values below -1 would be set to -1, and the values above 1 would be set to 1. The whole equation is defined as follows (31, 32).

$$I = \begin{cases} -1, & \text{if } \frac{I - \text{mean}}{STD} < -11, \\ \frac{I - \text{mean}}{STD}, & \text{if } -11 \leq \frac{I - \text{mean}}{STD} \leq 11, \\ 1, & \text{if } \frac{I - \text{mean}}{STD} > 11, \end{cases} \text{ other}$$

Where I refers to the CT intensity value, mean is the window level of -400, and the STD is set as the half of window width of 1500.

Before feeding the images into the deep learning network, we resampled each of the CT image to a spacing of $0.2 \times 0.2 \times 1.0$ mm (3), extracted the nodule in a bounding box, and then resized the nodule bounding box to a 3D path with size of $144 \times 144 \times 32$ pixels. Note that the bounding box was expanded by 20% to include more surrounding lung parenchyma information. In this way, the small nodules could be enlarged instead of occupying only a small region in the patch. Similarly, large nodules could be shrunk so that the box could include the whole nodule. To avoid overfitting and increase the robustness of the deep learning network, image augmentation, including rotation, scaling, and flipping, was performed on each image with a probability of 0.5. Rotation was randomly performed with an angle along an axis in a range of -5° to 5° . The scaling factor was randomly sampled in a range from 0.75 to 1.25. Flipping was adopted randomly along each axis.

The deep learning model was built by using a convolutional neural network (CNN), consisting of one input block, four downsample blocks, and one output block (Figure 1). A 3D convolution layer with a $3 \times 3 \times 3$ kernel filter is used as the input block. The downsample block consists four 3D convolution layers, each with $3 \times 3 \times 3$ filters and a stride of 2, followed by a batch normalization and a rectified linear unit (ReLU) layer, respectively. After that, the output block consists two fully connected layers followed by a ReLU layer and a softmax function to make a decision by providing the predicted probabilities for pre-IAC and IAC.

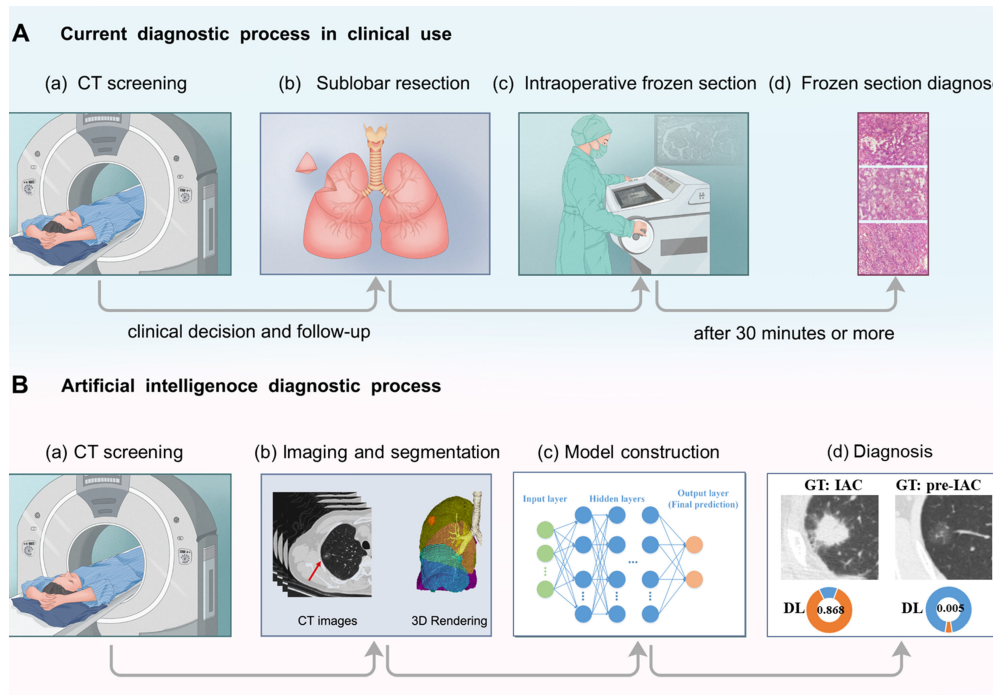


FIGURE 2

Diagram of (A) current and (B) artificial intelligence procedures to determine histological invasiveness. In the current diagnostic process in clinical use, sublobar resection is performed and intraoperative frozen sections decide the extent of surgery. In the other hand, in the workflow of deep learning approach, extensive information could be extracted from CT images, and help with the determination of tumor invasiveness. "GT" refers to ground truth. "DL" represents deep learning.

The proposed model was implemented using Python (version = 3.7.0) based on the platform of PyTorch (version = 1.7.0), and experiments were performed on a workstation with NVIDIA Quadro RTX 6000 24GB GPU and Intel(R) Xeon(R) Gold 6230R CPU. Adam was used as optimizer for stochastic gradient descent with an initial learning rate of 10^{-4} , weight decay of 0.01 and a batch size of 64 to update the network. The learning rate is halved if the validation performances do not improve during 100 epochs. To avoid potential overfitting, we used an early stop when the learning rate drops below 10^{-6} or 1000 epochs were exceeded. Focal loss function was applied (33, 34). Note that the deep learning model used only the image information where clinical features were not included.

2.6 Subcentimeter nodule classification model construction

Considering that small nodules are more difficult to discriminate than nodules with larger sizes, we collected subcentimeter nodules with sizes no greater than 10 mm from the training set, testing set 1, and testing set 2. We then trained a specific model on the subcentimeter nodules of the training set,

with the same training strategies used for deep learning model construction. The performance was evaluated on the testing set 1 and testing set 2 (Figure 1).

2.7 Observer study

For human performance comparisons, two radiologists, two junior surgeons, and two senior surgeons were recruited. They were blinded to the clinical records and pathological results and diagnosed all the nodules with only CT images. Each reader read the CT images independently and classified the nodules into pre-IAC or IAC, as with the deep learning model.

2.8 Statistical analysis

Age, sex, smoking history, surgical procedure, tumor size, and location of each patient were analyzed. Pearson's χ^2 test or Fisher's exact test was used to compare frequencies of categorical variables (all continuous variables were converted to categorical variables except for age, as shown in Table 1). The Mann-Whitney U test was used to analyze the age between the two

groups. The diagnostic performance of artificial intelligence models, observers, and frozen section diagnoses was evaluated by the area under the receiver operating characteristic (ROC) curve (AUC) and other evaluation metrics, such as accuracy, sensitivity, specificity, and Matthews correlation coefficient (MCC). The DeLong test was performed to compare the AUC curves of the deep learning models and observer studies and intraoperative frozen section, and the 95% confidence interval (95% CI) of the AUC was also assessed. In addition, the statistical significance of the difference in accuracy between deep learning models, observers, and frozen section diagnoses was evaluated using Pearson's χ^2 . All statistical analyses reported in this study were performed with Python (Version 3.7.0) and R (Version 4.0.2), and a P value less than 0.05 was considered statistically significant.

3 Results

3.1 Clinicopathological characteristics of all nodules in pre-IAC group and IAC group

A total of 1017 nodules (pre-IAC/IAC: 422/595) were included. The clinicopathological characteristics are summarized in [Table 1](#). Significant differences were found in terms of age, sex, smoking history, nodule diameter, and surgical type in the main set ($P < 0.05$). There were also significant differences between AIS/MIA and IAC in terms of age, nodule diameter, and surgical type in the testing set 2 ($P < 0.05$). Detailed information of the nodules for the overall and subcentimeter nodule classification is provided in [Supplementary Material Table S1](#).

TABLE 1 Clinicopathologic characteristics of the patients in the main set (including the training set and testing set 1) and testing set 2.

Characteristic	Main set			Testing set 2		
	AIS/MIA	IAC	P-value	AIS/MIA	IAC	P-value
Mean age	52	59	<0.001	53	61	<0.001
Sex			<0.001			0.88
Female	276	302		32	46	
Male	98	225		16	22	
Smoking history			<0.001			0.078
Yes	193	376		14	29	
No	181	151		34	39	
Diameter (cm)			<0.001			<0.001
≤ 1.0	301	50		38	16	
1.0–2.0	72	343		9	41	
≥ 2.0	1	134		1	11	
Nodule type			<0.001			<0.001
Solid nodule	35	270		0	28	
Subsolid nodule	339	257		48	40	
Location			0.856			0.544
RUL	128	182		17	17	
RML	30	36		4	4	
RLL	69	102		8	17	
LUL	106	140		16	22	
LLL	41	67		3	8	
Surgical type			<0.001			<0.001
Wedge resection	137	39		21	9	
Segmentectomy	84	56		10	9	
Lobectomy	153	432		17	50	

AIS, adenocarcinoma in situ; MIA, minimally invasive adenocarcinoma; IA, invasive adenocarcinoma; RUL, right upper lobe; RML, right middle lobe; RLL, right lower lobe; LUL, left upper lobe; LLL, left lower lobe. p-values were calculated using t-tests and Pearson's chi-squared tests.

3.2 Evaluation of classification performance on all nodules

3.2.1 Deep learning model

The deep learning model was trained on 540 epochs, and after convergence, the weights were used for testing. In [Table 2](#), the results show that the deep learning model achieved an AUC of 97.9% (95% CI: 96.8–99.0) with a sensitivity of 91.8%, specificity of 91.5% and accuracy of 91.6% on the training set, and AUC of 0.946 (95% CI: 89.9–99.4) with a sensitivity of 86.5%, specificity of 91.4%, and accuracy of 88.5% on the testing set 1. The AUC, sensitivity, specificity and accuracy on testing set 2 are 0.862 (95% CI: 79.4–93.0), 73.5%, 91.7%, and 81.0%, respectively. Note that the testing set 1 was acquired in the same time period with training set (2015–2017), while the testing set 2 was collected 4 years later (2019–2020). This may contribute the slightly reduced performance in testing set 2. The distribution differences of the deep features between the main set and testing set 2 were illustrated in [Supplementary Material Figure S2](#).

3.2.2 Observer study with radiologists and surgeons

For the results of testing set 1, the two radiologists achieved the highest averaged accuracy of 83.3% and AUC of 0.809 (95% CI: 71.1–90.7), the two junior thoracic surgeons obtained a mean accuracy of 79.9% and AUC of 0.823 (95% CI: 72.8–91.8), and the two senior thoracic surgeons achieved a mean accuracy of 74.1% and AUC of 0.799 (95% CI: 67.5–85.8). All of the averaged AUC of the observer studies were significantly lower than that of the deep learning model by the DeLong test ($P < 0.05$). Significantly decreased accuracy was found in the assessment of senior thoracic surgeons than that of deep learning with Pearson's χ^2 test.

For the testing set 2, the mean accuracy of radiologists, junior thoracic surgeons, and senior thoracic surgeons is 78.4%, 75.4%, and 69.4%, separately, meanwhile, the averaged AUC of the three observer studies is 0.776 (95% CI: 68.7–86.5), 0.768 (95% CI: 67.8–85.8) and 0.720 (95% CI: 66.3–84.7), respectively. Significantly decreased AUC was only found in the senior thoracic surgeons' assessment than that of the deep learning model (DeLong test, $P < 0.05$). Detailed mean AUC, accuracy, sensitivity, specificity, MCC, and F1-score of the six observers are shown in [Table 2](#).

3.2.3 Intraoperative frozen section analysis

Due to the availability, in this study, intraoperative frozen section diagnosis was analyzed in the testing set 2 for distinguishing pre-IAC from IAC in clinical practice. The accuracy of frozen sections for overall nodules was 74.1%, which was lower than that of the deep learning approach (81.0%) ([Table 2](#)). Intraoperative frozen section analysis yielded AUC values of 0.755 (95% CI: 66.3–84.7). Compared

to frozen section analysis, the deep learning approach achieved significantly higher AUC values at 0.862 ($P < 0.05$) ([Figure 3](#)).

3.2.4 Evaluation of classification performance on nodules with subcentimeter size

Nodules with subcentimeter size refer to the nodules with sizes no greater than 10 mm. In comparison to large nodules, they are more difficult to be differentiated between pre-IAC and IAC due to their small size. Considering that, we particularly repeated the above experiments for these subcentimeter size nodules.

As shown in [Table 3](#), the deep learning model achieved a sensitivity of 95.6%, specificity of 93.4%, accuracy of 93.7%, and AUC of 98.5% (95% CI: 97.3–99.6) on the training set, and a sensitivity of 60.0%, specificity of 90.0%, accuracy of 85.7%, and AUC of 89.3% (95% CI: 77.2–100.0) on the testing set 1. In testing set 2, the deep learning model achieved a sensitivity of 40.0%, specificity of 97.0%, accuracy of 85.7%, and AUC of 0.646 (95% CI: 42.9–86.4).

For subcentimeter nodules, deep learning models also yielded higher accuracies than the six observers ([Table 3](#)). Notably, the mean sensitivities of the two radiologists were higher than those of the artificial intelligence models in both testing set 1 and testing set 2, at 80.0% and 50.0%, respectively.

Likewise, the accuracy of frozen sections for subcentimeter nodules was 70.8%, lower than the accuracy of the artificial intelligence model ([Table 3](#)). Intraoperative frozen section analysis yielded AUC values of 0.642 (95% CI: 39.7–88.7) for subcentimeter nodules, which is lower than that of the deep learning approach, at 0.646 ($P > 0.05$) ([Figure 3](#)).

4 Discussion

Accurately discriminating pre-IAC from IAC is of great value for preoperative clinical guidance since there are significant differences in the 5-year disease-free survival rate between pre-IAC and IAC (9, 35). AI techniques can capture subtle information from CT images and learn a large number of features or deep representations of a given pulmonary nodule without any additional clinical information. AI techniques integrated with medical images have shown advantages in the invasive classification of lung adenocarcinoma (23, 36, 37). For instance, Wang et al. (21) used 886 ground-glass nodules (GGNs) from 794 patients to predict the invasiveness of lung adenocarcinoma using a deep learning network with an AUC of 0.941. In the clinic, the type of lung adenocarcinoma is identified by histological examination (e.g., biopsy and surgical resection), and diagnosis through CT image review is error-prone and time-consuming. In our study, the deep learning model achieved good discrimination on both testing set 1 and testing set 2 in terms of the overall nodule size (with AUCs of 0.946 and 0.862,

respectively). Although histological examination may still be the gold standard, the method presented in this study provides a convincing, non-invasive method for initial diagnosis before surgical resection.

In this study, the deep learning approach achieved better AUC and accuracy than observers in overall and subcentimeter nodules. The deep learning approach achieved a significantly higher AUC than that of human experts for overall nodules in the testing set 2 ($P < 0.05$). The diagnostic accuracy of well-trained radiologists was slightly lower than that of the deep learning model and higher than the accuracies of thoracic surgeons. Radiologists and surgeons typically focus on visible features such as size, solid components, lesion margin, and other qualitative features, which might be less sensitive to the local evidence that may be exploited by deep learning models. The low accuracy of thoracic surgeons in distinguishing pre-IAC from IAC may relate to the insufficient training and experience of surgeons. Previous studies have reported that deep learning-derived models can achieve equivalent and even higher performance than radiologists; the results of our study support this assertion.

Intraoperative frozen sections are a reliable and routinely used procedure for deciding the extent of surgery (Figure 2A). This study shows that the deep learning approach achieved comparable performance to frozen sections in determining tumor invasiveness, which could largely improve the current nodule screening process using CT images. For instance, our deep learning model might provide additional information on suspicious nodules, and doctors could integrate this information with patient history and clinical symptoms to guide the treatment plan. Patients with pre-IAC nodules predicted by a deep learning model might be more suitable for follow-up monitoring, avoiding invasive surgery. In addition, it only takes a few minutes to detect a

patient's lung nodules in CT images based on AI, while intraoperative frozen sections take hours to complete, which can greatly reduce the patient's waiting time. Furthermore, to our knowledge, comparisons of the diagnostic accuracy of frozen sections and CT-derived deep learning approaches have not yet been reported. Qiu et al. (38) and Wang et al. (39) compared the diagnostic accuracy of CT-based radiomics methods with that of frozen section analysis for the pathological classification of early-stage lung adenocarcinoma. Qiu et al. (38) reported that the AUC of the nomogram was 0.815, and that of the frozen section analysis was 0.670 ($P = 0.00095$). In this study, the AUC of the deep learning approach was 0.862 in the testing set 2 for overall nodules and 0.755 for intraoperative frozen section, which is higher than the study of Qiu et al. (38). The study of Qiu et al. (38) classified AAH, AIS, MIA and lepidic predominant adenocarcinoma (LPA) into pre-IAC because of the high 5-year survival of LPA, which made it more difficult for pathologists to distinguish LPA from other invasive adenocarcinomas in frozen sections. This may have contributed to the lower AUC of frozen sections in their study. The study of Wang et al. (39) reported no significant difference in the overall diagnostic accuracy between the radiomics method and FS (68.8% vs. 70.0%, $P = 0.836$), which is consistent with the results of our study.

Clinically, many factors affect intraoperative frozen section diagnoses, such as tumor size, sampling issues, and even nodule density. Liu et al. (40) reported that the diagnostic accuracy of FS for tumors smaller than 1 cm and larger than 1 cm in diameter was 79.6% and 90.8%, respectively. Yeh et al. (41) reported an average frozen section diagnostic accuracy of 64% (54% to 74%) for discriminating among AIS, MIA, and invasive adenocarcinomas by five pathologists. In this study, the accuracies of frozen sections for overall and subcentimeter nodules were 74.1% and 70.8%, respectively. Discrepancies were mostly due to the underestimation of AIS and MIA. A

TABLE 2 The performance of overall nodules with various methods for predicting pathological invasiveness.

	F1-score	Sensitivity	Specificity	MCC	ACC	AUC
Training set						
	0.928	0.918	0.915	0.829	0.916	0.979 [0.968,0.990]
Testing set 1						
Deep Learning Model	0.900	0.865	0.914	0.769	0.885	0.946 [0.899,0.994]
Radiologists*	0.869	0.913	0.714	0.666	0.833	0.809 [0.711,0.907]
Thoracic Surgeons (Junior)*	0.813	0.724	0.913	0.624	0.799	0.823 [0.728,0.918]
Thoracic Surgeons (Senior)*#	0.740	0.615	0.929	0.546	0.741	0.779 [0.675,0.883]
Testing set 2						
Deep Learning Model	0.820	0.735	0.917	0.644	0.810	0.862 [0.794,0.930]
Radiologists	0.818	0.829	0.720	0.558	0.784	0.776 [0.687,0.865]
Thoracic Surgeons (Junior)	0.759	0.662	0.885	0.544	0.754	0.768 [0.678,0.858]
Thoracic Surgeons (Senior)*	0.675	0.551	0.896	0.463	0.694	0.720 [0.623,0.817]
Frozen Section*	0.820	0.676	0.833	0.624	0.741	0.755 [0.663,0.847]

*Significant difference found between this diagnostic method of AUC and deep learning model by the DeLong test ($P < 0.05$).

#Significant difference found between this diagnostic method of accuracy and the deep learning model by Pearson's χ^2 test ($P < 0.05$).

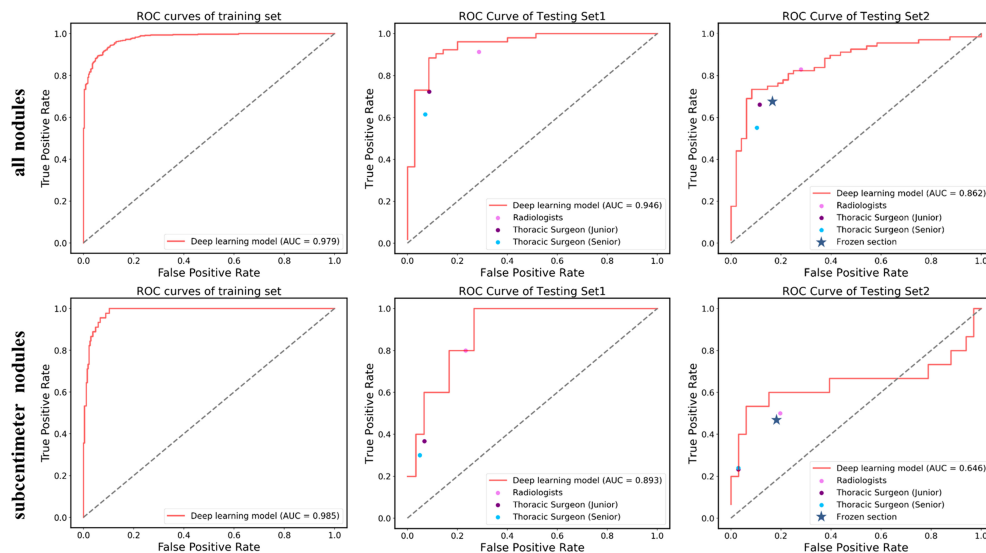


FIGURE 3

ROC curves showing the performance of the deep learning model and current methods in distinguishing pre-IAC from IAC in testing set 1 and testing set 2. Note that the results of frozen sections as well as radiologists and surgeons do not have probabilities and they were shown as line or dots in the figure.

high percentage of AIS/MIA and concurrent subcentimeter nodules may be one of the reasons for the high accuracy of the study of Liu et al. (40). Moreover, Zhu et al. (42) analyzed 803 cases and reported that misdiagnosis by frozen sections because of sampling error might lead to incomplete resection. Our study results suggest that a deep learning approach could serve as a reliable and complementary method when pathological evaluation cannot be performed intraoperatively.

However, this study still has several limitations. First, this is a retrospective study conducted at a single institution and is therefore subject to potential biases concerning patient selection, measurements, and observers. Prospective and multicenter trials are required in future studies. Second, intraoperative frozen sections also aid in determining the resection margin, which is not supported yet in the proposed deep learning approach. Therefore, another interesting research direction for the deep

TABLE 3 The performance of subcentimeter nodules (<10 mm) with various methods for predicting pathological invasiveness.

	F1-score	Sensitivity	Specificity	MCC	ACC	AUC
Training set						
	0.811	0.956	0.934	0.787	0.937	0.985 [0.973,0.996]
Testing set 1						
Deep Learning Model	0.545	0.600	0.900	0.464	0.857	0.893 [0.772,1.00]
Radiologists	0.554	0.800	0.767	0.481	0.771	0.783 [0.597,0.969]
Thoracic Surgeons (Junior)	0.422	0.367	0.932	0.340	0.843	0.667 [0.430,0.904]
Thoracic Surgeons (Senior)	0.367	0.300	0.950	0.360	0.857	0.683 [0.452,0.914]
Testing set 2						
Deep Learning Model	0.545	0.400	0.970	0.486	0.857	0.646 [0.429,0.864]
Radiologists	0.515	0.500	0.803	0.324	0.708	0.661 [0.422,0.900]
Thoracic Surgeons (Junior)	0.349	0.233	0.970	0.311	0.740	0.585 [0.324,0.846]
Thoracic Surgeons (Senior)	0.345	0.239	0.970	0.334	0.740	0.585 [0.324,0.846]
Frozen Section	0.500	0.467	0.818	0.297	0.708	0.642 [0.397,0.887]

Note that no significant difference was found between the AUC curves by the DeLong test ($P>0.05$), and no significant difference was found between the accuracies by Pearson's χ^2 test ($P>0.05$).

learning approach is to estimate appropriate surgery margin in clinical application. Third, efficient integration of the deep learning approach into clinical workflows still needs to be explored. Fourth, the sample size of subcentimeter nodules in the testing set was relatively low, which may decrease the model generalizability. Future work should include a large number of subcentimeter nodules to improve the performance of a deep learning approach in predicting tumor invasiveness.

5 Conclusion

We used a deep learning approach that demonstrated plausible performance, and its ability to distinguish tumor invasiveness was comparable to that of intraoperative frozen section analysis. This deep learning approach has potential value in clinically guiding surgical strategies, but it still needs to be verified in prospective and multicenter trials.

Data availability statement

The raw data supporting the conclusions of this article will be made available by the authors, without undue reservation.

Ethics statement

The study was conducted in accordance with the Declaration of Helsinki (as revised in 2013). The study was approved by the Institutional Review Board of Shanghai Chest Hospital, and individual consent for this retrospective analysis was waived.

Author contributions

Conception and design: YL, YZ, BY. Administrative support: YZ, YH, HY. Provision of study materials or patients: BY, YH, HY. Collection and assembly of data: YL, RH, JH, KX, YG, XianZ, YWu. Data analysis and interpretation: YL, YWe, XiaoZ, ML, CT, LY, BL, YH, ZS. All authors contributed to the article and approved the submitted version.

References

1. Sung H, Ferlay J, Siegel RL, Laversanne M, Soerjomataram I, Jemal A, et al. Global cancer statistics 2020: GLOBOCAN estimates of incidence and mortality worldwide for 36 cancers in 185 countries. *CA Cancer J Clin* (2021) 71:209–49. doi: 10.3322/caac.21660
2. Siegel RL, Miller KD, Fuchs HE, Jemal A. Cancer statistics, 2021. *CA Cancer J Clin* (2021) 71:7–33. doi: 10.3322/caac.21654
3. Yang D, Liu Y, Bai C, Wang X, Powell CA. Epidemiology of lung cancer and lung cancer screening programs in China and the united states. *Cancer Lett* (2020) 468:82–7. doi: 10.1016/j.canlet.2019.10.009
4. Ginsberg RJ, Rubinstein LV. Randomized trial of lobectomy versus limited resection for T1 N0 non-small cell lung cancer. Lung cancer study group. *Ann Thorac Surg* (1995) 60:615–22; discussion 622–3. doi: 10.1016/0003-4975(95)00537-U

Funding

This work was supported by the Interdisciplinary Program of Shanghai Jiao Tong University (grant no. YG2014QN22), Cooperative Research Project of Shanghai Jiao Tong University Collaborative Innovation Center of Translational Medicine (TM201822), Shanghai Science and Technology Support Project (No. 19441908900), National Science and Technology Innovation 2030-Major Project (2021ZD0111103), and National Natural Science Foundation of China (82172030, 82001812).

Acknowledgments

We thank Dr. Zhichao Liu for providing valuable suggestions in the revision of this manuscript.

Conflict of interest

YWe, YG, XianZ, YWu, YZ and FS are employees of Shanghai United Imaging Intelligence Co., Ltd. The company has no role in performing the surveillance and interpreting the data.

The remaining authors declare that the research was conducted in the absence of any commercial or financial relationships that could be construed as a potential conflict of interest.

Publisher's note

All claims expressed in this article are solely those of the authors and do not necessarily represent those of their affiliated organizations, or those of the publisher, the editors and the reviewers. Any product that may be evaluated in this article, or claim that may be made by its manufacturer, is not guaranteed or endorsed by the publisher.

Supplementary material

The Supplementary Material for this article can be found online at: <https://www.frontiersin.org/articles/10.3389/fonc.2022.995870/full#supplementary-material>

5. Landreneau RJ, Normolle DP, Christie NA, Awais O, Wizorek JJ, Abbas G, et al. Recurrence and survival outcomes after anatomic segmentectomy versus lobectomy for clinical stage I non-small-cell lung cancer: a propensity-matched analysis. *J Clin Oncol* (2014) 32:2449–55. doi: 10.1200/JCO.2013.50.8762
6. El-Sherif A, Gooding WE, Santos R, Pettiford B, Ferson PF, Fernando HC, et al. Outcomes of sublobar resection versus lobectomy for stage I non-small cell lung cancer: A 13-year analysis. *Ann Thorac Surg* (2006) 82:408–15; discussion 415–6. doi: 10.1016/j.athoracsur.2006.02.029
7. Suzuki K, Watanabe SI, Wakabayashi M, Saji H, Aokage K, Moriya Y, et al. A single-arm study of sublobar resection for ground-glass opacity dominant peripheral lung cancer. *J Thorac Cardiovasc Surg* (2020) 163(1):289–301. doi: 10.1016/j.jtcvs.2020.09.146
8. Travis WD, Brambilla E, Noguchi M, Nicholson AG, Geisinger KR, Yatabe Y, et al. International association for the study of lung cancer/american thoracic society/european respiratory society international multidisciplinary classification of lung adenocarcinoma. *J Thorac Oncol* (2011) 6:244–85. doi: 10.1097/JTO.0b013e318206a221
9. Yanagawa N, Shiono S, Abiko M, Ogata SY, Sato T, Tamura G. New IASLC/ATS/ERS classification and invasive tumor size are predictive of disease recurrence in stage I lung adenocarcinoma. *J Thorac Oncol* (2013) 8:612–8. doi: 10.1097/JTO.0b013e318287c3eb
10. Huang KY, Ko PZ, Yao CW, Hsu CN, Fang HY, Tu CY, et al. Inaccuracy of lung adenocarcinoma subtyping using preoperative biopsy specimens. *J Thorac Cardiovasc Surg* (2017) 154:332–339.e1. doi: 10.1016/j.jtcvs.2017.02.059
11. Huang CS, Hsu PK, Chen CK, Yeh YC, Chen HS, Wu MH, et al. Preoperative biopsy and tumor recurrence of stage I adenocarcinoma of the lung. *Surg Today* (2019) 50:673–84. doi: 10.1007/s00595-019-01941-3
12. Ahn SY, Yoon SH, Yang BR, Kim YT, Park CM, Goo JM. Risk of pleural recurrence after percutaneous transthoracic needle biopsy in stage I non-small-cell lung cancer. *Eur Radiol* (2019) 29:270–8. doi: 10.1007/s00330-018-5561-5
13. Inoue M, Honda O, Tomiyama N, Minami M, Sawabata N, Kadota Y, et al. Risk of pleural recurrence after computed tomographic-guided percutaneous needle biopsy in stage I lung cancer patients. *Ann Thorac Surg* (2011) 91:1066–71. doi: 10.1016/j.athoracsur.2010.12.032
14. Marchevsky AM, Changsri C, Gupta I, Fuller C, Houck W, McKenna RJ Jr. Frozen section diagnoses of small pulmonary nodules: Accuracy and clinical implications. *Ann Thorac Surg* (2004) 78:1755–9. doi: 10.1016/j.athoracsur.2004.05.003
15. Walts AE, Marchevsky AM. Root cause analysis of problems in the frozen section diagnosis of in situ, minimally invasive, and invasive adenocarcinoma of the lung. *Arch Pathol Lab Med* (2012) 136:1515–21. doi: 10.5858/arpa.2012-0042-OA
16. Lee SM, Park CM, Goo JM, Lee HJ, Wi JY, Kang CH. Invasive pulmonary adenocarcinomas versus preinvasive lesions appearing as ground-glass nodules: differentiation by using CT features. *Radiology* (2013) 268:265–73. doi: 10.1148/radiol.13120949
17. Cohen JG, Reymond E, Lederlin M, Medici M, Lantuejoul S, Laurent F, et al. Differentiating pre- and minimally invasive from invasive adenocarcinoma using CT-features in persistent pulmonary part-solid nodules in Caucasian patients. *Eur J Radiol* (2015) 84:738–44. doi: 10.1016/j.ejrad.2014.12.031
18. Zhang Y, Shen Y, Qiang JW, Ye JD, Zhang J, Zhao RY. HRCT features distinguishing pre-invasive from invasive pulmonary adenocarcinomas appearing as ground-glass nodules. *Eur Radiol* (2016) 26:2921–8. doi: 10.1007/s00330-015-4131-3
19. Niu R, Shao X, Shao X, Wang J, Jiang Z, Wang Y. Lung adenocarcinoma manifesting as ground-glass opacity nodules 3 cm or smaller: evaluation with combined high-resolution CT and PET/CT modality. *AJR Am J Roentgenol* (2019) 213:W236–245. doi: 10.2214/AJR.19.21382
20. Zhan Y, Peng X, Shan F, Feng M, Shi Y, Liu L, et al. Attenuation and morphologic characteristics distinguishing a ground-glass nodule measuring 5–10 mm in diameter as invasive lung adenocarcinoma on thin-slice CT. *AJR Am J Roentgenol* (2019) 213:W162–170. doi: 10.2214/AJR.18.21008
21. Wang X, Li Q, Cai J, Wang W, Xu P, Zhang Y, et al. Predicting the invasiveness of lung adenocarcinomas appearing as ground-glass nodule on CT scan using multi-task learning and deep radiomics. *Transl Lung Cancer Res* (2020) 9:1397–406. doi: 10.21037/tlcr-20-370
22. Xia X, Gong J, Hao W, Yang T, Lin Y, Wang S, et al. Comparison and fusion of deep learning and radiomics features of ground-glass nodules to predict the invasiveness risk of stage-I lung adenocarcinomas in CT scan. *Front Oncol* (2020) 10:418. doi: 10.3389/fonc.2020.00418
23. Zhao W, Wang J, Sun Y, Li C, Wu W, Jin L, et al. 3D deep learning from CT scans predicts tumor invasiveness of subcentimeter pulmonary adenocarcinomas. *Cancer Res* (2018) 78:6881–9. doi: 10.1158/0008-5472.CAN-18-0696
24. Park S, Park G, Lee SM, Kim W, Park H, Jung K, et al. Deep learning-based differentiation of invasive adenocarcinomas from preinvasive or minimally invasive lesions among pulmonary subsolid nodules. *Eur Radiol* (2021) 31:6239–47. doi: 10.1007/s00330-020-07620-z
25. Chaunzwa TL, Hosny A, Xu Y, Shafer A, Diao N, Lanuti M, et al. Deep learning classification of lung cancer histology using CT images. *Sci Rep* (2021) 11:5471. doi: 10.1038/s41598-021-84630-x
26. Lecun Y, Bengio Y, Hinton G. Deep learning. *Nature* (2015) 521:436. doi: 10.1038/nature14539
27. Ashraf SF, Yin K, Meng CX, Wang Q, Wang Q, Pu J, et al. Predicting benign, preinvasive, and invasive lung nodules on computed tomography scans using machine learning. *J Thorac Cardiovasc Surg* (2021) 163(4):1496–505. doi: 10.1016/j.jtcvs.2021.02.010
28. Gu D, Liu G, Xue Z. On the performance of lung nodule detection, segmentation and classification. *Comput Med Imaging Graph*. (2021) 89:101886. doi: 10.1016/j.compmedimag.2021.101886
29. Dettlerbeck FC, Boffa DJ, Kim AW, Tanoue LT. The eighth edition lung cancer stage classification. *Chest* (2017) 151:193–203. doi: 10.1016/j.chest.2016.10.010
30. Mu G, Chen Y, Wu D, Zhan Y, Zhou X, Gao Y. Relu cascade of feature pyramid networks for CT pulmonary nodule detection. In: Suk H-I, Liu M, Yan P, editors. *Machine learning in medical imaging*. Cham: Springer International Publishing (2019). p. 444–52.
31. Shi F, Chen B, Cao Q, Wei Y, Zhou Q, Zhang R, et al. Semi-supervised deep transfer learning for benign-malignant diagnosis of pulmonary nodules in chest CT images. *IEEE Trans Med Imaging* (2022) 41:771–81. doi: 10.1109/TMI.2021.3123572
32. Liu J, Cui Z, Sun Y, Jiang C, Chen Z, Yang H, et al. Multi-scale segmentation network for rib fracture classification from CT images. *machine learning in medical imaging*. Cham: Springer International Publishing (2021) p. 546–54.
33. Liu J, Duan X, Zhang R, Sun Y, Guan L, Lin B. Relation classification via BERT with piecewise convolution and focal loss. *PloS One* (2021) 16:e0257092. doi: 10.1371/journal.pone.0257092
34. Tran GS, Nghiem TP, Nguyen VT, Luong CM, Burie JC. Improving accuracy of lung nodule classification using deep learning with focal loss. *J Healthcare Eng* (2019) 2019:5156416. doi: 10.1155/2019/5156416
35. Russell PA, Wainer Z, Wright GM, Daniels M, Conron M, Williams RA. Does lung adenocarcinoma subtype predict patient survival? A clinicopathologic study based on the new international association for the study of lung Cancer/American thoracic Society/European respiratory society international multidisciplinary lung adenoc. *J Thorac Oncol* (2011) 6:1496–504. doi: 10.1097/JTO.0b013e318221f701
36. Sun Y, Li C, Jin L, Gao P, Zhao W, Ma W, et al. Radiomics for lung adenocarcinoma manifesting as pure ground-glass nodules: invasive prediction. *Eur Radiol* (2020) 30:3650–9. doi: 10.1007/s00330-020-06776-y
37. Gong J, Liu J, Hao W, Nie S, Zheng B, Wang S, et al. A deep residual learning network for predicting lung adenocarcinoma manifesting as ground-glass nodule on CT images. *Eur Radiol* (2020) 30:1847–55. doi: 10.1007/s00330-019-06533-w
38. Qiu ZB, Zhang C, Chu XP, Cai FY, Yang XN, Wu YL, et al. Quantifying invasiveness of clinical stage IA lung adenocarcinoma with computed tomography texture features. *J Thorac Cardiovasc Surg* (2020) 163(3):805–15. doi: 10.1016/j.jtcvs.2020.12.092
39. Wang B, Tang Y, Chen Y, Hamal P, Zhu Y, Wang T, et al. Joint use of the radiomics method and frozen sections should be considered in the prediction of the final classification of peripheral lung adenocarcinoma manifesting as ground-glass nodules. *Lung Cancer* (2020) 139:103–10. doi: 10.1016/j.lungcan.2019.10.031
40. Liu S, Wang R, Zhang Y, Li Y, Cheng C, Pan Y, et al. Precise diagnosis of intraoperative frozen section is an effective method to guide resection strategy for peripheral small-sized lung adenocarcinoma. *J Clin Oncol* (2016) 34:307–13. doi: 10.1200/JCO.2015.63.4907
41. Yeh YC, Nitadori J, Kadota K, Yoshizawa A, Rekhtman N, Moreira AL, et al. Using frozen section to identify histological patterns in stage I lung adenocarcinoma of ≤ 3 cm: Accuracy and interobserver agreement. *Histopathology* (2015) 66:922–38. doi: 10.1111/his.12468
42. Zhu E, Xie H, Dai C, Zhang L, Huang Y, Dong Z, et al. Intraoperatively measured tumor size and frozen section results should be considered jointly to predict the final pathology for lung adenocarcinoma. *Mod Pathol* (2018) 31:1391–9. doi: 10.1038/s41379-018-0056-0



OPEN ACCESS

EDITED BY

Lin Wu,
Hunan Cancer Hospital, Xiangya
School of Medicine, Central South
University, China

REVIEWED BY

Zhenjian Zhuo,
Guangzhou Medical University, China
Jian Zhou,
Fudan University, China

*CORRESPONDENCE

Anquan Shang
shanganquan@tongji.edu.cn
Wenqiang Quan
qwq@tongji.edu.cn

[†]The authors have contributed equally
to this work

SPECIALTY SECTION

This article was submitted to
Thoracic Oncology,
a section of the journal
Frontiers in Oncology

RECEIVED 21 May 2022

ACCEPTED 06 October 2022

PUBLISHED 24 October 2022

CITATION

Zhang W, Wang W, Wu J, Tian J,
Yan W, Yuan Y, Yao Y, Shang A and
Quan W (2022) Immune cell-
lipoprotein imbalance as a marker for
early diagnosis of non-small cell lung
cancer metastasis.
Front. Oncol. 12:942964.
doi: 10.3389/fonc.2022.942964

COPYRIGHT

© 2022 Zhang, Wang, Wu, Tian, Yan,
Yuan, Yao, Shang and Quan. This is an
open-access article distributed under
the terms of the [Creative Commons
Attribution License \(CC BY\)](https://creativecommons.org/licenses/by/4.0/). The use,
distribution or reproduction in other
forums is permitted, provided the
original author(s) and the copyright
owner(s) are credited and that the
original publication in this journal is
cited, in accordance with accepted
academic practice. No use,
distribution or reproduction is
permitted which does not comply with
these terms.

Immune cell-lipoprotein imbalance as a marker for early diagnosis of non-small cell lung cancer metastasis

Wei Zhang^{1†}, Weiwei Wang^{1,2†}, Junlu Wu^{1†}, Jiale Tian¹,
Wenhui Yan³, Yi Yuan¹, Yiwen Yao⁴, Anquan Shang^{1*}
and Wenqiang Quan^{1*}

¹Department of Laboratory Medicine, Shanghai Tongji Hospital, School of Medicine, Tongji University, Shanghai, China, ²Department of Pathology, Tinghu People's Hospital, Yancheng, China, ³Department of Laboratory Medicine, Yangzhi Rehabilitation Hospital (Shanghai Sunshine Rehabilitation Center), Tongji University School of Medicine, Shanghai, China, ⁴Department of Internal Medicine V-Pulmonology, Allergology, Respiratory Intensive Care Medicine, Saarland University Hospital, Homburg, Germany

The underlying molecular mechanisms and evolutionary patterns of lung cancer metastasis remain unclear, resulting in a lack of effective indicators for early diagnosis of metastasis. We retrospectively analyzed 117 patients with primary non-small cell lung cancer (NSCLC) admitted to Tongji Hospital of Tongji University in 2021, of which 93 patients with tumor metastasis were set as the metastasis group. 24 patients without metastasis were set as the non-metastasis group. The differences of each index in the two groups of patients and the expression levels in different TNM stages were compared. This study intends to evaluate the diagnostic value and net clinical benefit of common blood-related indicators Neutrophil/lymphocyte (NLR), lymphocyte/monocyte (LMR), High density lipoprotein/neutrophil (HNR), High density lipoprotein/monocyte (HMR) and combined assays in NSCLC metastasis for the early diagnosis of patients with NSCLC metastasis. It was found that the level of NLR was higher in metastatic NSCLC than non-metastatic, but the level of LMR, HNR and HMR was lower. The levels of NLR, LMR, HNR and HMR in patients with different TNM stages showed that NLR levels increased with TNM stage, while LMR, HNR and HMR levels decreased. The threshold probability range of the 4 combined tests was greater and the overall clinical benefit rate was higher compared to the individual tests. Our findings suggest that NLR, LMR, HNR and HMR have better diagnostic value for NSCLC metastasis. This study provides a clinical basis for investigating the mechanisms by which immune cells and lipid metabolism-related proteins remodel the microenvironment prior to NSCLC metastasis.

KEYWORDS

NLR, LMR, HNR, NSCLC, risk assessment, diagnostic markers

Introduction

Lung cancer is the second most common cancer in the world in terms of human incidence, is highly aggressive and metastatic, and is the leading cause of cancer deaths (1, 2). Studies show (3), that 2.2 million people in the United States were diagnosed with lung cancer in 2018 alone, and nearly 1.6 million died from lung cancer. Non-small cell lung cancer (NSCLC) accounts for 85% of lung cancers and is the common type of lung cancer, including squamous, adenocarcinoma and large cell lung cancer (4–6). Reports show that patients with NSCLC generally have poor treatment outcomes, with an overall 5-year survival rate of less than 15% (7). The main reason for this is that patients develop asymptomatic cancer metastases, which increases the risk of treatment and mortality for patients (8), and the 5-year survival rate for lung cancer patients without metastatic spread is about 35%, however, the 5-year survival rate for lung cancer patients with metastases is less than 5% (9), and patient death due to metastases. However, the 5-year survival rate of lung cancer patients with metastasis is less than 5% (10), and death due to metastasis is the main cause of death. Therefore, the occurrence of early metastasis in lung cancer patients is of great importance for the selection of appropriate treatment plans. Currently, non-invasive tests such as long-non-coding RNA (Lnc RNA), neuron-specific enolase (NSE), circulating tumor DNA (ct DNA) and microRNAs have good diagnostic value for early diagnosis and cancer staging of lung cancer (11–14), however, there are few reports on the diagnosis of metastasis in non-small cell lung cancer. Liquid biopsy and tissue biopsy are the gold standard for cancer diagnosis, however, due to the limitations of their operation such as invasiveness, complexity, inability to monitor longitudinally and continuous monitoring, and clinical variability of patients (15, 16), monitoring cannot be routinely performed in lung cancer patients. There are still no non-invasive markers that effectively predict the development of metastasis in patients with non-small cell lung cancer.

Inflammation is one of the markers of the body's immune status and also an important factor affecting the tumor microenvironment, which can play a role in the occurrence and development of various types of cancer by promoting cancer cell proliferation and metastasis (17). Inflammation plays a very important role in carcinogenesis and development, and chronic inflammation accompanies all stages of tumorigenesis. Complete

blood counts such as neutrophils, single core packs, and lymphocytes are routine preoperative tests used to reflect the inflammatory status of the body, and reports show (18, 19) that these indicators have good diagnostic performance in the early diagnosis and prognosis of many tumors such as colorectal cancer and nasopharyngeal carcinoma. Many cancers lead to metabolic disorders in the body, and disorders of lipid metabolism have been reported to play a key role in the pathogenesis of cancer. Studies have found correlations between serum lipids and many types of tumors such as breast cancer and gastric cancer (20). High-density lipoprotein cholesterol, a serum lipid, has been shown to correlate with tumor incidence and mortality (21). Neutrophil/lymphocyte (NLR), lymphocyte/monocyte (LMR), HDL cholesterol/neutrophil (HNR), and HDL cholesterol/monocyte (HMR) are calculated from blood counts and parameters in serum lipids, which have also been shown to be predictive of tumor prognosis (22). This study was designed to evaluate the diagnostic value of NLR, LMR, HNR, HMR and the combination of the four in patients with NSCLC metastases, to determine the optimal threshold values, and to assess the net clinical benefit of each individual and combined test for the early diagnosis of patients with NSCLC metastases.

Materials and methods

Medical record information

Retrospective analysis of 117 patients first diagnosed with NSCLC admitted to Tongji Hospital of Tongji University in 2021, the diagnostic staging criteria of non-small cell lung cancer were based on: the International Association for the Study of Lung Cancer (IASLC) published the eighth edition of TNM staging of lung cancer (23, 24), according to the TNM staging criteria, T stage T0 *in situ* tumor, T1-T2 stage tumor encircling lung tissue and dirty layer pleura, tumor invasion of The 24 patients who met all the criteria were regarded as non-metastatic and set up as the non-metastatic group, including T0 stage *in situ* tumor, T1-T2 stage tumor encircling lung tissue and dirty pleura, tumor invading the main bronchus, no regional lymph node metastasis in N stage, and no distant metastasis in M stage. In stage T2, the tumor invaded the main bronchus, invaded the dirty pleura, invaded any organ in stage T3-T4; in stage N1, ipsilateral hilar lymph node and intrapulmonary lymph node metastasis, and in stage N2-N3; in stage M, the tumor met M1 by distant metastasis, and 93 patients who met any of the above mentioned criteria or above were considered to have metastasis and set up as the metastasis group.

Patients with NSCLC are examined by one or more types of imaging, such as chest radiography, CT, magnetic resonance imaging (MRI), positron emission tomography-computed tomography (PET-CT), ultrasound, etc. Imaging, histological specimens by ultrasound or CT-guided percutaneous lung

Abbreviations: NSCLC, Non-small cell lung cancer; NLR, Neutrophil/lymphocyte; LMR, lymphocyte/monocyte; HNR, High density lipoprotein/neutrophil; HMR, High density lipoprotein/monocyte; NSE, neuron-specific enolase; Lnc RNA, long-non-coding RNA; ct DNA, circulating tumor DNA; IASLC, International Association for the Study of Lung Cancer; MRI, magnetic resonance imaging; PET-CT, positron emission tomography-computed tomography; NPV, negative predictive value; PPV, positive predictive value; AUC, area under the curve; DCA, decision curves.

biopsy, superficial lymph node or subcutaneous node biopsy, pleurodesis biopsy or thoracoscopic pleural biopsy, bronchoscopy and sampling biopsy, and one or more histological or cytological examinations.

Inclusion and exclusion criteria

Inclusion criteria: patients with primary NSCLC diagnosed by surgical pathology, not treated with radiotherapy before enrollment, not receiving radiotherapy and other antitumor treatments, no recent infectious symptoms and chronic infectious diseases.

Exclusion criteria: those with other types of tumors, those with missing clinical data, those with uncertain clinical stage or metastasis, those with organ dysfunction, those with hematologic disorders, those with immune deficiencies, and those with autoimmune diseases.

Clinical information and patient examination

Patients' gender, age, smoking history, neutrophils (ANC), lymphocytes (ALC), monocytes (AMC), platelets (PLT), glucose (GLU), triglycerides (TG), cholesterol (TC), high-density lipoprotein (HDL), low-density lipoprotein (LDL), TNM stage, and type of lung cancer were included in the monitoring indexes, and the inclusion of monitoring indexes was based on the patient's visit to treatment. Blood samples were collected for the first time prior to treatment, and neutrophils, lymphocytes, monocytes, and platelets were measured using a Myriad BC-6800 machine, and blood glucose, triglycerides, cholesterol, HDL, and LDL were measured using a Beckman AU5800 machine. Because the data were analyzed retrospectively, written informed consent from the subjects was waived.

Statistical analysis

SPSS 25.0 was used to statistically analyze the data that met the requirements, and the normal test was used to analyze the measurement data according to the shapiro-wilk test, and the normally distributed data were expressed by ($\bar{x} \pm SD$), and the t-test for two independent samples was used to compare between groups of normally distributed measurement data, and the χ^2 test or fisher's exact probability method. The median (M) and percentile (P25, P75) were used to express the measures of skewed distribution, and the Mann-Whitney U test was used to compare the measures of skewed distribution between two groups, and the Kruskal-Wallis H test for independent samples was used to compare the measures of skewed distribution between multiple groups, and pairwise comparisons between

groups were performed for the overall test with differences, and pairwise comparisons between groups were performed using the Bonferroni method was used to correct for significance levels. The ROC curves of the relevant indexes and combined tests were plotted using graphpad prism software, and the sensitivity, specificity, best critical value, Youden index, negative predictive value (NPV) and positive predictive value (PPV) of each relevant index in NSCLC metastasis were calculated using medcalc software, and the accuracy of the test was judged by the area under the curve (AUC). Binary logistic regression analysis was used to calculate the joint predictors of NLR, LMR, HNR, and HMR, and Delong test was used to compare the AUC of each index. The cutoff values and quartiles (P25, P50, P75) were used as cutoff points, respectively, and the risk of NLR, LMR, HNR, and HMR levels in NSCLC metastasis was evaluated using binary logistic regression analysis. Clinical decision curves (DCA) were drawn using R software 4.1.0 (<https://www.r-project.org/>) to evaluate the net clinical benefit of NLR, LMR, HNR, HMR and the 4 joint trials. The net clinical benefit rate for each index was determined by the net benefit at different threshold probabilities, which was calculated by subtracting the proportion of false-positive patients from the proportion of true-positive patients and by weighing the relative harms of forgoing the intervention against the negative consequences of unnecessary intervention. This study used the rmda package in R software 4.1.0. Differences were considered statistically significant at $P < 0.05$.

Results

Comparison of clinical baseline information between the two groups of patients

The differences were not statistically significant ($P > 0.05$) when comparing gender, age, tumor type, smoking history, PLT, ANC, GLU, TG, TC, HDL and LDL between the two groups, and the differences were statistically significant ($P < 0.05$) when comparing TNM stage, ALC and AMC between the two groups, (Table 1).

Expression levels of NLR, LMR, HNR, HMR in two groups of patients

The level of NLR in the lung cancer metastasis group was higher than that in the non-transferred group, and the difference was statistically significant ($Z = -3.584$, $P < 0.001$), (Figure 1A); the level of LMR in the lung cancer metastasis group was lower than that in the non-transferred group, and the difference was statistically significant ($Z = -3.691$, $P < 0.001$), (Figure 1B); the level of HNR in the lung cancer metastasis group was lower than that in the non-transferred group, and the difference was

TABLE 1 The analysis of the clinical data of the NSCLC patients in the metastatic and nonmetastatic groups.

Inspection items		No transfer group (n=24)	Transfer group (n=93)	c2/t/z value	P value
Gender	male	17	77	1.054	0.305
	female	7	16		
Age (year)		62.5 (53, 71)	66 (60,71)	1.301	0.193
History of smoking	no	8	23	0.725	0.395
	Yes	16	70		
Type	LACC	12	39	–	0.149
	SQCC	10	52		
	LCLC	2	2		
TNM	I	9	0	–	<0.001
	II	15	2		
	III	0	29		
	IV	0	62		
ANC (×10 ⁹ /L)		3.25 (2.35,4.10)	3.70 (2.55,4.90)	-1.486	0.137
ALC (×10 ⁹ /L)		1.40 (0.90,1.80)	1.00 (0.70,1.30)	-2.884	0.004
AMC (×10 ⁹ /L)		0.40 (0.23,0.50)	0.50 (0.40,0.65)	-2.324	0.020
PLT (×10 ⁹ /L)		175 (137,234)	192 (134,239)	-0.614	0.539
GLU (mmol/L)		4.67 (4.20,5.15)	4.79 (4.37,5.72)	-1.144	0.253
TG (mmol/L)		1.19 (0.75,1.55)	1.02 (0.81,1.53)	-0.240	0.811
TC (mmol/L)		4.61 ± 1.27	4.27 ± 0.97	-1.114	0.265
HDL (mg/dl)		44.00 (39.58,52.76)	39.63 (32.46,48.08)	-1.856	0.063
LDL (mg/dl)		106.14 (75.34,138.37)	97.10 (79.90,115.89)	-0.749	0.454

statistically significant ($Z=-2.352$, $P=0.019$), (Figure 1C); the HMR level in the lung cancer metastasis group was lower than that in the non-metastatic group, and the difference was statistically significant ($Z=-2.518$, $P<0.001$), (Figure 1D).

Expression levels of NLR, LMR, HNR, and HMR in patients with different stages

TNM stage III patients had higher NLR levels than stage I and stage II, with statistically significant differences ($P < 0.01$); stage III and stage IV patients had lower LMR levels than stage II, with statistically significant differences ($P < 0.01$); stage III patients had lower HNR levels than stage I, with statistically significant differences ($P<0.01$); stage III patients had lower HMR levels than stage I, with statistically significant differences ($P<0.01$). The difference was statistically significant ($P<0.01$); the difference was not statistically significant ($P>0.05$) when comparing the HMR levels of patients in each stage of TNM (Table 2; Figure 2).

Diagnostic value of each index in NSCLC metastasis

The joint predictors of NLR, LMR, HNR, and HMR were calculated using binary logistic regression analysis with the

transferred or untransferred subgroup Y (transferred = 1, untransferred = 0) as the dependent variable and NLR (X1), LMR (X2), HNR (X3), and HMR (X4) as the independent variables, with the regression equation $Y = 4.413 + 0.033X1 - 0.970X2 - 0.102X3 + 0.013X4$, and the joint predictors were used as four joint test indicators for outcome analysis.

ROC curves for each index and combined test were produced using graphpad prism software and are shown in Figures 3A–O. The AUC value of the neutrophil assay was 0.599 and the cutoff value was $3.7 \times 10^9/L$, and the sensitivity and specificity were 49.46% and 70.83%, and the PPV and NPV were 86.8% and 26.6%, respectively; the AUC value of the lymphocyte assay was 0.691 and the cutoff value was $1.2 \times 10^9/L$, and the sensitivity and specificity were 74.19% and 62.50%, PPV and NPV were 88.5% and 38.5%, respectively; the AUC value of PLT assay was 0.541 and the cutoff value was $296 \times 10^9/L$, the sensitivity and specificity were 16.13% and 100.00%, PPV and NPV were 100.0% and 23.5%, respectively; the AUC value of GLU assay was The sensitivity and specificity were 36.56%, 83.33%, 89.5% and 25.3% for PPV and NPV, respectively, at an AUC value of 0.576 and a cutoff value of 5.2 mmol/L for GLU; 68.82% and 50.00% for sensitivity and specificity at an AUC value of 0.516 and a cutoff value of 1.27 mmol/L for TG The sensitivity and specificity of the AUC value of 0.574 and the cutoff value of 4.28 mmol/L for TC assay were 53.76% and 62.50%, and the PPV and NPV were 84.7% and 25.9%, respectively; the AUC value of 0.623 and the cutoff value of The sensitivity and specificity were 54.84%,

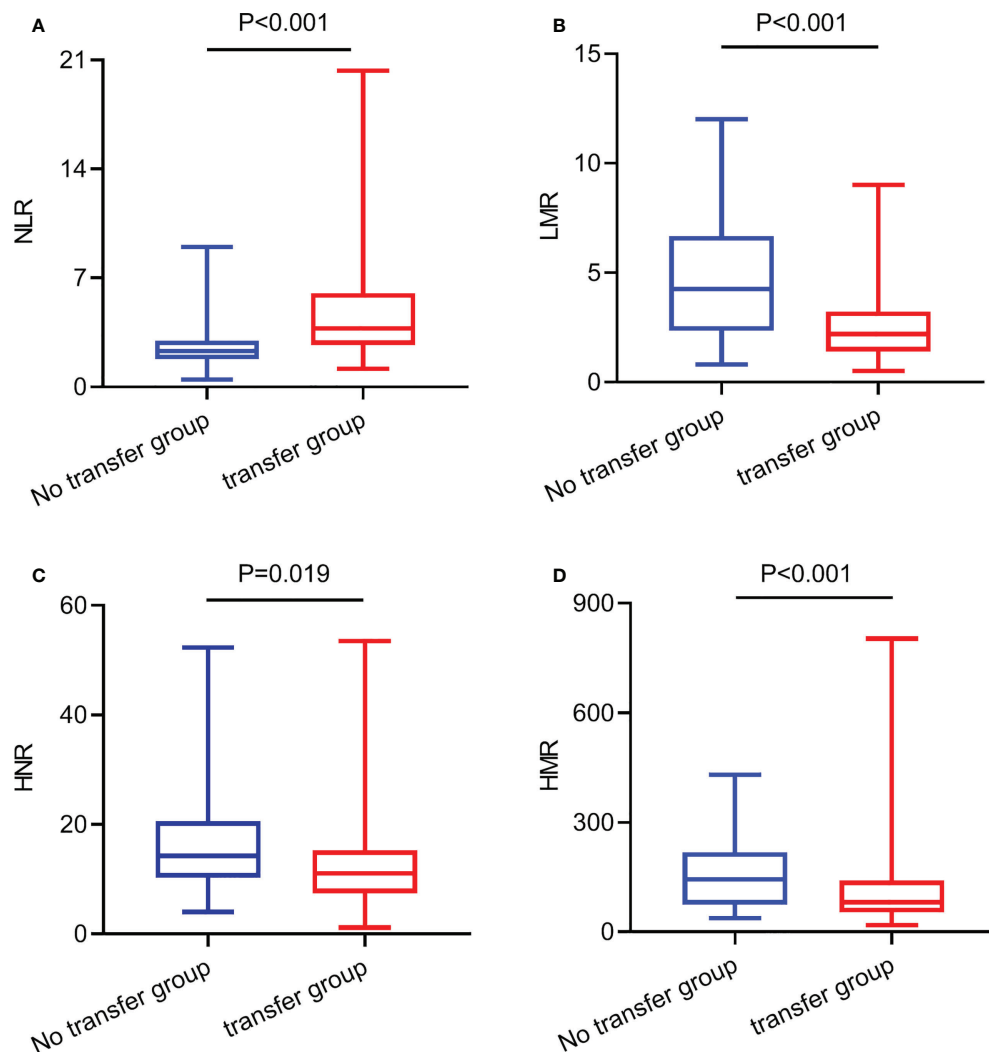


FIGURE 1

The expression levels of NLR, LMR, HNR, and HMR in metastatic and non-metastatic NSCLC patients. (A) The expression levels of NLR in metastatic and non-metastatic NSCLC patients. (B) The expression levels of LMR in metastatic and non-metastatic NSCLC patients. (C) The expression levels of HNR in metastatic and non-metastatic NSCLC patients. (D) The expression levels of HMR in metastatic and non-metastatic NSCLC patients.

75.00%, 89.5% and 30.0% for PPV and NPV, respectively, at 40.42 mg/dl; the sensitivity and specificity were 74.19%, 50.00%, and 85.2% and 33.3% for PPV and NPV, respectively, at 0.550 AUC and 112.2 mg/dl for LDL. The sensitivity and specificity of the NLR assay were 61.29% and 83.33% at an AUC value of 0.738 and a cutoff value of 3.08, and the PPV and NPV were 93.4% and 35.7%, respectively; the sensitivity and specificity of the HNR assay were 58.06% and 70.06% at an AUC value of 0.656 and a cutoff value of 11.61, respectively. The sensitivity and specificity of AUC value of 0.656 and cutoff value of 11.61 for HNR were 58.06% and 70.83%, and the PPV and NPV were 88.5% and 30.4%, respectively; the sensitivity and specificity of AUC value of

0.745 and cutoff value of 3.33 for LMR were 81.72% and 58.33%, and the PPV and NPV were 88.4% and 45.2%, respectively; the AUC value of 0.667 and cutoff value of 104.9. The sensitivity and specificity were 67.74%, 62.5%, 87.5% and 33.3% for PPV and NPV, respectively, at an AUC of 0.667 and a cutoff value of 104.9 for HMR; the sensitivity and specificity were 97.85%, 100.00%, and 100.00% for PPV and NPV, respectively, at an AUC of 0.993 and a cutoff value of 2 for TNM staging. 100.00% and 92.3%; the sensitivity and specificity were 68.82% and 87.50%, and the PPV and NPV were 95.5% and 42.0%, respectively, when the AUC value of the 4 joint tests was 0.846 and the cutoff value was 0.844; (Table 3).

TABLE 2 The expression levels of NLR, LMR, HNR, and HMR in patients of different stages.

Group	Number	NLR	LMR	HNR	HMR
stage I	9	2.78 (1.56,2.86)	3.00 (2.33,4.50)	17.68 (12.18,30.68)	178.60 (72.40,204.53)
stage II	17	2.29 (1.93,3.00)	4.50 (2.80,7.00)	13.69 (10.12,20.23)	144.58 (86.10,246.70)
stage III	29	5.44 (3.22,8.20)	2.00 (1.40,2.80)	8.44 (6.13,13.17)	80.44 (52.78,114.33)
stage IV	62	3.23 (2.51,4.61)	2.24 (1.40,3.24)	11.24 (8.04,15.34)	81.27 (53.12,126.85)

It can be concluded from the data in Table 3 that the AUC values for the four combinations of NLR, LMR, HNR, HMR and NLR+LMR+HNR+HMR were higher and had better diagnostic performance. The AUCs of the joint NLR, LMR, HNR, HMR and NLR+LMR+HNR+HMR were compared using Medcalc

software, and the differences were not statistically significant ($P > 0.05$) when the AUCs of the individual tests were compared with each other, and the differences were statistically significant ($P < 0.05$) when the AUCs of the 4 joint tests were compared with each individual test (Table 4).

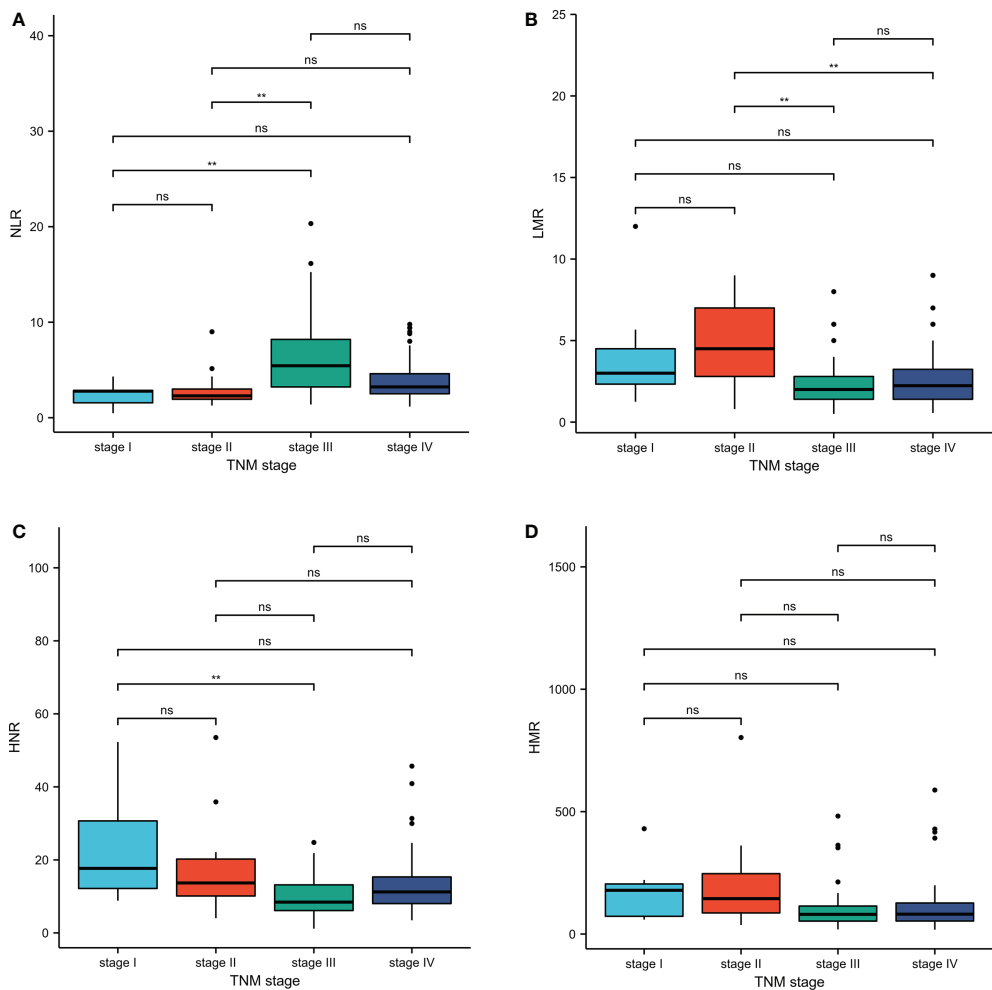


FIGURE 2 Inter-group comparison of NLR, LMR, HNR, and HMR in different stages of metastatic and non-metastatic NSCLC groups. (A) Inter-group comparison of NLR in different stages of metastatic and non-metastatic NSCLC groups. (B) Inter-group comparison of LMR in different stages of metastatic and non-metastatic NSCLC groups. (C) Inter-group comparison of HNR in different stages of metastatic and non-metastatic NSCLC groups. (D) Inter-group comparison of HMR in different stages of metastatic and non-metastatic NSCLC groups. ns, $p \geq 0.05$; ** $p < 0.01$.

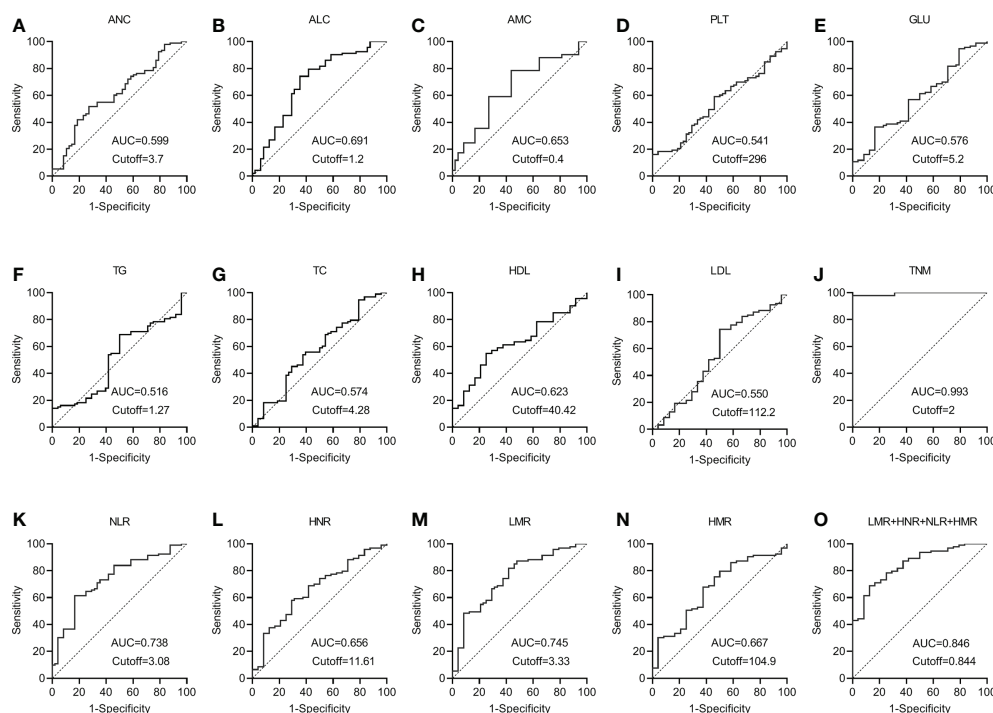


FIGURE 3

The diagnostic value of different blood markers in NSCLC metastasis. (A) The diagnostic value of ANC in NSCLC metastasis. (B) The diagnostic value of ALC in NSCLC metastasis. (C) The diagnostic value of AMC in NSCLC metastasis. (D) The diagnostic value of PLT in NSCLC metastasis. (E) The diagnostic value of GLU in NSCLC metastasis. (F) The diagnostic value of TG in NSCLC metastasis. (G) The diagnostic value of TC in NSCLC metastasis. (H) The diagnostic value of HDL in NSCLC metastasis. (I) The diagnostic value of LDL in NSCLC metastasis. (J) The diagnostic value of TNM in NSCLC metastasis. (K) The diagnostic value of NLR in NSCLC metastasis. (L) The diagnostic value of HNR in NSCLC metastasis. (M) The diagnostic value of LMR in NSCLC metastasis. (N) The diagnostic value of HMR in NSCLC metastasis. (O) The diagnostic value of LMR+HNR+NLR+HMR in NSCLC metastasis.

Clinical decision curve analysis of NLR, LMR, HNR, HMR and the combination of the four tests in NSCLC metastasis

The net clinical benefit of the model was assessed using the clinical decision curve (DCA), which was determined by the net benefit under different threshold probabilities. The net benefit was determined by subtracting the proportion of false-positive patients from the proportion of true-positive patients and by weighing the relative harms of not intervening and the negative consequences of intervening unnecessarily. The clinical decision curves showed that the net clinical benefit of the prediction models was greater than that of all patients when the threshold probabilities were 9%-68% for NLR alone, 2%-56% for LMR alone, 7%-39% for HNR alone, 18%-36% for HMR alone, and 1%-65% for the threshold probabilities when all four were combined. metastatic or non-metastatic scenarios. The graphical results show that the overall clinical benefit rate of the 4 joint tests was better than that of the single test, as shown in Figure 4.

Risk assessment of NLR, LMR, HNR, HMR in predicting NSCLC metastasis

The risk of NLR, LMR, HNR, and HMR levels in NSCLC metastasis was evaluated using binary logistic regression analysis with cutoff values (two group classification) and quartiles (P25, P50, P75) as cutoff points (four group classification), respectively. The dependent variable *y* is grouped according to whether metastasis is present (metastasis = 1, no metastasis = 0), and the median and quartile cutoff values of NLR, LMR, HNR, and HMR are grouped as independent variables. The risk value of each index for predicting NSCLC metastasis in the different groups is calculated. In the forest map, the odds ratio (or) is used as an indicator of the effect size of each indicator. In the forest map, the vertical coordinate line takes the estimated value of the effect point = 1 as an invalid line. If the horizontal line segment in the forest map intersects with the vertical coordinate line, it means that there is no statistical difference in risk between groups. If the horizontal line segment in the forest map does not intersect with the vertical coordinate line and lies on the

TABLE 3 The analysis of the expression levels of each test items in NSCLC metastasis.

Inspection items	Youden index	Cutoff value	AUC	AUC 95%CI	Sensitivity	Specificity	PPV (%)	NPV (%)
ANC	0.203	3.7	0.599	0.504-0.688	49.46	70.83	86.8	26.6
ALC	0.367	1.2	0.691	0.599-0.773	74.19	62.50	88.5	38.5
AMC	0.258	0.4	0.653	0.559-0.738	59.14	66.67	87.3	29.6
PLT	0.161	296	0.541	0.446-0.633	16.13	100.00	100	23.5
GLU	0.199	5.2	0.576	0.481-0.667	36.56	83.33	89.5	25.3
TG	0.188	1.27	0.516	0.422-0.609	68.82	50.00	89.5	25.3
TC	0.163	4.28	0.574	0.479-0.665	53.76	62.50	84.7	25.9
HDL	0.298	40.42	0.623	0.529-0.711	54.84	75.00	89.5	30.0
LDL	0.242	112.2	0.550	0.455-0.642	74.19	50.00	85.2	33.3
NLR	0.446	3.08	0.738	0.649-0.815	61.29	83.33	93.4	35.7
HNR	0.289	11.61	0.656	0.563-0.741	58.06	70.83	88.5	30.4
LMR	0.401	3.33	0.745	0.656-0.821	81.72	58.33	88.4	45.2
HMR	0.302	104.9	0.667	0.574-0.752	67.74	62.50	87.5	33.3
TNM	0.979	2	0.993	0.956-1.000	97.85	100.00	100.0	92.3
Joint tests	0.563	0.844	0.846	0.768-0.906	68.82	87.50	95.5	42.0

right side of the vertical coordinate line, it means that the risk of the current analysis group is greater than that of the reference group.

Patients were first divided into low level and high level groups based on the cutoff values of NLR (3.08), LMR (3.33), HNR (11.61), and HMR (104.9). The OR for the risk of developing NSCLC metastasis was 7.917 (95% CL, 2.502-25.046) ($P < 0.05$) in patients with high level NLR compared with low level NLR ($P < 0.05$), while the corrected OR was 6.087 (95% CL, 1.161-31.905) ($P < 0.05$); compared with high level HNR, patients with low level HNR The OR for the risk of developing NSCLC metastasis was 3.363 (95% CL, 1.272-8.886) compared with high level HNR ($P < 0.05$), while the corrected OR was 4.963 (95% CL, 1.163-21.172) ($P < 0.05$); compared with high level LMR, the OR for the risk of developing NSCLC metastasis in patients with low level LMR was 6.259 (95% CL,

2.380-16.461) ($P < 0.05$), with a concurrent corrected OR of 1.957 (95% CL, 0.376-10.184) ($P > 0.05$); the OR for the risk of NSCLC metastasis in patients with low-level HMR compared with high-level HMR was 3.500 (95% CL, 1.376- 8.904) ($P < 0.05$), while the corrected OR was 2.616 (95% CL, 0.438-15.617) ($P > 0.05$); (Figures 5, 6; Tables 5, 6).

Next, according to NLR ($Q1 \leq 2.4$; $2.4 < Q2 \leq 3.22$; $3.22 < Q3 \leq 5.29$; $Q4 > 5.29$), HNR ($Q1 \leq 7.73$; $7.73 < Q2 \leq 11.38$; $11.38 < Q3 \leq 17.48$; $Q4 > 17.48$), LMR ($Q1 \leq 1.5$; $1.5 < Q2 \leq 2.38$; $2.38 < Q3 \leq 3.75$; $Q4 > 3.75$), HMR ($Q1 \leq 57.75$; $57.75 < Q2 \leq 87.34$; $87.34 < Q3 \leq 147.515$; $Q4 > 147.515$) quartiles, and the patients were sequentially divided into Q1, Q2, Q3, and Q4 groups from low to high levels. Compared with the lowest NLR level group (Q1), the ORs for the risk of NSCLC metastasis in the Q2, Q3, and Q4 groups were 2.513 (0.826-7.642), 6.373 (1.574-25.801), and 21.412 (2.567-178.625), respectively, while the corrected ORs were 3.225 (0.841- 12.368), 8.354 (1.132-61.656), and 74.616 (1.165-4777.312), respectively; compared with the highest HNR level group (Q4), the ORs for the risk of NSCLC metastasis in the Q1, Q2, and Q3 groups were 6.075 (1.181-31.244), 2.250 (0.650-7.785), and 1.181 (0.381-3.665), while the corrected ORs were 21.007 (0.532-829.579), 8.63 (1.333-55.852), and 2.405 (0.516-11.207), respectively; compared with the highest LMR level group (Q4), the risk of NSCLC metastasis in the Q1, Q2, and Q3 groups was ORs were 12.567 (2.502-63.117), 5.200 (1.427-18.948), and 4.333 (1.287-14.588), respectively, with concurrent corrected ORs of 0.219 (0.005-9.137), 0.460 (0.027-7.904), and 1.489 (0.237- 9.360); compared with the highest HMR level group (Q4), the ORs for the risk of NSCLC metastasis in the Q1, Q2, and Q3 groups were 14.737 (1.74-124.827), 1.447 (0.475-4.410), and 2.526 (0.738-8.649), respectively, while the corrected ORs were 6.149 (0.059-640.262), 1.334 (0.091-19.578), and 3.540 (0.554-22.628); (Figures 7, 8; Tables 7, 8).

TABLE 4 The analysis of AUC area of NLR, LMR, HNR, HMR and Joint tests.

Inspection items	Z value	P value
Joint trial with NLR	2.170	0.030
Joint trial with LMR	2.273	0.023
Joint trial with HMR	3.311	<0.001
Joint trial with HNR	3.012	0.003
NLR with LMR	0.090	0.928
NLR with HNR	1.734	0.083
NLR with HMR	0.811	0.417
LMR with HNR	0.951	0.342
LMR with HMR	1.610	0.107
HNR with HMR	0.136	0.892

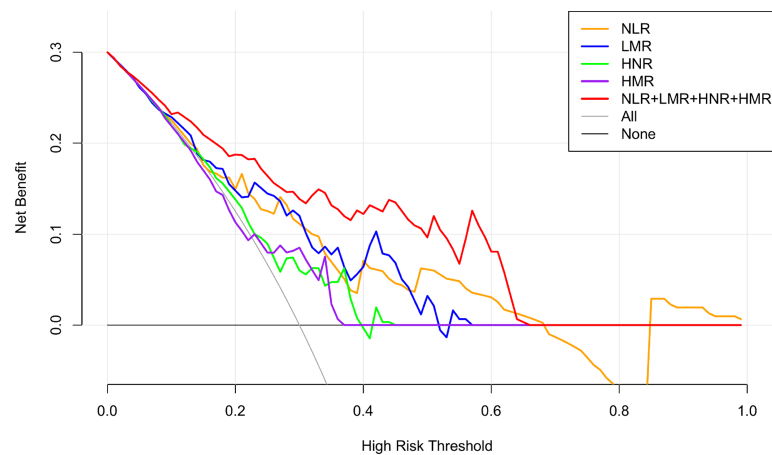


FIGURE 4
NLR, LMR, HNR, HMR and the clinical decision curve of NSCLC metastasis. (Note: the x-axis represents the threshold probability, the Y-axis represents the net benefit, the black line represents the assumption that all patients did not have metastases, and the gray line represents the assumption that all patients did have metastases).

Discussion

Lung cancer is one of the prevalent malignancies worldwide and the leading cause of cancer deaths. Reports show nearly 800,000 new lung cancer cases in China in 2018, with more than 400,000 deaths in men and 200,000 deaths in women, of which NSCLC accounts for the majority of lung cancer (25). With the newer advances in targeted therapy and surgical techniques, the prognosis of NSCLC patients has significantly improved, however, most patients have already developed local or distal metastases at the first visit or follow-up, delaying the optimal treatment window, thus non-invasive biomarkers that can identify the occurrence of metastases in NSCLC are crucial.

In this study, we analyzed the diagnostic value of NLR, LMR, HNR, and HMR in NSCLC metastasis, and the results showed that the level of NLR in the metastatic group of NSCLC was higher than that in the non-metastatic group ($P < 0.001$), and the levels of LMR, HNR, and HMR in the metastatic group were lower than those in the non-metastatic group ($P < 0.001$). A comparative analysis of the levels of NLR, LMR, HNR, and HMR in patients with different stages was also performed, and the results showed that NLR levels showed an increasing trend with increasing TNM stages, and LMR, HNR, and HMR levels showed a decreasing trend with increasing TNM stages. The report showed that (26–28) NLR, LMR, HDL and other indicators have a certain correlation with tumor occurrence,

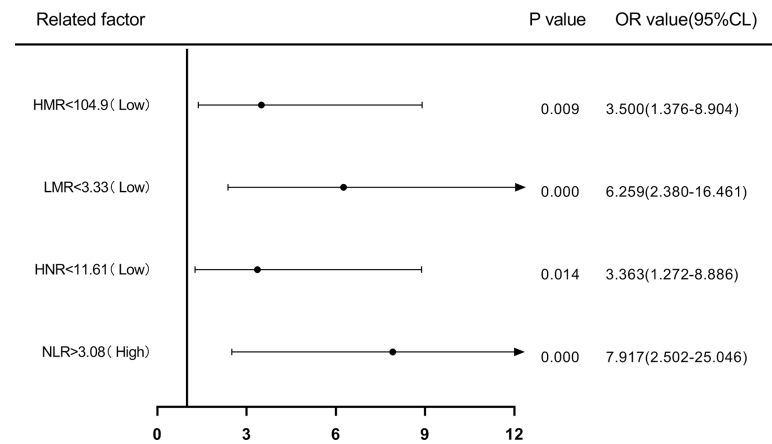


FIGURE 5
Forest plot of one-way logistic regression analysis of NLR, LMR, HNR, and HMR (two classification groups) in predicting NSCLC metastasis.

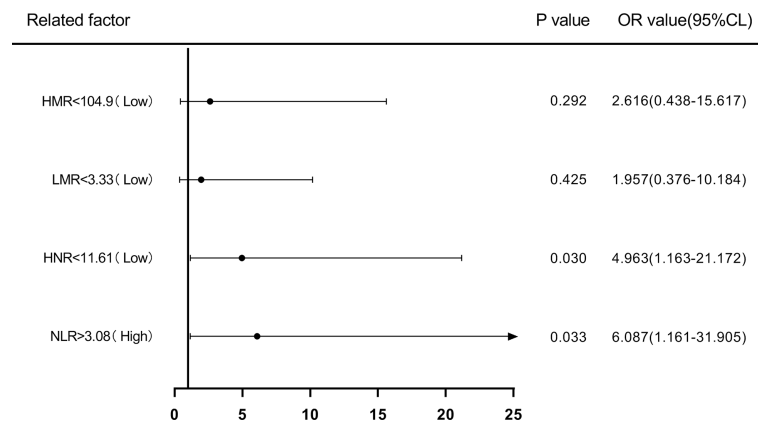


FIGURE 6

Forest plot of multifactorial logistic regression analysis of NLR, LMR, HNR, and HMR (two groups of classification) in predicting NSCLC metastasis. (Note: multifactor correction included variables ANC, ALC, AMC, HDL).

TABLE 5 Univariate Logistic regression analysis of NLR, LMR, HNR, and HMR (two categories) in predicting NSCLC transfer.

Related factors	B	S.E.	Wald	P value	OR value	95%CI	
						lower limit	upper limit
NLR>3.08 (High)	2.069	0.588	12.396	0.000	7.917	2.502	25.046
HNR<11.61 (Low)	1.213	0.496	5.982	0.014	3.363	1.272	8.886
LMR<3.33 (Low)	1.834	0.493	13.818	0.000	6.259	2.380	16.461
HMR<104.9 (Low)	1.253	0.476	6.914	0.009	3.500	1.376	8.904

TABLE 6 Multivariate Logistic regression analysis of NLR, LMR, HNR, and HMR (classified in the two-group categories) in the prediction of NSCLC metastasis.

Related factors	B	S.E.	Wald	P value	OR value	95%CI	
						lower limit	upper limit
NLR>3.08 (High)	1.806	0.845	4.566	0.033	6.087	1.161	31.905
HNR<11.61 (Low)	1.602	0.740	4.684	0.030	4.963	1.163	21.172
LMR<3.33 (Low)	0.671	0.842	0.636	0.425	1.957	0.376	10.184
HMR<104.9 (Low)	0.961	0.912	1.112	0.292	2.616	0.438	15.617

multivariate adjustment included variables ANC, ALC, AMC, HDL.

development and metastasis, which is basically consistent with this study, indicating that NLR, LMR, HNR and HMR have a certain value in NSCLC metastasis.

Using medcalc software to produce the area under the ROC curve for each index and combined test, the AUC values of NLR, LMR, HNR, HMR and NLR+LMR+HNR+HMR were higher than other indexes, indicating that these four indexes have better diagnostic value in NSCLC metastasis. NLR is a commonly used index calculated from the indexes ANC, ALC, which respond to inflammation. Reports show that (29) elevated NLR can be used as a predictor of tumor types such as breast cancer, gastric cancer,

ovarian cancer, pancreatic cancer, etc. The AUC value of LMR test is 0.745, and LMR is an inflammatory index calculated from ALC and AMC. Lymphocytes play an important role in resisting tumors, and decreased lymphocytes will lead to a weakened response of the body to resist tumors, while monocytes, as participants in the inflammatory response (30). The ANC and AMC have a role in promoting tumor progression. The ANC can secrete pro-angiogenic and anti-apoptotic factors, which indirectly provide an environment for tumor cell growth and metastasis (31). HDL plays a role in tumor cell development by suppressing the immune response, and reduced HDL levels

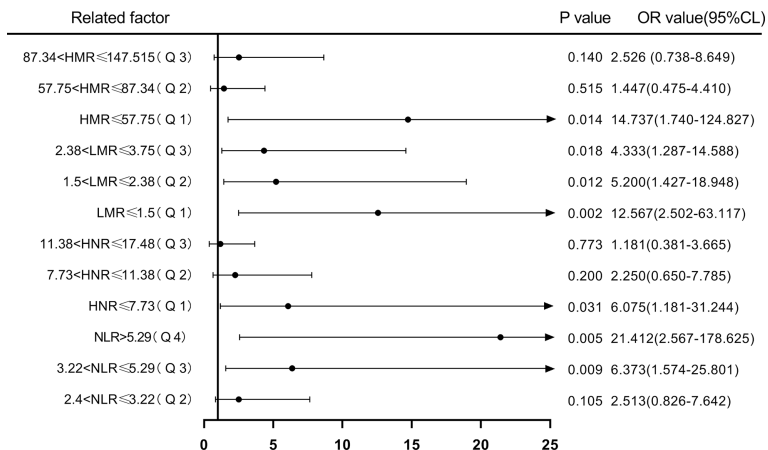


FIGURE 7
Forest plot of one-way logistic regression analysis of NLR, LMR, HNR, and HMR (four groups of classification) in predicting NSCLC metastasis.

predict poor tumor prognosis. Patients with poor prognosis, and for every 10 mg/dl increase in HDL level, cancer incidence is reduced by 36%, and HDL level shows a positive correlation with overall survival of tumor patients (32). By comparing the AUCs of NLR, LMR, HNR, HMR and the 4 joint tests, the AUCs of each single test index were not statistically significant when compared with each other ($P > 0.05$), and the 4 joint tests were higher than the AUCs of each single test ($P < 0.05$), indicating that the 4 joint tests were superior to the single test indexes in the diagnostic performance of NSCLC metastasis. The clinical decision curve analysis of NLR, LMR, HNR, HMR and the 4 joint indicators also showed that each single indicator had a better clinical benefit rate in different threshold probability ranges, and the overall clinical

benefit rate of the combined indicators was better than that of the single indicators. The overall clinical benefit rate of the combined assay was better than that of the single assay, suggesting that the combined assay of the four clinical indicators can be used as a reference indicator for the disease progression of NSCLC patients.

The risk of NLR, LMR, HNR, and HMR levels in NSCLC metastasis was evaluated using binary logistic regression analysis with cutoff values (two groups of classification) and quartiles (P25, P50, P75) as cut points (four groups of classification), respectively. The results showed that when the cutoff value was used as the cut point, the OR for the risk of NSCLC metastasis was 6.087 ($P < 0.05$) in patients with high level NLR compared

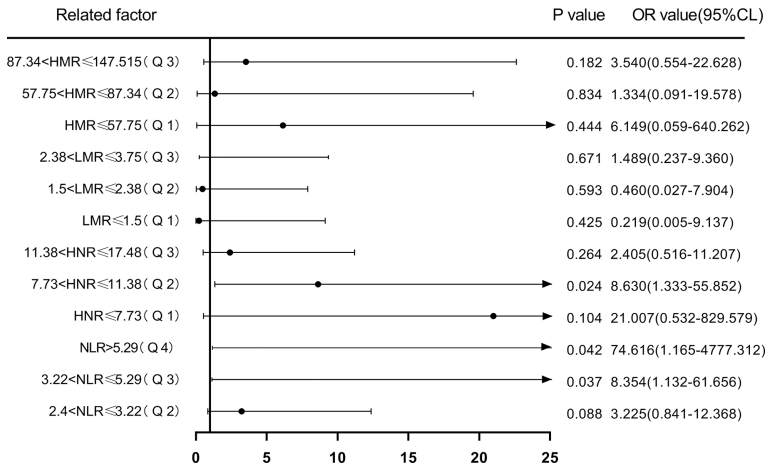


FIGURE 8
Forest plot of multifactorial logistic regression analysis of NLR, LMR, HNR, and HMR (four groups of classification) in predicting NSCLC metastasis. (Note: multifactor correction included variables ANC, ALC, AMC, HDL).

TABLE 7 Univariate Logistic regression analysis of NLR, LMR, HNR, and HMR (all four categories) in the prediction of NSCLC metastasis.

Related factors	B	S.E.	Wald	P value	OR value	95%CI	
						lower limit	upper limit
NLR (Q2)	0.921	0.568	2.635	0.105	2.513	0.826	7.642
NLR (Q3)	1.852	0.713	6.737	0.009	6.373	1.574	25.801
NLR (Q4)	3.064	1.082	8.014	0.005	21.412	2.567	178.625
HNR (Q1)	1.804	0.836	4.662	0.031	6.075	1.181	31.244
HNR (Q2)	0.811	0.633	1.639	0.200	2.250	0.650	7.785
HNR (Q3)	0.167	0.578	0.083	0.773	1.181	0.381	3.665
LMR (Q1)	2.531	0.823	9.448	0.002	12.567	2.502	63.117
LMR (Q2)	1.649	0.660	6.245	0.012	5.200	1.427	18.948
LMR (Q3)	1.466	0.619	5.605	0.018	4.333	1.287	14.588
HMR (Q1)	2.690	1.090	6.091	0.014	14.737	1.740	124.827
HMR (Q2)	0.370	0.568	0.423	0.515	1.447	0.475	4.410
HMR (Q3)	0.927	0.628	2.178	0.140	2.526	0.738	8.649

TABLE 8 Multivariate Logistic regression analysis of NLR, LMR, HNR, HNR and HMR (classified four groups) in the prediction of NSCLC metastasis.

Related factors	B	S.E.	Wald	P value	OR value	95%CI	
						lower limit	upper limit
NLR (Q2)	1.171	0.686	2.914	0.088	3.225	0.841	12.368
NLR (Q3)	2.123	1.020	4.333	0.037	8.354	1.132	61.656
NLR (Q4)	4.312	2.122	4.129	0.042	74.616	1.165	4777.312
HNR (Q1)	3.045	1.876	2.636	0.104	21.007	0.532	829.579
HNR (Q2)	2.155	0.953	5.116	0.024	8.630	1.333	55.852
HNR (Q3)	0.878	0.785	1.249	0.264	2.405	0.516	11.207
LMR (Q1)	-1.517	1.903	0.635	0.425	0.219	0.005	9.137
LMR (Q2)	-0.776	1.451	0.286	0.593	0.460	0.027	7.904
LMR (Q3)	0.398	0.938	0.180	0.671	1.489	0.237	9.360
HMR (Q1)	1.816	2.370	0.587	0.444	6.149	0.059	640.262
HMR (Q2)	0.288	1.371	0.044	0.834	1.334	0.091	19.578
HMR (Q3)	1.264	0.946	1.784	0.182	3.540	0.554	22.628

multivariate adjustment included variables ANC, ALC, AMC, HDL.

with the low level group after correction, and the OR for the risk of NSCLC metastasis was 3.363 ($P < 0.05$) in patients with low level HNR compared with high level. When quartiles were used as cut points for four-group classification, the ORs for the risk of NSCLC metastasis in patients in the corrected high level NLR (Q3, Q4) group compared with the low level Q1 group were 8.354 and 74.616, respectively ($P < 0.05$); the OR for the risk of NSCLC metastasis in patients in the low level HNR Q2 group compared with the high level Q4 group was 8.63 ($P < 0.05$). The remaining differences were not statistically significant in the low-level LMR and HMR groups compared with the high-level group ($P > 0.05$). The results suggest that NLR and HNR can be used as risk predictors for the development of metastasis in NSCLC patients, however, LMR and HMR are not sufficient as risk predictors for the development of metastasis in NSCLC patients.

In summary, NLR, LMR, HNR, and HMR have good diagnostic value in NSCLC metastasis. NLR and HNR can be used as risk predictors for metastasis in patients with NSCLC, and NLR, LMR, HNR, and HMR can be easily calculated based on blood cell counts and lipid tests, and the advantage of being easy to perform in primary care institutions. It is worth noting that the present study is a retrospective study with a small sample size, and there may be bias in diagnostic value and unavoidable selection bias. Because of the ratio of follow-up time, the study could not evaluate the long-term prognosis of patients with metastases. More samples will be collected and a prospective study will be designed in a later period to evaluate the long-term metastasis of patients, such as 3–5 years, whether transmission has occurred, to better evaluate the diagnostic value of each index in NSCLC patients with metastasis.

Data availability statement

The original contributions presented in the study are included in the article. Further inquiries can be directed to the corresponding authors.

Ethics statement

The study was approved by the Ethics Committee of Shanghai Tongji hospital (2021KYSB061), and the methods were designed according to the Declaration of Helsinki. Because the data were analyzed retrospectively, written informed consent from the subjects was waived.

Author contributions

WZ: formal analysis, investigation, visualization, writing-original draft. WW: investigation, methodology. JW: investigation, methodology. JT: investigation, methodology. WY: investigation, methodology. YYu: methodology, supervision. YYa: methodology, supervision. AS: resources, project administration. WQ: conceptualization, funding acquisition, methodology, writing-review and editing. All authors contributed to the article and approved the submitted version.

References

- Zanini D, Manfredi LH, Pelinson LP, Pimentel VC, Cardoso AM, Carmo Araújo Gonçalves VD, et al. ADA activity is decreased in lymphocytes from patients with advanced stage of lung cancer. *Med Oncol* (2019) 36:78. doi: 10.1007/s12032-019-1301-1
- Stratmann JA, Lacko R, Ballo O, Shaid S, Gleiber W, Vehreschild M, et al. Colonization with multi-drug-resistant organisms negatively impacts survival in patients with non-small cell lung cancer. *PloS One* (2020) 15:e0242544. doi: 10.1371/journal.pone.0242544
- Rice SR, Saboury B, Houshmand S, Salavati A, Kalbasi A, Goodman CR, et al. Quantification of global lung inflammation using volumetric 18F-FDG PET/CT parameters in locally advanced non-small-cell lung cancer patients treated with concurrent chemoradiotherapy: A comparison of photon and proton radiation therapy. *Nucl Med Commun* (2019) 40:618–25. doi: 10.1097/MNM.0000000000000997
- Bica-Pop C, Cojocneanu-Petric R, Magdo L, Raduly L, Gulei D, Berindan-Neagoe I. Overview upon miR-21 in lung cancer: Focus on NSCLC. *Cell Mol Life Sci* (2018) 75:3539–51. doi: 10.1007/s00018-018-2877-x
- Reli V, Trerotola M, Guerra E, Alberti S. Abandoning the notion of non-small cell lung cancer. *Trends Mol Med* (2019) 25:585–94. doi: 10.1016/j.molmed.2019.04.012
- Gardner LD, Loffredo PhD CA, Langenberg P, George D, Deepak J, Harris CC, et al. Associations between history of chronic lung disease and non-small cell lung carcinoma in Maryland: Variations by sex and race. *Ann Epidemiol* (2018) 28:543–8. doi: 10.1016/j.annepidem.2018.04.012
- Zhang F, Wang J, Fu J, Hu L, Zheng X, Wang Y, et al. Clinical value of combined detection of reactive oxygen species modulator 1 and adenosine deaminase in pleural effusion in the identification of NSCLC associated malignant pleural effusion. *J Clin Lab Anal* (2020) 34:e23091. doi: 10.1002/jcla.23091
- Rice SR, Molitoris JK, Vyfhuis M, Edelman MJ, Burrows WM, Feliciano J, et al. Lymph node size predicts for asymptomatic brain metastases in patients with non-small-cell lung cancer at diagnosis. *Clin Lung Cancer* (2019) 20:e107-107e114. doi: 10.1016/j.clcc.2018.09.014
- Chicas-Sett R, Zafra-Martin J, Morales-Orue I, Castilla-Martinez J, Berenguer-Frances MA, Gonzalez-Rodriguez E, et al. Immunoradiotherapy as an effective therapeutic strategy in lung cancer: From palliative care to curative intent. *Cancers (Basel)* (2020) 12(8):2178. doi: 10.3390/cancers12082178
- Ma Z, Wei K, Yang F, Guo Z, Pan C, He Y, et al. Tumor-derived exosomal miR-3157-3p promotes angiogenesis, vascular permeability and metastasis by targeting TIMP/KLF2 in non-small cell lung cancer. *Cell Death Dis* (2021) 12:840. doi: 10.1038/s41419-021-04037-4
- Wadowska K, Bil-Lula I, Trembecki Ł, Śliwińska-Mossoń M. Genetic markers in lung cancer diagnosis: A review. *Int J Mol Sci* (2020) 21(13):4569. doi: 10.3390/ijms21134569
- Singh A, Kant R, Saluja TS, Tripathi T, Srivastava K, Naithani M, et al. Differential diagnosis of non-small cell lung carcinoma by circulating microRNA. *J Cancer Res Ther* (2020) 16:127–31. doi: 10.4103/jcrt.JCRT_872_19
- Qian C, Dai N, Xu M, Luo H, Feng Y, Zhang M, et al. ctDNA facilitated the diagnosis of a patient with synchronous urothelial carcinoma and non-small cell lung cancer: case report. *Ann Transl Med* (2020) 8:1323. doi: 10.21037/atm-20-6552
- Huang Y, Liu G, Ma H, Tian Y, Huang C, Liu F, et al. Plasma lncRNA FEZF1-AS1 as a potential biomarker for diagnosis of non-small-cell lung carcinoma. *Med (Baltimore)* (2020) 99:e21019. doi: 10.1097/MD.00000000000021019
- Voigt W, Manegold C, Pilz L, Wu YL, Müllauer L, Pirker R, et al. Beyond tissue biopsy: A diagnostic framework to address tumor heterogeneity in lung cancer. *Curr Opin Oncol* (2020) 32:68–77. doi: 10.1097/CCO.0000000000000598

Funding

This work was supported by the National Natural Science Foundation of China (81902984); the “Gan Quan Xin Xing” talent training program of Shanghai Tongji Hospital (HRBC2005), the Yancheng city medical science and technology development plan project (YK2019112) and the Medical Research Project of Jiangsu Provincial Health and Health Commission (2019179).

Conflict of interest

The authors declare that the research was conducted in the absence of any commercial or financial relationships that could be construed as a potential conflict of interest.

Publisher's note

All claims expressed in this article are solely those of the authors and do not necessarily represent those of their affiliated organizations, or those of the publisher, the editors and the reviewers. Any product that may be evaluated in this article, or claim that may be made by its manufacturer, is not guaranteed or endorsed by the publisher.

16. Esagian SM, Grigoriadou GI, Nikas IP, Boikou V, Sadow PM, Won JK, et al. Comparison of liquid-based to tissue-based biopsy analysis by targeted next generation sequencing in advanced non-small cell lung cancer: A comprehensive systematic review. *J Cancer Res Clin Oncol* (2020) 146:2051–66. doi: 10.1007/s00432-020-03267-x
17. Shoji F, Kozuma Y, Toyokawa G, Yamazaki K, Takeo S. Complete blood cell count-derived inflammatory biomarkers in early-stage non-Small-Cell lung cancer. *Ann Thorac Cardiovasc Surg* (2020) 26:248–55. doi: 10.5761/atcs.0a.19-00315
18. Chen L, Qian J, Lin L, Lin J, Chen Q, Zhuang Z, et al. Prognostic value of preoperative lymphocyte-to-monocyte ratio in oral cancer patients and establishment of a dynamic nomogram. *Oral Dis* (2021) 27:1127–36. doi: 10.1111/odi.13629
19. Stojkovic Lalosevic M, Pavlovic Markovic A, Stankovic S, Stojkovic M, Dimitrijevic I, Radoman Vujacic I, et al. Combined diagnostic efficacy of neutrophil-to-Lymphocyte ratio (NLR), platelet-to-Lymphocyte ratio (PLR), and mean platelet volume (MPV) as biomarkers of systemic inflammation in the diagnosis of colorectal cancer. *Dis Markers* (2019) 2019:6036979. doi: 10.1155/2019/6036979
20. Hao B, Peng X, Bi B, Yu M, Sang C, Chen Z. Preoperative serum high-density lipoprotein cholesterol as a predictor of poor survival in patients with clear cell renal cell cancer. *Int J Biol Markers* (2019) 34:168–75. doi: 10.1177/1724600819831404
21. Ganjali S, Ricciuti B, Pirro M, Butler AE, Atkin SL, Banach M, et al. High-density lipoprotein components and functionality in cancer: State-of-the-Art. *Trends Endocrinol Metab* (2019) 30:12–24. doi: 10.1016/j.tem.2018.10.004
22. Liu J, Li S, Zhang S, Liu Y, Ma L, Zhu J, et al. Systemic immune-inflammation index, neutrophil-to-lymphocyte ratio, platelet-to-lymphocyte ratio can predict clinical outcomes in patients with metastatic non-small-cell lung cancer treated with nivolumab. *J Clin Lab Anal* (2019) 33:e22964. doi: 10.1002/jcla.22964
23. Rami-Porta R, Asamura H, Travis WD, Rusch VW. Lung cancer - major changes in the American joint committee on cancer eighth edition cancer staging manual. *CA Cancer J Clin* (2017) 67:138–55. doi: 10.3322/caac.21390
24. Lim W, Ridge CA, Nicholson AG, Mirsadraee S. The 8th lung cancer TNM classification and clinical staging system: Review of the changes and clinical implications. *Quant Imaging Med Surg* (2018) 8:709–18. doi: 10.21037/qims.2018.08.02
25. Liu S, Zang H, Zheng H, Wang W, Wen Q, Zhan Y, et al. miR-4634 augments the anti-tumor effects of RAD001 and associates well with clinical prognosis of non-small cell lung cancer. *Sci Rep* (2020) 10:13079. doi: 10.1038/s41598-020-70157-0
26. Cupp MA, Cariolou M, Tzoulaki I, Aune D, Evangelou E, Berlanga-Taylor AJ. Neutrophil to lymphocyte ratio and cancer prognosis: An umbrella review of systematic reviews and meta-analyses of observational studies. *BMC Med* (2020) 18:360. doi: 10.1186/s12916-020-01817-1
27. Mandaliya H, Jones M, Oldmeadow C, Nordman II. Prognostic biomarkers in stage IV non-small cell lung cancer (NSCLC): Neutrophil to lymphocyte ratio (NLR), lymphocyte to monocyte ratio (LMR), platelet to lymphocyte ratio (PLR) and advanced lung cancer inflammation index (ALI). *Transl Lung Cancer Res* (2019) 8:886–94. doi: 10.21037/tlcr.2019.11.16
28. Penson P, Long DL, Howard G, Howard VJ, Jones SR, Martin SS, et al. Associations between cardiovascular disease, cancer, and very low high-density lipoprotein cholesterol in the REasons for geographical and racial differences in stroke (REGARDS) study. *Cardiovasc Res* (2019) 115:204–12. doi: 10.1093/cvr/cvy198
29. Han F, Liu Y, Cheng S, Sun Z, Sheng C, Sun X, et al. Diagnosis and survival values of neutrophil-lymphocyte ratio (NLR) and red blood cell distribution width (RDW) in esophageal cancer. *Clin Chim Acta* (2019) 488:150–8. doi: 10.1016/j.cca.2018.10.042
30. Liu XZ, Wang JM, Ji YX, Zhao DB. Monocyte-to-high-density lipoprotein cholesterol ratio is associated with the presence and size of thyroid nodule irrespective of the gender. *Lipids Health Dis* (2020) 19:36. doi: 10.1186/s12944-020-1196-z
31. Yalon M, Toren A, Jabarin D, Fadida E, Constantini S, Mehrian-Shai R. Elevated NLR may be a feature of pediatric brain cancer patients. *Front Oncol* (2019) 9:327. doi: 10.3389/fonc.2019.00327
32. Wang Y, Sun XQ, Lin HC, Wang DS, Wang ZQ, Shao Q, et al. Correlation between immune signature and high-density lipoprotein cholesterol level in stage II/III colorectal cancer. *Cancer Med* (2019) 8:1209–17. doi: 10.1002/cam4.1987



OPEN ACCESS

EDITED BY

Alberto Sandri,
San Luigi Gonzaga Hospital, Italy

REVIEWED BY

Ming Li,
Fudan University, China
Yang Wo,
Qingdao University, China

*CORRESPONDENCE

Jialong Zhu
Zhujialong3@163.com
Gening Jiang
geningjiang@tongji.edu.cn

[†]These authors have contributed
equally to this work

SPECIALTY SECTION

This article was submitted to
Thoracic Oncology,
a section of the journal
Frontiers in Oncology

RECEIVED 15 April 2022

ACCEPTED 31 October 2022

PUBLISHED 17 November 2022

CITATION

Ge T, Zhu S, Sun L, Yin L, Dai J, Qian J,
Chen X, Zhang P, Zhu J and Jiang G
(2022) Development and validation of
nomogram prognostic model for
early-stage T1-2N0M0 small cell lung
cancer: A population-based analysis.
Front. Oncol. 12:921365.
doi: 10.3389/fonc.2022.921365

COPYRIGHT

© 2022 Ge, Zhu, Sun, Yin, Dai, Qian,
Chen, Zhang, Zhu and Jiang. This is an
open-access article distributed under
the terms of the [Creative Commons
Attribution License \(CC BY\)](#). The use,
distribution or reproduction in other
forums is permitted, provided the
original author(s) and the copyright
owner(s) are credited and that the
original publication in this journal is
cited, in accordance with accepted
academic practice. No use,
distribution or reproduction is
permitted which does not comply with
these terms.

Development and validation of nomogram prognostic model for early-stage T1-2N0M0 small cell lung cancer: A population-based analysis

Tao Ge^{1†}, Shuncang Zhu^{1†}, Liangdong Sun^{1†}, Laibo Yin^{2†},
Jie Dai¹, Jiayi Qian¹, Xiangru Chen¹, Peng Zhang¹,
Jialong Zhu^{2*} and Gening Jiang^{1*}

¹Department of Thoracic Surgery, Shanghai Pulmonary Hospital, Tongji University School of Medicine, Shanghai, China, ²Department of Thoracic and Cardiovascular Surgery, The First Affiliated Hospital, School of Medicine, Shihezi University, Shihezi, China

Background: Survival outcomes of early-stage T1-2N0M0 small cell lung cancer (SCLC) patients differ widely, and the existing Veterans Administration Lung Study Group (VALSG) or TNM staging system is inefficient at predicting individual prognoses. In our study, we developed and validated nomograms for individually predicting overall survival (OS) and lung cancer-specific survival (LCSS) in this special subset of patients.

Methods: Data on patients diagnosed with T1-2N0M0 SCLC between 2000 and 2015 were extracted from the Surveillance, Epidemiology, and End Results (SEER) database. All enrolled patients were split into a training cohort and a validation cohort according to the year of diagnosis. Using multivariable Cox regression, significant prognostic factors were identified and integrated to develop nomograms for 1-, 3-, and 5-year OS and LCSS prediction. The prognostic performance of our new model was measured by the concordance index (C-index) and calibration curve. We compared our latest model and the 8th AJCC staging system using decision curve analyses (DCA). Kaplan–Meier survival analyses were applied to test the application of the risk stratification system.

Results: A total of 1,147 patients diagnosed from 2000 to 2011 were assigned to the training cohort, and 498 cases that were diagnosed from 2012 to 2015 comprised the validation cohort. Age, surgery, lymph node removal (LNR), and chemotherapy were independent predictors of LCSS. The variables of sex, age, surgery, LNR, and chemotherapy were identified as independent predictors of OS. The above-mentioned prognostic factors were entered into the nomogram construction of OS and LCSS. The C-index of this model in the training cohort was 0.663, 0.702, 0.733, and 0.658, 0.702, 0.733 for predicting 1-, 3-, and 5-year OS and LCSS, respectively. Additionally, in the validation cohort, there were 0.706, 0.707, 0.718 and 0.712, 0.691, 0.692. The calibration

curve showed accepted prediction accuracy between nomogram-predicted survival and actual observed survival, regardless of OS or LCSS. In addition, there were significant distinctions in the survival curves of OS and LCSS between different risk groups stratified by prognostic scores. Compared with the 8th AJCC staging system, our new model also improved net benefits.

Conclusions: We developed and validated novel nomograms for individual prediction of OS and LCSS, integrating the characteristics of patients and tumors. The model showed superior reliability and may help clinicians make treatment strategies and survival predictions for early-stage T1-2N0M0 SCLC patients.

KEYWORDS

small cell lung cancer, nomogram, prognosis, Surveillance, Epidemiology, and End Results (SEER), lung cancer-specific survival

Introduction

Lung cancer remains the leading cause of cancer-related deaths and an important public health concern affecting both men and women worldwide (1). Small cell lung cancer (SCLC) accounts for approximately 15%–20% of lung cancer patients and is characterized by high vascularity, high cellular proliferation, rapid progression, and early metastatic spread (2). Approximately 30% of SCLC patients were non-metastatic at initial diagnosis (3). Compared to NSCLC, for which the 5-year survival rate is 18%, SCLC has only a 6.2% 5-year survival rate (4).

With the improvement of patients' health awareness and the popularity of computed tomography (CT) screening for long-term smokers, it is more likely to increase the incidence of early-stage lung cancer diagnosis (5). However, approximately 5% of SCLC patients present with early-stage T1-2N0M0 disease, which has a better prognosis with a 5-year survival rate of up to 50% (6–8). In this group of patients, a surgical approach can be proposed as part of multidisciplinary treatment after excluding mediastinal lymph node involvement, according to the current National Comprehensive Cancer Network (NCCN) guidelines (9). Most previous clinical guidelines and treatment strategies for SCLC were based on the Veterans Administration Lung Study Group (VALSG) staging system, in which SCLC patients were roughly divided into limited-stage and extensive-stage. However, individual survival differs widely at the same stage. It has been recommended that the American Joint Committee on Cancer (AJCC) TNM staging system replace the VALSG staging system because the TNM system could contribute to more appropriate treatment selections and more precise assessments of prognosis (10, 11). Nevertheless, in addition to the TNM staging status, some studies have revealed that clinical characteristics like sex, age, location,

surgical procedure, adjuvant chemotherapy, or radiotherapy were also noteworthy factors influencing individual survival outcomes of SCLC cancer patients (12–14). Hence, a more refined model with better individualized prognostic discrimination is required to solve this problem.

Nomogram models have been widely recognized as a feasible tool to predict individual prognosis for cancer patients and could benefit treatment strategy-making and clinical trials (15, 16). It mainly depends on both patient and disease features. The unique advantage of the nomogram is that it provides the score of each influencing factor according to the contribution degree of each influencing factor in the regression model. It then calculates the total score of an individual to obtain the predicted value of the individual. To date, there have been no nomogram studies regarding the OS and LCSS of early-stage T1-2N0M0 SCLC patients. Thus, the objective of this study was to derive and validate a prognostic nomogram to quantitatively predict survival outcomes in early-stage T1-2N0M0 SCLC patients using a large cohort from the SEER database, which would help clinicians make better clinical decisions and further improve the survival of patients.

Methods

Patient selection

The SEER is an authoritative source for cancer statistics that covers approximately 28% of the US population and contains data on cancer occurrences in 18 areas of the United States, which can help reduce the cancer burden among the U.S. population. The data of 100,585 patients diagnosed with SCLC from 2000 to 2015 were retrieved from the SEER database using

SEER*Stat version 8.3.9 (National Cancer Institute, Bethesda, MD, USA). The study cohort consisted of patients with the following International Classification of Disease for Oncology, Third Edition (ICD-O-3), morphology codes: 8041/3, 8042/3, 8043/3, 8044/3, and 8045/3; and the site codes: C34.0, C34.1, C34.2, C34.3, C34.8, and C34.9. The exclusion criteria were as follows: (I) not receiving regular follow-up or no follow-up; (II) patients having at least one prior malignancy; (III) not being pathologically confirmed by immunohistochemistry; and (IV) patients with missing information concerning the primary tumor size (T), regional lymph node (N), or distant metastasis (M) stage and clinical information. After that, we also excluded patients who underwent pneumonectomy and whose information about the removed lymph nodes was unknown.

Variables

The extracted clinical information contained sex, age (<65 years, ≥65 years), race, primary site (upper lobe, lower lobe, middle lobe, main bronchus, overlapping lesion), laterality (left, right), tumor size (≤3 cm, 3–4 cm, 4–5 cm), pathological grade (moderate, well, poor, undifferentiated, unknown), surgery (lobectomy, others, non-surgery), lymph nodes removal (LNR) (<4, ≥4 regional lymph nodes), radiotherapy or not, chemotherapy or not, survival months, causes of death, vital status. In terms of surgery, all other surgical approaches are classified as others except for lobectomy because the number of some surgical procedures is so limited that we cannot analyze them separately. In addition, we converted the TNM stages based on the 6/7th edition to those of the 8th AJCC staging system for each patient using tumor size, tumor CS extension, and the 6/7th edition N/M stages (17). We assembled the tumor sizes of ≤1 cm, 1–2 cm, and 2–3 cm as the group of ≤3 cm because no significant difference in survival was found among these patients (18). For chemotherapy or radiotherapy, we were unable to define neoadjuvant or adjuvant therapy due to the lack of sequence of the treatment. Regrettably, the information on the visceral pleural invasion for lung cancer was unavailable before 2010. The information regarding prophylactic cranial radiation was missing during this period. The primary outcomes were defined as OS and LCSS. The time of the last follow-up was November 2020. OS was defined as the interval between cancer diagnosis and death resulting from any cause or the last follow-up for patients still alive. LCSS was defined as the length of time from cancer diagnosis to death from lung cancer.

Development and evaluation of the nomogram prognostic model

According to our exclusion criteria, 1,645 patients were included for analysis. A total of 1,147 patients who were diagnosed from 2000 to 2011 were assigned to the training

cohort and used to develop the nomogram prognostic models. Four hundred and ninety-eight patients diagnosed from 2012 to 2015 were assigned to the validation cohort and used to validate the model. To identify independent prognostic factors for OS and LCSS to build our prognosis model, we performed a univariate COX proportional hazard regression analysis. Significant factors from the univariate analysis (P -value <0.05) entered the multivariate COX proportional hazard regression analysis to obtain the hazard ratio (HR) and corresponding 95% confidential interval (CI) for every independent prognostic variable. The prognostic nomograms for OS and LCSS were constructed based on the risk factors calculated by the final multivariate Cox regression model.

The performance and evaluation of a nomogram mainly depend on two facets: discrimination and calibration accuracy. The discrimination refers to the efficiency of the model to distinguish patients with different survival outcomes. The concordance index (C-index) is recognized as a tool to measure discrimination and represents a concordance measure analogous to the area under the receiver operating characteristic (ROC). The theoretical value of the C-index ranges from 0 (indicating no better than random chance) to 1.0 (indicating perfect prediction) (16). Calibration curves of the nomogram for 1-, 3-, and 5-year survival were plotted to measure the consistency between predicted survival probability and actual survival proportion in the training and validation cohorts. A perfectly calibrated model would present a 45-degree curve. The estimation of discrimination and calibration was performed by bootstrapping 1,000 times. The conventional staging model, the AJCC 8th TNM staging system, was also assessed for prognostic performance. In addition, the area under the curve (AUC) of the time-dependent ROC was calculated for each month, from months 1 to 60. We conducted the comparisons of AUCs between the proposed nomogram and the AJCC 8th staging system. The decision curve analysis (DCA) was also conducted to evaluate the benefits and advantages of our new predicting model over the existing 8th edition AJCC TNM staging system (19).

The patients of every cohort were divided into two different risk groups (low-risk and high-risk) according to the prognostic scores of every patient on the nomogram. The cut-off values were defined using the X-tile software version 3.6.1 (Copyright: Camp/Rimm, Yale University), which could recognize the optimal cut-off values for continuous variables by calculating the largest Chi-square and minimum p -values. These cut-off values were then applied to the different TNM categories and the validation cohort; the respective log-rank P values were calculated to compare the difference in survival.

Statistical analysis

Chi-squared tests were used to analyze the categorical variables. OS and LCSS survival analyses were performed

using the Kaplan–Meier method. Kaplan–Meier survival analysis was used to assess distinctions in prognosis with a log-rank P-value. A two-sided P-value <0.05 was deemed significant. All data analyses were performed using SPSS 26.0 (SPSS, Chicago, IL) and RStudio version 4.1.0 (RStudio, Boston, MA, USA). The R packages ‘survival,’ ‘rms,’ ‘riskRegression,’ ‘survminer,’ and ‘ggDCA’ were used for nomogram construction and evaluation. Furthermore, the R packages ‘DynNom,’ ‘DNbuilder,’ and ‘rsconnect’ were applied for developing a user-friendly web-based interface for our nomogram.

Results

Characteristics of the training and validation cohorts

We selected 1,645 eligible patients with stage T1–2N0M0 (Figure 1). The distribution of clinical characteristics of patients and pathological characteristics of tumors is presented in Table 1. Based on the year of diagnosis, the included patients were divided into two distinct cohorts: 1,147 patients diagnosed from 2000 to 2011 were assigned to the training cohort, whereas cases that were diagnosed from 2012 to 2015 were used as the validation cohort ($n = 498$). In the training cohort, females were the predominant sex. Most of the patients were aged ≥ 65 years old. Caucasians were the predominant race. The most common site of the tumor was the upper lobe, followed by the lower lobe. The number of patients with right-side primary tumors was 653 (56.93%) in the training cohort. The distribution of tumor size was 61.38%, 22.14%, and 16.48% for ≤ 3 cm, 3–4 cm, and 4–5 cm,

respectively. Over half of the patients did not receive surgery. Lobectomy was the predominant surgical approach in the patients receiving surgical treatment, and most patients underwent lymph node removal of fewer than four lymph nodes. In the training cohort, more than half of the patients were treated with chemotherapy and radiotherapy. The above demographics of the patients in the validation cohort were similar to those in the training cohort. The differentiated grade of most tumors in both cohorts was unknown. In comparing the training and validation cohorts, the demographic variables were not significant, except for the variables of grade and LNR.

Independent prognostic factors in the training cohort

There were 1,027 events (deaths) in the training cohort, of which 799 patients died of cancer. The mean follow-up duration was 38.30 months (median, 20 months; range, 1–225 months). In univariate analysis, sex, age, tumor size, surgery, LNR, and chemotherapy were significantly associated with OS (Table 2), and these factors were also significantly associated with LCSS except for the factor of sex (Table 3). After multivariate analysis, sex, age, surgery, LNR, and chemotherapy were proven to be associated with OS (Table 2). In the group aged ≥ 65 years, no surgery, less than four regional lymph nodes removed, and no chemotherapy were demonstrated to have a higher hazard of death from lung cancer through multivariate analysis (Table 3). In terms of surgical procedures, lobectomy was associated with the lowest risk of death.

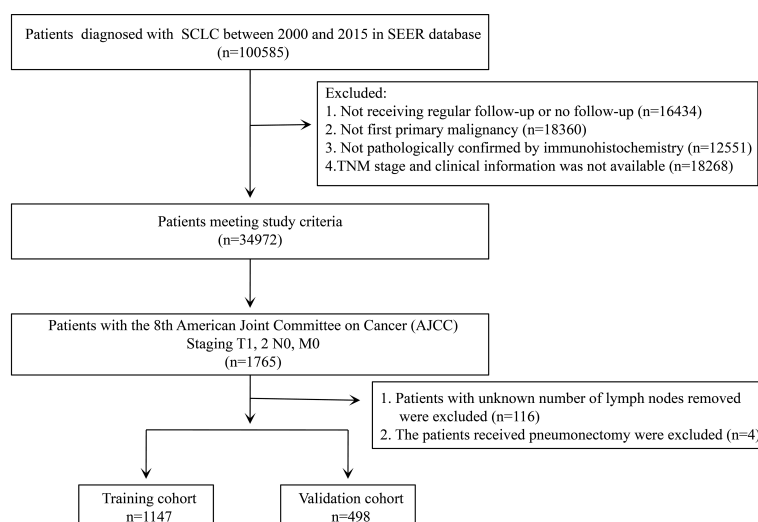


FIGURE 1

The flow chart shows the process of patient selection.

TABLE 1 Demographic and clinicopathologic characteristics of the training and validation cohort.

Characteristics	Training cohort (%)	Validation cohort (%)	P-value
No. of cases	1,147	498	
Sex			0.056
Male	544 (47.43)	210 (42.17)	
Female	603 (52.57)	288 (57.83)	
Age			0.206
<65 y	367 (32.00)	143 (28.71)	
≥65 y	780 (68.00)	355 (71.29)	
Race			0.097
White	1,020 (88.93)	424 (85.14)	
Black	89 (7.76)	51 (10.24)	
Others	38 (3.31)	23 (4.62)	
Primary site			0.522
Upper lobe	664 (57.89)	304 (61.04)	
Lower lobe	341 (29.73)	145 (29.12)	
Middle lobe	75 (6.54)	27 (5.42)	
Main bronchus	64 (5.58)	20 (4.02)	
Overlapping lesion	3 (0.26)	2 (0.40)	
Laterality			1.000
Left	494 (43.07)	215 (43.17)	
Right	653 (56.93)	283 (56.83)	
Tumor size (cm)			0.050
≤3	704 (61.38)	333 (66.87)	
3–4	254 (22.14)	104 (20.88)	
4–5	189 (16.48)	61 (12.25)	
Grade			<0.001
Moderate + well	18 (1.57)	11 (2.21)	
Poor	200 (17.44)	95 (19.08)	
Undifferentiated	368 (32.08)	86 (17.27)	
Unknown	561 (48.91)	306 (61.45)	
Surgery			0.104
Non-surgery	825 (71.93)	346 (69.48)	
Lobectomy	181 (15.78)	99 (19.88)	
Others	141 (12.29)	53 (10.64)	
LNR(number)			0.005
<4	976 (85.09)	395 (79.32)	
≥4	171 (14.91)	103 (20.68)	
Chemotherapy			0.593
No	363 (31.65)	165 (33.13)	
Yes	784 (68.35)	333 (66.87)	
Radiotherapy			0.373
No	568 (49.52)	234 (46.99)	
Yes	579 (50.48)	264 (53.01)	

LNR, lymph node removal.

Developing the prognostic nomogram model for OS and LCSS

Significant variables of age, surgery, LNR, and chemotherapy were finally selected for the development of a nomogram model for 1-, 3-, and 5-year LCSS (Figure 2B). Besides, the variable of sex was also used to develop the nomogram model for 1-, 3-, and 5-year OS (Figure 2A). Each variable was assigned a point score ranging from 0 to 100. In the nomograms for OS and LCSS, the surgical procedure showed the largest contribution to prognosis, with a score of 100, followed by LNR. The factor of LNR showed a larger contribution in the nomogram model for OS than for LCSS, with a point of 87.5. Notably, the lobectomy demonstrated a great influence on survival prediction regardless of OS or LCSS. Each factor can be assigned a corresponding point by drawing a line straight upward to the “Point axis.” Individual risk scores were calculated by summing up the scores of each variable. The probabilities of survival at 1, 3, and 5 years were easily determined by locating their corresponding points on the survival scale.

Calibration and validation of the nomogram

There were 344 events (deaths) in the validation cohort, of which 265 patients died of cancer. The mean follow-up duration was 30.34 months (median, 24 months; range, 1–83 months).

The C-indexes of the training cohort were 0.663 (95% confidence interval [CI] 0.626–0.701), 0.702 (95% CI 0.669–0.735), 0.733 (95% CI 0.698–0.769) for 1-, 3-, and 5-year OS and 0.658 (95% CI 0.615–0.700), 0.702 (95% CI 0.666–0.738), 0.733 (95% CI 0.695–0.772) for 1-, 3-, and 5-year LCSS, respectively. In the validation cohort, they were 0.706 (95% CI 0.642–0.770), 0.707 (95% CI 0.657–0.758), 0.718 (95% CI 0.651–0.785) for 1-, 3-, and 5-year OS and 0.712 (95% CI 0.642–0.783), 0.691 (95% CI 0.637–0.745), 0.692 (95% CI 0.618–0.767) for 1-, 3-, and 5-year LCSS, respectively. The data indicated the brilliant discrimination ability of the nomogram (Figures 3, 4). These calibration curves of the training cohort and validation cohort also presented acceptable consistency between the model prediction and the actual observation for 1-, 3-, and 5-year OS and LCSS (Figure 5). Concerning the prognostic ability of OS and LCSS, we conducted comparisons of the model performance between our nomograms and the 8th edition AJCC TNM staging system. The 1-, 3-, and 5-year time-dependent ROC curves of the two models are shown in Figures 3, 4. All AUCs of the nomogram model were significantly higher than the 8th edition AJCC TNM staging system in the training cohort (Figures 3A–

TABLE 2 Univariable and multivariate Cox proportional hazards regression analysis for overall survival.

Variables	Univariate cox regression		Multivariate cox regression	
	HR (95% CI)	P-value	HR (95% CI)	P-value
Sex				
Female	1		1	
Male	1.23 (1.08–1.39)	0.001	1.13 (1.00–1.28)	0.045
Age				
<65 y	1		1	
≥65 y	1.53 (1.34–1.76)	<0.001	1.49 (1.29–1.70)	<0.001
Race				
White	1			
Black	1.07 (0.85–1.35)	0.555		
Others	1.12 (0.81–1.56)	0.488		
Primary site				
Upper lobe	1		1	
Lower lobe	0.98 (0.85–1.12)	0.732	0.94 (0.82–1.08)	0.407
Middle lobe	0.94 (0.73–1.22)	0.652	1.06 (0.82–1.36)	0.675
Main bronchus	1.41 (1.08–1.83)	0.010	1.18 (0.90–1.54)	0.232
Overlapping lesion	4.33 (1.39–13.5)	0.012	5.32 (1.70–16.66)	0.004
Laterality				
Left	1			
Right	1.02 (0.90–1.16)	0.722		
Tumor size (cm)				
≤3	1		1	
3–4	1.26 (1.09–1.47)	0.002	1.09 (0.93–1.27)	0.288
4–5	1.21 (1.03–1.44)	0.024	1.08 (0.91–1.29)	0.365
Grade				
Moderate + well	1			
Poor	0.77 (0.47–1.27)	0.309		
Undifferentiated	0.97 (0.60–1.59)	0.913		
Unknown	1.13 (0.70–1.84)	0.609		
Surgery				
Non-surgery	1		1	
Lobectomy	0.36 (0.30–0.44)	<0.001	0.52 (0.39–0.68)	<0.001
Others	0.62 (0.51–0.75)	<0.001	0.62 (0.50–0.76)	<0.001
LNR (number)				
<4	1		1	
≥4	0.35 (0.28–0.43)	<0.001	0.55 (0.42–0.73)	<0.001
Chemotherapy				
No	1		1	
Yes	0.78 (0.69–0.89)	<0.001	0.64 (0.55–0.73)	<0.001
Radiotherapy				
No	1			
Yes	0.93 (0.82–1.05)	0.258		

LNR, lymph node removal; HR, hazard ratio; CI, confidence interval.

C, 4A–C) and validation cohort (Figures 3D–F, 4D–F), which verified the strong and robust prognostic power of our nomograms. Furthermore, we also compared the continuous trends of the prognostic performance of each model and found the AUCs of our nomogram models were significantly higher

than that of the 8th edition AJCC TNM staging system throughout the calculation period (from months 1–60), whether in the training (Figures 6A, C) or validation cohorts (Figures 6B, D). After that, the DCA analysis suggested a significantly increased net benefit of the new nomogram over

TABLE 3 Univariable and multivariate Cox proportional hazards regression analysis for lung cancer-specific survival.

Variables	Univariate cox regression		Multivariate cox regression	
	HR (95% CI)	P-value	HR (95% CI)	P-value
Sex				
Female	1			
Male	1.13 (0.98–1.29)	0.096		
Age				
<65 y	1		1	
≥65 y	1.40 (1.20–1.63)	<0.001	1.34 (1.15–1.56)	<0.001
Race				
White	1			
Black	1.09 (0.84–1.41)	0.517		
Others	1.14 (0.79–1.64)	0.479		
Primary site				
Upper lobe	1			
Lower lobe	1.04 (0.89–1.22)	0.601		
Middle lobe	0.91 (0.67–1.22)	0.517		
Main bronchus	1.43 (1.06–1.93)	0.018		
Overlapping lesion	3.42 (0.85–13.75)	0.083		
Laterality				
Left	1			
Right	1.03 (0.90–1.19)	0.656		
Tumor size (cm)				
≤3	1		1	
3–4	1.28 (1.08–1.52)	0.005	1.08 (0.91–1.29)	0.379
4–5	1.34 (1.11–1.61)	0.002	1.18 (0.98–1.43)	0.088
Grade				
Moderate + well	1			
Poor	0.96 (0.52–1.77)	0.885		
Undifferentiated	1.23 (0.67–2.26)	0.494		
Unknown	1.38 (0.76–2.52)	0.287		
Surgery				
None	1		1	
Lobectomy	0.33 (0.26–0.41)	<0.001	0.47 (0.34–0.66)	<0.001
Others	0.56 (0.45–0.70)	<0.001	0.56 (0.44–0.72)	<0.001
LNR (number)				
<4	1		1	
≥4	0.31 (0.24–0.40)	<0.001	0.53 (0.38–0.75)	<0.001
Chemotherapy				
No	1		1	
Yes	0.79 (0.68–0.91)	0.002	0.62 (0.53–0.73)	<0.001
Radiotherapy				
No	1			
Yes	0.88 (0.77–1.01)	0.070		

LNR, lymph node removal; HR, hazard ratio; CI, confidence interval.

the 8th edition AJCC TNM staging system with wide and practical ranges of threshold probabilities regardless of the OS (Figures 7A–C) or LCSS (Figures 7D–F), which further verified the better individual prognostic performance of our nomograms in the clinical appliance.

Performance of the new risk stratification model

The cutoff values for the high-risk group and low-risk group developed from X-tile software were 196.0 and 181.0 for OS and

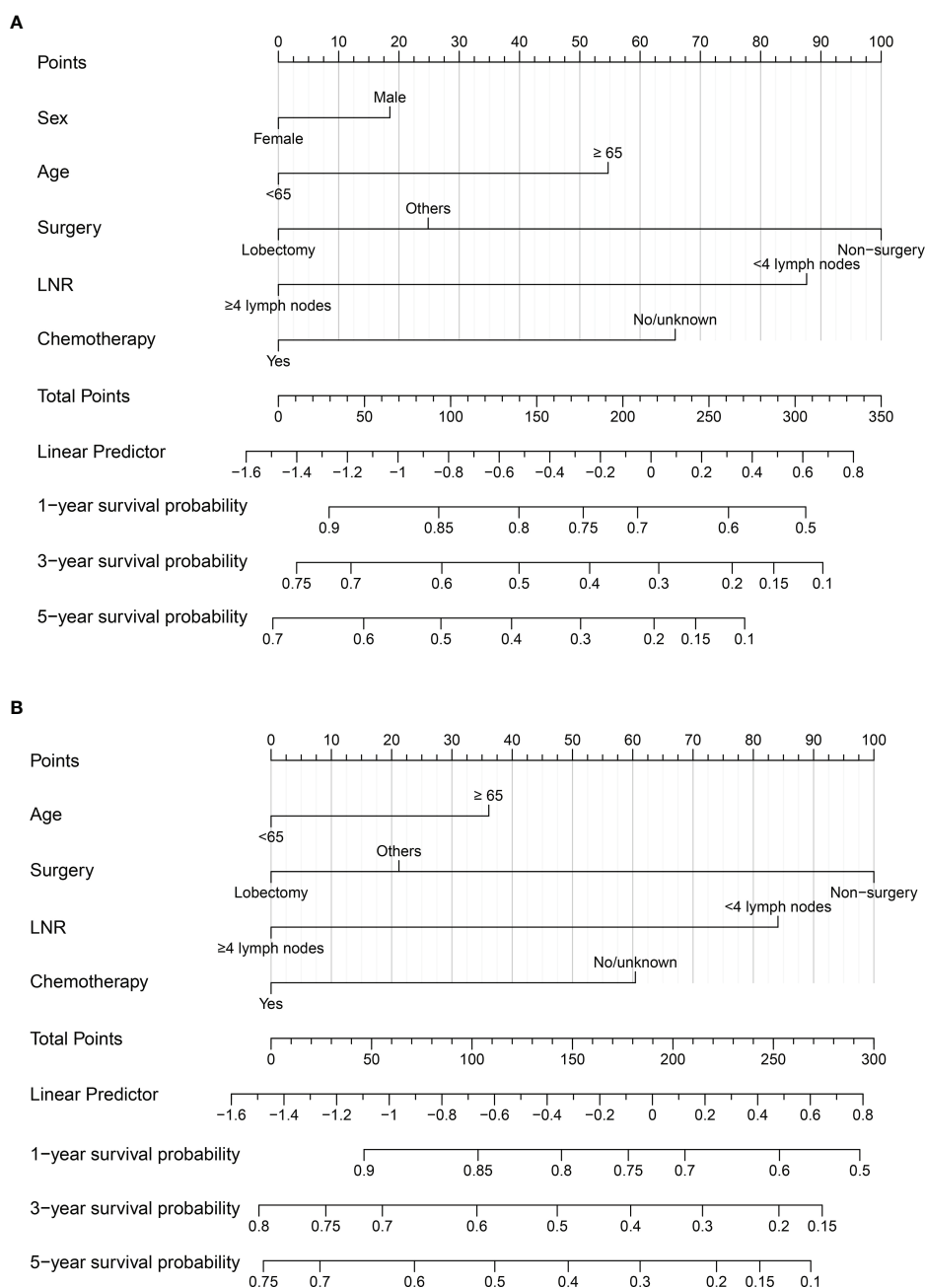


FIGURE 2

(A) Nomogram to predict 1-, 3-, and 5-year OS probability for early-stage T1-2N0M0 SCLC patients; (B) Nomogram to predict 1-, 3-, and 5-year LCSS probability for early-stage T1-2N0M0 SCLC patients. LNR, lymph nodes removal; SCLC, small cell lung cancer; OS, overall survival; LCSS, lung cancer-specific survival.

LCSS, respectively. All 1,147 patients in the training cohort were divided into the high-risk group (total points >196.0 for OS, >181.0 for LCSS) and the low-risk group (total points ≤196.0 for OS, ≤181.0 for LCSS) based on the cutoff value. The survival curves for OS and LCSS showed significant distinctions between the two different risk groups in the training cohort ($P < 0.0001$,

Figures 8A, 9A). Significant differences in OS and LCSS were also observed between almost all subgroups when patients were stratified by AJCC stages ($P < 0.001$, Figures 8B–D, 9B–D). The same grouping method was then applied to the validation cohort, and significant distinctions in survival curves for OS and LCSS between the two different risk groups were also

observed, even within certain AJCC staging categories (Figures 8E–H, 9E–H).

Development of web servers for the nomogram

For the convenient application of our nomogram, we created a user-friendly website. The website can calculate an individualized survival probability as long as you input certain clinical variables of a T1-2N0M0 SCLC patient and a certain prediction time (months). After that, it can also provide the corresponding survival plot for this case. The public online version of our nomogram is available at <https://shanghaisuzhousclcnomogrampredictability.shinyapps.io/DynNomapp/> and <https://shanghaisuzhousclcnomogrampredictability.shinyapps.io/DynNomappLCSS/>. Clinicians can use the websites freely and do not need to input any passwords.

Discussion

SCLC is well recognized as an easily aggressive tumor that will present hematogenous metastases and lymph node metastases at an early stage. So T1-2N0M0 SCLC is a relatively uncommon clinical scenario. Existing VALSG or

TNM staging systems are not efficient in predicting the individual prognosis of early-stage T1-2N0M0 SCLC patients. Therefore, we constructed and validated novel nomogram prognostic models for OS and LCSS based on surgery and other clinicopathological variables to compensate for these limitations using a large population-based database of T1-2N0M0 SCLC patients. To our knowledge, this was the first comprehensive nomogram to provide a personalized predictive model for the OS and LCSS of early-stage T1-2N0M0 SCLC patients. Our new model demonstrated considerable discrimination ability and calibration accuracy both in the training and validation cohorts, which displayed good repeatability and reliability compared to the established model. After that, the nomograms showed a significant benefit in clinical application compared with the 8th TNM staging system through DCA analyses. Our risk stratification model depended on our nomograms and also could effectively stratify different risk patients by distinguishing OS and LCSS. So our models could help clinicians assess the survival of early-stage SCLC patients and better weigh the risks and benefits of more aggressive or more conservative anticancer therapies.

Several previous studies have published nomograms regarding survival prediction for SCLC patients. Xie and colleagues developed a nomogram using a cohort of 938 cases to predict OS for SCLC, incorporating peripheral blood markers (4). However, neither the study nor the independent validation

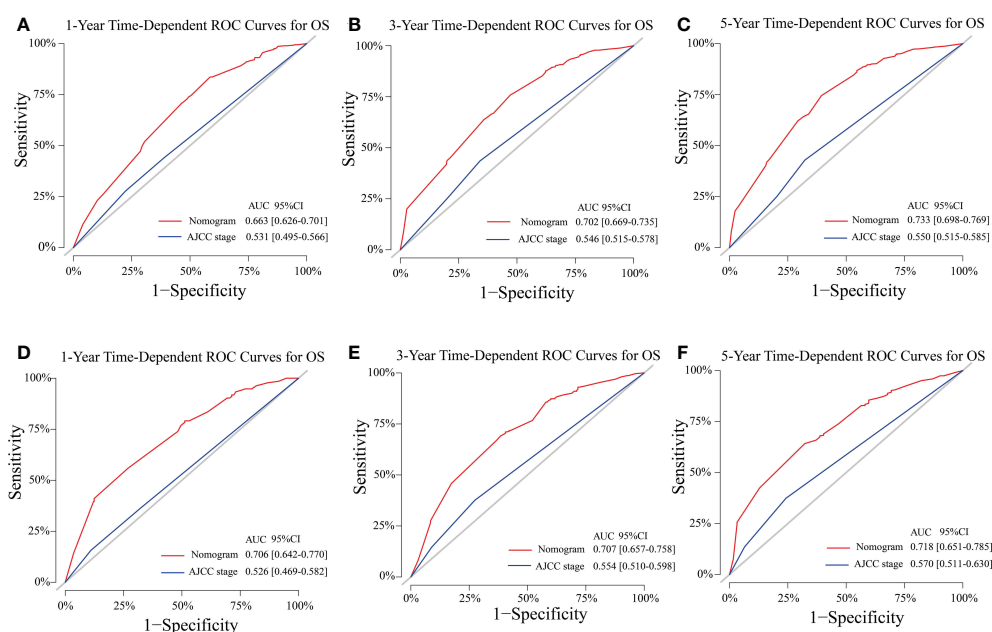


FIGURE 3

Model performance of the proposed nomogram. (A–F) Time-dependent ROC curves of the two prognostic models for predicting 1-, 3-, and 5-year OS. The AUCs of the two prognostic models at each time point of interest were presented in the training (A–C) and validation cohorts (D–F). ROC, receiver operating characteristic; AUC, area under the curve; OS, overall survival; AJCC, American Joint Committee on Cancer; CI, confidence interval.

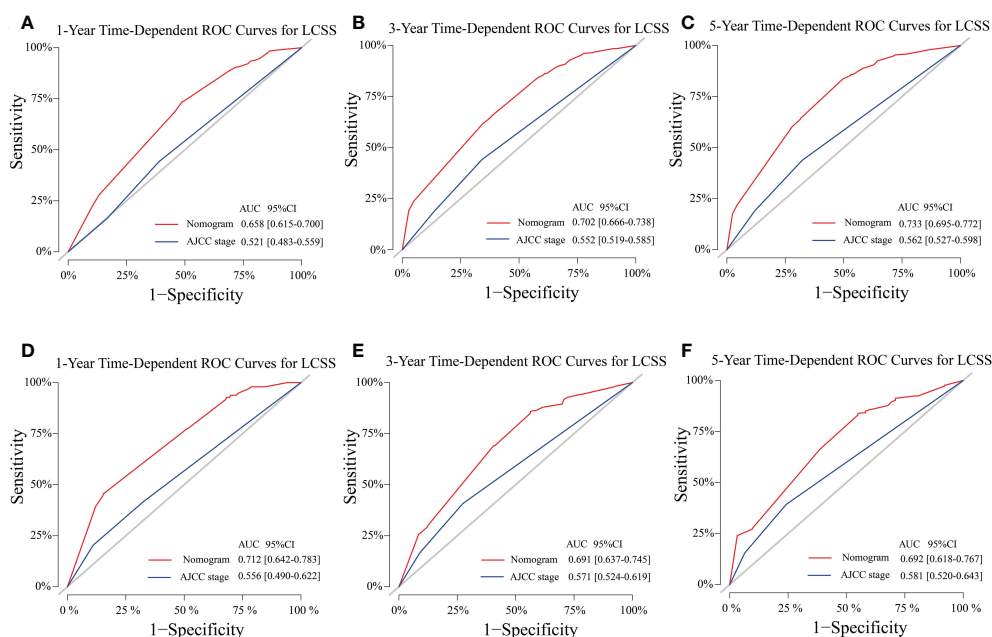


FIGURE 4

Model performance of the proposed nomogram. (A–F) Time-dependent ROC curves of the two prognostic models for predicting 1-, 3-, and 5-year LCSS. The AUCs of the two prognostic models at each time point of interest were presented in the training (A–C) and validation cohorts (D–F). ROC, receiver operating characteristic; AUC, area under the curve; LCSS, lung cancer-specific survival; AJCC American Joint Committee on Cancer; CI confidence interval.

assigned to the model applied the more accurate TNM staging system, nor did they assign an independent validation for the model. Due to the lack of early-stage T1-2N0M0 SCLC competing risk analyses in their model, we cannot compare the results between Xie's model and our model in this study. In 2017, Wang et al. developed a prognostic nomogram for predicting the survival of SCLC patients using the National Cancer Database (NCDB) (20). This study applied the 8th TNM staging system and treatment patterns. However, the model incorporated the entire stages, which failed to provide accurate prediction for a special subset of patients. Besides, this study did not refer to the surgical procedure or the status of lymph node removal. While in 2021, Zeng et al. demonstrate a nomogram model for OS of resected limited-stage SCLC patients using the SEER database and an independent SCLC cohort at their single institution (21). Their predictive model could not only provide an accurate prediction for resected limited-stage SCLC but also provide the specific surgical procedure and lymph node status. But the model involves different stages, not merely the early-stage T1-2N0M0. Above all, prognostic models did not reveal predictors of death resulting from lung cancer-specific causes. Li and colleagues investigated the mortality of stage I SCLC patients in the presence of competing risks and conducted nomograms to predict probabilities of both lung cancer-specific death and death resulting from other causes (22). This study applied the 6th staging system and simply pointed out

whether surgery was necessary or not without mentioning the concrete surgical procedure or lymph nodes removed, which means it might not be completely suitable for stage I SCLC patients. In contrast, our new model was constructed specially for early-stage T1-2N0M0 patients based on the characteristics of patients and tumor biology using a large population database and included common surgical procedures and the removal of lymph nodes. Besides, our new model was the first study to conduct the prediction of LCSS to provide the most beneficial treatment modalities and a more accurate probability of survival for this specific subset of patients. Notably, our new model received an ideal C-index by independent validation, so it has certain generalizability and can provide an accurate prediction.

Through univariate and multivariate analysis, sex, age, surgery, LNR, and chemotherapy were recognized as independent prognostic parameters of OS. Some of these factors have been studied in previous research on the survival of SCLC (23–27). After that, we also find that age, surgery, LND, and chemotherapy were associated with the LCSS by COX regression analyses. Sex did not affect lung cancer-specific mortality, which was consistent with the studies of Li et al. (22). But the male patients had worse OS than the female patients. Our study found the factor of age showed a larger contribution in the nomogram model for OS than for LCSS, which means that old patients may be more likely to die from other causes. Elder patients had worse survival than younger

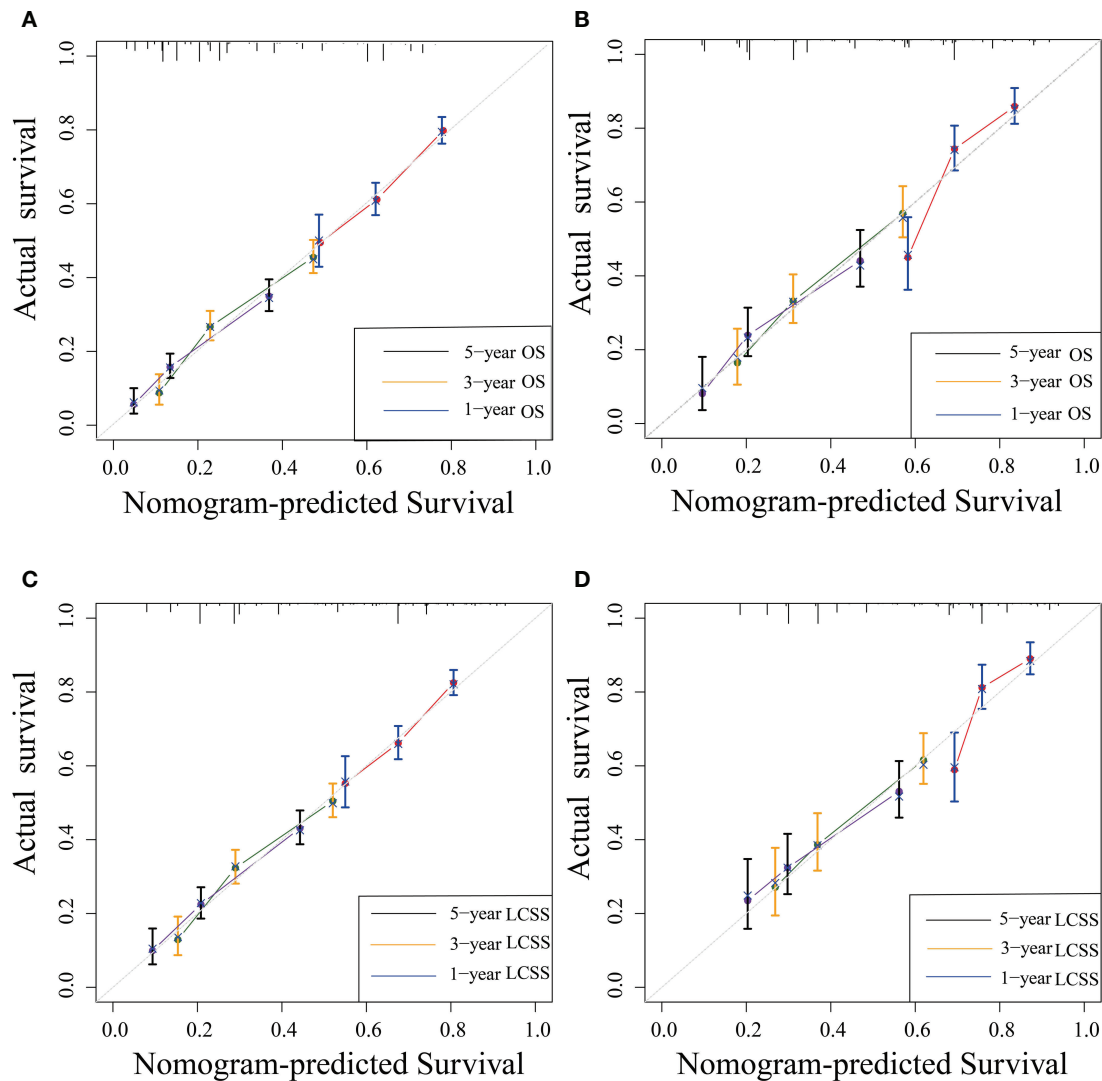


FIGURE 5

Nomogram calibration curves for nomogram-predicted survival (x-axis) and actual observed survival (y-axis). Calibration curves for OS (A, B) and LCSS (C, D) in the training (A, C) and validation cohort (B, D); curves for 1-, 3-, and 5-year OS and LCSS were present as blue, yellow, and black lines, respectively. OS, overall survival; LCSS, lung cancer-specific survival.

patients, which might be because of degenerative changes in various aspects of organ function and an increased prevalence of all types of comorbidities (28). So elder patients may require additional treatment and intensive follow-up. Our study showed that patients diagnosed with T1-2N0M0 SCLC without any lymph node metastasis should also undergo surgical resection of lymph nodes. And the ones with more lymph node removal performed had better survival regardless of OS or LCSS, which suggested conducting lymphadenectomy for early-stage T1-2N0M0 SCLC patients. This result was similar to the results of Zeng et al. and Yang et al. (21, 29). Notably, the

surgical procedure was a crucial independent predictor for OS and LCSS in our study, of which lobectomy posed the superior choice with better survival. There have been similar results in the previous study (7, 14, 30, 31). In our study, although the detailed location of the tumor was further refined based on lobes, the association between prognosis and the location of the tumor remained nonsignificant. In addition, we also find that there was no association between tumor size and prognosis in this subset of SCLC patients, regardless of the OS or LCSS.

However, several limitations existed in our study. First, certain biases may exist due to the inherent nature of this

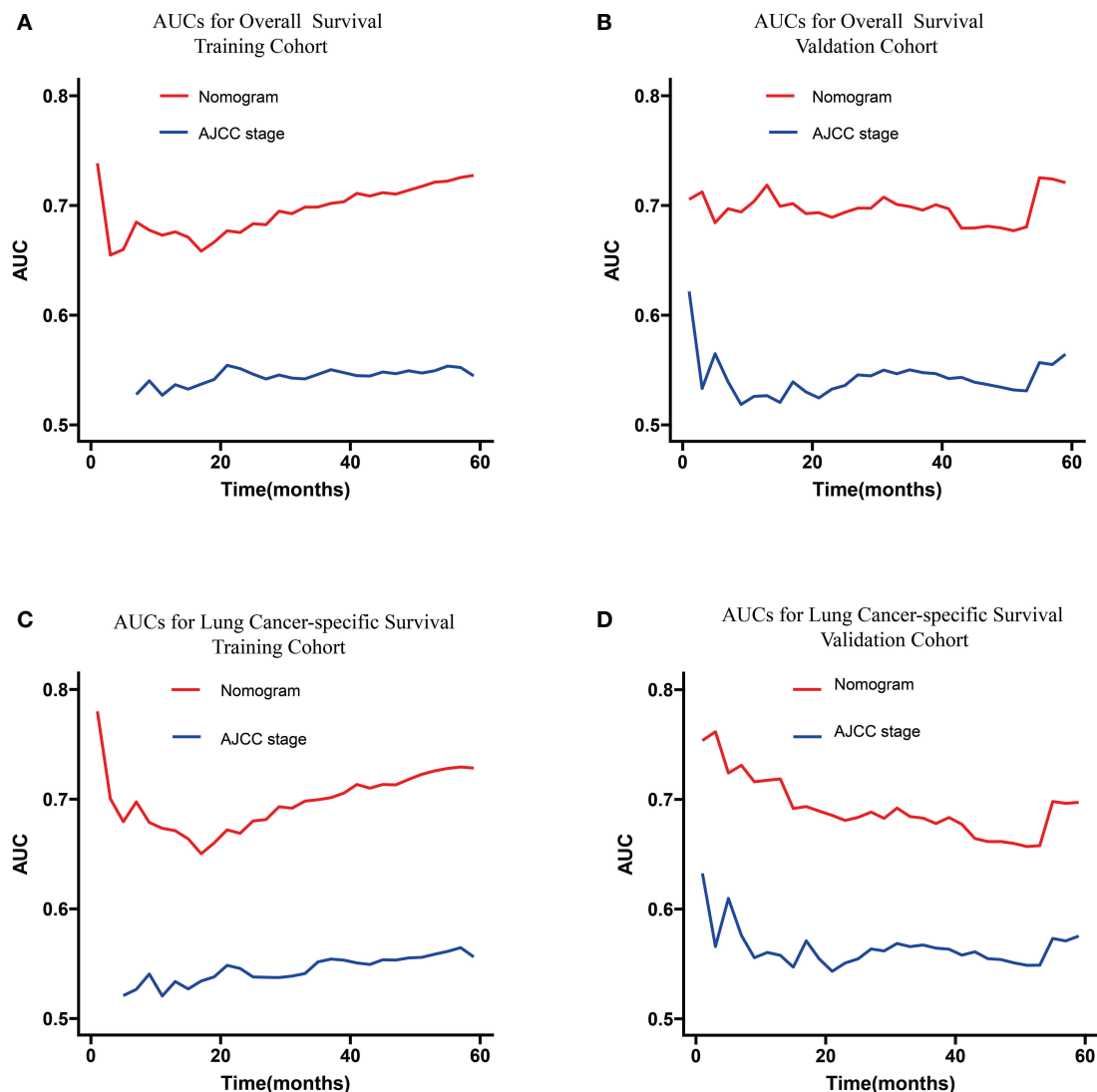


FIGURE 6

Continuous AUCs of the nomogram (red) and 8th edition AJCC TNM staging system (blue) in the training (A, C) and validation cohorts (B, D) throughout the period of 1–60 months. AUC, area under the curve; AJCC, American Joint Committee on Cancer.

retrospective study. Second, certain shortcomings existed in using the SEER database, which lacked routinely available data including performance score, smoking status, pulmonary functions, body index, and comorbidities. Especially the variable of comorbidity will affect physicians in deciding the treatment strategies and evaluating the prognosis. After that, some available clinicopathological information about the patients is incomplete (e.g., the status of lymph node resection is unknown). Due to the dependence on the SEER database, we cannot conduct a more predictive survival analysis that includes the above-mentioned parameters.

Moreover, several treatment-related variables were not included in our models, such as the sequence of chemotherapy and radiotherapy with surgery, the plans of chemotherapy, the number of cycles, the doses and methods of radiotherapy, and the further treatment after recurrence, so that our study cannot be able to evaluate the effects of treatment sequence, regimens, and courses on patients' survival. We cannot externally validate the nomogram using data from our institution because of severe data loss. Hence, there should be a further multicenter prospective study that incorporates relatively complete clinicopathological variables

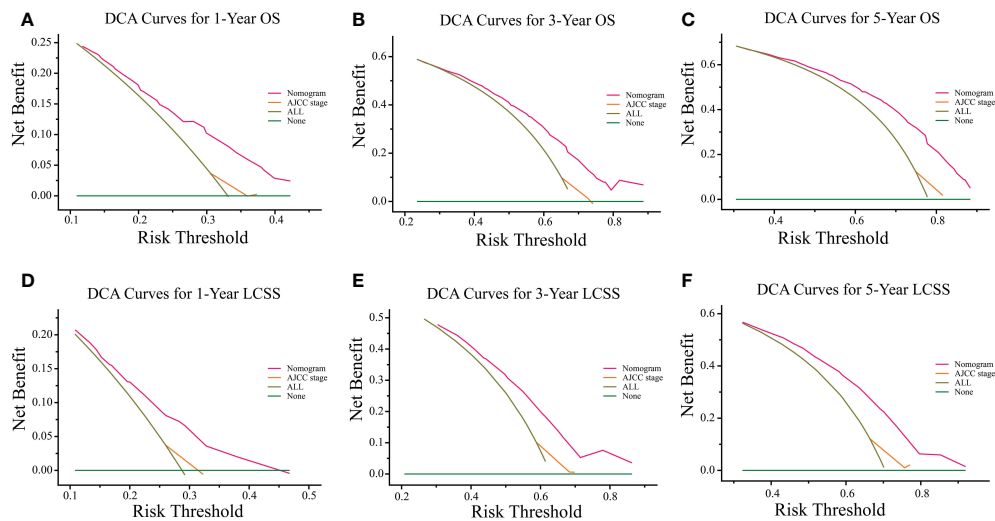


FIGURE 7

DCA curves of the proposed nomogram and 8th edition AJCC TNM staging system for 1-, 3-, and 5-year OS (A–C) and LCSS (D–F). The x-axis represents the risk threshold, and the y-axis measures the net benefit. The green horizontal solid line along the x-axis assumes that overall death occurred in no patients, whereas the light green solid line assumes that all patients will have overall death at a specific threshold probability. The pink solid line represents the nomogram. The orange solid line represents the 8th edition AJCC TNM staging system. DCA, decision curve analysis; OS, overall survival; LCSS, lung cancer-specific survival; AJCC, American Joint Committee on Cancer.

and detailed information on treatment to create a more precise predictive model. But we considered that our model for OS and LCSS, conducted depending on other vital clinical factors that could be obtained in the SEER database with a larger sample,

could provide some valuable implications in clinical practice for early-stage T1-2N0M0 SCLC patients.

In conclusion, our study found that the selection of surgical procedures was a crucial factor and that lymph node removal

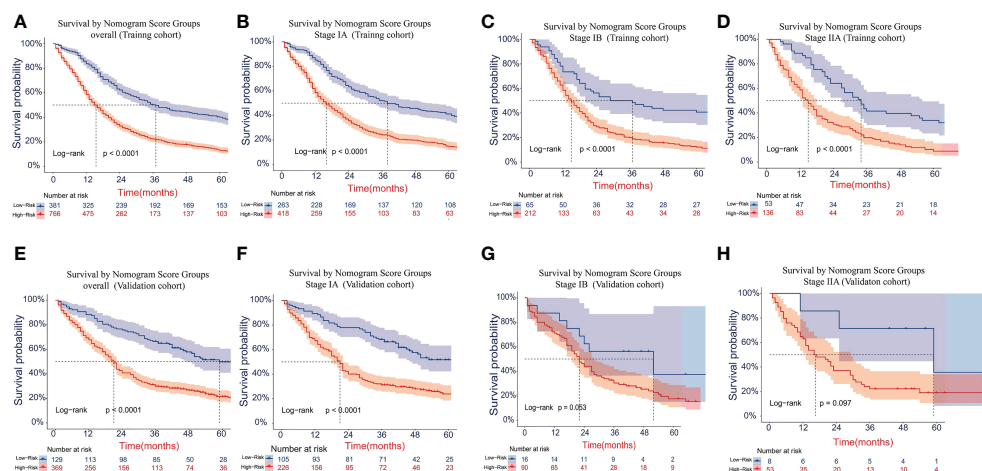


FIGURE 8

Kaplan–Meier survival curves for OS in the overall and stage-stratified patients in the training (A–D) and validation (E–H) cohorts to test the risk stratification system based on the training cohort. The red line represents the high-risk group, and the blue line represents the low-risk group. OS, overall survival.

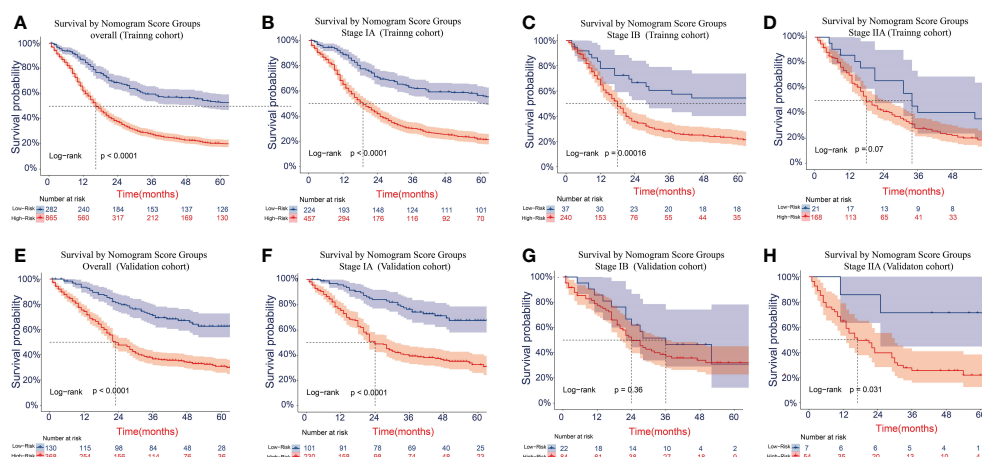


FIGURE 9

Kaplan–Meier survival curves for LCSS in the overall and stage-stratified patients in the training (A–D) and validation (E–H) cohorts to test the risk stratification system based on the training cohort. The red line represents the high-risk group, and the blue line represents the low-risk group. LCSS, lung cancer-specific survival.

should be stressed even in node-negative SCLC patients because it was positively related to prognosis. Additionally, we developed and validated a prognostic nomogram for predicting 1-, 3-, and 5-year OS and LCSS in early-stage T1-2N0M0 SCLC patients with good discrimination and calibration, which has not been proposed in previous studies. Our model also showed certain reliability and could provide clinician suggestions to improve the prognosis, make treatment strategies, and design clinical trials. Besides, we implemented the nomogram in a user-friendly web server for clinicians and patients.

Data availability statement

The raw data supporting the conclusions of this article will be made available by the authors, without undue reservation.

Author contributions

All authors participated in manuscript writing and approved the final version of the manuscript. TG, SZ, LS, and LY conceived and designed the analysis. Collection and assembly of data were performed by TG, SZ, JQ, and XC. Analysis and interpretation of the data were supported by TG, SZ, LS, and JD. PZ, JZ, and GJ conducted a critical review of the manuscript, contributing important intellectual content. All authors contributed to the article and approved the submitted version.

Funding

This work was supported by the Clinical Research Plan of SHDC (Grant No. SHDC2020CR2020B), the Funding of Shanghai Pulmonary Hospital (Grant No.FKCY1904, No.FKLY20004), and the Oasis Scholars Funding of Shihezi University.

Conflict of interest

The authors declare that the research was conducted in the absence of any commercial or financial relationships that could be construed as a potential conflict of interest.

Publisher's note

All claims expressed in this article are solely those of the authors and do not necessarily represent those of their affiliated organizations, or those of the publisher, the editors and the reviewers. Any product that may be evaluated in this article, or claim that may be made by its manufacturer, is not guaranteed or endorsed by the publisher.

References

- Siegel RL, Miller KD, Jemal A. Cancer statistics, 2018. *CA Cancer J Clin* (2018) 68(1):7–30. doi: 10.3322/caac.21442
- Gazdar AF, Bunn PA, Minna JD. Small-cell lung cancer: What we know, what we need to know and the path forward. *Nat Rev Cancer* (2017) 17(12):725–37. doi: 10.1038/nrc.2017.87
- Rudin CM, Ismaila N, Hann CL, Malhotra N, Movsas B, Norris K, et al. Treatment of small-cell lung cancer: American society of clinical oncology endorsement of the American college of chest physicians guideline. *J Clin Oncol* (2015) 33(34):4106–11. doi: 10.1200/Jco.2015.63.7918
- Xie D, Marks R, Zhang MR, Jiang GN, Jatoi A, Garces YI, et al. Nomograms predict overall survival for patients with small-cell lung cancer incorporating pretreatment peripheral blood markers. *J Thorac Oncol* (2015) 10(8):1213–20. doi: 10.1097/Jto.0000000000000585
- Aberle DR, Adams AM, Berg CD, Black WC, Clapp JD, Fagerstrom RM, et al. Reduced lung-cancer mortality with low-dose computed tomographic screening. *New Engl J Med* (2011) 365(5):395–409. doi: 10.1056/NEJMoa1102873
- Yu JB, Decker RH, Detterbeck FC, Wilson LD. Surveillance epidemiology and end results evaluation of the role of surgery for stage I small cell lung cancer. *J Thorac Oncol* (2010) 5(2):215–9. doi: 10.1097/JTO.0b013e3181cd3208
- Schreiber D, Rineer J, Weedon J, Vongtama D, Wortham A, Kim A, et al. Survival outcomes with the use of surgery in limited-stage small cell lung cancer should its role be re-evaluated? *Cancer* (2010) 116(5):1350–7. doi: 10.1002/cncr.24853
- Shepherd FA, Crowley J, Van Houtte P, Postmus PE, Carney D, Chansky K, et al. The international association for the study of lung cancer - lung cancer staging project: Proposals regarding the clinical staging of small cell lung cancer in the forthcoming (Seventh) edition of the tumor, node, metastasis classification for lung cancer. *J Thorac Oncol* (2007) 2(12):1067–77. doi: 10.1097/JTO.0b013e31815bdc0d
- National Comprehensive Cancer Network Website. *National comprehensive cancer network guidelines for small cell lung cancer version 2.2018*. Available at: https://www.nccn.org/professionals/physician_gls/pdf/sclc.pdf (Accessed 17 Jan 2018).
- Jhun BW, Lee KJ, Jeon K, Suh GY, Chung MP, Kim H, et al. Clinical applicability of staging small cell lung cancer according to the seventh edition of the tmn staging system. *Lung Cancer* (2013) 81(1):65–70. doi: 10.1016/j.lungcan.2013.03.005
- Groome PA, Bolejack V, Crowley JJ, Kennedy C, Krasnik M, Sobin LH, et al. The iaslc lung cancer staging project: Validation of the proposals for revision of the T, n, and m descriptors and consequent stage groupings in the forthcoming (Seventh) edition of the tmn classification of malignant tumours. *J Thorac Oncol* (2007) 2(8):694–705. doi: 10.1097/JTO.0b013e31812d05d5
- Abedallaa N, Tremblay L, Baey C, Fabre D, Planchard D, Pignon JP, et al. Effect of chemotherapy in patients with resected small-cell or Large-cell neuroendocrine carcinoma. *J Thorac Oncol* (2012) 7(7):1179–83. doi: 10.1097/JTO.0b013e3182572ead
- Che K, Shen H, Qu X, Pang Z, Jiang Y, Liu S, et al. Survival outcomes for patients with surgical and non-surgical treatments in stages I-iii small-cell lung cancer. *J Cancer* (2018) 9(8):1421–9. doi: 10.7150/jca.23583
- Wong AT, Rineer J, Schwartz D, Schreiber D. Assessing the impact of postoperative radiation therapy for completely resected limited-stage small cell lung cancer using the national cancer database. *J Thorac Oncol* (2016) 11(2):242–8. doi: 10.1016/j.jtho.2015.10.011
- Grimes DA. The nomogram epidemic: Resurgence of a medical relic. *Ann Intern Med* (2008) 149(4):273–5. doi: 10.7326/0003-4819-149-4-200808190-00010
- Balachandran VP, Gonen M, Smith JJ, DeMatteo RP. Nomograms in oncology: More than meets the eye. *Lancet Oncol* (2015) 16(4):e173–80. doi: 10.1016/s1470-2045(14)71116-7
- Rami-Porta R, Bolejack V, Giroux DJ, Chansky K, Crowley J, Asamura H, et al. The iaslc lung cancer staging project: The new database to inform the eighth edition of the tmn classification of lung cancer. *J Thorac Oncol* (2014) 9(11):1618–24. doi: 10.1097/Jto.0000000000000334
- Abdel-Rahman O. Validation of the ajcc 8th lung cancer staging system among patients with small cell lung cancer. *Clin Transl Oncol* (2018) 20(4):550–6. doi: 10.1007/s12094-017-1739-6
- Vickers AJ, Elkin EB. Decision curve analysis: A novel method for evaluating prediction models. *Med Decis Making* (2006) 26(6):565–74. doi: 10.1177/0272989x06295361
- Wang SD, Yang L, Ci B, Maclean M, Gerber DE, Xiao GH, et al. Development and validation of a nomogram prognostic model for sclc patients. *J Thorac Oncol* (2018) 13(9):1338–48. doi: 10.1016/j.jtho.2018.05.037
- Zeng QP, Li JG, Tan FW, Sun N, Mao YS, Gao YS, et al. Development and validation of a nomogram prognostic model for resected limited-stage small cell lung cancer patients. *Ann Surg Oncol* (2021) 28(9):4893–904. doi: 10.1245/s10434-020-09552-w
- Li JJ, Zheng QW, Zhao XH, Zhao J, An TT, Wu MN, et al. Nomogram model for predicting cause-specific mortality in patients with stage I small-cell lung cancer: A competing risk analysis. *BMC Cancer* (2020) 20(1):793. doi: 10.1186/s12885-020-07271-9
- Wolf M, Holle R, Hans K, Drings P, Havemann K. Analysis of prognostic factors in 766 patients with small-cell lung-cancer (Sclc) - the role of sex as a predictor for survival. *Brit J Cancer* (1991) 63(6):986–92. doi: 10.1038/bjc.1991.215
- Foster NR, Mandrekar SJ, Schild SE, Nelson GD, Rowland KM, Deming RL, et al. Prognostic factors differ by tumor stage for small cell lung cancer: A pooled analysis of north central cancer treatment group trials. *Cancer* (2009) 115(12):2721–31. doi: 10.1002/cncr.24314
- Zhang C, Yang HT, Zhao H, Lang BP, Yu XD, Xiao P, et al. Clinical outcomes of surgically resected combined small cell lung cancer: A two-institutional experience. *J Thorac Dis* (2017) 9(1):151–8. doi: 10.21037/jtd.2017.01.07
- Leuzzi G, Lococo F, Alessandrini G, Sperduti I, Spaggiari L, Venuta F, et al. Prognostic impact of node-spreading pattern in surgically treated small-cell lung cancer: A multicentric analysis. *Lung* (2017) 195(1):107–14. doi: 10.1007/s00408-016-9954-4
- Forget P, Machiels JP, Coulie PG, Berliere M, Poncelet AJ, Tombal B, et al. Neutrophil: Lymphocyte ratio and intraoperative use of ketorolac or diclofenac are prognostic factors in different cohorts of patients undergoing breast, lung, and kidney cancer surgery. *Ann Surg Oncol* (2013) 20:S650–S60. doi: 10.1245/s10434-013-3136-x
- Aarts MJ, Aerts JG, van den Borne BE, Biesma B, Lemmens VE, Kloover JS. Comorbidity in patients with small-cell lung cancer: Trends and prognostic impact. *Clin Lung Cancer* (2015) 16(4):282–91. doi: 10.1016/j.clcc.2014.12.003
- Yang CJ, Chan DY, Shah SA, Yerokun BA, Wang XF, D'Amico TA, et al. Long-term survival after surgery compared with concurrent chemoradiation for node-negative small cell lung cancer. *Ann Surg* (2018) 268(6):1105–12. doi: 10.1097/SLA.0000000000002287
- Veronesi G, Bottoni E, Finocchiaro G, Alloisio M. When is surgery indicated for small-cell lung cancer? *Lung Cancer* (2015) 90(3):582–9. doi: 10.1016/j.lungcan.2015.10.019
- Liu Y, Shan L, Shen J, Liu L, Wang J, He J, et al. Choice of surgical procedure - lobectomy, segmentectomy, or wedge resection - for patients with stage T1-2n0m0 small cell lung cancer: A population-based study. *Thorac Cancer* (2019) 10(4):593–600. doi: 10.1111/1759-7714.12943



OPEN ACCESS

EDITED BY
Xiaomin Niu,
Shanghai Jiao Tong University, China

REVIEWED BY
Monika Szturmowicz,
National Institute of Tuberculosis and
Lung Diseases, Poland
Teodora Donisan,
Mayo Clinic, United States

*CORRESPONDENCE
Guoguang Lu
lugg@enzemed.com
Tao Li
taolee1986@163.com

[†]These authors have contributed
equally to this work and share
first authorship

[‡]Lead contact: Tao Li

SPECIALTY SECTION
This article was submitted to
Thoracic Oncology,
a section of the journal
Frontiers in Oncology

RECEIVED 05 August 2022

ACCEPTED 16 November 2022

PUBLISHED 01 December 2022

CITATION
Jin X, Hu L, Fang M, Zheng Q, Yuan Y,
Lu G and Li T (2022) Development and
validation a simple scoring system to
identify malignant pericardial effusion.
Front. Oncol. 12:1012664.
doi: 10.3389/fonc.2022.1012664

COPYRIGHT
© 2022 Jin, Hu, Fang, Zheng, Yuan, Lu
and Li. This is an open-access article
distributed under the terms of the
Creative Commons Attribution License
(CC BY). The use, distribution or
reproduction in other forums is
permitted, provided the original
author(s) and the copyright owner(s)
are credited and that the original
publication in this journal is cited, in
accordance with accepted academic
practice. No use, distribution or
reproduction is permitted which does
not comply with these terms.

Development and validation a simple scoring system to identify malignant pericardial effusion

Xi Xia Jin^{1†}, Lingling Hu^{1†}, Meidan Fang^{1†}, Qiaofei Zheng¹,
Yuan Yuan¹, Guoguang Lu^{1*} and Tao Li^{2**}

¹Department of Clinical Laboratory, Taizhou Hospital of Zhejiang Province, Taizhou Enze Medical Center (Group), Linhai, Zhejiang, China, ²Department of Cardiovascular medicine, Taizhou Hospital of Zhejiang Province, Taizhou Enze Medical Center (Group), Linhai, Zhejiang, China

Background: Malignant pericardial effusion (MPE) is a serious complication in patients with advanced malignant tumors, which indicates a poor prognosis. However, its clinical manifestations lack specificity, making it challenging to distinguish MPE from benign pericardial effusion (BPE). The aim of this study was to develop and validate a scoring system based on a nomogram to discriminate MPE from BPE through easy-to-obtain clinical parameters.

Methods: In this study, the patients with pericardial effusion who underwent diagnostic pericardiocentesis in Taizhou Hospital of Zhejiang Province from February 2013 to December 2021 were retrospectively analyzed. The eligible patients were divided into a training group (n = 161) and a validation group (n = 66) according to the admission time. The nomogram model was established using the meaningful indicators screened by the least absolute shrinkage and selection operator (LASSO) and multivariate logistic regression. Then, a new scoring system was constructed based on this nomogram model.

Results: The new scoring system included loss of weight (3 points), no fever (4 points), mediastinal lymph node enlargement (2 points), pleural effusion (6 points), effusion adenosine deaminase ($ADA \leq 18U/L$) (5 points), effusion lactate dehydrogenase ($LDH > 1033U/L$) (7 points), and effusion carcinoembryonic antigen ($CEA > 4.9g/mL$) (10 points). With the optimal cut-off value was 16 points, the area under the curve (AUC), specificity, sensitivity, positive predictive value (PPV), negative predictive value (NPV), positive likelihood ratio (PLR), negative likelihood ratio (NLR) for identifying MPE were 0.974, 95.1%, 91.0%, 85.6%, 96.8%, 10.56 and 0.05, respectively, in the training set and 0.950, 83.3%, 95.2%, 90.9%, 90.9%, 17.50, and 0.18, respectively, in the validation set. The scoring system also showed good diagnostic accuracy in

differentiating MPE caused by lung cancer from tuberculous pericardial effusion (TPE) and MPE including atypical cell from BPE.

Conclusion: The new scoring system based on seven easily available variables has good diagnostic value in distinguishing MPE from BPE.

KEYWORDS

malignant pericardial effusion, diagnosis, nomogram, scoring system, atypical cell

Introduction

Pericardial effusion (PE) is a common clinical syndrome that usually caused by infection, iatrogenic, and connective tissue diseases. Malignant pericardial effusion is the result of cancer invading the pericardium. Secondary involvement of pericardium is much more common than primary cardiac malignancies, and the most common causes include lung cancer, breast cancer, malignant melanoma, lymphoma, and leukemia (1). The incidence rate of pericardial involvement in malignant tumors is about 10–20% in all cancer patients. The incidence of MPE may increase with the increase of global cancer incidence rate and the overall survival rate (2, 3). MPE which indicates a poor prognosis is a serious complication of patients with advanced malignant tumors (4). The misdiagnosed and delayed treatment will directly lead to increased mortality. Therefore, rapid and accurate identification of MPE is not only the basis of diagnosis but also very important to inpatient treatment.

At present, pericardial biopsy and pericardiocentesis are still the main means to diagnose MPE. However, the pericardial biopsy is not easy to accept because of its invasiveness and potential complications. The cytological analysis is the gold standard for diagnosing MPE. But the evaluation of results largely depends on the professional knowledge of pathologists. The sensitivity is only 30–50%, and a large number of samples are required (5, 6). Moreover, it is difficult to diagnose some atypical cells only with cytological specimens. With the help of some auxiliary tools, this gray area can be reduced, which is helpful to achieve a clear diagnosis (7). Previous studies have shown that some laboratory indicators, such as various tumor markers, vascular endothelial growth factor, and serum BNP (8–10), have certain value in the differential diagnosis of benign and malignant PE. But the diagnostic accuracy still needs to be improved, and some new markers have not been widely used in clinical practice. Therefore, it is very important to design a simple, economical, and less traumatic method to identify MPE.

Abbreviations: TP, total protein; ALB, albumin; ADA, adenosine deaminase; GLU, glucose; LDH, lactate dehydrogenase; CEA, carcinoembryonic antigen; hs-CRP, high-sensitivity C-reactive protein; ESR, erythrocyte sedimentation ratio.

In this study, we conducted a retrospective study to develop a nomogram model based on clinical features and laboratory data to identify MPE from BPE. Next, we aimed to develop a new scoring system based on this nomogram for clinical practical application.

Materials and methods

Patient selection

We retrospectively analyzed the data of patients with pericardial effusion who underwent diagnostic pericardiocentesis in Taizhou Hospital of Zhejiang Province from February 2013 to December 2021. All patients met the following criteria: (1) PE confirmed by chest X-ray, CT, or ultrasound; (2) Patients undergoing diagnostic pericardiocentesis. Exclusion criteria: (1) patients with pericardial effusion of unknown etiology; (2) Patients with more than 30% missing information.

This study was approved by the ethics committee of Taizhou hospital, Zhejiang Province (K20220104). Informed consent was abandoned because it was a retrospective study.

Data collection

Relevant data of the selected patients were collected, including: (1) clinical information, including gender, age, chest distress, chest pain, anepithymia, loss of weight, fever (fever is defined as body temperature > 37.5°C), heart rate, pleural effusion, size of effusion, pericardial hematocele, mediastinal lymph node enlargement; (2) blood laboratory data include high sensitivity C-reactive protein (hs CRP), total protein (TP), albumin (ALB), ADA, glucose (GLU), LDH, erythrocyte sedimentation rate (ESR), CEA; (3) Laboratory data of pericardial effusion include karyocyte count, effusion TP, effusion ALB, effusion ADA, effusion GLU, effusion LDH and effusion CEA. All numerical variables were converted into categorical variables according to the cut-off value which were obtained using receiver operating characteristic (ROC) curves (Supplementary Figure 1).

Diagnostic criteria

MPE is diagnosed if the patient meets at least one of the following criteria: (1) tumor cells are detected in pericardial effusion cytology or pericardial biopsy; (2) proof of primary tumor; (3) atypical cells are detected in pericardial effusion and there is clinical evidence of tumor spread and exclusion of other potential causes of pericardial effusion (1, 11).

BPE is diagnosed if the patient meets at least one of the following criteria: (1) no cancer cells are detected in pericardial effusion cytology or pleural biopsy; (2) PE disappeared after etiological treatment and thoracic puncture. All BPE was confirmed by clinical and laboratory examination without any tumor signs.

Tuberculous pericardial effusion (TPE) is diagnosed if the patient meets at least one of the following criteria: (1) pericardial effusion or biopsy smear shows acid fast bacilli, or Mycobacterium tuberculosis culture or polymerase chain reaction is positive in other clinical samples; (2) Granulomatous inflammation in pericardial biopsy specimens; (3) After empirical antituberculosis treatment, the clinical manifestations and imaging findings of pericardial effusion were resolved.

Statistical analysis

All data were statistically analyzed using R (Version: 4.0.5). Chi square test or Fisher's exact test and lasso regression were used to screen the risk factors of MPE in the training set. Odds ratios (ORs) and their 95% confidence intervals (CIs) were estimated. A nomogram was developed to present the model according to the independent risk factors selected by multivariate logistic regression. The prediction accuracy of the

model was evaluated by ROC curve AUC, calibration curve, decision curve analysis (DCA), and clinical impact curve (CIC). In order to make the prediction model more suitable for doctors' use in clinical work, we modified the nomogram to the scoring system, and evaluated the diagnostic accuracy of this scoring system using AUC, specificity, sensitivity, PPV, NPV, PLR, and NLR in the training set and verification set. $P < 0.05$ was considered to be statistically significant.

Results

Patient characteristics

A total of 273 patients were diagnosed with pericardial effusion. 46 patients were excluded because they did not meet the inclusion criteria. A total of 227 patients (85 MPE and 142 BPE) were included in this study. The patient selection flow chart is shown in Figure 1. In 85 cases of MPE, tumor cells were found in 57 cases, atypical cells were found in 28 cases, and tumor cells or atypical cells were not found in 142 cases of BPE. The etiological classification of included patients is shown in Table 1. 85 patients with MPE and 142 patients with BPE were divided into a training group (admission in 2017 and later) and a validation group (admission before 2017).

Development and validation of nomogram and new scoring system

Most parameters such as heart rate, fever, weight loss, massive PE, mediastinal lymph node enlargement, pleural

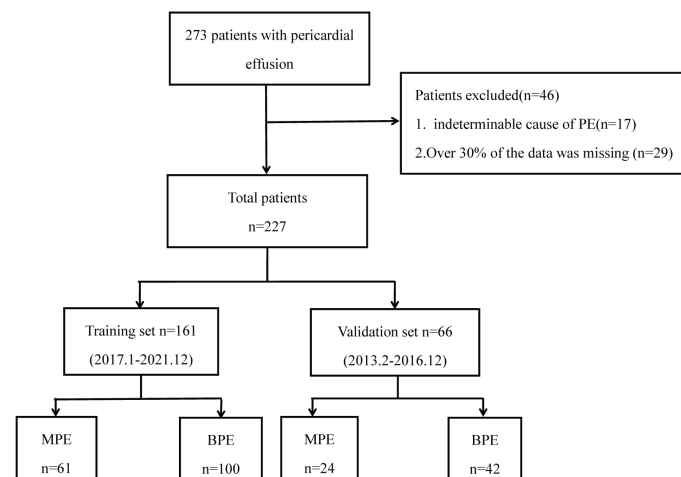


FIGURE 1
Flow chart of participant selection.

TABLE 1 Baseline characteristics of the study set.

Paremeters	Training set (n = 161)	Validation set (n = 66)
Age (years)	67.0 (59.0, 76.0)	60.0 (49.2, 72.0)
Gender (%)		
Male	99 (61.5)	21 (47.0)
Female	62 (38.5)	35 (53.0)
Malignant pleural effusion (%)		
Lung cancer	46 (75.4)	18 (75.0)
Esophageal carcinoma	2 (3.3)	0 (0.0)
Breast carcinoma	5 (8.2)	3 (12.5)
Gastrointestinal carcinoma	4 (6.6)	1 (4.2)
Non-Hodgkin lymphoma	2 (3.3)	1 (4.2)
Cancer of unknown primary	2 (3.3)	1 (4.2)
Benign pleural effusion (%)		
Tuberculosis	26(26.0)	15 (35.7)
Cardiac injury syndromes	5 (5.0)	1 (2.4)
Autoimmune	5 (5.0)	2 (4.8)
Congestive heart failure	19 (19.0)	5 (11.9)
Cirrhosis	3 (3.0)	1 (2.4)
Nephrotic syndrome	8 (8.0)	1 (2.4)
Traumatic	3 (3.0)	1 (2.4)
Hypothyroidism	4 (4.0)	1 (2.4)
Infectious	6 (6.0)	2 (4.8)
Idiopathic	21 (21.0)	13 (31.0)

effusion, CEA, effusion LDH, effusion CEA, TP, ADA, effusion ADA, and effusion GLU were significantly different between MPE and BPE groups in the training set (Supplementary Table S1). Then we used a multivariable logistic regression model to get the optimal features, including loss of weight, fever, mediastinal lymph node enlargement, pleural effusion,

effusion ADA, effusion LDH, and effusion CEA (Figure 2, Table 2). Next, a nomogram was developed to distinguish MPE from BPE based on the logistic regression model (Figure 3A). The ROC curve AUC of the nomogram was 0.974 (95%CI = 0.948-0.998), which had high diagnostic value (Figure 3B). The calibration curve showed that the predicted value of the nomogram diagnosis MPE was in good agreement with the actual observed value (Figure 3C). DCA showed that PE patients would benefit from the use of this nomogram model, rather than all or no treatment (Figure 3D). CIC analysis showed when the threshold probability was greater than 30% of the predictive scoring probability, the predictive model determines that MPE was highly matched with the actual MPE, which confirms that the predictive model had a very high clinical efficiency (Figure 3E).

The nomogram model with an AUC of 0.970 (95%CI = 0.938-1.000) showed good discrimination ability in the validation set (Figure 3F). The calibration curve showed that the predicted value of the nomogram was in good agreement with the actual observed value (Figure 3G). DCA showed that PE patients would benefit from using this nomogram model (Figure 3H). CIC showed the model prediction was accurate in predicting high risk MPE cases when the risk threshold was about 0.3~1.0 (Figure 3I).

In order to make the prediction model more suitable for doctors using in clinical work, we converted the nomogram to the scoring system: loss of weight (3 points), no fever (4 points), mediastinal lymph node enlargement (2 points), pleural effusion (6 points), effusion ADA ≤ 18 U/L (5 points), effusion LDH >1033 U/L (7 points), and effusion CEA >4.9 g/mL (10 points) (Table 3). The optimal cut-off value for MPE diagnosis was 16 points according to the ROC curve. When the total score exceeded 16 points, PE were more likely to be diagnosed as MPE, while the total score was lower than 16 points, PE was

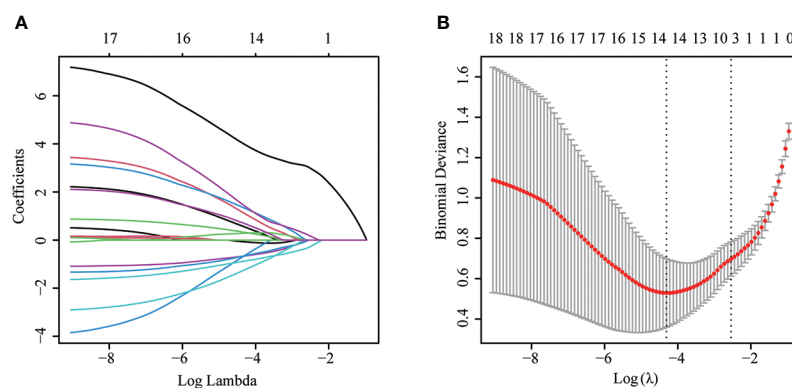


FIGURE 2

The LASSO logistic proportional hazard regression to screen risk factors for MPE. (A) The plot of partial likelihood deviance of LASSO logistic regression. (B) Plot of LASSO coefficient profiles.

TABLE 2 Multivariate logistic regression analysis of the clinical parameters in the training set.

Parameters	OR (95%CI)	P value
heartrate≥100	10.57 (0.81-138.69)	0.073
loss of weight	30.26 (1.71-536.80)	0.020
size	2.57 (0.65-10.13)	0.177
fever	0.05 (0.01-0.54)	0.013
Mediastinal lymph node enlargement	8.99 (1.01-79.78)	0.049
Pleural Effusion	29.58 (1.17-745.95)	0.040
TP>62.7g/L	0.35 (0.05-2.44)	0.287
ADA>9U/L	1.82 (0.27-12.44)	0.540
CEA>4.5ng/ml	0.96 (0.09-10.79)	0.970
Effusion ADA>18U/L	0.02 (0.00-0.98)	0.049
Effusion GLU>5.23mmol/L	0.19 (0.02-1.59)	0.125
Effusion LDH>1033U/L	164.58 (3.18-8515.92)	0.011
Effusion CEA>4.9ng/mL	1684.04 (21.49-131981.48)	0.001
ESR>20mm/H	0.25 (0.03-2.00)	0.193

OR, odds ratio; CI, confidence interval; TP, total protein; ADA, adenosine deaminase; GLU, glucose; LDH, lactate dehydrogenase; ESR, erythrocyte sedimentation; CEA, carcino embryonic antigen. Parameters with P values less than 0.05 were shown in bold values.

more likely to be diagnosed as BPE. The AUC, specificity, sensitivity, PPV, NPV, PLR and NLR were 0.974, 95.1%, 91.0%, 85.6%, 96.8%, 10.56, and 0.054, respectively, in the training set (Table 4). When the critical point was also set to 16, AUC, specificity, sensitivity, PPV, NPV, PLR, and NLR were 0.950, 83.3%, 95.2%, 90.9%, 90.9%, 17.5, and 0.175, respectively, in the validation set (Table 4).

Diagnostic significance of scoring system in differentiating lung cancer complicated with MPE from TPE

Because tuberculosis was still the main cause of pericardial effusion in developing countries, and TPE with atypical symptoms was easy to be confused with MPE cause by lung cancer in the clinical environment, we specially apply this scoring system to distinguish MPE caused by lung cancer from TPE. We found that the AUC value of the scoring system used to distinguish MPE caused by lung cancer from TPE was 0.980 (95% CI = 0.959-1.000). When the total score exceeded 16, it had good specificity, sensitivity, PPV, NPV, PLR, and NLR values, as shown in Table 4.

Diagnostic significance of scoring system in differentiating MPE with atypical cells from BPE

It was difficult to diagnose some atypical cells only with cytological specimens, and some auxiliary tools were often needed to achieve a clear diagnosis. Therefore, we specially apply this scoring system to distinguish MPE from BPE. We

found that the AUC value of the scoring system to identify MPE with atypical cells from BPE was 0.940 (95% CI = 0.884-0.996), which had a good diagnostic performance. When the total score exceeded 16, it had good specificity, sensitivity, PPV, NPV, PLR, and NLR values (Table 4).

Discussion

MPE is a common symptom of tumor invading pericardium, sometimes even the first symptom of tumor patients (12). The existence of MPE will not only seriously affect the life quality of patients but also represent the late stage of the disease. The average survival time of these patients is rarely more than 12 months (13). In addition, about 1/3 cancer patients with PE will have pericardial tamponade, resulting in hemodynamic instability and death (14). The clinical manifestations of patients with MPE lack of specificity, and distinguishing MPE from BPE may be a high challenge. Exfoliative cytology and diagnostic pericardial biopsy of pericardial effusion are of decisive significance for the diagnosis of MPE, but the sensitivity of these methods is relatively low. In this study, the sensitivity of cytology is 67.1%. Therefore, the primary goal of this study is to establish an accurate and efficient early diagnosis model of MPE.

Pericardial effusion specimens are not common, so there are few reports on the early diagnosis of MPE compared with pleural effusion or peritoneal effusion. Karatolios K et al. analyzed CEA, CA19-9, CA72-4, squamous cell carcinoma antigen (SCC), and neuron specific enolase (NSE) in the pericardial effusion of 29 patients with MPE and 25 patients with BPE, and found that measuring the level of CA 72-4 in pericardial fluid has certain diagnostic value for MPE (15). Nakamura T et al. analyzed 125

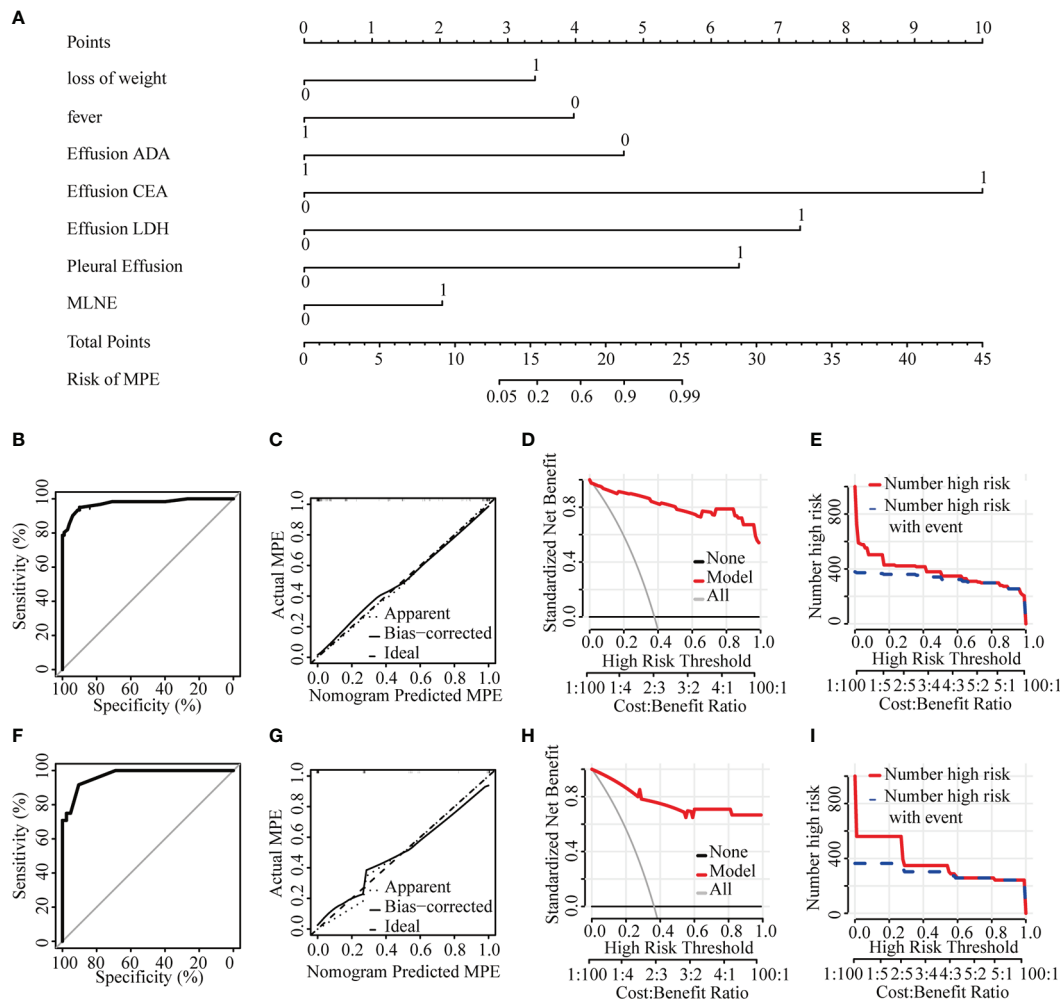


FIGURE 3

Diagnostic model of the discrimination for MPE and BPE. (A) Nomogram for identifying MPE from BPE. (B) ROC curve in the training set. (C) Calibration curve in the training set. (D) Clinical decision curve in the training set. (E) Clinical impact curve in the training set. (F) ROC curve in the validation set. (G) Calibration curve in the validation set. (H) Clinical decision curve in the validation set. (I) Clinical impact curve in the validation set. ADA, adenosine deaminase; CEA, carcino embryonic antigen; LDH, lactate dehydrogenase; MPE, malignant pericardial effusion; MLNE, mediastinal lymph node enlargement.

TABLE 3 Scoring system developed from a nomogram of the training set.

Parameters	Score modified from nomogram
Fever (No)	4
Loss of weight	3
Pleural Effusion (Yes)	6
Mediastinal lymph node enlargement (Yes)	2
Effusion ADA ≤ 18 U/L	5
Effusion LDH > 1033 U/L	7
Effusion CEA > 4.9 g/mL	10

ADA, adenosine deaminase; LDH, lactate dehydrogenase; CEA, carcino embryonic antigen.

PE patients who underwent pericardiocentesis and found that low pericardial blood glucose level and high CT attenuation value had a certain suggestive effect on MPE (16). However, most biomarkers are used alone and cannot provide adequate evidence to identify MPE and BPE accurately. With the development of analytical methods, the establishment of prediction models based on multiple clinical characteristics or indicators has attracted more and more attention and application in medical research and clinical practice (17, 18).

Nomogram is to predict the probability of individual specific clinical outcomes through a certain function transformation relationship by constructing a multivariate regression model. And it transforms the complex regression equation into simple

TABLE 4 Accuracy of the prediction score for differentiating MPE from BPE.

Parameters	Training set	Validation set	Lung cancer with MPE/BPE	MPE with atypical cell/BPE
AUC	0.974 (0.949-0.999)	0.950 (0.898-1.000)	0.980 (0.959-1.000)	0.940 (0.884-0.996)
Sensitivity (%)	95.1 (85.4-98.7)	83.3 (61.8-94.5)	92.2 (82.0-97.1)	85.7 (66.4-95.3)
Specificity (%)	91.0 (83.2-95.5)	95.2 (82.6-99.2)	95.1 (82.2-99.2)	92.3 (86.2-95.9)
PPV (%)	85.6 (75.5-93.3)	90.9 (69.4-98.4)	96.7 (87.7-99.4)	68.6 (50.6-82.6)
NPV (%)	96.8 (90.3-99.2)	90.9 (77.4-97.0)	88.6 (74.6-95.7)	97.0 (92.1-99.0)
PLR	10.56 (5.65-19.75)	17.50 (4.47-68.48)	18.90 (4.88-73.16)	11.06 (6.15-19.91)
NLR	0.05 (0.02-0.16)	0.18 (0.07-0.43)	0.08 (0.035-0.19)	0.16 (0.06-0.38)

MPE, malignant pericardial effect; BPE, beneficial pericardial effect; AUC, area under curve; PPV, positive predictive value; NPV, negative predictive value; PLR, positive likelihood ratio; NLR, negative likelihood ratio.

and visual graphics so that the results of the prediction model can be displayed more intuitively and has a higher use value. In this study, we collected 29 routine parameters easily obtained in the clinical practice of 227 patients with PE and established a nomogram model to distinguish MPE and BPE based on lasso regression and multiple logistic regression model. The nomogram model includes loss of weight, fever, mediastinal lymph node enlargement, pleural effusion, effusion ADA, effusion LDH, and effusion CEA.

In order to make the model more suitable for doctors to use in clinical work, we transformed the nomogram into a scoring system. Patients with a score of more than 16 are more likely to be diagnosed with MPE. We used sensitivity, specificity, PPV, NPV, PLR, and NLR to evaluate the accuracy of the scoring system and found that the scoring system has good diagnostic performance. Therefore, the scoring system is a quantitative and valuable tool which can be used to quickly distinguish MPE from BPE. Szturmowicz M et al. has developed a scoring system based on mediastinal lymph node enlargement, effusion Cyfra 21-1, effusion CEA, bloody effusion, signs of imminent cardiac tamponade and heart rate faster than 90 beats/min (19). On this basis, we have established a new scoring system combining the clinical features and effusion biochemical parameters, which has improved the diagnostic accuracy to a certain extent.

Lung cancer related MPE and TPE have many similarities in clinical characteristics and laboratory indicators. Some patients with malignant pericardial effusion cannot find tumor cells and are easy to be misdiagnosed as tuberculous pericardial effusion (20). Therefore, finding a new method to differentiate lung cancer with MPE and TPE is of great significance. We applied the scoring system to the diagnosis of these two diseases and found that the scoring system has good diagnostic performance in distinguishing MPE and TPE related to lung cancer. When the total score exceeded 16, the patient is more likely to be diagnosed with MPE.

Our study aims to design a new quantitative tool so that clinicians can predict the probability of MPE and BPE, and then help doctors choose treatment options and predict prognosis. Our scoring system is based on various common clinical and

laboratory indicators. These indicators have been carried out in most hospitals, even grass-roots hospitals, and are suitable for wide clinical applications. Therefore, we recommend that the new scoring model would be widely used in most hospitals to distinguish MPE from BPE quickly.

There are still some deficiencies in this study. Firstly, this study was a single center retrospective study, which may have some bias. Secondly, only internal validation was carried out for the model, and no further external validation was carried out. Third, no other tumor markers except CEA were evaluated for pericardial effusion. Therefore, prospective studies with a larger sample size from multiple centers were needed to verify the diagnostic model.

Conclusion

In conclusion, loss of weight, fever, mediastinal lymph node enlargement, pleural effusion, effusion ADA, effusion LDH, and effusion CEA are of great significance in distinguishing MPE from BPE. Although the scoring system developed in this study has high diagnostic value in distinguishing MPE and BPE, it still needs to be further verified in a multicenter prospective study.

Data availability statement

The raw data supporting the conclusions of this article will be made available by the authors, without undue reservation.

Ethics statement

The studies involving human participants were reviewed and approved by the ethics committee of Taizhou hospital, Zhejiang Province (K20220104). Written informed consent for participation was not required for this study in accordance with the national legislation and the institutional requirements.

Author contributions

TL and GL design and conceptualized the study. XJ design and conceptualized study, analyzed the data and drafted the manuscript. MF and LH collected the data and revised the manuscript. QZ and YY collected the data. All authors contributed to the article and approved the submitted version.

Acknowledgments

The authors thank all patients for their participation in this study.

Conflict of interest

The authors declare that the research was conducted in the absence of any commercial or financial relationships that could be construed as a potential conflict of interest.

References

- Adler Y, Charron P, Imazio M, Badano L, Baron-Esquivias G, Bogaert J, et al. ESC Guidelines for the diagnosis and management of pericardial diseases: The task force for the diagnosis and management of pericardial diseases of the European society of cardiology (ESC) Endorsed by: The European association for cardiothoracic surgery (EACTS). *Eur Heart J* (2015) 36(42):2921–64. doi: 10.1093/eurheartj/ehv318
- Kim SR, Kim EK, Cho J, Chang SA, Park SJ, Lee SC, et al. Effect of anti-inflammatory drugs on clinical outcomes in patients with malignant pericardial effusion. *J Am Coll Cardiol* (2020) 76(13):1551–61. doi: 10.1016/j.jacc.2020.08.003
- Schusler R, Meyerson SL. Pericardial disease associated with malignancy. *Curr Cardiol Rep* (2018) 20(10):92. doi: 10.1007/s11886-018-1040-5
- Wang S, Zhao J, Wang C, Zhang N. Prognosis and role of clinical and imaging features in patients with malignant pericardial effusion: a single-center study in China. *BMC Cardiovasc Disord* (2021) 21(1):565. doi: 10.1186/s12872-021-02331-9
- Bildirici U, Celikyurt U, Acar E, Bulut O, Sahin T, Kozdag G, et al. The value of serum tumour markers in the prediction of aetiology and follow up of patients with pericardial effusion. *Cardiovasc J Afr* (2012) 23(3):143–6. doi: 10.5830/CVJA-2011-029
- Chen B, Meinertzhagen IA, Shaw SR. Circadian rhythms in light-evoked responses of the fly's compound eye, and the effects of neuromodulators 5-HT and the peptide PDF. *J Comp Physiol A* (1999) 185(5):393–404. doi: 10.1007/s003590050400
- Puri M, Sen R, Gupta M, Kalra R, Bhargava S, Puri K. DNA Ploidy analysis and cell block immunohistochemistry in the diagnosis of malignant effusions. *Acta Cytol* (2020) 64(3):256–64. doi: 10.1159/000501790
- Carasso S, Grosman-Rimon L, Nassar A, Kusnec F, Ghanim D, Elbaz-Greener G, et al. Serum BNP levels are associated with malignant pericardial effusion. *Int J Cardiol Heart Vasc* (2019) 23:100359. doi: 10.1016/j.ijcha.2019.100359
- Karalios K, Pankuweit S, Maisch B. Diagnostic value of biochemical biomarkers in malignant and non-malignant pericardial effusion. *Heart Failure Rev* (2012) 18(3):337–44. doi: 10.1007/s10741-012-9327-x
- Karalios K, Pankuweit S, Moosdorf RG, Maisch B. Vascular endothelial growth factor in malignant and benign pericardial effusion. *Clin Cardiol* (2012) 35(6):377–81. doi: 10.1002/clc.21967
- Pennacchioni A, Nanni G, Sgura FA, Imberti JF, Monopoli DE, Rossi R, et al. Percutaneous pericardiocentesis for pericardial effusion: predictors of mortality and outcomes. *Internal Emergency Med* (2021) 16(7):1771–7. doi: 10.1007/s11739-021-02642-x
- Vakamudi S, Ho N, Cremer PC. Pericardial effusions: Causes, diagnosis, and management. *Prog Cardiovasc Dis* (2017) 59(4):380–8. doi: 10.1016/j.pcad.2016.12.009
- Chahine J, Shekhar S, Mahalwar G, Imazio M, Collier P, Klein A. Pericardial involvement in cancer. *Am J Cardiol* (2021) 145:151–9. doi: 10.1016/j.amjcard.2020.12.092
- Imazio M, Colopi M, De Ferrari GM. Pericardial diseases in patients with cancer: contemporary prevalence, management and outcomes. *Heart* (2020) 106(8):569–74. doi: 10.1136/heartjnl-2019-315852
- Karalios K, Maisch B, Pankuweit S. [Tumor markers in the assessment of malignant and benign pericardial effusion]. *Herz* (2011) 36(4):290–5. doi: 10.1007/s00059-011-3451-6
- Nakamura T, Okune M, Yasuda M, Watanabe H, Ueno M, Yamaji K, et al. Impact of pericardial fluid glucose level and computed tomography attenuation values on diagnosis of malignancy-related pericardial effusion. *BMC Cardiovasc Disord* (2021) 21(1):272. doi: 10.1186/s12872-021-02091-6
- Hou ZL, Kang Y, Yang GZ, Wang Z, Wang F, Yu YX, et al. Pleural effusion-based nomogram to predict outcomes in unselected patients with multiple myeloma: a large single center experience. *Ann Hematol* (2021) 100(7):1789–801. doi: 10.1007/s00277-021-04484-1
- Xu S, Qi J, Li B, Bie ZX, Li YM, Li XG. Risk prediction of pleural effusion in lung malignancy patients treated with CT-guided percutaneous microwave ablation: a nomogram and artificial neural network model. *Int J Hyperthermia* (2021) 38(1):220–8. doi: 10.1080/02656736.2021.1885755
- Szturmowicz M, Pawlak-Cieslik A, Fijalkowska A, Gatarek J, Skoczylas A, Dybowska M, et al. The value of the new scoring system for predicting neoplastic pericarditis in the patients with large pericardial effusion. *Support Care Cancer* (2017) 25(8):2399–403. doi: 10.1007/s00520-017-3645-4
- Liu J, Zeng Y, Ma W, Chen S, Zheng Y, Ye S, et al. Preliminary investigation of the clinical value of vascular endothelial growth factor and hypoxia-inducible factor-1 α in pericardial fluid in diagnosing malignant and tuberculous pericardial effusion. *Cardiology* (2010) 116(1):37–41. doi: 10.1159/000313465

Publisher's note

All claims expressed in this article are solely those of the authors and do not necessarily represent those of their affiliated organizations, or those of the publisher, the editors and the reviewers. Any product that may be evaluated in this article, or claim that may be made by its manufacturer, is not guaranteed or endorsed by the publisher.

Supplementary material

The Supplementary Material for this article can be found online at: <https://www.frontiersin.org/articles/10.3389/fonc.2022.1012664/full#supplementary-material>

SUPPLEMENTARY FIGURE 1

Receiver operative characteristic (ROC) analysis were used to determine the optimal cut-offs of categorical variables. age (A), effusion TP (B), effusion ALB (C), effusion ADA (D), effusion GLU (E), effusion LDH (F), effusion CEA (G), TP (H), ALB (I), ADA (J), GLU (K), LDH (L), CEA (M), hs-CRP (N), ESR (O) and Karyocyte count (P).



OPEN ACCESS

EDITED BY

Alberto Sandri,
San Luigi Gonzaga Hospital, Italy

REVIEWED BY

Liyuan Zhang,
Second Affiliated Hospital of Soochow
University, China
Sheng Lin,
The Affiliated Hospital of Southwest
Medical University, China

*CORRESPONDENCE

Shude Chai
✉ chaishude_edu@163.com
Xuequan Huang
✉ hxuequan@163.com
Junjie Wang
✉ junjiawang_edu@sina.cn

[†]These authors share first authorship

SPECIALTY SECTION

This article was submitted to
Thoracic Oncology,
a section of the journal
Frontiers in Oncology

RECEIVED 31 May 2022

ACCEPTED 30 December 2022

PUBLISHED 07 February 2023

CITATION

Huo B, Ji Z, He C, Yang W, Ma Y, Huo X,
Wang Z, Zhao X, Dai J, Wang H, Chen G,
Wang R, Song Y, Zhang K, Huang X, Chai S
and Wang J (2023) Safety and efficacy of
stereotactic ablative brachytherapy as a
salvage therapy for recurrent chest wall
cancer: A retrospective, multicenter study.
Front. Oncol. 12:957497.
doi: 10.3389/fonc.2022.957497

COPYRIGHT

© 2023 Huo, Ji, He, Yang, Ma, Huo, Wang,
Zhao, Dai, Wang, Chen, Wang, Song, Zhang,
Huang, Chai and Wang. This is an open-
access article distributed under the terms of
the [Creative Commons Attribution License](https://creativecommons.org/licenses/by/4.0/)
(CC BY). The use, distribution or
reproduction in other forums is permitted,
provided the original author(s) and the
copyright owner(s) are credited and that
the original publication in this journal is
cited, in accordance with accepted
academic practice. No use, distribution or
reproduction is permitted which does not
comply with these terms.

Safety and efficacy of stereotactic ablative brachytherapy as a salvage therapy for recurrent chest wall cancer: A retrospective, multicenter study

Bin Huo^{1†}, Zhe Ji^{2†}, Chuang He^{3†}, Wanying Yang⁴, Yanli Ma⁵,
Xiaodong Huo¹, Zhe Wang⁶, Xinxin Zhao⁷, Jinchao Dai⁸,
Haitao Wang¹, Guanglie Chen⁷, Ruoyu Wang⁶, Yuqing Song⁵,
Kaixian Zhang⁴, Xuequan Huang^{3*}, Shude Chai^{1*}
and Junjie Wang^{2*}

¹Department of Oncology, The Second Hospital of Tianjin Medical University, Tianjin, China,

²Department of Radiation Oncology, Peking University Third Hospital, Beijing, China, ³Center of
Minimally Invasive Intervention, Southwest Hospital of Army Medical University, Chongqing, China,

⁴Department of Oncology, Tengzhou Central People's Hospital, Tengzhou, China, ⁵Department of
Oncology, Staff Hospital of Chengde Iron and Steel Group Co. Ltd., Chengde, China, ⁶Department of
Radiation Oncology, Affiliated Zhongshan Hospital of Dalian University, Dalian, China, ⁷Department of
Oncology Radiotherapy, The First People's Hospital of Kerqin District, Tongliao, China, ⁸Department of
Nuclear Medicine, Qingdao Central Hospital, Qingdao, China

Purpose: To evaluate the safety and efficacy of stereotactic ablative brachytherapy (SABT) as a salvage therapy for patients with recurrent chest wall cancer (rCWC) who have previously received external beam radiotherapy (EBRT) or surgery.

Materials and methods: Between November 2013 and October 2020, a total of 130 patients (including 75 men with a median age of 63 years) with rCWC treated with SABT were enrolled in this multicenter retrospective study. There were 97 cases of non-small-cell lung carcinoma, 24 cases of breast cancer, and 9 cases of thymic cancer. Of the patients included, 102 patients previously received surgery and 58 patients received EBRT, with systemic treatment progressing after recurrence. None of them were suitable or refused to undergo salvage EBRT or surgery again.

Results: During the 22 (4–70)-month median patient follow-up, 59 patients died. The local control (LC) rates at 6, 12, 24, and 36 months were 88.3%, 74.3%, 50.4%, and 36.7%, respectively. The 1-, 2- and 3-year survival rates were 85%, 56%, and 42%, respectively. The median overall survival was 26 months (95% CI, 18.9–33.1 months). The pain relief rate was 81%, and the median to remission time was 10 days. Univariate and multivariate analyses showed that independent prognostic factors for LC included tumor size and postoperative D90. On the other hand, independent prognostic factors for survival include the Karnofsky performance status (KPS) score, tumor size, and D90 19 patients (14.6%) developed grade I/II skin reaction complications. No grade III or severer complications occurred.

Conclusion: SABB is safe and effective as a salvage therapy for rCWC following EBRT/surgery. For patients with a KPS score greater than 80, prescribed dose greater than 130 Gy, and tumor size less than 4 cm may bring better results.

KEYWORDS

recurrent chest wall cancer, stereotactic ablative brachytherapy, reirradiation, external beam radiotherapy (EBRT), salvage therapy

Introduction

Chest wall cancer (CWC) can arise from a variety of tumors, including breast cancer, lung cancer, mesothelioma, sarcoma, and thymic cancer. The primary treatment was surgical resection, but 50% of patients relapsed after surgery or radiotherapy (1–3). Once systemic therapy (chemotherapy or targeted therapy) progressed, the treatment options were limited; 5-year survival was only 17% (4–6). Retreatment with EBRT is promising, although the recurrence of the lesion within the previously irradiated field remains to be resolved. Hence, only well-selected patients can be considered for EBRT with higher toxicity (7, 8). Brachytherapy (BT) has the exceptional ability to deliver extremely high doses that external beam radiotherapy (EBRT) could never achieve within treated lesions, with the added benefit that doses drop off rapidly outside the target lesion by minimizing the exposure of uninvolved surrounding normal tissue (9). Stereotactic ablative BT (SABB) was designed to improve the ablative effect of radiation, which was achieved *via* improved image guidance and the calculation of ablative dose, shorter treatment duration, and better organ preservation (10). Recently collected data suggest that SABB has been shown to be safe and effective in the treatment of head and neck, thoracic, abdominal, retroperitoneal, and vertebral cancers, particularly for locally advanced or recurrent solid cancers following EBRT (11–15). Several single-institution retrospective studies of recurrent CWC (rCWC) patients have been published previously (16–18). Here, our multicenter retrospective study provided the long-term survival outcome data in rCWC patients treated with SABB and the data for real-world clinical practice.

Materials and methods

Patient selection criteria

This was a retrospective study, and 130 patients were enrolled [75 men and 55 women; the median age of 63 (32–85) years was related to rCWC receiving SABB treatment at eight medical centers in China between November 2013 and October 2020. There were 97 cases of non-small-cell lung carcinoma (40 cases of squamous cell carcinoma and 57 cases of adenocarcinoma), 24 cases of breast cancer, and 9 cases of thymic cancer. Of the patients included, 102 patients previously received surgery and 58 patients received EBRT, with systemic treatment progressing after recurrence and none of whom were candidates for or refused salvage surgery and/or repeat EBRT.

The study enrolled patients with squamous cell lung cancer or driver-negative adenocarcinoma of the lung who had failed previous multiline chemotherapy. The driver-positive adenocarcinoma of the lung, who had failed previous targeted therapies. The characteristics of the patients are listed in Table 1. We analyzed several indicators such as the local control (LC) rate, progression-free survival (PFS), overall survival (OS), and complications. We evaluated tumor response according to Response Evaluation Criteria in Solid Tumors (RECIST) v1.1 (19). Local disease control included complete response, partial response, and stable disease. Time to tumor progression from the SABB procedure was defined as time to progression. The time from SABB surgery to death from any cause or last follow-up was defined as OS. Complications were identified by Common Terminology Criteria for Adverse Events (CTCAE) v4.0 (CTCA) (20).

Preoperative preparation and preplanning

All patients underwent blood routine, coagulation, and biochemical tests before SABB to rule out contraindications. The patient was secured on a CT scan bed and fixed in a custom-made vacuum bag in supine, prone, or lateral positions. Plain and contrast-enhanced CT scans were performed 1–2 days before treatment with a thickness of 5 mm. According to the requirements of the American Association of medical physicists (AAPM), the image data is transmitted to BT-TPS (Beijing University of Aeronautics and Astronautics and Beijing Astronomical Technology Co., Ltd.) for pre-planning (22, 23). The 90% gross tumor volume (GTV (GTV D90) dose should be as close as possible to the prescribed dose, while the organs at risk (OAR) dose should be as low as possible. The median prescription dose was 120 Gy (range, 100–160 Gy). The radionuclides used in the treatment were iodine 125 seeds (4.5 mm × 0.8 mm in size, with a half-life of 59.6 days; the activities of the seeds were 0.45–0.83 mCi (median 0.65 mCi).

Stereotactic ablative brachytherapy protocol

The SABB protocol was as follows (24, 25): (1) the patient is placed on a CT simulator and fixed with a vacuum pad for a CT scan. (2) The body surface projection of the tumor target area was delineated, and local anesthesia and intercostal nerve block were performed. (3) Simple CT guided or use a coplanar or non-coplanar template to place the first pin on the body surface projection of the

TABLE 1 Clinical characteristics of the 130 patients.

	n	%
Gender		
Male	75	57.7
Female	55	42.3
Median age (years)		
<70	92	70.8
≥70	38	29.2
KPS		
<80	59	45.4
≥80	71	57.7
Primary tumor		
Lung cancer	97	74.6
Breast cancer	24	18.5
Thyroid cancer	9	6.9
Previous therapy		
Previous surgery	102	78.5
Previous radiotherapy	58	44.6
Guidance mode		
Coplanar template guided	61	46.9
3D-PNCT guided	20	15.4
Simple CT guided	49	37.7
Tumor size		
≤4	55	42.3
>4	75	57.7

tumor as planned. The seed needles were all inserted into the target site; (4) A CT scan was performed to determine the exact position of the reference needle; (5) when the position of the reference needle did not match the predetermined position, the needle was adjusted in real time until the deviation was less than 2 mm; (6) the needle was inserted into the target area all at once; (7) the CT scan was repeated to confirm the position of all the tips and, in the same way, adjust for deviations of more than 2 mm; (8) the ^{125}I seeds were delivered in a backward fashion with the Mick 200-TPV Applicator: TP transperineal (Mick Radio-Nuclear Inc., USA: Mount Vernon, NY); (9) The CT scan was performed again to confirm the distribution of ^{125}I seeds in the targets. CT images were transmitted to BT-TPS for postplanning dose assessment. The patient will be discharged 1–2 days after SABT. All procedures follow the International Commission on Radiological Protection Recommendation (26). The dosimetric parameters, e.g., D90, were identified.

Follow-up

The subjects were followed up by CT at the first month after SABT, every 3 months for 2 years, every 6 months for 3–5 years, and

every year thereafter. The evaluation of tumor response was based on CT images after SABT.

Statistical analysis

Statistical analyses were performed using SPSS 26.0 (IBM Corp., Armonk, NY, USA). The survival rate was estimated by the Kaplan–Meier method, univariate analysis by the logarithmic rank test, and multivariate analysis by Cox regression. $P \leq 0.05$ was set as statistically significant.

Results

Patients

The 130 patients enrolled had a median age of 63 ± 11.7 years. A total of 59 patients died during a median follow-up of 22 (4–70) months; 71 patients survived (12 patients lost to follow-up since October 2020; Figure 1).

Seed implantation

The median lesion diameter was 4.65 ± 1.61 cm (range, 1.5–8.9 cm). The median number of implanted seeds was 57 ± 20.65 (range, 23–128). The median seed radioactivity was 0.65 ± 0.07 mCi (range, 0.6–0.8 mCi). The median GTV D90 was 126 ± 15.27 Gy (range, 95–180 Gy).

Treatment response

The median follow-up period was 22 months (range, 4–70 months). The LC rates at 6, 12, 24, and 36 months were 88.3%, 74.3%, 50.4%, and 36.7%, respectively (Figure 2). Univariate analysis showed that sex, age, past surgical history, past radiotherapy history, implantation mode, pathological type, and physical status score were independent of LC ($p = 0.119, 0.270, 0.993, 0.068, 0.550, 0.083$, and 0.522 , respectively). LC in patients with D90 ≥ 130 Gy was significantly better than that in patients with D90 < 130 Gy ($p < 0.001$). LC in patients with tumor size ≤ 4 cm was significantly better than that in patients with tumor size > 4 cm ($p < 0.001$). In addition, multivariate analysis showed that the tumor size and postoperative D90 were independent prognostic factors for LC (Figure 3). The pain relief rate was 81%, and the median to remission time was 10 days.

Survival

The 1-, 2-, and 3-year survival rates were 85%, 56%, and 42%, respectively, with a median OS of 26 months (Figure 2). The 6-, 12-, 24-, and 36-month survival rates were 81.3%, 60.3%, 29.1%, and 20.3%, respectively. The median PFS was 13 months; 52.3% of patients had metastasis, 20.8% had local progression, and 26.9% had long-term LC. Univariate analysis showed that sex, age, past

surgical history, past radiotherapy history, and implantation mode were not related to OS ($P = 0.520, 0.111, 0.941, 0.178, \text{ and } 0.099$, respectively). Patients with $D90 \geq 130$ Gy showed significantly better OS than patients with $D90 < 130$ Gy ($p < 0.001$). Patients with tumor size ≤ 4 cm had significantly better OS compared to patients with tumor size > 4 cm ($p = 0.006$). Patients with good performance status ($KPS \geq 80$) showed better OS than those with poor performance status ($KPS < 80$) ($p < 0.001$). Patients with the chest wall recurrence of breast cancer had longer OS than lung cancer ($p = 0.005$). Multivariate analysis showed that factors significantly associated with OS included the KPS score, tumor size, and postoperative D90 (all $p < 0.001$; Figure 3).

Complications

There were 19 cases (14.6%) with grade I/II skin reaction and local skin pigmentation. No influencing factors were found to be associated with skin toxicity. No rib fracture, burst, pneumothorax, radiation pneumonia, and other adverse events occurred. There were no treatment-related adverse events of grade 3 or above.

Discussion

This multicenter retrospective study presents the long-term follow-up results of SABT as salvage therapy. After a median follow-up of 22 months, patients showed relatively high rates of LC, OS, and improvement in the quality of life, particularly pain. The KPS score, tumor size, and postoperative D90 were significantly correlated with OS. The main complication was a mild skin reaction.

The management of rCWC after surgery and/or radiotherapy has been a challenging issue. EBRT as a salvage treatment option is promising for rCWC in previously exposed areas. However, challenges remain because it is difficult to deliver adequate doses to the target without affecting normal tissue, especially for tumors that had previously received full-dose therapy (27, 28). Hyperthermia combined with reirradiation or a high dose rate after loading is an

effective treatment option in recent years (3, 29, 30). However, it is also limited by the tolerance of normal tissues, which often makes it difficult to increase the target dose, the overall efficacy is not satisfactory, and there are serious or even fatal treatment-related adverse reactions, such as ulceration, necrosis, chest fibrosis, and pneumonia (31, 32). SABT appears to be a viable alternative to adjuvant therapy. SABT may have the following advantages (9, 10): (1) compared with EBRT, the implanted radioactive seeds can irradiate the tumor continuously and without interval; (2) the radiation dose of the target can be increased high enough to achieve ablation effect; at the same time, the dose of correctly implanted seeds will rapidly decrease, thus not affecting normal tissue; (3) because of the minimally invasive nature of SABT, patients will soon recover and resume their daily lives after treatment.

For patients who develop recurrence in a previously radiated chest wall, the treatment options are more difficult. The overall clinical response rate was 38%–42.3% for radiation alone. There have been several small trials exploring reirradiation with the addition of local hyperthermia therapy. The 3-year LC rate was 25%. The overall clinical response rate was 60%–71% (33). Previous SABT data for rCWC patients were all obtained from single-center retrospective studies. Jiang et al. (16) reported 20 patients with refractory rCWC. The median follow-up time was 11.5 months. The 1-, 2-, 3- and 4-year tumor control rates were all 88.7%, respectively. The 1- and 2-, 3-, and 4-year OS rates were 53.3% and 35.6%, 35.6%, and 35.6% respectively. Shi et al. (17) reported 31 patients with a recurrent chest wall malignant tumor. The 6-month effective rate was 77.4%, and the LC rate was 83.9%. Jiang et al. (18) reported 19 cases of SABT guided by a three-dimensional (3D) non-coplanar template. The median follow-up time was 8 months. Complete response was observed in 18.1%, and partial response was observed in 59.1%; stable disease was observed in 8.1%, and the pain relief rate was 87.5%. Our study is consistent with those of previous studies, and higher LC rates were obtained. The 6- and 12-month LC rates were 88.3% and 74.3%, respectively. The chest wall recurrence tumor focus shallow, fixed, rich bone structure is conducive to 3D-printing non co-planar template (PNCT) fixation; the template is easier to meet the preoperative dosimetry requirements and can

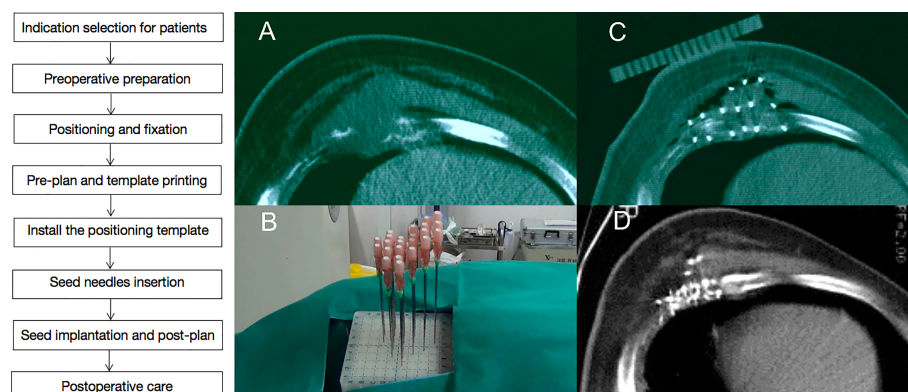


FIGURE 1

A case of recurrent chest wall cancer (rCWC) following surgery and adjuvant radiotherapy. (A) CT images of rCWC; (B) template-assisted CT-guided puncture the tumor target area; (C) ^{125}I seeds were implanted as a salvage treatment; and (D) 3 months after the seed implantation, partial response was observed.

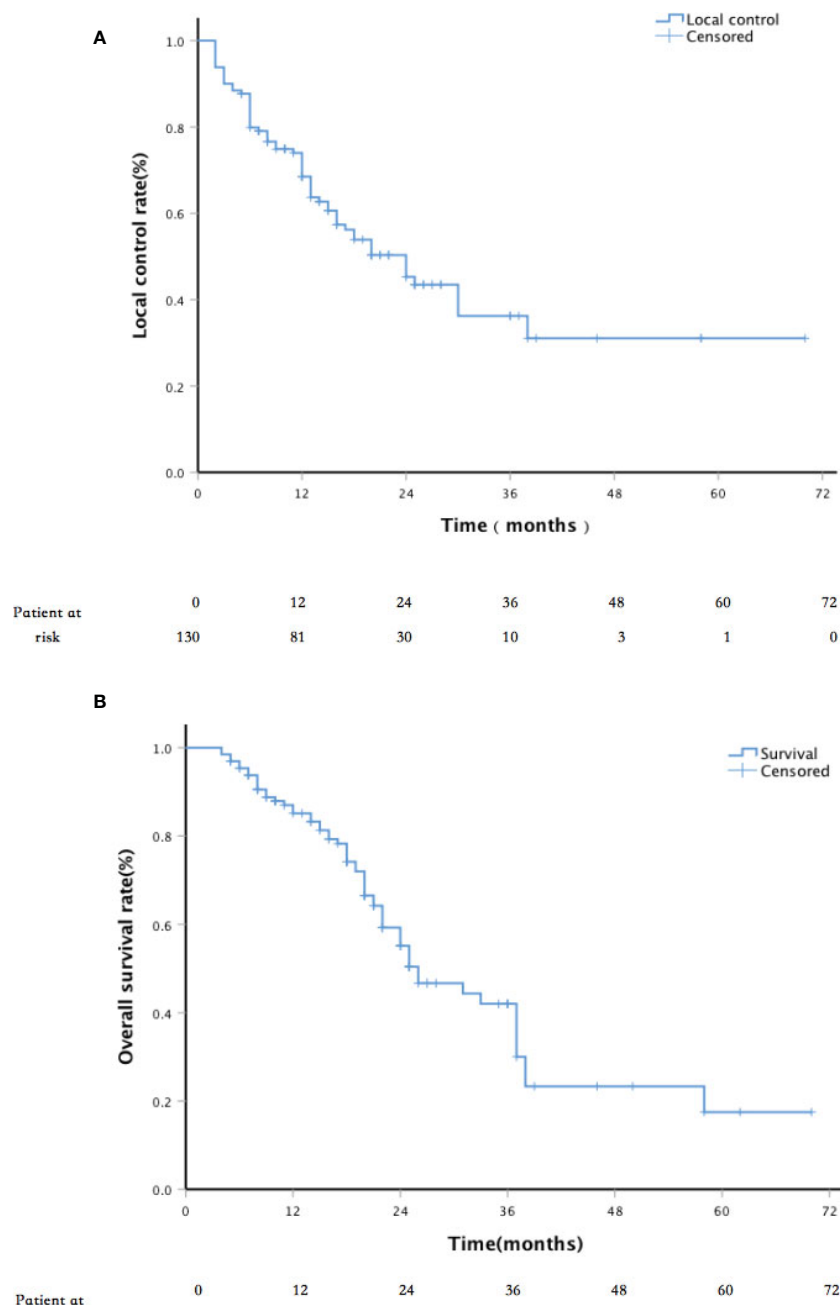


FIGURE 2

(A) Kaplan–Meier plots of local control (LC) and (B) Kaplan–Meier plots of survival.

simplify the procedure; and the operator in a relatively short learning time can be skilled. The high rate of LC and the major causes of progression or death are metastasis to other sites suggest the need to explore and combine better systemic therapy to improve OS.

In terms of safety, 24%–33% of patients \geq grade 3 acute toxicity occurred using hyperthermia and radiation. The main adverse reactions were skin edema, ulceration and fibrosis (34), chest wall pain (neurogenic) (35), and rib fracture (36, 37); the incidence of moderate and severe skin ulcers was as high as 14% (38). The average duration of chest wall pain was 25 months (2–63 months), and 36% of patients never had relief from chest wall pain. A total of 34 (29%) of the 118 cases resulted in rib fractures with an average time of 22

months (3–46 months). The results of this study showed that the complications of SBT were mild and acceptable, mainly manifested as local skin pigmentation, without rib fracture, rupture, pneumothorax, radiation pneumonia, and other adverse events. No treatment-related adverse events of grade 3 or above occurred. Retreatment after radiotherapy remains a therapeutic challenge, but both the efficacy and toxicity of SBT are acceptable. There is even a history of radiation therapy similar to that of patients without radiation therapy. As a result, SBT has significant security advantages. The improvement of pain is good, the median onset time is short, and the quality of life of patients could be significantly improved.

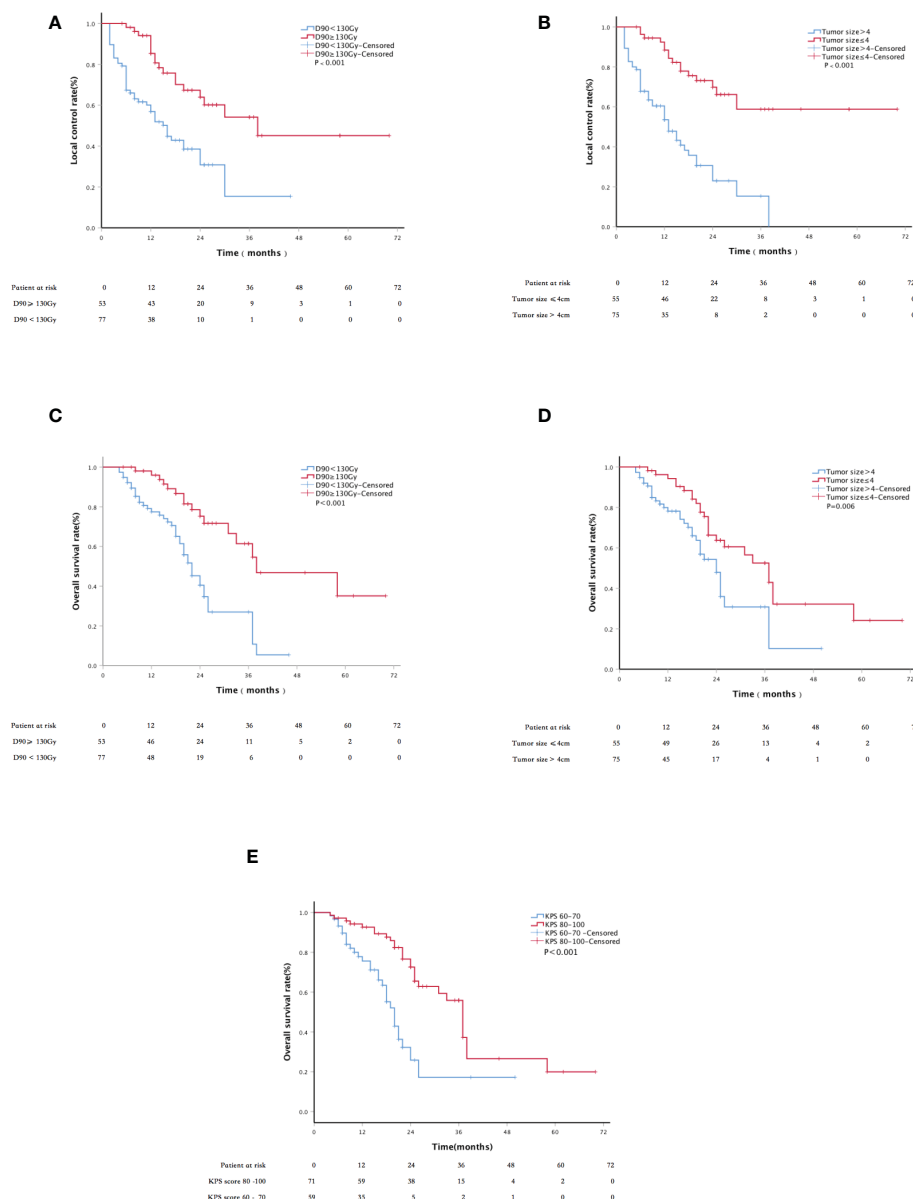


FIGURE 3

Kaplan–Meier curve about LC and survival: (A) the LC of patients with D90 \geq 130 Gy and D90 < 130 Gy; (B) the LC of tumor size \leq 4 cm and tumor size > 4 cm; (C) the overall survival (OS) of patients with D90 \geq 130 Gy and D90 < 130 Gy; (D) the OS of patients with tumor size \leq 4 cm and tumor size > 4 cm; and (E) the OS of patients with KPS scores 60–70 and 80–100.

This study has several limitations. First, as a multicenter study, the proportion of patients in different center groups is different, which may lead to potential bias. Secondly, the study was a one-arm retrospective study with 12 patients interviewed since October 2020, which may also lead to some bias. Thirdly, SABB serves as salvage therapy for the patients, but there is currently a lack of control group receiving standard salvage surgery or repeat EBRT. In addition, this group of patients is heterogeneous in the pathologic type, involving many different tumor species. There were no significant differences between lung cancer and breast cancer in the LC from SABB. Patients with the chest wall recurrence of breast cancer had better OS compared to patients with lung cancer. The sample size of different pathological types in the study group was quite different, and there might be some

bias. However, this study was the first multicenter study including more than 100 patients to investigate the long-term safety and efficacy of SABB as salvage therapy in patients with rCWC. Therefore, randomized controlled prospective studies are warranted in the future.

Conclusion

As salvage therapy following EBRT/surgery in patients with rCWC, SABB is safe and effective and has promising efficacy compared to historical data. Patients with a KPS score greater than 80, prescribed dose greater than 130 Gy, and tumor size less than 4 cm may bring better results.

Data availability statement

The original contributions presented in the study are included in the article/[Supplementary Material](#). Further inquiries can be directed to the corresponding authors.

Ethics statement

The studies involving human participants were reviewed and approved by The Second Hospital of Tianjin Medical University. The patients/participants provided their written informed consent to participate in this study.

Author contributions

Study concepts and design: SC, XuH, and JW. Literature research: BH and ZJ. Clinical studies: WY, YM, XiH, ZW, XZ, JD, HW, GC, RW,YS, and KZ. Experimental studies/data analysis: XiH, ZW, XZ, JD, and HW. Statistical analysis: ZJ and CH. Manuscript preparation: BH and CH. Manuscript editing: BH and ZJ. SC, XuH, and JW reviewed and edited the manuscript. All authors contributed to the article and approved the submitted version.

References

- Zagar TM, Higgins KA, Miles EF, Vujaskovic Z, Dewhurst MW, Clough RW, et al. Durable palliation of breast cancer chest wall recurrence with radiation therapy, hyperthermia, and chemotherapy. *Radiother Oncol* (2010) 97(3):535–40. doi: 10.1016/j.radonc.2010.10.020
- Wang L, Yan X, Zhao J, Chen C, Chen C, Chen J, et al. Expert consensus on resection of chest wall tumors and chest wall reconstruction. *Transl Lung Cancer Res* (2021) 10(11):4057–83. doi: 10.21037/tlcr-21-935
- Besson N, Hennequin C, Guillemin S, Fumagalli I, Martin V, Michaud S, et al. Plesiobrachytherapy for chest wall recurrences of breast cancer after mastectomy and radiotherapy for breast cancer. *Brachytherapy* (2018) 17(2):425–31. doi: 10.1016/j.brachy.2017.10.005
- Incarbone M, Pastorino U. Surgical treatment of chest wall tumors. *World J Surg* (2001) 25(2):218–30. doi: 10.1007/s002680020022
- Sandri A, Donati G, Blanc CD, Nigra VA, Gagliasso M, Barmasse R, et al. Anterior chest wall resection and sternal body wedge for primary chest wall tumour: reconstruction technique with biological meshes and titanium plates. *J Thorac Dis* (2020) 12(1):17–21. doi: 10.21037/jtd.2019.06.45
- Arciero C, Thompson P, Meisel JL, Taylor CE, Torres MA, Wood WC, et al. Multidisciplinary approaches to chest wall recurrences of breast cancer. *Oncol (Williston Park)* (2018) 32(8):392–6.
- Demmy TL, Nwogu CE, Yendamuri S. Thoracoscopic chest wall resection: what is its role? *Ann Thorac Surg* (2010) 89:S2142–2145. doi: 10.1016/j.athoracsurg.2010.02.110
- Wouters MW, van Geel AN, Nieuwenhuis L, van Tinteren H, Verhoef C, van Coevorden F, et al. Outcome after surgical resections of recurrent chest wall sarcomas. *J Clin Oncol* (2008) 26:5113–8. doi: 10.1200/JCO.2008.17.4631
- Wei S, Li C, Li M, Xiong Y, Jiang Y, Sun H, et al. Radioactive iodine-125 in tumor therapy: Advances and future directions. *Front Oncol* (2021) 11:717180. doi: 10.3389/fonc.2021.717180
- Xue H, Qiu B, Wang H, Jiang P, Sukocheva O, Fan R, et al. Stereotactic ablative brachytherapy: Recent advances in optimization of radiobiological cancer therapy. *Cancers* (2021) 13:3493. doi: 10.3390/cancers13143493
- Ji Z, Jiang Y, Tian S, Guo F, Peng R, Xu F, et al. The effectiveness and prognostic factors of CT-guided radioactive I-125 seed implantation for the treatment of recurrent head and neck cancer after external beam radiation therapy. *Int J Radiat Oncol Biol Phys* (2019) 103(3):638–45. doi: 10.1016/j.ijrobp.2018.10.034
- Yu X, Li J, Zhong X, He J. Combination of iodine-125 brachytherapy and chemotherapy for locally recurrent stage III non-small cell lung cancer after concurrent chemoradiotherapy. *BMC Cancer* (2015) 15:656. doi: 10.1186/s12885-015-1657-3
- Jiang W, Jiang P, Wei S, Jiang Y, Ji Z, Sun H, et al. The accuracy and safety of CT-guided iodine-125 seed implantation assisted by 3D non-coplanar template for retroperitoneal recurrent carcinoma. *World J Surg Oncol* (2020) 18(1):307. doi: 10.1186/s12957-020-02087-0
- Henriquez López I, González-San Segundo C, Vegas JO, Gutierrez C, Hervas A, Cabeza Rodriguez MA, et al. Salvage brachytherapy for locally-recurrent prostate cancer after radiation therapy: A comparison of efficacy and toxicity outcomes with high-dose rate and low-dose rate brachytherapy. *Radiother Oncol* (2019) 141:156–63. doi: 10.1016/j.radonc.2019.09.006
- Yao L, Cao Q, Wang J, Yang J, Meng N, Guo F, et al. CT-guided 125I seed interstitial brachytherapy as a salvage treatment for recurrent spinal metastases after external beam radiotherapy. *BioMed Res Int* (2016) 2016:8265907. doi: 10.1155/2016/8265907
- Jiang P, Liu C, Wang J, Yang R, Jiang Y, Tian S. Computed tomography (CT)-guided interstitial permanent implantation of 125I seeds for refractory chest wall metastasis or recurrence. *Technol Cancer Res Treat* (2015) 14(1):11–8. doi: 10.7785/tcr.2012.500402
- Shi S, Zheng G, Zhang S, Lv J, Feng Z, Chai S, et al. CT guided coplanar template assisted in the treatment of metastatic or recurrent chest wall malignant tumor with 125I seed implantation. *Chin J Radiol Med Prot* (2017) 37(7):539–42. doi: 10.3760/cma.j.issn.0254-5098.2017.07.013
- Jiang W, Chen Y, Ji Z, Jiang Y, Qiu B, Sun H, et al. The accuracy and dosimetric analysis of 3D-printing non-coplanar template-assisted iodine-125 seed implantation for recurrent chest wall cancer. *J Contemp Brachyther* (2021) 13(3):273–9. doi: 10.5114/jcb.2021.106250
- Eisenhauer EA, Therasse P, Bogaerts J, Schwartz LH, Sargent D, Ford R, et al. New response evaluation criteria in solid tumours: Revised RECIST guideline (version 1.1). *Eur J Cancer* (2009) 45(2):0–247. doi: 10.1016/j.ejca.2008.10.026
- Chen AP, Setser A, Anadkat MJ, Cotliar J, Olsen EA, Garden BC, et al. Grading dermatologic adverse events of cancer treatments: The common terminology criteria for adverse events version 4.0. *J Am Acad Dermatol* (2012) 67(5):1025–39. doi: 10.1016/j.jaad.2012.02.010
- Qiu B, Jiang P, Ji Z, Huo X, Sun H, Wang J. Brachytherapy for lung cancer. *Brachytherapy* (2021) 20(2):454–66. doi: 10.1016/j.brachy.2020.11.009
- Fraass B, Doppke K, Hunt M, Kutcher G, Starkschall G, Stern R, et al. American Association of physicists in medicine radiation therapy committee task group 53: Quality assurance for clinical radiotherapy treatment planning. *Med Phys* (1998) 25(10):1773–829. doi: 10.1118/1.598373

Conflict of interest

Authors YM and YS are employed by the Staff Hospital of Chengde Iron and Steel Group Co. Ltd.

The remaining authors declare that the research was conducted in the absence of any commercial or financial relationships that could be construed as a potential conflict of interest.

Publisher's note

All claims expressed in this article are solely those of the authors and do not necessarily represent those of their affiliated organizations, or those of the publisher, the editors and the reviewers. Any product that may be evaluated in this article, or claim that may be made by its manufacturer, is not guaranteed or endorsed by the publisher.

Supplementary material

The Supplementary Material for this article can be found online at: <https://www.frontiersin.org/articles/10.3389/fonc.2022.957497/full#supplementary-material>

23. Nath R, Anderson LL, Meli JA, Olch AJ, Stitt JA, Williamson JF. Code of practice for brachytherapy physics: Report of the AAPM radiation therapy committee task group no. 56. *Am Assoc Phys Med Med Phys* (1997) 24(10):1557–98. doi: 10.1118/1.597966
24. Wang J, Chai S, Wang R, Zheng G, Zhang K, Huo B, et al. Expert consensus on computed tomography-assisted three-dimensional-printed coplanar template guidance for interstitial permanent radioactive 125I seed implantation therapy. *J Cancer Res Ther* (2019) 15(7):1430–4. doi: 10.4103/jcrt.JCRT_434_19
25. Ji Z, Jiang Y, Guo F, Peng R, Sun H, Fan J, et al. Safety and efficacy of CT-guided radioactive iodine-125 seed implantation assisted by a 3D printing template for the treatment of thoracic malignancies. *J Cancer Res Clin Oncol* (2020) 146(1):229–36. doi: 10.1007/s00432-019-03050-7
26. Optimization and decision-making in radiological protection. A report of a task group of committee 4 of the international commission on radiological protection. *Ann ICRP* (1989) 20(1):1–60.
27. Buchholz TA, Ali S, Hunt KK. Multidisciplinary management of locoregional recurrent breast cancer. *J Clin Oncol* (2020) 38(20):2321–8. doi: 10.1200/JCO.19.02806
28. Chagpar A, Kuerer HM, Hunt KK, Strom EA, Buchholz TA. Outcome of treatment for breast cancer patients with chest wall recurrence according to initial stage: Implications for post-mastectomy radiation therapy. *Int J Radiat Oncol Biol Phys* (2003) 57(1):128–35. doi: 10.1016/s0360-3016(03)00431-0
29. Auoragh A, Strnad V, Ott OJ, Beckmann MW, Fietkau R. Re-irradiation of the chest wall for local breast cancer recurrence: Results of salvage brachytherapy with hyperthermia. re-bestrahlung der brustwand bei lokalen brustkrebsrezidiven: Ergebnisse der salvage-brachytherapie mit hyperthermie. *Strahlenther Onkol* (2016) 192(9):617–23. doi: 10.1007/s00066-016-1010-z
30. Oldenburg S, Van Os RM, Van rij CM, Crezee J, Van de Kamer JB, Rutgers EJ, et al. Elective re-irradiation and hyperthermia following resection of peSABTstent locoregional recurrent breast cancer: A retrospective study. *Int J Hyperther* (2010) 26(2):136–44. doi: 10.3109/02656730903341340
31. Oldenburg S, Rasch CRN, van Os R, Kusumanto YH, Oei BS, Venselaar JL, et al. Reirradiation + hyperthermia for recurrent breast cancer en cuirasse. rebestrahlung + hyperthermie bei brustkrebs in form von cancer en cuirasse. *Strahlenther Onkol* (2018) 194(3):206–14. doi: 10.1007/s00066-017-1241-7
32. Oldenburg S, Griesdoorn V, van Os R, Kusumanto YH, Oei BS, Venselaar JL, et al. Reirradiation and hyperthermia for irresectable locoregional recurrent breast cancer in previously irradiated area: Size matters. *Radiother Oncol* (2015) 117(2):223–8. doi: 10.1016/j.radonc.2015.10.017
33. Jones EL. Randomized trial of hyperthermia and radiation for superficial tumors. *J Clin Oncol* (2005) 23(13):3079–85. doi: 10.1200/JCO.2005.05.520
34. Hoppe BS, Laser B, Kowalski AV, Fontenla SC, Pena-Greenberg E, Yorke ED, et al. Acute skin toxicity following stereotactic body radiation therapy for stage I non-Small-Cell lung cancer: Who's at risk? *Int J Radiat oncol biol Phys* (2009) 72(5):1283–6. doi: 10.1016/j.ijrobp.2008.08.036
35. Mccammon R, Scheffer TE, Gaspar LE, Zaemisch R, Gravidahl D, Kavanagh B. Observation of a dose-control relationship for lung and liver tumors after stereotactic body radiation therapy. *Int J Radiat Oncol Biol Phys* (2009) 73(1):112–8. doi: 10.1016/j.ijrobp.2008.03.062
36. Pettersson N, Nyman J, Johansson KA. Radiation-induced rib fractures after hypofractionated stereotactic body radiation therapy of non-small cell lung cancer: A dose- and volume-response analysis. *Radiother Oncol J Eur Soc Ther Radiol Oncol* (2009) 91(3):360–8. doi: 10.1016/j.radonc.2009.03.022
37. Voroney JPP, Hope A, Dahele MR, Purdie TG, Franks KN, Pearson S, et al. Chest wall pain and rib fracture after stereotactic radiotherapy for peripheral non-small cell lung cancer. *Int J Radiat Oncol biol Phys* (2008) 72(1):S35–6. doi: 10.1097/JTO.0b013e3181ae2962
38. Li G, Mitsumori M, Ogura M, Horii N, Kawamura S, Masunaga S, et al. Local hyperthermia combined with external irradiation for regional recurrent breast carcinoma. *Int J Clin Oncol* (2004) 9(3):179–83. doi: 10.1007/s10147-004-0395-3

Frontiers in Oncology

Advances knowledge of carcinogenesis and tumor progression for better treatment and management

The third most-cited oncology journal, which highlights research in carcinogenesis and tumor progression, bridging the gap between basic research and applications to improve diagnosis, therapeutics and management strategies.

Discover the latest Research Topics

See more →

Frontiers

Avenue du Tribunal-Fédéral 34
1005 Lausanne, Switzerland
frontiersin.org

Contact us

+41 (0)21 510 17 00
frontiersin.org/about/contact

